Subdivision Schemes for Curve Design and Image Analysis

Doctoral Dissertation submitted to

Faculty of Mathematics and Applications   Faculty of Informatics

in partial fulfillment of the requirements for the degree of

Doctor of Philosophy

presented by

Elena Volontè

under the supervision of

Milvia Rossini   **Kai Hormann**
Università degli Studi Milano Bicocca   Università della Svizzera italiana

December 2017

Dissertation Committee

- Internal Members

  Evanthia Papadopoulou   Università della Svizzera italiana, Switzerland
  Lourenco Beirao Da Veiga   Università degli Studi Milano Bicocca, Italy

- External Members

  Costanza Conti   Università degli Studi di Firenze, Italy
  Ulrich Reif   Technische Universität Darmstadt, Germany

Dissertation accepted on 29 December 2017

Research Advisor	PhD Program Director
Milvia Rossini	**Roberto Paoletti**
Kai Hormann	**Walter Binder**

I certify that except where due acknowledgement has been given, the work presented in this thesis is that of the author alone; the work has not been submitted previously, in whole or in part, to qualify for any other academic award; and the content of the thesis is the result of work which has been carried out since the official commencement date of the approved research program.

Elena Volontè
Milano, 29 December 2017

I have not failed. I've just found
10,000 ways that won't work.

Thomas Edison

Abstract

Subdivision schemes are able to produce functions, which are smooth up to pixel accuracy, in a few steps through an iterative process. They take as input a coarse control polygon and iteratively generate new points using some algebraic or geometric rules. Therefore, they are a powerful tool for creating and displaying functions, in particular in computer graphics, computer-aided design, and signal analysis.

A lot of research on univariate subdivision schemes is concerned with the convergence and the smoothness of the limit curve, especially for schemes where the new points are a linear combination of points from the previous iteration. Much less is known for non-linear schemes: in many cases there are only ad hoc proofs or numerical evidence about the regularity of these schemes. For schemes that use a geometric construction, it could be interesting to study the continuity of geometric entities. Dyn and Hormann [2012] propose sufficient conditions such that the subdivision process converges and the limit curve is tangent continuous. These conditions can be satisfied by any interpolatory scheme and they depend only on edge lengths and angles. The goal of my work is to generalize these conditions and to find a sufficient constraint, which guarantees that a generic interpolatory subdivision scheme gives limit curves with continuous curvature. To require the continuity of the curvature it seems natural to come up with a condition that depends on the difference of curvatures of neighbouring circles. The proof of the proposed condition is not completed, but we give a numerical evidence of it.

A key feature of subdivision schemes is that they can be used in different fields of approximation theory. Due to their well-known relation with multiresolution analysis they can be exploited also in image analysis. In fact, subdivision schemes allow for an efficient computation of the wavelet transform using the filterbank. One current issue in signal processing is the analysis of anisotropic signals. Shearlet transforms allow to do it using the concept of multiple subdivision schemes. One drawback, however, is the big number of filters needed for analysing the signal given. The number of filters is related to the determinant of the expanding matrix considered. Therefore, a part of my work is devoted to find expanding matrices that give a smaller number of filters compared to the shearlet case. We present a family of anisotropic matrices for any dimension d with smaller determinant than shearlets. At the same time, these matrices allow for the definition of a valid directional transform and associated multiple subdivision schemes.

Acknowledgements

First of all, I would like to thank prof. Mira Bozzini for encouraging me to do the PhD, and for having followed me in a great part of my studies. Many thanks to dr. Milvia Rossini, who guided me from the bachelor thesis up to now. She has always been helpful and available to listen my problems. I have to thank both of them for giving me the possibility to collaborate with several professors, such as prof. Tomas Sauer and dr. Mariantonia Cotronei, who I am grateful to for the nice and fruitful meetings and for the availability to answer to all my questions.

I am particularly grateful to prof. Kai Hormann for the opportunity he gave me to spend half of my PhD studies at the Università della Svizzera Italiana. It has been a great chance to know a different university environment and to experience a different way to work. It was very exciting for me and it helped me to increase my skills. Nevertheless, I have to thank him for the patience with my bad English: I hope he can see my little improvements.

I have to thank my colleagues at the Università della Svizzera italiana who welcomed me in the group. In particular, I have to thank Dima for always being available when I needed something, Teseo that is the mentor of the group and always has the answer to any problem, and Emiliano for the fun at the conferences and for listening my outbursts.

Per quanto riguarda i miei colleghi italiani devo per prima cosa ringraziare quelli che mi hanno fatto compagnia nelle conferenze: Alberto, Daniela, Valentina e soprattutto Paola con cui abbiamo condiviso tutto il percorso universitario nelle gioie ma soprattutto nei dolori.

Anche se non propriamente una collega devo ringraziare Silvia con cui ho condiviso le ansie del dottorato e ci siamo supportate a vicenda, anche se non eravamo più nella stessa università. Nonostante le esperienze diverse è stato utile avere qualcuno che ti capisse.

Devo ringraziare tutti i dottorandi di Matematica in Bicocca, che sono in troppi per essere elencati. In particolare devo ringraziare quelli con cui ho passato più tempo: Bianca, Elia, Alessandro, ma soprattutto Federico e Benedetta. Grazie di avermi sempre fatto sentire parte del gruppo anche se per lunghi periodi non ci sono stata.

Infine devo assolutamente ringraziare i miei genitori che mi hanno insegnato a dare sempre il massimo, a non arrendermi mai e a cercare sempre di spingermi oltre. Senza questa motivazione non avrei mai intrapreso questo percorso.

Last but not least, devo ringraziare Jacopo, che ha vissuto con me ogni istante di questi quattro lunghi anni, che mi ha supportato in ogni momento e che dicendomi di abbandonare mi ha spronato invece ad andare avanti. Grazie per la pazienza.

Thanks to everyone I met during these four years: you all taught me something.

Contents

II   Subdivision Schemes for Image Analysis   97

Outline   99

5   Wavelets   103

6   Shearlets   115

7   Anisotropic Scaling Matrices   135

Conclusions   175

Bibliography   177

Introduction

The first subdivision scheme is given by De Rham [1947]. Later on, two other famous schemes are introduced by Chaikin [1974]; Deslauriers and Dubuc [1989]. The basic idea of subdivision is to start with a coarse control polygon and iteratively generate new points that converge to a smooth limit curve. The new points are generated from the previous ones using some algebraic or geometric rules.

The idea is not new, because it is the same principle that Archimedes used in *The Measurement of a Circle* to approximate a circle by increasing the number of vertices of a regular polygon (see Fig. 1). But, with the invention of computers, it becomes a faster and cheaper way to plot a curve. These two characteristics allow for the exploitation in graphic design: even complex smooth curves can be described in terms of a small number of control points, and the curves themselves can be generated efficiently by applying just few subdivision steps. Other advantages include the rotational invariance and the locality of the subdivision rules. On the one hand, this means that the resulting limit curve can be rotated and translated by applying the same transformations to the initial control points. On the other hand, changing the position of one of the control points influences only a small part of the limit curve.

Subdivision schemes are a powerful tool not only for graphic design, because the connection with multiresolution analysis theory allows to exploit them also in signal processing and in general in the approximation theory. Whenever we define a multiresolution analysis to approximate a function at different levels, subdivision schemes are
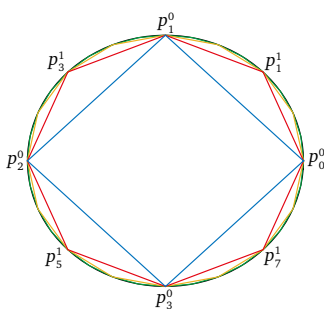
Figure 1. "First" attempt of iterative process to approximate a circle by Archimedes.

used to efficiently compute the approximation.

Motivation

The thesis is focused on both applications: one in designing curves and studying their geometric regularity (Part I), and one in image processing using subdivision schemes to generate a directional multiple multiresolution analysis to analyse anisotropic phenomena (Part II).

Being an iterative process, the first inquiry about a subdivision scheme is if it converges. For this reason a lot of research on subdivision schemes concerns the convergence and the smoothness of the limit curve [Dyn and Levin, 1995; Dyn, 2002; Wallner and Dyn, 2005]. Linear schemes are well investigated in this sense. A linear scheme is a scheme where the new points are a linear combination of points from the previous iteration. A famous example of linear scheme is the family of interpolatory 2N-point schemes presented by Deslauriers and Dubuc [1989]; where the new points are a linear combination of 2N points from the previous step.

There are other schemes, called non-linear schemes, where the new points depend in a non-linear way on the points from the previous step or they are computed with a geometric construction. Examples of such schemes are the incenter scheme [Deng and Wang, 2010; Hernández-Mederos et al., 2013], the angle-based 4-point scheme or the circle-based 4-point scheme [Dyn and Hormann, 2012]. The name of these schemes is evocative of the fact that the construction depends on some geometric quantities. These types of schemes are not generally exploited, because of the difficulties to study their convergence, but they are an interesting tool to guarantee some geometric properties of the limit curve. Usually, for non-linear schemes with a geometric construction, ad hoc proofs are provided or there is only numerical evidence of the regularity of the limit curve.

The first paper that tries to cover this lack of studies is that of Dyn and Hormann [2012] where they give sufficient conditions on the convergence and tangent continuity of an interpolatory geometric scheme. The peculiarity of their approach is to study the regularity of a curve considering entities like tangents and curvatures that are independent on the curve parametrization. In this way they require the geometric continuity of the limit curve instead of the analytic continuity of the derivatives.

The conditions that Dyn and Hormann [2012] present depend on the edge length and the external angle of the triangles defined by three consecutive point of the subdivision process. In particular, the summability of the sequence of maximum edge lengths gives the convergence of the scheme, while the summability of the maximum modulo of angles ensures that the limit curve is tangent continuous.

The conditions proposed by Dyn and Hormann [2012] give at maximum the G^1 continuity of the limit curve. In the literature there are some geometric schemes [Deng and Wang, 2010; Deng and Ma, 2012, 2014; Hernández-Mederos et al., 2013] that claim to generate limit curve with continuous curvature. In order to give a proof of this regularity

in the first part of my work I focus on finding a geometric condition for the curvature continuity of the limit curve. The curvature of a curve at a point p can be defined as the reciprocal of the radius of the osculating circle. An osculating circle is the limit of the circles passing through three point q, p, r when q and r converge to p. With this in mind, we consider the curvatures of the circles passing through three consecutive points and we take their difference. The core of my work is to prove that the summability of this sequence is sufficient for generating a limit curve with continuous curvature. Unfortunately, the proof is not completed but we give a numerical evidence of the proposed condition and of the missing points in the proof.

Different is the use of subdivision schemes in image analysis. Due to their relation with a multiresolution analysis, interpolatory subdivision schemes allow for the construction of a filterbank that can be used to analyse and synthesize a signal (see e.g [Chui, 1992b; Madych, 1993; Mallat, 1989; Meyer, 1995; Strang and Nguyen, 1996]).

One crucial issue in signal processing is the analysis of anisotropic signals with the aim to catch directionality of the signal. When dealing with anisotropic phenomena, wavelets do not provide optimally sparse representations. For this reason directional transforms were introduced [Candès and Donoho, 2004; Labate et al., 2005; Do and Vetterli, 2005]. Among them, the shearlets transform is interesting because it is connected to a multiresolution analysis similar to those of wavelets: the multiple multiresolution analysis [Kutyniok and Sauer, 2009; Kutyniok et al., 2012]. Related to a multiple multiresolution analysis, there were introduced the multiple subdivision schemes [Sauer, 2010]. A multiple subdivision scheme is a scheme where in each iteration the expanding matrix M_i and the subdivision scheme $\mathcal{S}_i$ are chosen from a finite dictionary $\{M_i, \mathcal{S}_i\}_{i \in \mathbb{Z}_s}$.

The expanding matrices M_i are the key ingredient in a multiresolution analysis because there are responsible for the refinement. For the multiple subdvision scheme we require that all the combinations of M_i are expanding, namely the set of matrices $\{M_i\}_{i \in \mathbb{Z}_s}$ are jointly expanding. In order to define a directional transform, it is crucial that the expanding matrices satisfy the slope resolution property. All the directions in the space can be reached applying an appropriate combination of the matrices M_i to a reference line.

In the shearlets case the expanding matrices considered are the product of a diagonal matrix, the so-called parabolic matrix, with a pseudo rotation matrix called shear matrix and they satisfy all the previous properties [Sauer, 2012]. The drawback is that the diagonal matrix considered has large determinant that leads to a high number of filters and a quite substantial complexity in implementations.

In the second part of my work I want to overcome this problem by studying the existence of different matrices that allow us to define a directional transform in any dimension d with smaller determinant. We propose a family of shear-like matrices, product of an anisotropic diagonal matrix and a shear matrix, whose determinant, for increasing d, is considerable lower than the shearlet case. We prove that in any dimension the elements of this family are expanding, jointly expanding and they provide the slope res-

olution property. In this sense we are able to define an appropriate directional transform suitable for image analysis. For dimension $d > 2$, we also study the possibility of relaxing the structure of the matrix considering the general case of an anisotropic expanding matrix with small determinant.

Structure

The thesis is divided in two parts, one about subdivision schemes for curve design and the second one about schemes for image analysis. Before these two parts, in Chapter 1, I introduce the main concepts about subdivision schemes that I will use along the thesis. In particular, in Section 1.1, I recall some general background notions about successions and series. I give the definition of subdivision schemes and the main classification between linear, non-linear, interpolatory, approximating, stationary, non-stationary schemes in Section 1.2. The main results presented in the literature about the convergence and regularity of the limit curve are recalled in Section 1.3. Finally, in Section 1.4, I give some examples of linear schemes.

In Part I of the thesis I focus on curve design and the study of sufficient conditions to require a certain order of geometric regularity. In Chapter 2, I recall the main differences between analytic continuity and geometric continuity (Sec. 2.1) and I give some examples of geometric schemes (Sec. 2.2). In Chapter 3, I present the work of Dyn and Hormann [2012] showing, in Section 3.1, the sufficient conditions that generate a G^1 continuous limit curve by an interpolatory scheme. In Section 3.2 I display some examples of geometric schemes that satisfy these conditions. Chapter 4 is mainly devoted to explain the results of the collaboration with Kai Hormann during the period that I spent at Università della Svizzera italiana. In Section 4.1 I present the condition that we elaborate in order to ensure that a geometric interpolatory subdivision scheme generates a limit curve with continuous curvature. In order to test the validity of this condition, we made some numerical examples that I report in Section 4.2. Finally in Section 4.3 there are my attempts to prove that the condition suggested is sufficient to generate curvature continuous limit curve. The proof is not complete but I give a numerical evidence of the missing points.

In Part II of the thesis I study which matrices allow to define a directional transform suitable for image analysis. Before giving the detail of my work, I present the problem introducing wavelets and shearlet theory respectively in Chapters 5 and 6. It is necessary to recall the general definition of the wavelet transform (Sec. 5.1) in order to explain the relation with multiresolutive analysis and subdivision schemes (Sec. 5.2). Furthermore, in Section 5.3 we introduce the theory of filterbanks that allows to exploit subdivision schemes for the analysis of a signal. The same description is given for the shearlet transform (Sec. 6.1) exploiting in this case the more general concept of multiple multiresolution analysis and multiple subdivision scheme (Sec. 6.2). In Chapter 7 I present the joint work with Mira Bozzini, Milvia Rossini and Tomas Sauer, in particular Section 7.1 shows which are the fundamental properties that the expanding matrices

have to satisfy in order to generate a directional transform. Then, in Section 7.2 I introduce a new family of integer matrices with minimum determinant in the set of matrices that are product of an anisotropic diagonal matrix and a shear matrix. Moreover, the proposed set of matrices satisfies all the previous properties. In Section 7.3 I study the possibility for any dimension $d > 2$ to relax the structure of the expanding matrices in order to minimize even more the value of the determinant. The effectiveness of the presented matrices is shown by several numerical examples on images in Section 7.4.

Chapter 1

Subdivision schemes

Subdivision schemes are the common background of my research presented in this thesis. It is worthwhile to make a little excursion on the basic notions and results about subdivision schemes in literature.

Definition 1.1. *A subdivision scheme $\mathcal{S}$ takes an ordered set of control points $P = \{p_i\}_{i \in \mathbb{Z}} \subset \mathbb{R}^d$ and iteratively generates new points*

$$P^0 := P, \qquad P^{j+1} := \mathcal{S}P^j, \quad j \geq 0,$$

by applying some simple rules

$$p_{vi}^{j+1} = f_0(p_{i-k}^j, \ldots, p_{i+k}^j), \ p_{vi+1}^{j+1} = f_1(p_{i-k}^j, \ldots, p_{i+k}^j), \ \ldots, \ p_{vi+v-1}^{j+1} = f_{v-1}(p_{i-k}^j, \ldots, p_{i+k}^j). \tag{1.1}$$

The points are denoted by two indices: the lower index i indicates the position of the point inside the control polygon, the upper index j indicates the level of subdivision. Figure 1.1 shows a simple example of univariate subdivision scheme where the points of the previous level are kept by the scheme and a new point is inserted between each pair of old points.

The number of rules for computing the new points is called the *arity v* of a subdivision scheme. The arity also coincides with the factor by which the number of points is multiplied in each step. For instance, a binary scheme duplicates the number of control
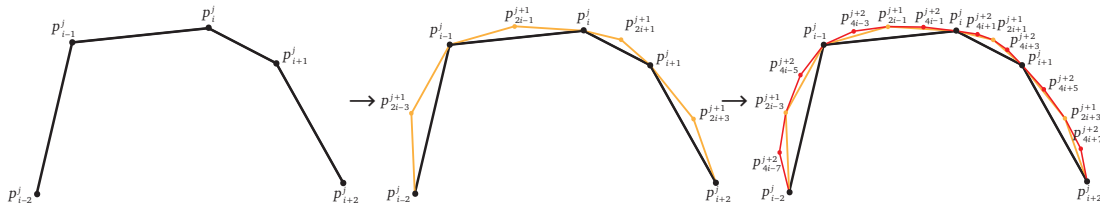

Figure 1.1. Two iterations of a univariate binary subdivision scheme.

points and a ternary scheme triplicates the points. If the functions f_n, $n = 0, \ldots, \nu - 1$ depend on at most $2k + 1$ points, then $2k + 1$ is called the *support* of the subdivision scheme.

1.1   Background material

A subdivision scheme associates a sequence of points to a given finite set of points. In this sense we should recall some basic notions on sequences.

The space of bi-infinite sequences from $\mathbb{Z}^d$ to $\mathbb{R}$ is denoted by $\ell(\mathbb{Z}^d)$. Instead with $\ell_p(\mathbb{Z}^d)$ we denote the sequences with finite p-norm

$$\|c\|_{\ell_p(\mathbb{Z}^d)} = \left(\sum_{\alpha \in \mathbb{Z}^d} |c(\alpha)|^p \right)^{1/p} < \infty$$

where $1 \leq p < \infty$. For $p = \infty$ we consider the sequences with norm

$$\|c\|_{\ell_\infty(\mathbb{Z}^d)} = \sup_{\alpha \in \mathbb{Z}^d} |c(\alpha)|.$$

Finally, $\ell_{00}(\mathbb{Z}^d)$ is composed of all sequences from $\mathbb{Z}^d$ to $\mathbb{R}$ with finite support. We denote by $\ell^d(\mathbb{Z})$ the vector sequences from $\mathbb{Z}$ to $\mathbb{R}^d$. So a subdivision scheme is an operator $\mathcal{S}\colon \ell_{00}^d(\mathbb{Z}) \to \ell_{00}^d(\mathbb{Z})$.

Since we consider infinite and finite sequences all along the thesis, it is useful to recall some general results on Cauchy sequences, convergent and summable scalar sequences. For further details see [Rudin et al., 1964].

Definition 1.2. *An infinite scalar sequence $a = \{a_n\}_{n \in \mathbb{N}} \in \ell(\mathbb{N})$ converges to A if for every $\epsilon > 0$, there exists an integer n_0 such that $|a_n - A| < \epsilon$ for any $n \geq n_0$ and we write*

$$\lim_{n \to \infty} a_n = A.$$

Definition 1.3. *A sequence $a = \{a_n\} \in \ell(\mathbb{N})$ is called a Cauchy sequence if for any $\epsilon > 0$, there exists n_0 such that $|a_n - a_m| < \epsilon$ for any $n, m \geq n_0$.*

For Cauchy sequences there is a well-known result.

Theorem 1.1. *In $\mathbb{R}^d$, $d \in \mathbb{N}$, every Cauchy sequence converges.*

An example of an infinite sequence is the geometric sequence.

Definition 1.4. *A sequence $a = \{a_n\} \in \ell(\mathbb{N})$ is called a geometric sequence if there exists some $\mu \in \mathbb{R}$ such that for all $n \in \mathbb{N}$ he have $a_{n+1}/a_n = \mu$. The general term of the sequence can be rewritten as $a_n = c\mu^n$ with some constant c.*

Different values of μ give different behaviour of the geometric sequence.

Proposition 1.2. *Let $\mu \neq 0$, in the limit the geometric sequence $a_n = \mu^n$ behave as*

$$\lim_{n \to \infty} \mu^n = \begin{cases} +\infty & \mu > 1 \\ 1 & \mu = 1 \\ 0 & |\mu| < 1 \\ \nexists & \mu \leq -1 \end{cases}$$

From the definition of sequences we define the concept of series.

Definition 1.5. *Given a sequence $a = \{a_n\} \in \ell(\mathbb{N})$ we associate another sequence*

$$s_n = \sum_{k=1}^{n} a_k$$

called the partial sum. *If the sequence $\{s_n\}$ is convergent and converges to $s < \infty$, then the series*

$$\sum_{n=1}^{\infty} a_n = s < \infty$$

converges. In this case the sequence $\{a_n\}$ is called summable. *Otherwise, if the sequence $\{s_n\}$ diverge, the corresponding series diverges.*

Definition 1.3 of a Cauchy sequence gives a sufficient and necessary condition for the convergence of the series.

Proposition 1.3. *A sequence $\{a_k\}$ is summable if and only if for every $\epsilon > 0$ there exists some n_0 such that*

$$\left| \sum_{k=n}^{m} a_k \right| < \epsilon$$

for any $m > n \geq n_0$.

Proposition 1.4. *If the series $\sum a_n$ converges, then the general term of the series converges to zero, $\lim_{n \to \infty} a_n = 0$.*

Note that convergence to 0 of the general term a_n is a necessary but not a sufficient condition to have the convergence of the series.

Applying Proposition 1.4 to a geometric sequence it is possible to prove

Proposition 1.5. *The series*

$$\sum_{n=0}^{\infty} \mu^n = \frac{1}{1 - \mu}$$

converges if and only if $|\mu| < 1$.

To compare the behaviour of two different sequences we recall the big O notation and the concept of asymptotic sequences.

Definition 1.6. *Given two sequences $\{a_n\}_{n\in\mathbb{N}}$ and $\{b_n\}_{n\in\mathbb{N}}$ we say that $a_n = O(b_n)$ if there exists a constant $c > 0$ such that there exists some n_0, such that for all $n \geq n_0$,*

$$|a_n| \leq c\,|b_n|.$$

Two sequences $\{a_n\}_{n\in\mathbb{N}}$ and $\{b_n\}_{n\in\mathbb{N}}$ are called asymptotic $a_n \sim b_n$ *if for all $\epsilon > 0$, there exists some n_0 such that for all $n \geq n_0$,*

$$\left|\frac{a_n}{b_n} - 1\right| < \epsilon \quad \Rightarrow \quad \lim_{n\to\infty} \frac{a_n}{b_n} = 1$$

For more details we refer to [Erdélyi, 2010; Knuth, 1976].

Simple operations like summation and multiplication are well-defined on big O notation:

(i) $O(a_n)O(b_n) = O(a_n b_n)$.

(ii) $O(a_n) + O(a_n) = O(a_n)$.

(iii) If the sequence $a_n = O(1)$ is bounded then $O(a_n) + O(a_n^2) = O(a_n)$.

Proof: Let $b_n = O(a_n)$ and $d_n = O(a_n^2)$. By Definition 1.6 there exist $c_1, c_2 > 0$ such that

$$|b_n| \leq c_1\,|a_n|, \quad |d_n| \leq c_2\,|a_n|^2.$$

Moreover $a_n = O(1)$ implies that there exists some $c_3 > 0$ such that $|a_n| \leq c_3$. Putting all together we obtain

$$|b_n + d_n| \leq |b_n| + |d_n| \leq c_1\,|a_n| + c_2\,|a_n|^2 = (c_1 + c_2\,|a_n|)\,|a_n| \leq (c_1 + c_2 c_3)\,|a_n|.$$

$\square$

In Chapters 3 and 4 we give some sufficient conditions for the regularity of the limit curve generated by the scheme in terms of summability of a sequence. In the proof of the curvature continuity (Proposition 4.9) we require a stricter condition then summability.

Definition 1.7. *A sequence $\{a_n\}_{n\in\mathbb{N}}$ is said to behave like a convergent geometric sequence if there exists some $0 < \mu < 1$ such that*

$$a_n = O(\mu^n) \quad \Rightarrow \quad |a_n| \leq c\mu^n,$$

where c is a positive constant.

1.2 Classification of subdivision schemes

Once we have defined a subdivision scheme, we can classify the subdivision schemes with respect to certain characteristics. Here we present the main types of schemes that we consider throughout the thesis.
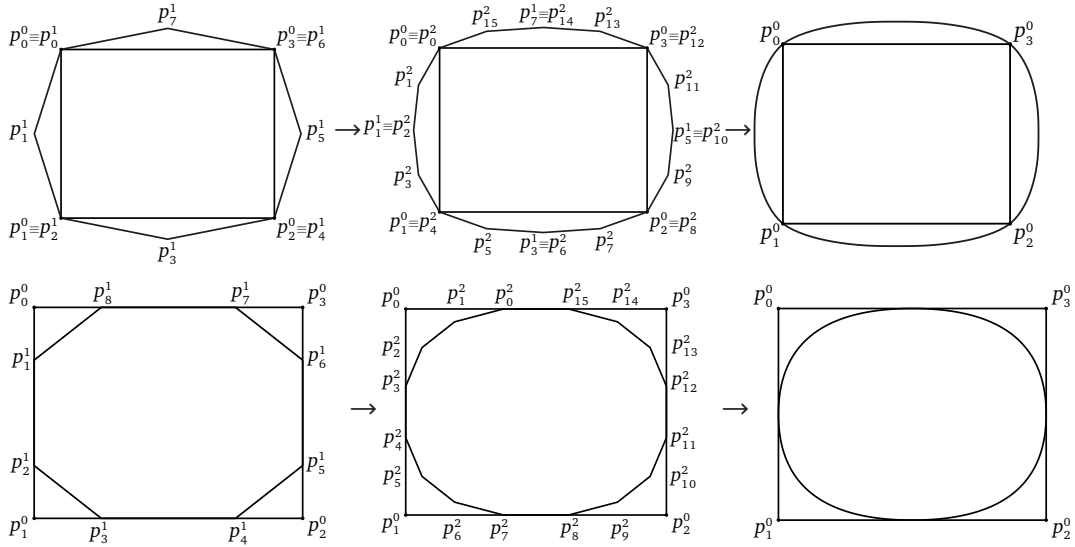
Figure 1.2. Subdivision process for an interpolatory scheme (top) and an approximating scheme (bottom).

1.2.1   Interpolatory vs approximating schemes

The first characterization that we consider is between interpolatory and approximating schemes.

If the first rule in (1.1) is the Dirac delta function $f_0 = \delta$, then the subdivision scheme keeps the points from the previous step,

$$p_{vi}^{j+1} = \delta_{i,k}\, p_k^j = p_i^j$$

and is called *interpolatory*. This denomination comes from the fact that the limit curve passes through the starting points (see Fig. 1.2). Otherwise, if the first rule f_0 in (1.1) is generic, then the scheme is called *approximating*. In this case the limit curve approximates the initial control polygon (see Fig. 1.2).

An example of an interpolatory subdivision scheme is the well-known 4-point scheme by Deslauriers and Dubuc [1989] with rules

$$\begin{aligned}
p_{2i}^{j+1} &= p_i^j, \\
p_{2i+1}^{j+1} &= -\frac{1}{16}p_{i-1}^j + \frac{9}{16}p_i^j + \frac{9}{16}p_{i+1}^j - \frac{1}{16}p_{i+2}^j.
\end{aligned} \tag{1.2}$$

It is a binary scheme where the even points p_{2i}^{j+1} are the points kept from the previous step while the odd points p_{2i+1}^{j+1} are new points computed as a linear combination of 4 points from the previous step. The name of the scheme comes from the value of the support. The action of (1.2) is displayed in Figure 1.3.
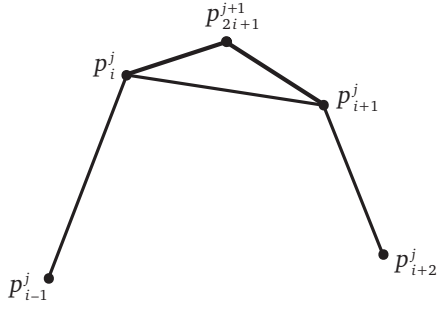
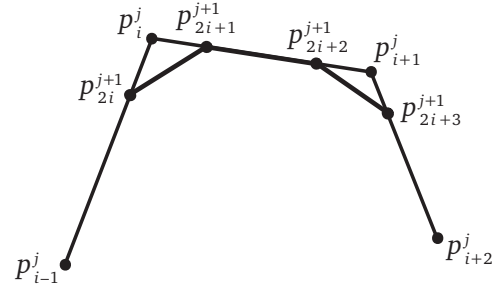Figure 1.3. Construction of the new point for the 4-point scheme.

Figure 1.4. Construction of the new points for the B-spline scheme.

An example of an approximating scheme is the quadratic B-spline scheme with rules

$$p_{2i}^{j+1} = \frac{1}{4}p_{i-1}^{j} + \frac{3}{4}p_{i}^{j}, \tag{1.3}$$

$$p_{2i+1}^{j+1} = \frac{3}{4}p_{i}^{j} + \frac{1}{4}p_{i+1}^{j}.$$

In this case both the even and odd points are a linear combination of two points from the previous level. So the support of the scheme is 2. From Figure 1.4 we can observe that the points at level j are discarded at level $j+1$ and new points are computed. The name of the scheme is due to the fact that if we consider as starting points the Delta sequence $\delta = (\ldots, 0, 1, 0, \ldots)$ the limit curve generated is the quadratic B-spline basic function centred at the origin.

For all the rest of the thesis we consider only interpolatory schemes. The reasons for this choice are many and are explained better in the following chapters.

1.2.2   Linear vs non-linear schemes

In the two previous examples, the 4-point scheme (1.2) and the quadratic B-spline scheme (1.3), the new points are a linear combination of points from the previous level. If the rules of the subdivision scheme (1.1) are such that the new points at level $j+1$ are linear combinations of the points at level j,

$$p_{i}^{j+1} = (\mathcal{S}P^{j})_{i} = \sum_{\ell=-k}^{k} a_{i-\nu\ell}\, p_{\ell}^{j}, \tag{1.4}$$

then we call $\mathcal{S}$ a *linear* subdivision scheme. Equation (1.4) collects in one expression all the ν rules in (1.1). If we want to separate the different rules, then we need to write i modulo ν

$$p_{\nu i}^{j+1} = (\mathcal{S}P^{j})_{\nu i} = \sum_{\ell=-k}^{k} a_{\nu(i-\ell)}\, p_{\ell}^{j}, \quad p_{\nu i+1}^{j+1} = (\mathcal{S}P^{j})_{\nu i+1} = \sum_{\ell=-k}^{k} a_{\nu(i-\ell)+1}\, p_{\ell}^{j}, \quad \ldots \tag{1.5}$$

The vector $a = \{a_i\}_{i \in \mathbb{Z}} \in \ell_{00}(\mathbb{Z})$ includes all the coefficients of the rules and is called the *mask* of the scheme. For the 4-point scheme (1.2) the mask is

$$a^{[4]} = \left\{ \dots, 0, -\frac{1}{16}, 0, \frac{9}{16}, 1, \frac{9}{16}, 0, -\frac{1}{16}, 0, \dots \right\}, \tag{1.6}$$

while the mask of the quadratic B-spline is

$$a^{[B]} = \left\{ \frac{1}{4}, \frac{3}{4}, \frac{3}{4}, \frac{1}{4} \right\}. \tag{1.7}$$

The submasks of the scheme are the vectors that collects the coefficients of the rules in (1.5). They can be extracted from the mask considering the elements modulo the arity ν. In the case of binary schemes we have two submasks: the even submask $a_{[0]}$ and the odd submask $a_{[1]}$. They are called in this way because the even submask extracts the even elements of the mask, while the odd submask takes all the odd elements. For example, the mask of the 4-point scheme can be split into

$$a_{[0]} = \{\dots, 0, 1, 0, \dots\}, \quad a_{[1]} = \frac{1}{16}\{-1, 9, 9, -1\}.$$

An interpolatory scheme can be easily recognized, because the even submask is the delta sequence $\delta_{0,i}$.

Expression (1.4) gives the rules for a linear univariate scheme. For arbitrary dimension d the subdivision rules of a linear scheme become

$$p_i^{j+1} = (\mathcal{S}P^j)_i = \sum_{\ell \in \mathbb{Z}^d} a_{i - M\ell} \, p_\ell^j, \tag{1.8}$$

where $i \in \mathbb{Z}^d$ and M is an expanding matrix, namely a matrix with all eigenvalues greater than 1 in absolute value. We always consider masks a with a finite number of coefficients, $a \in \ell_{00}(\mathbb{Z}^d)$. In this general case the arity of the scheme is given by the determinant of the matrix M, $\nu = |\det M|$. For example, in two dimensions ($d = 2$) with $M = \left(\begin{smallmatrix} 2 & 0 \\ 0 & 2 \end{smallmatrix} \right)$ the rules appear as

$$p_{i,k}^{j+1} = \sum_{n,m \in \mathbb{Z}} a_{i-2n, k-2m} \, p_{n,m}^j, \quad i, k \in \mathbb{Z}.$$

Differently, a *non-linear* scheme is a subdivision process where the rules f_k, $k = 0, \dots, \nu - 1$ have a non-linear dependency on the points from the previous level. This definition includes a wide range of subdivision schemes and we distinguish between different types of non-linear rules. One type are manifold-valued schemes, where the non linearity of the schemes is determined by adapting a linear scheme to the geometry of a manifold, see [Wallner and Dyn, 2005; Wallner, 2006; Xie and Yu, 2007; Moosmüller, 2016]). Other non-linear schemes are generated by substitution of a linear average with a non-linear one as the geometric mean, see [Schaefer et al., 2008]. The 4-point scheme rules are defined by evaluating an interpolating polynomial. A non-linear version
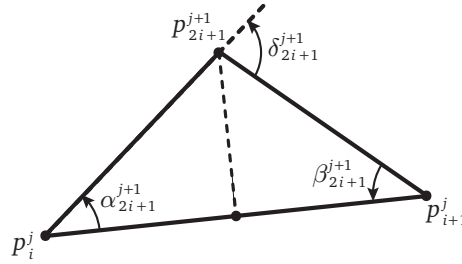
Figure 1.5. In the bisector scheme the point p_{2i+1}^{j+1} lies on the orthogonal bisector of the edge $p_i^j p_{i+1}^j$.

interpolates functions different from polynomials, see [Oswald, 2004; Xie and Yu, 2005], or it interpolates a piecewise smooth function as in the ENO (Essentially Non Oscillatory) and WENO (Weighted ENO) schemes, see [Harten et al., 1987; Liu et al., 1994].

My work addresses instead the class of so-called geometric schemes where the new points are computed with a geometric construction. By construction this type of schemes commute with similarity transformations: rotating and shifting the limit curve has the same effect as rotating and translating the initial points. An example of a family of geometric schemes is the *bisector* scheme. It is a binary interpolatory scheme where the new points p_{2i+1}^{j+1} lie on the bisector of the edge $\overrightarrow{p_i^j p_{i+1}^j}$

$$p_{2i+1}^{j+1} = \frac{p_i^j + p_{i+1}^j}{2} + \tan\left(\frac{\delta_{2i+1}^{j+1}}{2}\right) \frac{(p_{i+1}^j - p_i^j)^\perp}{2}, \tag{1.9}$$

(see. Fig 1.5). The scheme is specified by giving an expression for the angle δ_{2i+1}^{j+1}. Clearly the new point p_{2i+1}^{j+1} depends non linearly on the points p_i^j and p_{i+1}^j from the previous level.

The first example of a geometric scheme is presented by Sabin and Dodgson [2004]. Other examples can be found in [Cashman et al., 2013; Chalmovianský and Jüttler, 2007; Deng and Wang, 2010; Deng and Ma, 2012, 2014; Hernández-Mederos et al., 2013; Dyn and Hormann, 2012; Yang, 2006; Zhao et al., 2009], some of them are presented in Section 2.2 in order to be used as numerical examples.

1.2.3 Stationary vs non-stationary schemes

Another distinction can be made between stationary and non stationary schemes. All the schemes considered until now are stationary. A *non-stationary* scheme is a subdivision operator where the rules depend on the level j of iteration,

$$p_{vi}^{j+1} = f_0^{(j)}(p_{i-k}^j, \ldots, p_{i+k}^j), \ldots, p_{vi+v-1}^{j+1} = f_{v-1}^{(j)}(p_{i-k}^j, \ldots, p_{i+k}^j).$$

The rules $f_k^{(j)}$, $k = 0, \ldots, \nu-1$, are level dependent or in general they can change between different levels. In case of linear schemes

$$p_i^{j+1} = \sum_{\ell \in \mathbb{Z}} a_{i-\nu\ell}^{(j)} \, p_\ell^j,$$

the mask itself depends on the level of iteration.

In the first part of the thesis we focus on stationary subdivision schemes while in the second part we introduce a generalization of non-stationary schemes called multiple schemes (see Definition 6.6). In this case we will see that in each iteration we change not only the subdivision rule but also the expanding matrix and the arity of the scheme. For an extensive explanation we refer to Section 6.2.

1.3   Regularity of subdivision schemes

The main effort in subdivision schemes is to study the convergence and the regularity of the schemes. Let focus on stationary schemes, by repeating infinitely many times the subdivision operator $\mathcal{S}$, it is natural to ask if the sequence of points generated, $\{p_i^j, \, i \in \mathrm{I}\}_{j\geq 0} \in \ell^d(\mathbb{Z})$ with $\mathrm{I} \subset \mathbb{Z}$ a closed interval, converges or not.

Definition 1.8. *A univariate stationary subdivision scheme $\mathcal{S}$ is called* convergent*, if for any closed interval $\mathrm{I} \subset \mathbb{Z}$ and any set $P^0 = \{p_i^0, i \in \mathrm{I}\}$ of control points there exists a continuous limit function $f^\infty : \mathbb{R} \to \mathbb{R}^d$ such that*

$$\lim_{j \to \infty} \sup_{i \in \mathrm{I}} \left| f^\infty(i/\nu^j) - (\mathcal{S}^j P^0)_i \right| = 0,$$

and $f^\infty \neq 0$ for some initial data P^0. The scheme $\mathcal{S}$ is said to be C^n continuous, if $f^\infty \in C^n(\mathbb{R})$.

If we consider the piecewise linear functions f^j, which interpolate the points of the scheme at certain values of the parametrization,

$$f^j\left(\frac{i}{\nu^j}\right) = p_i^j,$$

then Definition 1.12 means that the sequence of functions f^j is uniformly convergent,

$$\lim_{j \to \infty} f^j = f^\infty,$$

as shown in Figure 1.6.

Applying infinitely many times a subdivision scheme $\mathcal{S}$ to the delta sequence $\delta = \{\delta_{i,0}, \, i \in \mathbb{Z}\}$, we obtain a function ϕ that is called the *basic limit function*,

$$\phi := \lim_{j \to \infty} \mathcal{S}^j \delta = \mathcal{S}^\infty \delta. \tag{1.10}$$
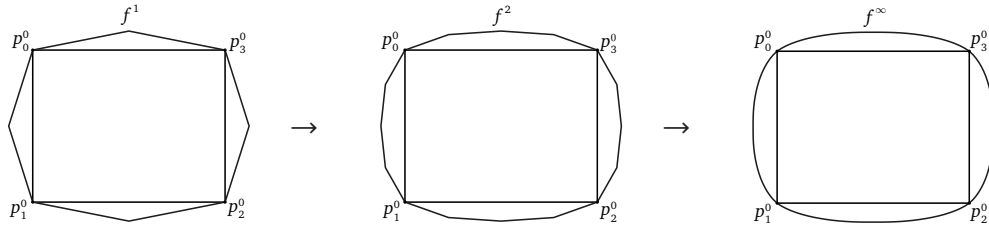
Figure 1.6. Uniform convergence of piecewise linear functions f^j to the limit curve f^∞.

This function is like a basis for any limit function generated by the scheme. In fact, for any initial points $P^0 = \{p_i^0\}$ and $f^\infty = \lim_{j\to\infty} \mathcal{S}^j P^0$, then

$$f^\infty(x) = \sum_{i\in\mathbb{Z}} p_i^0 \phi(x-i). \tag{1.11}$$

Furthermore, if we consider a linear subdivision scheme with mask a, then the basic limit function ϕ is a *refinable* function, [Micchelli and Prautzsch, 1989]

$$\phi(x) = \sum_{k\in\mathbb{Z}} a_k \phi(\nu x - k). \tag{1.12}$$

This follows from the definition of the linear scheme,

$$\phi(x) = (\mathcal{S}_a^\infty \delta)(x) = \mathcal{S}_a^\infty(\mathcal{S}_a \delta)(x) = \sum_{k\in\mathbb{Z}} a_k \phi(\nu x - k).$$

The spaces

$$V_j = \text{span}\{\phi(\nu^j \cdot -k),\ k\in\mathbb{Z}\} = \left\{ f(x) = \sum_{k\in\mathbb{Z}} c_k \phi(\nu^j x - k),\ k\in\mathbb{Z} \right\},$$

spanned by ϕ, are nested, that is $V_j \subset V_{j+1}$, due to the refinability of ϕ (1.12). The generation property (1.11) and the refinable property (1.12) of the basic limit function allow to define a multiresolution analysis. We can associate a multiresolution analysis to any linear stationary scheme, this allows to exploit the subdivision schemes in image analysis. The definition of a multiresolution analysis and further explanations are given in Section 5.2.

In general it is hard to prove the convergence of a scheme using Definition 1.12 because we should know a priori the expression of the limit function f^∞. In literature there are several sufficient and necessary conditions to require a certain regularity.

For a generic linear scheme (1.8) the mask a is such that

$$\sum_{k\in\mathbb{Z}^d} a_k = \nu,$$

where $\nu = |\det M|$.

Proposition 1.6 [Han and Jia, 1998]**.** *A necessary condition for the uniform convergence of the linear stationary scheme $\mathcal{S}_a$ (1.8) with arity $\nu = |\det M|$ is that*

$$\sum_{k \in \mathbb{Z}} a_{i-Mk} = 1, \qquad \forall i \in \mathbb{Z}^d. \tag{1.13}$$

For a univariate binary scheme it is equivalent to require that

$$\sum_{i \in \mathbb{Z}} a_{2i} = \sum_{i \in \mathbb{Z}} a_{2i+1} = 1,$$

as proved in [Dyn et al., 1991]. Equation (1.13) is often called *sum rule* of order one.

Once we consider a univariate linear scheme with arity ν (1.4), it is possible to rewrite the rules in matrix form $P^{j+1} = S_a P^j$,

$$
\begin{pmatrix} p^{j+1}_{\nu i-k} \\ \vdots \\ p^{j+1}_{\nu i} \\ p^{j+1}_{\nu i+1} \\ \vdots \\ p^{j+1}_{\nu i+k} \end{pmatrix}
=
\begin{pmatrix}
a_{[0],-k} & \cdots & a_{[0],k} & 0 \\
\vdots & \vdots & \vdots & \vdots \\
a_{[\nu-1],-k} & \cdots & a_{[\nu-1],k} & 0 \\
0 & a_{[0],-k} & \cdots & a_{[0],k} \\
\vdots & \vdots & \vdots & \vdots \\
0 & a_{[\nu-1],-k} & \cdots & a_{[\nu-1],k}
\end{pmatrix}
\begin{pmatrix} p^{j}_{i-k} \\ \vdots \\ p^{j}_{i} \\ p^{j}_{i+1} \\ \vdots \\ p^{j}_{i+k} \end{pmatrix},
\tag{1.14}
$$

introducing the subdivision matrix S_a. The eigenvalues and eigenvectors of the subdivision matrix S_a give other necessary conditions for the regularity of the limit curve.

Proposition 1.7 [Dyn et al., 1991]**.** *Let S_a be the subdivision matrix associated with the stationary subdivision scheme $\mathcal{S}_a$, whose eigenvalues are sorted in decreasing modulus. If the subdivision scheme $\mathcal{S}_a$ is convergent, then*

$$1 = \lambda_0 > |\lambda_1|.$$

Proposition 1.8 [Warren, 1995]**.** *Let S_a be a subdivision matrix with eigenvalues ordered by decreasing modulus. If the associated subdivision scheme $\mathcal{S}_a$ produces C^k continuous limit functions, then*

$$\lambda_i = \frac{1}{\nu^i}, \qquad i = 0, \ldots, k.$$

The analysis with the local subdivision matrix can be useful in the multivariate setting for the analysis of the regularity in a neighbourhood of an extraordinary point. I do not give further details, if you are interested see [Peters and Reif, 2008].

Studying the subdivision matrix of linear stationary schemes gives only necessary conditions. To obtain sufficient conditions for the regularity of the scheme we introduce the concept of Laurent polynomials as done in [Dyn, 1992, 2002].

Definition 1.9. *Given a finite sequence $a \in \ell_{00}(Z^d)$, we call*

$$a^*(z) = \sum_{k \in \mathbb{Z}^d} a_k z^k, \qquad z \in (\mathbb{C} \setminus \{0\})^d,$$

where $z^k = \left(z_1^{k_1}, \ldots, z_d^{k_d} \right)$, the Laurent polynomial *of a.*

If a is the mask of a linear subdivision scheme, then the polynomial $a^*(z)$ is denominated the *symbol* of the scheme.

In terms of the Laurent polynomials, the sum rule of order one (1.13) corresponds to

$$a^*(1) = v, \qquad a^*(\xi) = 0 \quad \text{with} \quad \xi \in E = \left\{ \exp\left(\frac{2\pi i}{v} j \right), \, j = 1, \ldots, v-1 \right\}, \quad (1.15)$$

as shown in [Han and Jia, 1998; Conti and Hormann, 2011] for a univariate linear scheme with any arity v. In general the sum rules of order $n+1$ are

$$a^*(1) = v, \qquad \max_{k \le n} \max_{\xi \in E} \left| \frac{d^k a^*(\xi)}{dz^k} \right| = 0. \tag{1.16}$$

Corollary 1.9. *A necessary condition for a univariate linear stationary scheme $\mathcal{S}_a$ (1.8) with arity v to be convergent is that the symbol of the scheme satisfies*

$$a^*(1) = v, \qquad a^*(\xi_k) = 0,$$

for any $k = 1, \ldots, d-1$ and $\xi_k = \exp\left(\frac{2\pi i}{v} k \right)$.

In the binary case the necessary conditions become

$$a^*(1) = 2, \qquad a^*(-1) = 0, \tag{1.17}$$

namely that the symbol a^* can be rewritten as

$$a^*(z) = (1+z) b^*(z), \tag{1.18}$$

for a certain polynomial $b^*(z)$, such that $b^*(1) = 1$.

We denote with $\nabla : \ell(\mathbb{Z}) \to \ell(\mathbb{Z})$ the difference operator

$$\nabla c = \{ \nabla c_i = c_i - c_{i-1}, \, i \in \mathbb{Z} \}. \tag{1.19}$$

Proposition 1.10. *The polynomial $b^*(z)$ is the symbol of the difference scheme*

$$\nabla(\mathcal{S}_a p) = \mathcal{S}_b \nabla p.$$

Proof: We can observe that the refinement equation

$$p_i^{j+1} = \sum_{k\in\mathbb{Z}} a_{i-2k}p_k^j$$

turns out to be

$$(p^{j+1})^*(z) = a^*(z)(p^j)^*(z^2),$$

in the Laurent formalism. Then, the Laurent polynomial associated with the difference of points $\nabla p_i^j = p_i^j - p_{i-1}^j$ is

$$(\nabla p^j)^*(z) = (1-z)(p^j)^*(z).$$

Using (1.18) we conclude that $b^*(z)$ is the symbol related to the difference scheme

$$(\nabla p^{j+1})^*(z) = (1-z)(p^{j+1})^*(z) = (1-z)a^*(z)(p^j)^*(z^2) = b^*(z)(1-z^2)(p^j)^*(z^2)$$
$$= b^*(z)(\nabla p^j)^*(z^2).$$

$\square$

Using the symbol of the difference scheme $b^*(z)$, Dyn [2002] gives a sufficient condition for the convergence and regularity of a binary linear scheme $\mathcal{S}_a$.

Proposition 1.11 [Dyn, 2002]. *The univariate linear stationary scheme $\mathcal{S}_a$ converges if and only if the corresponding scheme for the differences $b^*(z) = \frac{a^*(z)}{1+z}$ is contractive for any initial data.*

Definition 1.10. *A scheme $\mathcal{S}$ is* contractive *if there exist some $\mu < 1$ and $L \in \mathbb{N}$ such that*

$$\max_{i\in\mathbb{Z}}\left\|p_i^{j+L}\right\| < \mu \max_{i\in\mathbb{Z}}\left\|p_i^j\right\|. \tag{1.20}$$

In case of a univariate linear scheme $\mathcal{S}_a$ this is equivalent to require that

$$\left\|(\mathcal{S}_a)^L\right\|_\infty = \left\|\mathcal{S}_{a^{(L)}}\right\|_\infty = \max\left\{\sum_{k\in\mathbb{Z}}\left|a_{i-2^Lk}^{(L)}\right| : i = 0,1,\ldots,2^L-1\right\} < 1 \tag{1.21}$$

where $a^{(L)}$ is the mask of the scheme with symbol

$$a_{(L)}^*(z) = a^*(z)a^*(z^2)\ldots a^*(z^L).$$

Proposition 1.12 [Dyn, 2002]. *If the scheme $\mathcal{S}_b$ is contractive, then the limit curves of the univariate linear scheme $\mathcal{S}_a$ with symbol*

$$a^*(z) = \left(\frac{1+z}{2}\right)^n (1+z)b^*(z)$$

are C^n continuous.

The previous results on Laurent polynomials are presented in the simple case of univariate binary schemes. They can be generalized to any arity v by observing that (1.15) factorizes the symbol $a^*(z)$ into

$$a^*(z) = (1 + z + \ldots + z^{v-1})b^*(z),$$

where $b^*(z)$ is again the symbol of the difference scheme $(\nabla S_a = S_b \nabla)$.

Proposition 1.13. *The univariate linear scheme S_a with arity v converges if and only if the corresponding scheme for the differences $b^*(z) = \frac{a^*(z)}{1+z+\ldots+z^{v-1}}$ is contractive for any initial data.*

Instead, if we want to generalize in the multivariate setting, then we should take into account the geometry of the mesh of points. The factorization of the symbol is different if we consider quadrilateral or triangular meshes. Both cases are treated in [Dyn, 2002].

In the multivariate setting the difference operator $\nabla : \ell(\mathbb{Z}^d) \to \ell(\mathbb{Z}^d)$ can be applied along different directions $e \in \mathbb{Z}^d$,

$$\nabla_e c = \{c_i - c_{i-e}, \ i \in \mathbb{Z}^d\}. \tag{1.22}$$

In a quadrilateral setting the direction chosen are the vectors along different axes $e_k \in \mathbb{Z}^d$ such that $(e_k)_i = \delta_{i,k}$. For example, in the bivariate case we consider $e_1 = (1,0)^T$ and $e_2 = (0,1)^T$.

Proposition 1.14 [Dyn, 2002]. *Let S_a be a bivariate linear scheme with symbol*

$$a^*(z_1, z_2) = (1 + z_1)(1 + z_2)b(z_1, z_2)$$

and the difference schemes related to the two directions e_1 and e_2 are defined as

$$b_1^*(z_1, z_2) = \frac{a(z_1, z_2)}{(1 + z_1)} = (1 + z_2)b(z_1, z_2),$$

$$b_2^*(z_1, z_2) = \frac{a(z_1, z_2)}{(1 + z_2)} = (1 + z_1)b(z_1, z_2).$$

The scheme S_a converges if and only if the schemes S_{b_1} and S_{b_2} are contractive.

Proposition 1.15 [Dyn, 2002]. *Let a bivariate linear scheme S_a with symbol*

$$a^*(z_1, z_2) = \left(\frac{1 + z_1}{2}\right)^{n+1} \left(\frac{1 + z_2}{2}\right)^{n+1} b^*(z_1, z_2)$$

be given. If the $n + 2$ symbols

$$b_i^*(z_1, z_2) = \left(\frac{1 + z_1}{2}\right)^{n+1-i} \left(\frac{1 + z_2}{2}\right)^i b^*(z_1, z_2)$$

are contractive for $i = 0, \ldots, n + 1$, then S_a generates C^n limit functions.

In case of a triangular mesh: we have to consider also the difference along $e_3 = (1,1)^T$. In this case the convergence results are slightly different.

Proposition 1.16 [Dyn, 2002]. *Let $\mathcal{S}_a$ be a bivariate linear scheme on a triangular mesh with symbol of the form*

$$a^*(z_1, z_2) = (1 + z_1)(1 + z_2)(1 + z_1 z_2) b^*(z_1, z_2),$$

and the symbols of the difference schemes along the direction e_i, $i = 1, 2, 3$ are

$$b_1^*(z_1, z_2) = \frac{a^*(z_1, z_2)}{(1 + z_1)}, \quad b_2^*(z_1, z_2) = \frac{a^*(z_1, z_2)}{(1 + z_2)}, \quad b_3^*(z_1, z_2) = \frac{a^*(z_1, z_2)}{(1 + z_1 z_2)}.$$

The scheme $\mathcal{S}_a$ is convergent if and only if the schemes $\mathcal{S}_{b_i}$, $i = 1, 2, 3$, are contractive.

All these results can be generalized to dimension d for any arity $\nu = |\det M|$ using the concept of the *canonical factor* introduced in [Sauer, 2010]. The definition of the canonical factor and more details are given in Section 6.2.

In the univariate setting the sum rule (1.13) gives the factor $(1 + z)$ of the symbol $a^*(z)$. In the multivariate case we need to be more careful, because the symbol belongs to the quotient ideal $\langle z^2 - 1 \rangle : \langle z - 1 \rangle$, so we can have different factorizations. In this case, it can be useful to come back to the general equation

$$\nabla \mathcal{S}_a = \mathcal{S}_b \nabla \tag{1.23}$$

of Proposition 1.10 and to use the formalism of the spectral radius.

Definition 1.11. *Let us consider a matrix $M \in \mathbb{R}^{n \times n}$. The* spectral radius *of the matrix is defined as*

$$\rho(M) := \max\{|\lambda_1|, \dots, |\lambda_n|\} = \lim_{r \to \infty} \|M^r\|^{\frac{1}{r}}.$$

Analogously, if we take a set of matrices $\{M_j\}_{j \in \mathbb{Z}_m} = \{M_0, \dots, M_{m-1}\}$, with $\mathbb{Z}_m := \{0, \dots, m-1\}$, then

$$\rho\left(\{M_j\}_{j \in \mathbb{Z}_m}\right) = \lim_{r \to \infty} \max_{\epsilon \in \mathbb{Z}_m^r} \left\| \prod_{i=1}^{r} M_{\epsilon_i} \right\|^{\frac{1}{r}}$$

represents the joint spectral radius *of the set.*

Considering the mask a of a binary scheme with finite support in $\{0, \dots, k\}^d$ we introduce the matrices

$$A_\epsilon = \left\{ a(2\alpha - \beta + \epsilon), \ \alpha, \beta \in \{0, \dots, k-1\}^d \right\}, \quad \epsilon \in \{0, 1\}^d$$

and the space $V = \{v \in \ell(\{0, \dots, k\}^d) : \sum_{\alpha \in \{0, \dots, k\}^d} v(\alpha) = 0\}$. Using the general relation (1.23), Charina et al. [2005a] prove that

$$\rho(A_\epsilon|_V) = \rho(\mathcal{S}_b|_\nabla)$$

where

$$\rho(A_\epsilon|_V) = \lim_{r \to \infty} \left\| \nabla \mathcal{S}_a^r \delta \right\|^{\frac{1}{r}},$$

$$\rho(\mathcal{S}_b|_\nabla) = \lim_{r \to \infty} \left\| \mathcal{S}_b^r|_\nabla \right\|^{\frac{1}{r}} = \lim_{r \to \infty} \max_{\|\nabla c\|=1} \left\| \mathcal{S}_b^r \nabla c \right\|^{\frac{1}{r}}.$$

The "contractivity" of the difference scheme gives the regularity and Hölder continuity of the subdivision scheme, similar to the Laurent formalism.

Proposition 1.17 [Charina et al., 2005b]. *Let $\mathcal{S}_a$ be a linear scheme such that there exists a difference scheme $\mathcal{S}_b$ that satisfies (1.23). The scheme $\mathcal{S}_a$ is convergent if and only if $\rho(\mathcal{S}_b|_\nabla) < 1$.*

Iterating the difference relation (1.23) and this proposition we have a subdivision scheme with higher order of regularity. In the univariate setting the spectral radius also gives the Hölder regularity of the limit curve.

Proposition 1.18 [Daubechies and Lagarias, 1992; Dyn, 1992]. *Let $a \in \ell(\mathbb{Z})$, then $\mathcal{S}_a$ converges to a continuous function if and only if the mask satisfies the sum rules (1.13) and $\rho(A_\epsilon|_V) = \rho < 1$. Moreover, the Hölder exponent of the limit function is $-\log_2 \rho$.*

The results obtained using the spectral radius are the same as those obtained with the Laurent formalism, but it is interesting to observe that even if we are considering two different factorizations b_1 and b_2 of a we have the same value for the restricted spectral radius $\rho(\mathcal{S}_{b_1}|_\nabla) = \rho(\mathcal{S}_{b_2}|_\nabla)$ (see [Charina et al., 2005b]). This can be useful in the multivariate setting.

The results presented so far can be applied only to stationary linear schemes. In the non-stationary setting the definition of convergence is slightly different.

Definition 1.12. *A non-stationary subdivision scheme $\{\mathcal{S}^{(j)}, j \geq 0\}$ is called* convergent, *if for any closed interval $\mathrm{I} \subset \mathbb{Z}$ and any set $P^0 = \{p_i^0, i \in \mathrm{I}\}$ of control points there exists a continuous limit function $f^\infty : \mathbb{R} \to \mathbb{R}^d$ such that*

$$\lim_{j \to \infty} \sup_{i \in \mathrm{I}} \left| f^\infty(i/\nu^j) - (\mathcal{S}^{(j-1)} \cdots \mathcal{S}^{(0)} P^0)_i \right| = 0,$$

and $f^\infty \neq 0$ for some initial data P^0. The scheme is said to be C^n continuous, if $f^\infty \in C^n(\mathbb{R})$.

At each iteration we apply a different scheme. In order to study the regularity of non-stationary schemes, we can exploit the concept of asymptotic equivalence with a stationary scheme.

Proposition 1.19 [Dyn and Levin, 1995]. *Consider a stationary subdivision scheme $\mathcal{S}_a$ with arity ν and a non-stationary scheme $\{\mathcal{S}_{a^{(j)}}, j \in \mathbb{N}\}$ with the same arity and support width. If $\mathcal{S}_a$ is C^n continuous and*

$$\sum_{k=0}^{\infty} \nu^{nk} \left\| \mathcal{S}_{a^{(j)}} - \mathcal{S}_a \right\|_\infty < \infty, \tag{1.24}$$

then the non-stationary scheme $\{\mathcal{S}_{a^{(j)}},\ j \in \mathbb{N}\}$ is C^n continuous.

Two schemes that satisfy (1.24) are called *asymptotically equivalent* of order $n+1$. A weaker condition than asymptotic equivalence is the concept of asymptotically similarity.

Definition 1.13 [Conti et al., 2015]**.** *Two subdivision schemes $\{\mathcal{S}_{a^{(j)}},\ j \geq 0\}$ and $\{\mathcal{S}_{b^{(j)}},\ j \geq 0\}$ are* asymptotically similar *if*

$$\lim_{j \to \infty} \left\| a^{(j)} - b^{(j)} \right\| = 0.$$

In order to exploit the asymptotically similarity of a non-stationary scheme $\{\mathcal{S}_{a^{(j)}},\ j \geq 0\}$ with arity v we have to consider a relaxed version of the sum rule (1.16). A non-stationary scheme satisfies the *approximate sum rules* of order $n+1$ if the sequences

$$\alpha_j = a^*_{(j)}(1) - v \quad \text{and} \quad \beta_j = \max_{k \leq n} \max_{\xi \in E \setminus \{1\}} v^{-jk} \left| \frac{d^k a^*_{(j)}(\xi)}{dz^k} \right|, \tag{1.25}$$

with $E = \left\{ \exp\left(\frac{2\pi i}{v} \ell\right),\ \ell = 1, \dots, v-1 \right\}$, satisfy

$$\sum_{j=1}^{\infty} \alpha_j < \infty, \qquad \sum_{j=1}^{\infty} v^{jn} \beta_j < \infty,$$

see [Charina et al., 2017].

Proposition 1.20 [Charina et al., 2017; Conti et al., 2015]**.** *If a non-stationary subdivision scheme $\{\mathcal{S}_{a^{(j)}},\ j \geq 0\}$ satisfies the approximate sum rule of order $n+1$, and is asymptotically similar to a stationary subdivision scheme $\mathcal{S}_a$ that is C^n continuous, then also the non-stationary scheme is C^n continuous.*

Instead, to study the regularity of a non-linear scheme we can use the proximity condition introduced by Wallner and Dyn [2005]; Wallner [2006]. First of all they introduce a convergence condition that is equivalent to requiring that the difference scheme is contractive as in Definition 1.10.

Definition 1.14 [Wallner and Dyn, 2005]**.** *A scheme $\mathcal{S}$ satisfies a* convergence condition *with $\mu_0 < 1$ if*

$$\left\| \nabla \mathcal{S}^\ell \right\|_\infty \leq \mu_0^\ell \left\| \nabla p \right\|_\infty, \quad \forall \ell \in \mathbb{N} \text{ and } \forall p \in \mathbb{R}^d. \tag{1.26}$$

Definition 1.15 [Wallner and Dyn, 2005]**.** *Given a linear subdivision scheme $\mathcal{S}_a$ and a generic scheme $\mathcal{S}$, the two schemes satisfy the* proximity condition *if for any set of points for which*

$$\sup_{i \in \mathbb{Z}} \| p_{i+1} - p_i \| = \| \nabla p \|_\infty < \epsilon,$$

there exists a positive constant C such that

$$\left\| \mathcal{S}_a p - \mathcal{S} p \right\|_\infty \leq C \left\| \nabla p \right\|_\infty^2. \tag{1.27}$$

Proposition 1.21 [Wallner and Dyn, 2005]. *Let a linear scheme $\mathcal{S}_a$ and a generic scheme $\mathcal{S}$ satisfy the proximity condition (1.27) for any set of points such that $\|\nabla p\| < \epsilon$. Moreover, suppose that $\mathcal{S}_a$ satisfies a convergence condition (1.26) with $\mu_0 < 1$, then there exists $\delta > 0$ and $\bar{\mu}_0 < 1$ such that $\mathcal{S}$ satisfies a convergence condition (1.26) with $\bar{\mu}_0$ for any set of points such that $\|\nabla p\| < \delta$. Choosing δ small enough we can have $\mu_0 - \bar{\mu}_0$ arbitrary small.*

The conditions for higher order regularity of a scheme $\mathcal{S}$ are given in [Wallner, 2006].

In Section 3.1 we will see that a similar condition to (1.20) and (1.26) is proposed by Dyn and Hormann [2012] as a sufficient condition in order to a have a convergent geometric scheme.

Moreover, Ewald et al. [2015] use something similar to the proximity condition (1.27) to prove the Hölder continuity for Geometric Local Uniform Equilinear schemes, also called GLUE schemes. A GLUE scheme is a scheme that commutes with similarities, where the rules depend on a finite number of points and they apply everywhere. Moreover, if we consider as control polygon a segment, then it is mapped to a segment with half spacing. Ewald et al. [2015] introduce the relative distortion that measures the deviation of a set of points from the linear behaviour. The decay of this relative distortion gives the existence and regularity of a geometric scheme like in Proposition 1.21.

1.4   Examples of subdivision schemes

In this section we recall some examples of stationary interpolatory linear schemes. We restrict ourself on this type of schemes because throughout the work we focus only on interpolatory schemes and examples of non-linear scheme are presented in Section 2.2. All the scheme presented in this section and Section 2.2 are used for numerical tests.

1.4.1   2N-point schemes

The family of 2N-point schemes by Deslauriers and Dubuc [1989], is the most famous family of interpolatory schemes. The name states the fact that the new points are linear combinations of 2N points from the previous level of iteration. An example of such schemes is the 4-point scheme with rules (1.2) already presented in Section 1.2. Here we want to explain the general construction.

The general rules of the binary 2N-point scheme for $N \in \mathbb{N}$ are given by

$$p_{2i+\ell}^{j+1} = \sum_{n=-N}^{N-1} \mathscr{L}_{i-n,2N-1}\left(t_{2i+\ell}^{(j+1)}\right) p_{i-n}^j, \qquad \ell = \{0,1\},$$

where $\mathscr{L}_{i-n,2N-1}$ is the Lagrange fundamental polynomial of degree $2N-1$ associated with the knots $t_{i-n}^{(j)} = \frac{i-n}{2^j}$ and $n = -N,\ldots,N-1$. A Lagrange polynomial associate to

the knots $\{t_i\}_{-N}^{N-1}$ is defined as

$$\mathcal{L}_{i,2N-1}(t) = \prod_{\substack{k=-N \\ k \neq i}}^{N-1} \frac{(t - t_k)}{(t_i - t_k)} \tag{1.28}$$

and has the fundamental property

$$\mathcal{L}_{i,2N-1}(t_k) = \delta_{i,k}. \tag{1.29}$$

Applying (1.29) in the previous rules for the 2N-points scheme we can deduce that it is an interpolatory scheme

$$p_{2i}^{j+1} = p_i^j, \tag{1.30}$$

$$p_{2i+1}^{j+1} = \sum_{n=-N}^{N-1} \mathcal{L}_{i-n,2N-1}\left(\frac{2i+1}{2^{j+1}}\right) p_{i-n}^j.$$

Let us compute the masks for the different schemes for some values of N.

- $N = 1$

  Consider the two linear Lagrange polynomials ($n = -1, 0$)

  $$\mathcal{L}_{i+1,1}\left(\frac{2i+1}{2^{j+1}}\right) = \frac{\frac{2i+1}{2^{j+1}} - \frac{i}{2^j}}{\frac{i+1}{2^j} - \frac{i}{2^j}} = \frac{1/2^{j+1}}{1/2^j} = \frac{1}{2}$$

  $$\mathcal{L}_{i,1}\left(\frac{2i+1}{2^{j+1}}\right) = \frac{\frac{2i+1}{2^{j+1}} - \frac{i+1}{2^j}}{\frac{i}{2^j} - \frac{i+1}{2^j}} = \frac{-1/2^{j+1}}{-1/2^j} = \frac{1}{2}$$

  and the rules for the 2-point scheme become

  $$p_{2i}^{j+1} = p_i^j, \tag{1.31}$$

  $$p_{2i+1}^{j+1} = \frac{1}{2}p_i^j + \frac{1}{2}p_{i+1}^j.$$

These rules insert at each level the mean of the two neighbouring points from the previous level, as shown in Figure 1.7. The mean of two points p_i^j, p_{i+1}^j lies on the edge $\overrightarrow{p_i^j p_{i+1}^j}$, so in the limit the scheme reproduces the initial control polygon and we expect that the scheme is C^0 continuous. From (1.31) the mask of the scheme and the symbol are

$$a^{[2]} = \left\{\frac{1}{2}, 1, \frac{1}{2}\right\}, \qquad (a^{[2]})^*(z) = \frac{1}{2}(1+z)^2,$$

so the mask and the symbol of the difference scheme are

$$b^{[2]} = \left\{\frac{1}{2}, \frac{1}{2}\right\}, \qquad (b^{[2]})^*(z) = \frac{1}{2}(1+z).$$

As the difference scheme is contractive $\left(\left\|b^{[2]}\right\|_\infty = 1/2\right)$, the 2-point scheme is convergent (C^0 continuous) according to Proposition 1.11.

- $N = 2$

  Consider the 4-point scheme. Computing the Lagrange polynomials we found the coefficients state in (1.2)

  $$\mathscr{L}_{i-1,3}\left(\frac{2i+1}{2^{j+1}}\right) = \prod_{n=-2}^{0} \frac{2n+1}{2(n-1)} = -\frac{1}{16},$$

  $$\mathscr{L}_{i,3}\left(\frac{2i+1}{2^{j+1}}\right) = \prod_{\substack{n=-2 \\ n \neq 0}}^{1} \frac{2n+1}{2n} = \frac{9}{16},$$

  $$\mathscr{L}_{i+1,3}\left(\frac{2i+1}{2^{j+1}}\right) = \prod_{\substack{n=-2 \\ n \neq -1}}^{1} \frac{2n+1}{2(n+1)} = \frac{9}{16},$$

  $$\mathscr{L}_{i+2,3}\left(\frac{2i+1}{2^{j+1}}\right) = \prod_{n=-2}^{0} \frac{2n+1}{2(n+2)} = -\frac{1}{16}.$$

  The mask and symbol of the scheme are

  $$a^{[4]} = \left\{-\frac{1}{16}, 0, \frac{9}{16}, 1, \frac{9}{16}, 0, -\frac{1}{16}\right\}, \quad (a^{[4]})^*(z) = \left(\frac{1+z}{2}\right)^4 z^{-3}(-1 + 4z - z^2)$$

  and Figure 1.3 shows the new point generated by this scheme. The associated difference scheme has the contractive mask

  $$b^{[4]} = \frac{1}{16}\{-1, 1, 8, 8, 1, -1\}, \quad \text{with} \quad \left\|b^{[4]}\right\|_\infty = \frac{5}{8} < 1.$$

  By Proposition 1.11 the 4-point scheme is convergent. In order to study if the scheme is C^1 continuous we factorize the symbol $(a^{[4]})^*$

  $$(a^{[4]})^*(z) = \frac{(1+z)^2}{2} \frac{(1+z)^2(-1+4z-z^2)}{8z^3} = \frac{(1+z)^2}{2}(c^{[4]})^*(z)$$

  and we consider the mask of the second-order differences

  $$c^{[4]} = \frac{1}{8}\{-1, 2, 6, 2, -1\} \tag{1.32}$$

  Since the norm of the mask is $\left\|c^{[4]}\right\|_\infty = 1$, we need to iterate the scheme to check if it is contractive. Iterating the scheme related to $c^{[4]}$ one time, we obtain

  $$c_{(2)}^{[4]} = \frac{1}{64}\{1, -2, -8, 2, 7, 16, 32, 16, 7, 2, -8, -2, 1\}, \quad \left\|c_{(2)}^{[4]}\right\| < 1.$$

  Hence the scheme is C^1 continuous by Proposition 1.12. The scheme has Hölder regularity $C^{2-\epsilon}$, but it is not C^2, because the mask of the third-order differences,

  $$d^{[4]} = \frac{1}{4}\{-1, 3, 3 - 1\}, \quad \left\|d_{(L)}^{[4]}\right\|_\infty = 1 \quad \forall L \in \mathbb{N},$$

  is not contractive.

- $N = 3$

  The Lagrange polynomials

  $$\mathscr{L}_{i-n,5}\left(\frac{2i+1}{2^{j+1}}\right) = \prod_{\substack{k=-3 \\ k \neq n}}^{2} \frac{2k+1}{2(k-n)},$$

  for $n = -3, \ldots, 2$, give the coefficients into the rules of the 6-point scheme

  $$p_{2i}^{j+1} = p_i^j \tag{1.33}$$

  $$p_{2i+1}^{j+1} = \frac{3}{256}p_{i-2}^j - \frac{25}{256}p_{i-1}^j + \frac{150}{256}p_i^j + \frac{150}{256}p_{i+1}^j - \frac{25}{256}p_{i+2}^j + \frac{3}{256}p_{i+3}^j.$$

  Figure 1.8 show the position of the new point p_{2i+1}^{j+1}. The mask and the symbol of the scheme are

  $$a^{[6]} = \frac{1}{2^8}\{3, 0, -25, 0, 150, 256, 150, 0, -25, 0, 3\},$$

  $$(a^{[6]})^*(z) = \left(\frac{1+z}{2}\right)^6 \frac{3 - 18z + 38z^2 - 18z^3 + 3z^4}{4z^5}.$$

  To prove that the 6-point scheme is convergent we have to study the difference scheme

  $$(a^{[6]})^*(z) = (1+z)\frac{(1+z)^5(3 - 18z + 38z^2 - 18z^3 + 3z^4)}{2^8 z^5} = (1+z)(b^{[6]})^*(z),$$

  $$b^{[6]} = \frac{1}{256}\{3, -3, -22, 22, 128, 128, 22, -22, -3, 3\}.$$

  By Proposition 1.11 the 6-point scheme is convergent, because the difference scheme is contractive, $\|b^{[6]}\|_\infty < 1$. To study if the scheme generates limit curves with higher order regularity we use Proposition 1.12 and we study the scheme for higher order differences. The scheme of the second-order differences is given by

  $$(a^{[6]})^*(z) = \frac{(1+z)^2}{2}\frac{(1+z)^4(3 - 18z + 38z^2 - 18z^3 + 3z^4)}{2^7 z^5} = \frac{(1+z)^2}{2}(c^{[6]})^*(z),$$

  $$c^{[6]} = \frac{1}{128}\{3, -6, -16, 38, 90, 38, -16, -6, 3\} \tag{1.34}$$

  and is contractive, $\left\|c_{(2)}^{[6]}\right\|_\infty < 1$. By Proposition 1.12, the 6-point scheme is C^1 continuous and also C^2 continuous because the scheme of third-order differences

  $$(a^{[6]})^*(z) = \frac{(1+z)^3}{4}\frac{(1+z)^3(3 - 18z + 38z^2 - 18z^3 + 3z^4)}{2^6 z^5} = \frac{(1+z)^3}{4}(d^{[6]})^*(z),$$

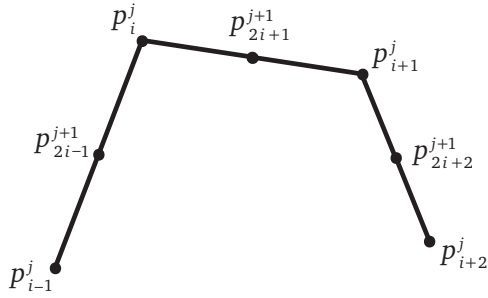 $$d^{[6]} = \frac{1}{64}\{3, -9, -7, 45, 45, -7, -9, 3\}$$

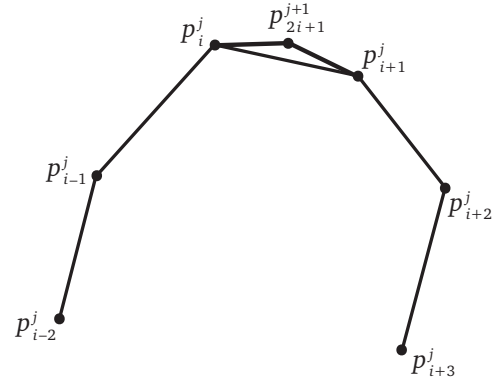Figure 1.7. Construction of the new point for the 2-point scheme.

Figure 1.8. Construction of new point for the 6-point scheme.

is contractive, $\left\|d_{(2)}^{[6]}\right\|_\infty < 1$. Instead the scheme is not C^3 continuous because the scheme

$$(a^{[6]})^*(z) = \frac{(1+z)^4}{8} \frac{(1+z)^2(3-18z+38z^2-18z^3+3z^4)}{2^5z^5} = \frac{(1+z)^4}{8}(f^{[6]})^*(z),$$

$$f^{[6]} = \frac{1}{32}\{3,-12,5,40,5,-12,3\},$$

have $\left\|f^{[6]}\right\|_\infty > 1$.

Note that the regularity of the 2N-point schemes does not grow linearly with N, to find the exact regularity see [Daubechies and Lagarias, 1992].

The examples of 2N-point schemes presented until now are binary scheme, but in general Deslauriers and Dubuc [1989] define schemes for any arity ν. The general rules are

$$p_{\nu i+\ell}^{j+1} = \sum_{n=-N}^{N-1} \mathscr{L}_{i-n,2N-1}\left(\frac{\nu i+\ell}{\nu^{j+1}}\right) p_{i-n}^j, \qquad \ell = \{0,\ldots,\nu-1\},$$

where we now consider as knots $t_{i-n}^{(j)} = \frac{i-n}{\nu^j}$ with $n = -N,\ldots,N-1$. By the fundamental property of the Lagrange polynomial (1.29) the scheme is interpolatory. In the simple case of 2-point scheme we can easily deduce the rules. In fact, the Lagrange polynomials give

$$\mathscr{L}_{i,2}\left(\frac{\nu i+\ell}{\nu^{j+1}}\right) = \frac{\frac{\nu i+\ell}{\nu^{j+1}} - \frac{i+1}{\nu^j}}{\frac{i}{\nu^j} - \frac{i+1}{\nu^j}} = 1 - \frac{\ell}{\nu},$$

$$\mathscr{L}_{i+1,2}\left(\frac{\nu i+\ell}{\nu^{j+1}}\right) = \frac{\frac{\nu i+\ell}{\nu^{j+1}} - \frac{i}{\nu^j}}{\frac{i+1}{\nu^j} - \frac{i}{\nu^j}} = \frac{\ell}{\nu},$$

for $\ell = 0, \ldots, \nu - 1$. The mask and the symbol of the 2-point scheme with arity ν are

$$a = \frac{1}{\nu}\{1, 2, \ldots, \nu-1, \nu, \nu-1, \ldots, 2, 1\}, \qquad a^*(z) = \frac{z^{-(\nu-1)}}{\nu}(1 + z + \ldots + z^{\nu-1})^2. \quad (1.35)$$

Using Proposition 1.13 we can prove that the 2-point scheme converges for any arity ν. Let us consider the difference scheme such that

$$a^*(z) = (1 + z + \ldots + z^{\nu-1})\frac{1 + z + \ldots + z^{\nu-1}}{\nu z^{\nu-1}} = (1 + z + \ldots + z^{\nu-1})b^*(z),$$

$$b = \frac{1}{\nu}\{1, 1, \ldots, 1\}.$$

The norm is

$$\|b\|_\infty = \max_i\left\{\sum_{\ell \in Z}|b_{\nu\ell+i}|\right\} = \frac{1}{\nu} < 1,$$

hence the difference scheme is contractive and the 2-point scheme converge.

1.4.2 4-point scheme with tension parameter
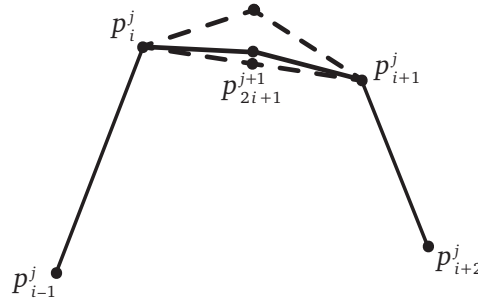
Figure 1.9. Construction of the new point for the 4-point scheme with tension parameter $w = 1/32$. The points generated by the 2-point scheme and the 4-point scheme are shown, for comparison, in dash line.

Another interesting example of an interpolatory linear scheme is the 4-point scheme with tension parameter w [Dyn et al., 1987]. It is defined as

$$p_{2i}^{j+1} = p_i^j \qquad\qquad (1.36)$$

$$p_{2i+1}^{j+1} = -wp_{i-1}^j + \left(\frac{1}{2} + w\right)p_i^j + \left(\frac{1}{2} + w\right)p_{i+1}^j - wp_{i+2}^j,$$

and has mask

$$a = \left\{-w, 0, \frac{1}{2} + w, 1, \frac{1}{2} + w, 0, -w\right\}.$$

In the special case $w = 0$ it reproduces the rules of the 2-point scheme, while for $w = 1/16$ we obtain the 4-point scheme. This scheme is a combination of the 2-point and the 4-point scheme. In fact,

$$a = (1-16w)\left\{\frac{1}{2}, 1, \frac{1}{2}\right\} + 16w\left\{-\frac{1}{16}, 0, \frac{9}{16}, 1, \frac{9}{16}, 0, -\frac{1}{16}\right\}$$
$$= (1-16w)\, a^{[2]} + 16w\, a^{[4]}.$$

If we take $w = 1/32$, then the resulting scheme is the mean of the 2-point and the 4-point scheme. The position of the new point p_{2i+1}^{j+1} in this case is shown in Figure 1.9. The points, connected with dash lines, are the points generated by the 2-point scheme and the 4-point scheme. We observe that p_{2i+1}^{j+1} is not exactly the mean of the points generated by the 2-point and the 4-point scheme but it is between these two points.

Varying w, also changes the regularity of the scheme, because the 2-point scheme is only convergent, while the 4-point scheme is C^1 continuous. In [Dyn et al., 1991] the behaviour of the scheme for different w is studied and they prove that if $w \in \left(-\frac{1}{2}, \frac{1}{2}\right)$ then the scheme is C^0 continuous, while the scheme is also C^1 continuous if $w \in \left(0, \frac{\sqrt{5}-1}{8}\right)$.

In the next chapters, we present some interpolatory geometric schemes, we give some results to study their regularity and we use them as numerical examples.

Part I

Subdivision Schemes for Curve Design

Outline

Linear schemes are well understood and studied (see e.g. [Conti and Hormann, 2011; Dyn et al., 1991, 1987; Dyn, 2002, 1992; Han and Jia, 1998]), but sometimes the resulting limit curves have some artefacts like loops and cups. For this reason, it is interesting to consider geometric subdivision schemes.

A geometric subdivision scheme is a non-linear scheme that, in each iteration, uses a geometric construction to generate the new points. In this way, the geometry of the initial control polygon is taken into account in the resulting limit curve. This produces less artefacts in the limit curve than a linear scheme.

The problem with geometric schemes is the lack of tools to study their regularity. We cannot use the well-known results of the linear case for this type of schemes, and it is complicate to find new methods.

Some studies are done for special cases of non-linear schemes, as those proposed by Floater and Micchelli [1998]; Schaefer et al. [2008]. These schemes take a binary linear scheme and they replace the binary linear average, as the arithmetic mean, with a non-linear average, as the harmonic mean or the geometric mean. This type of non-linear schemes is strictly related to their relative linear schemes and they inherit from them the smoothness.

Another possible approach uses the concept of asymptotic equivalence [Dyn and Levin, 1995] or the proximity condition [Wallner and Dyn, 2005] to a linear scheme. For example, Sabin and Dodgson [2004] show that the circle-preserving 4-point scheme is asymptotically equivalent to the linear 4-point scheme of Deslauriers and Dubuc [1989] and it inherits its C^1 continuity. The proximity condition is used instead by Wallner [2006] to prove the regularity of manifold-valued schemes. These two conditions do not cover all the possible non-linear schemes. For example the schemes presented in [Dyn and Hormann, 2012] do not satisfy the proximity condition. Moreover, the asymptotic equivalence and the proximity condition, with a linear scheme, allow to study the analytic continuity of the limit curve. This type of continuity needs that the limit curve is parametrized. For other non-linear schemes ad-hoc proofs are proposed, like in [Yang, 2006; Zhao et al., 2009; Deng and Wang, 2010; Hernández-Mederos et al., 2013], or only numerical evidence of the regularity of the limit curve is given [Deng and Ma, 2012, 2014; Cashman et al., 2013]. Dyn and Hormann [2012] are the first to give geometric conditions such that a non-linear interpolatory scheme converges and produces tangent

continuous limit curve. The key features of these conditions are the possibility to apply them to any type of interpolatory scheme and they are purely geometric, so they do not rely on any parametrization of the limit curve. Dyn and Hormann [2012] study the geometric continuity of the limit curve. The G^n continuity with respect to C^n continuity is independent on the parametrization of the curve and depends on geometric entities like edges, angles, tangents, circles.

In Section 2.1 we analyse the main differences between C^n continuity and G^n continuity giving some examples of curves that have one type of continuity and not the other. The conditions given by Dyn and Hormann [2012] are presented in Chapter 3. These conditions depend only on geometric quantities like edge lengths and angles generated by the subdivision control polygon. In particular, Dyn and Hormann [2012] show that the summability of maximum edge length is sufficient to have a convergent subdivision scheme, while the summability of the maximum of angles in absolute value gives a tangent continuous limit curve. These conditions prove the G^1 continuity of a geometric scheme.

In the literature there are some subdivision schemes [Deng and Wang, 2010; Deng and Ma, 2012, 2014; Hernández-Mederos et al., 2013] that claim to generate limit curves with continuous curvature. Therefore, my work is devoted on extending the conditions of Dyn and Hormann [2012], finding sufficient conditions for an interpolatory scheme to generate G^2 continuous limit curves. Instead of edges and angles, in this case we consider the circles passing through three consecutive points generated by the subdivision process. We look at the maximum difference of curvatures between neighbouring circles and we claim that the summability of this sequence is responsible to generate limit curves that are G^2 continuous. Unfortunately the proof is not complete yet; in Chapter 4 we give the idea of the proof and the results that we already proved with some numerical evidence for the missing points. Moreover, we present also some numerical examples to support the correctness of the proposed condition.

Acknowledgement

Chapter 2

Geometric subdivision schemes

All previous attempts to prove the regularity of a geometric subdivision scheme use the concept of asymptotic equivalence, proximity condition, or they are proofs suited for very specific subdivision schemes. As we saw in Section 1.3 the asymptotic equivalence and the proximity condition, even if they are general methods, provide only the analytic continuity of the limit curve. In this chapter we define what G^n continuity means and we make a comparison between analytic C^n continuity and geometric G^n continuity, giving some examples of curves with different type of regularity. The aim is to explain why it is necessary to change the approach if we consider geometric schemes.

In the second part of the chapter we recall some examples of geometric subdivision schemes presented in the literature that we use to test our sufficient condition. Finally, we introduce a new scheme that is designed to satisfy our G^2 condition.

2.1 C^n continuity vs G^n continuity

It is worthwhile to analyse the differences between a curve that is C^n continuous and a curve that is G^n continuous. For this reason, we recall some basic notions of differential geometry (see e.g. [Do Carmo, 1976]).

Definition 2.1. *A parametrized planar curve is a continuous map $\mathscr{C} : I \subset \mathbb{R} \to \mathbb{R}^2$, where I is an interval of $\mathbb{R}$.*

Definition 2.2. *A parametrized curve is C^n continuous, if it is n times differentiable and for any $x_0 \in I$*

$$\lim_{x \to x_0^-} \mathscr{C}^{(\ell)}(x) = \lim_{x \to x_0^+} \mathscr{C}^{(\ell)}(x) = \mathscr{C}^{(\ell)}(x_0), \quad \ell = 0, \dots, n.$$

$\mathscr{C}^{(\ell)}$ denotes the ℓ-th derivative of the curve $\mathscr{C}$.

Suppose that a curve is twice differentiable at any point and $\mathscr{C}'(x) \neq 0$, then the tangent vector and the curvature of the curve $\mathscr{C}$ are defined as

$$t = t(x) = \frac{\mathscr{C}'(x)}{\|\mathscr{C}'(x)\|},$$

$$k = k(x) = \frac{\det(\mathscr{C}'(x), \mathscr{C}''(x))}{\|\mathscr{C}'(x)\|^3}. \tag{2.1}$$

The determinant of two vectors is equal to the two dimensional cross product. If $\mathscr{C}'(x) \neq 0$ for any $x \in I$, the parametrization of the curve is said *regular*.

The concept of C^n continuity is strictly related to the parametrization of the curve, while geometric continuity is invariant with respect to the parametrization. First of all we need to introduce the concepts of tangents and curvature for an arbitrary curve independently of the parametrization.

We use the definitions given by Dyn and Hormann [2012] because they introduce sufficient conditions to require the G^1 continuity depending only on edges, angles and tangents.

Definition 2.3. *Any two distinct points $p, q \in \mathbb{R}^2$ determine a directed line $\overrightarrow{pq}$ from p to q with direction $(q - p)/\|q - p\|$.*

Definition 2.4. *The signed angle $\sphericalangle(s, t)$ between two directed lines s and t is the angle between the two directions measured from s to t, where counterclockwise angles are positive and clockwise angles are negative. For parallel directed lines s and t, we have $\sphericalangle(s, t) = 0$ if $\overrightarrow{s} = \overrightarrow{t}$ or $\sphericalangle(s, t) = \pi$ if $\overrightarrow{s} = -\overrightarrow{t}$.*

Definition 2.5. *Let $\mathscr{C}$ be a continuous curve and p, q two points on the curve. A direct line t is the directed tangent at p if the directed line $\overrightarrow{pq}$ converges to t as q approaches p along $\mathscr{C}$ from the right and $\overrightarrow{qp}$ converges to t as q approaches p from the left.*

Definition 2.6. *A curve $\mathscr{C}$ is said G^1 continuous if it has a directed tangent at each point $p \in \mathscr{C}$ and if the directed tangent at $q \in \mathscr{C}$ converges to the one at p as q approaches p along $\mathscr{C}$.*

This means that there are no jumps in the direction of the tangents along the curve.

In general, analytic continuity C^1 does not implies geometric continuity G^1.

Example 2.1. Consider the curve

$$\mathscr{C}(x) = (x^3, x^2), \quad x \in [-1, 1].$$

The first derivative at zero is zero but if we consider a sequence of points that converges to zero from the left they define the tangent $t = (0, -1)$. Instead if we consider a sequence of points that converges to zero from right, the directed tangent is $(0, 1)$. The tangents lie on the same line but with opposite directions as can be seen in Figure 2.1.
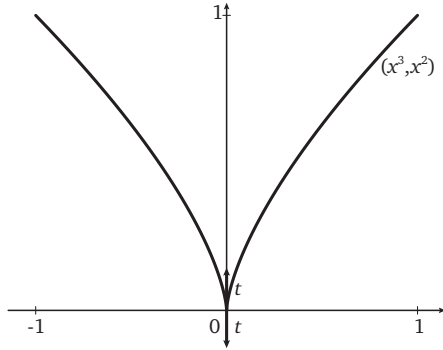
Figure 2.1. Example of a C^1 continuous curve that is not G^1 continuous: $\mathscr{C}(x) = (x^3, x^2)$ for $x \in [-1, 1]$.
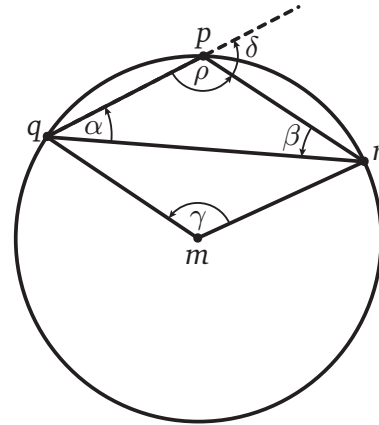

Figure 2.2. Circle passing through q, p and r.

In the same way for the G^2 continuity we consider a definition of the curvature that is independent of the parametrization of the curve.

Definition 2.7. *Let q, p, r be three points in $\mathbb{R}^2$. A discrete interpolating circle C is the circle passing through three points q, p, r. The absolute value of the discrete curvature k is the inverse of the radius*

$$|k| = \frac{1}{\|p - m\|}, \tag{2.2}$$

where m is the center of the circle, see Figure 2.2. The curvature is positive if q, p and r are in clockwise order otherwise is negative.

The concept of discrete curvature allows us to give a definition of curvature based on the notion of the osculating circle (see e.g. [Do Carmo, 1976; Farin, 2002]).

Definition 2.8. *Let $\mathscr{C}$ be a curve and q, p, r three points on the curve itself. If the discrete interpolating circle passing through q, p, r converges to a circle when q approaches p along the curve from the left and r approaches p along the curve from the right, then this limit circle is called* osculating circle*. The tangent of the circle at p is the directed tangent of the curve at p. The curvature of the curve at p is the reciprocal of the radius of the osculating circle.*

If the three points q, p and r are collinear at limit, then the osculating circle degenerates to the straight line passing through these points. In this case the direct tangent is give by $\overrightarrow{pr}$ and the curvature is zero.

Considering the discrete circle passing through q, p, r non collinear points (see Fig. 2.2), direct computations give the radius as

$$\|q - m\| = \frac{\frac{1}{2} \|r - q\|}{\sin(|\gamma|/2)},$$

where we consider the absolute value of the angle, because the radius of a circle is always positive. Any angle inscribed in a circle is half the central angle that subtends the same arc, so

$$|\gamma| = 2\pi - 2\,|\rho| = 2\pi - 2(\pi - |\delta|) = 2\,|\delta|,$$

and,

$$\|q - M\| = \frac{\|r - q\|}{2\sin(|\delta|)}.$$

Then, the discrete curvature (with sign) at the point p is

$$k = \frac{2\sin(\delta)}{\|r - q\|}. \tag{2.3}$$

The sign of the discrete curvature is given by the sign of the angle δ. In Figure 2.2, δ is positive, which is the reason why in Definition 2.7 we say the discrete curvature is positive for a clockwise triple of points. Moreover, if the three points q, p, r are collinear, then the angle $\delta = 0$ and also the curvature is zero.

It is possible to show that the curvature of the osculating circle is equivalent to the usual definition of curvature for a parametric curve (2.1). Let us consider a twice differentiable parametric curve $\mathscr{C}$ at a point $\mathscr{C}(x) = p$. We define the points q and r on $\mathscr{C}$ as

$$q = \mathscr{C}(x) - \mathscr{C}'(x)\Delta x_1 + \mathscr{C}''(x)\frac{\Delta x_1^2}{2} + O(\Delta x_1^3),$$

$$r = \mathscr{C}(x) + \mathscr{C}'(x)\Delta x_2 + \mathscr{C}''(x)\frac{\Delta x_2^2}{2} + O(\Delta x_2^3),$$

such that they converge to p with two different velocities $\Delta x_1, \Delta x_2 \to 0$. The unsigned curvature of $\mathscr{C}$ at p is the limit of the discrete curvature

$$\lim_{\Delta x_i \to 0} k(p) = \lim_{\Delta x_i \to 0} \frac{2\sin(|\delta|)}{\|r - q\|},$$

for $i = 1, 2$. The determinant between two vectors a and b is the norm of the two dimensional cross product

$$\|a \times b\| = |\det(a, b)| = \|a\|\,\|b\|\sin(\angle(a, b)).$$

Using the definitions of q, r we have

$$\lim_{\Delta x_i \to 0} k(p) = \lim_{\Delta x_i \to 0} \frac{2\sin(|\delta|)}{\|r-q\|} = \lim_{\Delta x_i \to 0} \frac{2\left\|\overrightarrow{qp} \times \overrightarrow{pr}\right\|}{\|p-q\|\,\|r-p\|\,\|r-q\|}$$

$$= \lim_{\Delta x_i \to 0} \frac{2\left\|\left(\mathscr{C}'(x)\Delta x_1 - \mathscr{C}''(x)\frac{\Delta x_1^2}{2}\right) \times \left(\mathscr{C}'(x)\Delta x_2 + \mathscr{C}''(x)\frac{\Delta x_2^2}{2}\right)\right\|}{\left\|\mathscr{C}'(x)\Delta x_1 - \mathscr{C}''(x)\frac{\Delta x_1^2}{2}\right\| \left\|\mathscr{C}'(x)\Delta x_2 + \mathscr{C}''(x)\frac{\Delta x_2^2}{2}\right\| \left\|\mathscr{C}'(x)(\Delta x_1 + \Delta x_2) + \mathscr{C}''(x)\frac{\Delta x_2^2 - \Delta x_1^2}{2}\right\|}$$

$$= \lim_{\Delta x_i \to 0} \frac{2\left\|(\mathscr{C}'(x) \times \mathscr{C}''(x))\frac{\Delta x_1 \Delta x_2^2}{2} + (-\mathscr{C}''(x) \times \mathscr{C}'(x))\frac{\Delta x_1^2 \Delta x_2}{2}\right\|}{\Delta x_1 \Delta x_2 \left\|\mathscr{C}'(x) - \mathscr{C}''(x)\frac{\Delta x_1}{2}\right\| \left\|\mathscr{C}'(x) + \mathscr{C}''(x)\frac{\Delta x_2}{2}\right\| \left\|\mathscr{C}'(x)(\Delta x_1 + \Delta x_2) + \mathscr{C}''(x)\frac{\Delta x_2^2 - \Delta x_1^2}{2}\right\|}$$

$$= \lim_{\Delta x_i \to 0} \frac{(\Delta x_2 + \Delta x_1)\left\|\mathscr{C}'(x) \times \mathscr{C}''(x)\right\|}{\left\|\mathscr{C}'(x) - \mathscr{C}''(x)\frac{\Delta x_1}{2}\right\| \left\|\mathscr{C}'(x) + \mathscr{C}''(x)\frac{\Delta x_2}{2}\right\| \left\|\mathscr{C}'(x)(\Delta x_1 + \Delta x_2) + \mathscr{C}''(x)\frac{\Delta x_2^2 - \Delta x_1^2}{2}\right\|}$$

$$= \lim_{\Delta x_i \to 0} \frac{\left\|\mathscr{C}'(x) \times \mathscr{C}''(x)\right\|}{\left\|\mathscr{C}'(x) - \mathscr{C}''(x)\frac{\Delta x_1}{2}\right\| \left\|\mathscr{C}'(x) + \mathscr{C}''(x)\frac{\Delta x_2}{2}\right\| \left\|\mathscr{C}'(x) + \mathscr{C}''(x)\frac{\Delta x_2 - \Delta x_1}{2}\right\|}$$

$$= \frac{\left\|\mathscr{C}'(x) \times \mathscr{C}''(x)\right\|}{\|\mathscr{C}'(x)\|^3} = \frac{\left|\det(\mathscr{C}'(x), \mathscr{C}''(x))\right|}{\|\mathscr{C}'(x)^3\|},$$

for $i = 1, 2$, which is equal to (2.1). We eliminate the higher terms because they decay to zero and they are irrelevant from a computational point of view. Moreover, we exploit the properties of the cross product.

The advantage of using the discrete curvature (2.3) instead of (2.1) is that the curve does not have to be twice differentiable and we do not need an explicit parametrization. Moreover, using (2.3) in a geometric subdivision scheme, we exploit only the angles and edges defined by the points. We are now able to define a G^2 continuous curve.

Definition 2.9. *A curve is said to be G^2 continuous if there exists an osculating circle at each point $p \in \mathscr{C}$ and the curvature of the osculating circle at $q \in \mathscr{C}$ converges to the curvature at p as q approaches p along $\mathscr{C}$.*

Example 2.2. Consider the curve

$$\mathscr{C}(x) = \begin{cases} \left(\sin\left(\frac{\pi}{2}x^3\right), \cos\left(\frac{\pi}{2}x^3\right) - 1\right) & x \in [-1, 0) \\ \left(\sin\left(\frac{\pi}{2}x^3\right), 1 - \cos\left(\frac{\pi}{2}x^3\right)\right) & x \in [0, 1] \end{cases},$$

displayed in Figure 2.3. The curve is composed by two sectors of unit circles: it is G^1 but not G^2 continuous at zero because the two circles have opposite curvatures. With the previous parametrization the curve $\mathscr{C}$ is C^2 continuous, in fact the second derivative is

$$\mathscr{C}''(x) = \begin{cases} \left(3\pi t \cos\left(\frac{\pi}{2}x^3\right) - \frac{9}{4}\pi^2 t^4 \sin\left(\frac{\pi}{2}x^3\right), -3\pi t \sin\left(\frac{\pi}{2}x^3\right) - \frac{9}{4}\pi^2 t^4 \cos\left(\frac{\pi}{2}x^3\right)\right) \\ \left(3\pi t \cos\left(\frac{\pi}{2}x^3\right) - \frac{9}{4}\pi^2 t^4 \sin\left(\frac{\pi}{2}x^3\right), 3\pi t \sin\left(\frac{\pi}{2}x^3\right) + \frac{9}{4}\pi^2 t^4 \cos\left(\frac{\pi}{2}x^3\right)\right) \end{cases},$$

and we have $\lim_{x \to 0^-} \mathscr{C}''(x) = \lim_{x \to 0^+} \mathscr{C}''(x) = (0, 0)$.
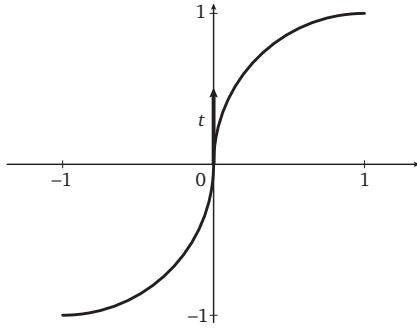
Figure 2.3. Example of a C^2 continuous curve that is not G^2 continuous because it is composed by two circles with opposite curvatures.
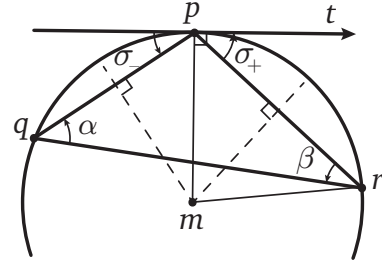
Figure 2.4. Discrete circle with tangent t and angles α and σ_+.

This example shows that the continuity of the second derivative does not imply the continuity of the curvature.

In Definition 2.7 we define the discrete interpolating circle as the circle passing through three points. In general, a circle can be described in several equivalent ways:

1. the circle with center m and radius $\|p - m\|$,

2. the circle passing through three points q, p and r,

3. the circle with tangent line t at p and curvature k.

4. the circle with tangent line t at p and passing through p and r.

These are the different descriptions that we use throughout the thesis. For each different description of the circle we can compute the curvature in different ways.

Lemma 2.1. *Let t be the tangent at p of the circle passing through q, p, r, then*

$$\sigma_+ := \sphericalangle(\overrightarrow{pr}, t) = \sphericalangle(\overrightarrow{qr}, \overrightarrow{qp}), \quad and \quad \sigma_- := \sphericalangle(-t, \overrightarrow{pq}) = \sphericalangle(\overrightarrow{rp}, \overrightarrow{rq}).$$

Proof: For the definition of the angles σ_+, σ_-, α, β we refer to Figure 2.4, and

$$\alpha = \sphericalangle(\overrightarrow{qr}, \overrightarrow{qp}) = \frac{1}{2}\sphericalangle(\overrightarrow{mr}, \overrightarrow{mp}) = \sigma_+,$$

because an angle inscribed in the circle is half of the central angle that subtends the same arc and some relations between complementary angles (see Fig. 2.4). In the same way we have

$$\sigma_- = \beta = \sphericalangle(\overrightarrow{pr}, \overrightarrow{qr}).$$

Then, the curvature of a circle with tangent t at p and passing through r or q is

$$k(p, r, t) = \frac{2\sin(\sigma_+)}{\|p - r\|} \quad \text{or} \quad k(q, p, t) = \frac{2\sin(\sigma_-)}{\|p - q\|}.$$
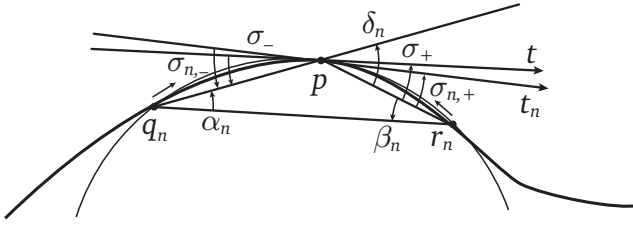
Figure 2.5. The sequences of points $\{q_n\}_n$ and $\{r_n\}_n$ that converge to p respectively from the left and right.
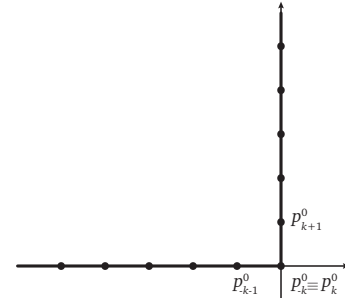
Figure 2.6. Limit curve generated by control points p_i^0 (2.7).

□

This remark allows us to prove that the osculating circle of a curve $\mathscr{C}$ at p is the limit of two sequences of circles with tangent t and passing through p, q_n and p, r_n, as q_n and r_n converge to p (see Fig. 2.5).

Proposition 2.2. *Let $\mathscr{C}$ be a G^1 continuous curve. Consider two sequences of points $\{q_n\}_{n\in\mathbb{N}}$ and $\{r_n\}_{n\in\mathbb{N}}$ on $\mathscr{C}$, which both converge to the same point $p \in \mathscr{C}$, respectively from the left and from the right. We denote by $k(q_n, p, t)$ the curvature of the circle that has the tangent t of the curve at p as directed tangent and passes through p and q_n, and likewise the curvature of the circle with tangent t, passing through p and r_n, by $k(p, r_n, t)$. If the two sequences of curvatures converge to the same limit*

$$\lim_{n\to\infty} k(q_n, p, t) = \bar{k} = \lim_{n\to\infty} k(p, r_n, t),$$

then

 (i) they converge to the same limit of the sequence of discrete curvatures

$$\lim_{n\to\infty} k(q_n, p, r_n) = \bar{k}.$$

 (ii) $\bar{k}$ is the curvature of the curve $\mathscr{C}$ at p.

Proof: Let us consider two sequences of points $\{q_n\}$ and $\{r_n\}$ on a curve $\mathscr{C}$ that approach p respectively from the left and the right and t the tangent of the curve at p (see Fig. 2.5).

The curvature of the circle that has tangent t of the curve at p as directed tangent and passes through p and q_n is

$$k(q_n, p, t) = \frac{2 \sin \sigma_-}{\|p - q_n\|}. \tag{2.4}$$

Analogously the curvature of the circle passing through r_n is

$$k(p, r_n, t) = \frac{2 \sin \sigma_+}{\|r_n - p\|}. \tag{2.5}$$

By hypothesis, both the the sequences converge to $\bar{k}$.

The discrete curvature of the circle passing through q_n, p and r_n is

$$k(q_n, p, r_n) = \frac{2 \sin \delta_n}{\|r_n - q_n\|}.$$

From Figure 2.5 and Lemma 2.1 we observe that

$$\delta_n = \alpha_n + \beta_n = \sigma_{n,+} + \sigma_{n,-} = \sphericalangle(\overrightarrow{pr_n}, t_n) + \sphericalangle(t_n, t) + \sphericalangle(t, t_n) + \sphericalangle(t_n, \overrightarrow{q_n p}) = \sigma_+ + \sigma_-,$$

$$(2.6)$$

$$\|r_n - q_n\| = \|p - q_n\| \cos \alpha_n + \|r_n - p\| \cos \beta_n.$$

Thus, the discrete curvature becomes

$$\begin{aligned}
k(q_n, p, r_n) &= \frac{2 \sin \delta_n}{\|r_n - q_n\|} = \frac{2 \sin(\sigma_+ + \sigma_-)}{\|p - q_n\| \cos \alpha_n + \|r_n - p\| \cos \beta_n} \\
&= \frac{2 \sin(\sigma_+) \cos(\sigma_-) + 2 \sin(\sigma_-) \cos(\sigma_+)}{\|r_n - p\| \cos \beta_n + \|p - q_n\| \cos \alpha_n}.
\end{aligned}$$

Since q_n and r_n converge to p, we can assume that from a certain n on, both $|\alpha_n|$ and $|\beta_n|$ are smaller than $\pi/2$ and the cosine of these angles is positive. Using (2.4), (2.5) and Lemma 2.3, the discrete curvature $k(q_n, p, r_n)$ is bounded,

$$k(q_n, p, r_n) \geq \min \left\{ k(p, r_n, t) \frac{\cos(\sigma_-)}{\cos(\beta_n)}; k(q_n, p, t) \frac{\cos(\sigma_+)}{\cos(\alpha_n)} \right\},$$

$$k(q_n, p, r_n) \leq \max \left\{ k(p, r_n, t) \frac{\cos(\sigma_-)}{\cos(\beta_n)}; k(q_n, p, t) \frac{\cos(\sigma_+)}{\cos(\alpha_n)} \right\}.$$

Using the relations between the angles in (2.6), the behaviour of the two terms, when $n \to \infty$, is

$$\begin{aligned}
\lim_{n \to \infty} k(p, r_n, t) \frac{\cos(\sigma_-)}{\cos(\beta_n)} &= \lim_{n \to \infty} k(p, r_n, t) \frac{\cos(\beta_n - \sphericalangle(t_n, t))}{\cos(\beta_n)} \\
&= \lim_{n \to \infty} k(p, r_n, t) \frac{\cos(\beta_n) \cos(\sphericalangle(t_n, t)) + \sin(\beta_n) \sin(\sphericalangle(t_n, t))}{\cos(\beta_n)} \\
&= \lim_{n \to \infty} k(p, r_n, t) (\cos(\sphericalangle(t_n, t)) + \tan(\beta_n) \sin(\sphericalangle(t_n, t))) \\
&= \bar{k}.
\end{aligned}$$

From the definition of the discrete interpolating circle we have that the sequence of curvatures $k(q_n, p, r_n)$ converges to the curvature of the curve at p, and the sequence of tangents t_n of the discrete circles converges to the directed tangent t of the curve at p,

$\lim_{n\to\infty} \sphericalangle(t_n, t) = 0$. Moreover, by hypothesis $k(p, r_n, t)$ converge to $\bar{k}$. Analogously,

$$
\begin{aligned}
\lim_{n\to\infty} k(q_n, p, t)\frac{\cos(\sigma_+)}{\cos(\alpha_n)} &= \lim_{n\to\infty} k(q_n, p, t)\frac{\cos(\alpha_n + \sphericalangle(t_n, t))}{\cos(\alpha_n)} \\
&= \lim_{n\to\infty} k(q_n, p, t)\frac{\cos(\alpha_n)\cos(\sphericalangle(t_n, t)) - \sin(\alpha_n)\sin(\sphericalangle(t_n, t))}{\cos(\alpha_n)} \\
&= \lim_{n\to\infty} k(q_n, p, t)(\cos(\sphericalangle(t_n, t)) - \tan(\alpha_n)\sin(\sphericalangle(t_n, t))) \\
&= \bar{k}.
\end{aligned}
$$

Using the squeeze theorem we then conclude

$$
\lim_{n\to\infty} k(q_n, p, r_n) = \bar{k}.
$$

$\square$

This general result is used later in the proof of our condition for G^2 continuous curves generated by an interpolatory scheme (see Section 4.3.2).

Lemma 2.3. *For any $a, b \in \mathbb{R}$ and $c, d > 0$ we have*

$$
\min\left\{\frac{a}{c}, \frac{b}{d}\right\} \le \frac{a+b}{c+d} \le \max\left\{\frac{a}{c}, \frac{b}{d}\right\}.
$$

Proof: If

$$
\frac{a}{c} \le \frac{b}{d} \quad \Rightarrow \quad
\begin{aligned}
a &\le \frac{bc}{d} \\
b &\ge \frac{ad}{c}
\end{aligned}
\quad \Rightarrow \quad
\begin{aligned}
\frac{a+b}{c+d} &\le \frac{b(\frac{c}{d}+1)}{c+d} \le \frac{b}{d} \\
\frac{a+b}{c+d} &\ge \frac{a(1+\frac{d}{c})}{c+d} \ge \frac{a}{c}
\end{aligned}
\quad .
$$

Otherwise

$$
\frac{a}{c} > \frac{b}{d} \quad \Rightarrow \quad
\begin{aligned}
b &< \frac{ad}{c} \\
a &> \frac{bc}{d}
\end{aligned}
\quad \Rightarrow \quad
\begin{aligned}
\frac{a+b}{c+d} &< \frac{a(1+\frac{d}{c})}{c+d} < \frac{a}{c} \\
\frac{a+b}{c+d} &> \frac{b(\frac{c}{d}+1)}{c+d} > \frac{b}{d}
\end{aligned}
\quad .
$$

$\square$

Before we introduce some examples of geometric subdivision schemes, we have to remark that a subdivision scheme can hardly generate a G^1 or G^2 limit curve for all input data. For example, if we consider as control points

$$
p_i^0 = \begin{cases}
(i, 0) & i < -k, \\
(0, 0) & |i| \le k, \\
(0, i) & i > k,
\end{cases}
\tag{2.7}
$$

then any subdivision scheme with support $2k + 1$ generates a limit curve composed by two perpendicular straight half lines as in Figure 2.6. In order to avoid this strange configuration, for the rest of the thesis we consider control polygons with distinctive neighbouring points, i.e. $p_i \ne p_{i+1} \ \forall i \in I \subset \mathbb{Z}$.
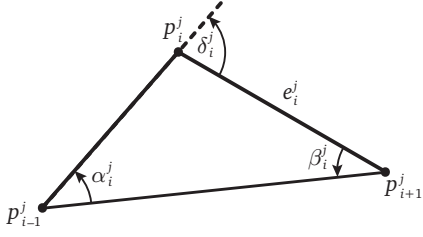
Figure 2.7. Definition of edge length e_i^j and angle δ_i^j.
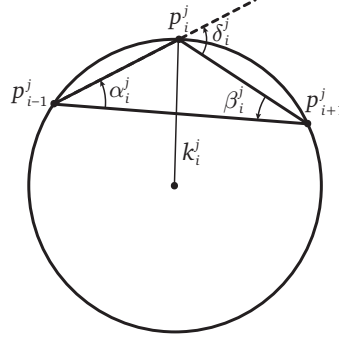
Figure 2.8. Definition of discrete curvature k_i^j.

2.2   Examples of geometric subdivision schemes

Here we recall some non-linear subdivision schemes presented in the literature that use a geometric construction. These schemes are of our interest, because they allow us to test the conditions, given in the following chapters, to study the convergence and regularity of the limit curve.

We introduce some notations that we use in the definitions of geometric schemes. At level j of the subdivision process we denote with

$$e_i^j = \left\| p_{i+1}^j - p_i^j \right\|$$

the edge length of $\overrightarrow{p_i^j p_{i+1}^j}$. Considering three consecutive points p_{i-1}^j, p_i^j and p_{i+1}^j generated by the subdivision scheme, they define a triangle with angles

$$\alpha_i^j := \sphericalangle(\overrightarrow{p_{i-1}^j p_{i+1}^j}, \overrightarrow{p_{i-1}^j p_i^j}), \quad \beta_i^j := \sphericalangle(\overrightarrow{p_i^j p_{i+1}^j}, \overrightarrow{p_{i-1}^j p_{i+1}^j}), \quad \delta_i^j := \sphericalangle(\overrightarrow{p_i^j p_{i+1}^j}, \overrightarrow{p_{i-1}^j p_i^j}),$$

(see Fig. 2.7). By a geometric constraint, for every triangle we have

$$\alpha_i^j + \beta_i^j = \delta_i^j.$$

The three consecutive points p_{i-1}^j, p_i^j and p_{i+1}^j define also a circle passing through them, whose curvature is denoted by k_i^j (see Fig. 2.8). Using (2.3), the curvature k_i^j is computed using the external angle δ_i^j and the edge length e_i^j,

$$k_i^j = \frac{2\sin\delta_i^j}{e_i^j}.$$

2.2.1 Incenter scheme

One example is the incenter scheme proposed by Deng and Wang [2010]. It takes as input a set of control points P^0 and tangents $T^0 = \{t_i^0\}$ for each point. It is interpolatory, so $p_{2i}^{j+1} = p_i^j$, and each new point p_{2i+1}^{j+1} is the incenter of the triangle formed by the edge $\overrightarrow{p_i^j p_{i+1}^j}$ and the two tangent lines t_i^j and $-t_{i+1}^j$,

$$p_{2i+1}^{j+1} = p_i^j + \frac{\sin\left(\frac{\theta_i^j}{2}\right)}{\sin\left(\frac{\gamma_i^j + \theta_i^j}{2}\right)} R\left(-\frac{\gamma_i^j}{2}\right)\left(p_{i+1}^j - p_i^j\right)$$

where $\gamma_i^j := \sphericalangle(t_i^j, \overrightarrow{p_i^j p_{i+1}^j})$ and $\theta_i^j := \sphericalangle(\overrightarrow{p_i^j p_{i+1}^j}, t_{i+1}^j)$, (see Fig. 2.9). With $R(\theta)$ we indicate the rotation matrix

$$R(\theta) = \begin{pmatrix} \cos(\theta) & -\sin(\theta) \\ \sin(\theta) & \cos(\theta) \end{pmatrix}.$$

For any new point p_i^{j+1}, they choose provisional tangents u_i^{j+1} such that

$$u_{2i}^{j+1} = t_i^j, \qquad u_{2i+1}^{j+1} = \frac{p_{i+1}^j - p_i^j}{\left\| p_{i+1}^j - p_i^j \right\|}.$$

The previous tangents are kept at the interpolating points, while at the new points the tangents are defined with the same direction as the edge $\overrightarrow{p_i^j p_{i+1}^j}$. Then, the new angles are

$$\bar{\gamma}_{2i}^{j+1} = \bar{\theta}_{2i}^{j+1} = \frac{\gamma_i^j}{2}, \qquad \bar{\gamma}_{2i+1}^{j+1} = \bar{\theta}_{2i+1}^{j+1} = \frac{\theta_i^j}{2}.$$

Deng and Wang [2010] claim that in order to obtain a curvature continuous subdivision scheme the tangents should be adjusted,

$$t_i^{j+1} = R\left(\sigma_i^{j+1}\right) u_i^{j+1} \quad \text{with} \quad \sigma_i^{j+1} = \frac{\epsilon\, \bar{\gamma}_i^{j+1} \bar{\gamma}_{i-1}^{j+1}}{\bar{\gamma}_i^{j+1} + \bar{\gamma}_{i-1}^{j+1}} \frac{r_i^{j+1} - r_{i-1}^{j+1}}{r_i^{j+1} + r_{i-1}^{j+1}},$$

where $0 < \epsilon \leq 1/2$ and r_i^{j+1} is the radius of the circle passing through p_i^{j+1} and p_{i+1}^{j+1} with tangents u_i^{j+1} and u_{i+1}^{j+1},

$$r_i^{j+1} = \frac{\left\| p_{i+1}^{j+1} - p_i^{j+1} \right\|}{2\sin\left(\bar{\gamma}_i^{j+1}\right)}.$$

Once the tangents have been adjusted, also the angles γ_i^{j+1} and θ_i^{j+1} are adjusted with the same value

$$\gamma_i^{j+1} = \bar{\gamma}_i^{j+1} + \sigma_i^{j+1}, \qquad \theta_i^{j+1} = \bar{\theta}_i^{j+1} - \sigma_{i+1}^{j+1}.$$
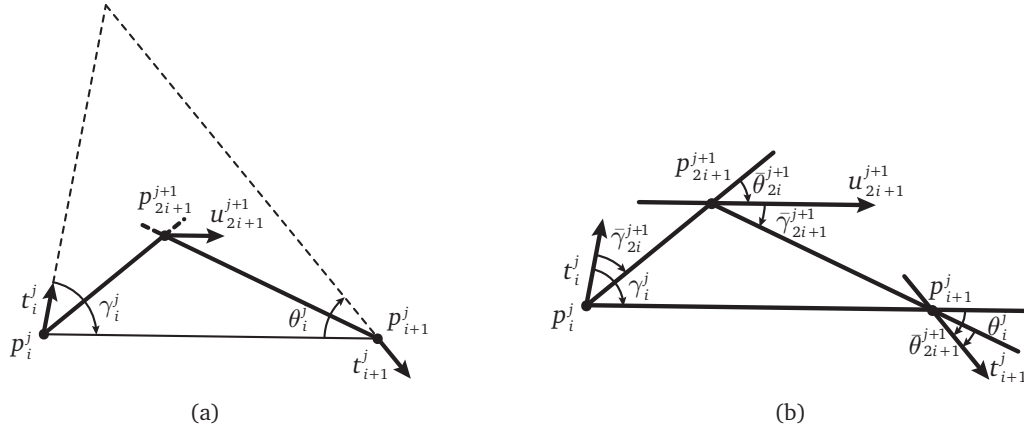
Figure 2.9. Construction of the new points for the incenter scheme (a) and the new tangents (b).

In the end, the scheme does not interpolate the initial tangents due to the correction with σ_i^{j+1}, for this reason it is not a Hermite scheme. In [Hernández-Mederos et al., 2013] a generalization of the incenter scheme is presented that does not correct the tangents and is really a Hermite scheme.

Deng and Wang [2010] prove that the limit curve generated by the incenter scheme is G^1 continuous and claim that it is also G^2 continuous. In the next chapters, we use this scheme to test out sufficient conditions in order to guarantee G^1 and G^2 continuity of the limit curve.

2.2.2 Angle-based 4-point scheme

The angle-based 4-point scheme is introduced in [Dyn and Hormann, 2012] as an example of a scheme that satisfies the G^1 condition presented there. It is an interpolatory bisector scheme (1.9),

$$p_{2i+1}^{j+1} = \frac{p_i^j + p_{i+1}^j}{2} + \tan\left(\alpha_{2i+1}^{j+1}\right)\frac{(p_{i+1}^j - p_i^j)^\perp}{2},$$

such that

$$\alpha_{2i+1}^{j+1} = \beta_{2i+1}^{j+1} = \frac{\delta_i^j + \delta_{i+1}^j}{8}.$$

The scheme depends on 4 points because the new point p_{2i+1}^{j+1} is constructed by quadrisecting and averaging the external angles δ_i^j and δ_{i+1}^j (see Fig. 2.10). Using the general relations between angles,

$$\delta_{2i}^{j+1} = \delta_i^j - \alpha_{2i+1}^{j+1} - \beta_{2i-1}^j, \qquad \delta_{2i+1}^{j+1} = \alpha_{2i+1}^{j+1} + \beta_{2i+1}^{j+1}, \qquad (2.8)$$

Figure 2.10. Construction of the new point p_{2i+1}^{j+1} for the angle-based 4-point scheme.
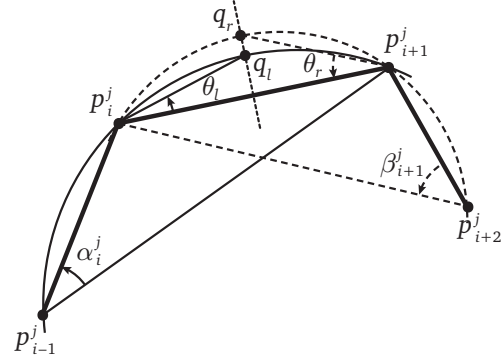
Figure 2.11. Construction of the new point p_{2i+1}^{j+1} for the circle-based 4-point scheme.

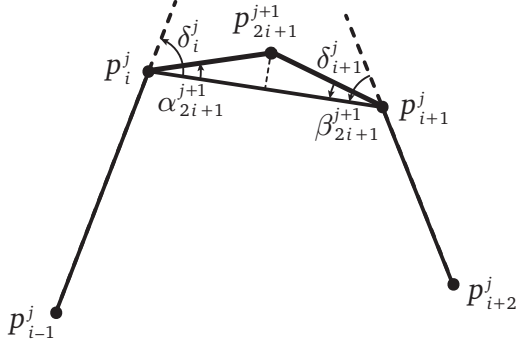we obtain in the specific case of the angle-based 4-point scheme,

$$\delta_{2i}^{j+1} = \delta_i^j - \frac{\delta_i^j + \delta_{i+1}^j}{8} - \frac{\delta_{i-1}^j + \delta_i^j}{8} = \frac{-\delta_{i-1}^j + 6\delta_i^j - \delta_{i+1}^j}{8}, \quad \delta_{2i+1}^{j+1} = \frac{\delta_i^j + \delta_{i+1}^j}{4}. \quad (2.9)$$

Note that the coefficients in (2.9) are the same as the mask of the second-order differences for the 4-point scheme (1.32).

The angle-based 4-point scheme generates a circle whenever the initial points are vertices of a regular polygon. In this case all the initial external angles are equal $\delta_i^0 = \delta^0$ and in the following levels $\delta^j = 2^{-j}\delta^0$, thanks to (2.9). Then, the scheme produces a sequence of regular polygons with common radius and centre, because the scheme is interpolatory. In the limit the regular polygons converge to the circle with the same radius and centre.

We postpone the discussion of G^1 continuity of this scheme to Section 3.2.

2.2.3 Circle-based 4-point scheme

Also the circle-based 4-point scheme is presented in [Dyn and Hormann, 2012] as an example of scheme that satisfies the G^1 condition given. It is an interpolatory bisector scheme where they average two circles. Namely, they consider the two circles that pass through $p_{i-1}^j, p_i^j, p_{i+1}^j$ and $p_i^j, p_{i+1}^j, p_{i+2}^j$ respectively and their intersections q_l and q_r with the perpendicular bisector of the edge $\overrightarrow{p_i^j p_{i+1}^j}$; see Figure 2.11. The new point p_{2i+1}^{j+1} is not the mean of q_l and q_r, but averages the angles $\theta_l = \sphericalangle(\overrightarrow{p_i^j p_{i+1}^j}, \overrightarrow{p_i^j q_l})$ and $\theta_r = \sphericalangle(\overrightarrow{p_i^j p_{i+1}^j}, \overrightarrow{p_i^j q_r})$, so that

$$\alpha_{2i+1}^{j+1} = \beta_{2i+1}^{j+1} = \frac{\theta_l + \theta_r}{2}.$$

By some geometric considerations, we observe that $\theta_l = \alpha_i^j/2$ and $\theta_r = \beta_{i+1}^j/2$, giving the relation

$$\alpha_{2i+1}^{j+1} = \beta_{2i+1}^{j+1} = \frac{\alpha_i^j + \beta_{i+1}^j}{4}. \tag{2.10}$$

Introducing (2.10) into the general relations for δ_{2i}^{j+1} and δ_{2i+1}^j (2.8), we obtain

$$\delta_{2i}^{j+1} = \frac{-\alpha_i^j + 3\delta_i^j - \beta_{i+1}^j}{4}, \qquad \delta_{2i+1}^{j+1} = \frac{\alpha_i^j + \beta_{i+1}^j}{2}. \tag{2.11}$$

This type of scheme clearly reproduces circles if the starting points are sampled on a common circle. If all the points lie on a circle, then the generating points q_l and q_r are the same point which lies again on the same circle. Every point generated by the scheme is on the circle and, at the limit, the scheme generates the circle itself.

For an arbitrary control polygon, the limit curve is circle-shaped as shown in Figure 2.12 (top left). This example is suited to show how a geometric scheme takes into account the geometry of the control polygon. Considering a control polygon with different edge lengths, a linear scheme, like the 4-point scheme, can produce artifacts, as can be observed in Figure 2.12 (right). Instead the circle based 4-point scheme follows the geometry of the control polygons (Fig. 2.12 left).

2.2.4 Circle-based 6-point scheme

In order to further test our condition for G^2 continuity, let us consider an interpolatory geometric scheme that is expected to produce limit curves with continuous curvatures. For simplicity, we choose a bisector scheme,

$$p_{2i+1}^{j+1} = \frac{p_i^j + p_{i+1}^j}{2} + \tan\left(\frac{\delta_{2i+1}^{j+1}}{2}\right) \frac{(p_{i+1}^j - p_i^j)^\perp}{2}.$$

To define the angle δ_{2i+1}^{j+1} we take inspiration from two different schemes: the angle-based 4-point scheme and the circle preserving variant of the 4-point scheme presented by Sabin and Dodgson [2004].

From the angle-based 4-point scheme, we keep the idea of using the mask of the second-order differences for the 4-point scheme to compute the new external angle δ_{2i+1}^{j+1} with respect to the angles δ_i^j, δ_{i+1}^j (2.9). To gain regularity with respect to the angle-based 4-point scheme, we consider the mask of the second-order differences of the 6-point scheme (1.34). We choose the 6-point scheme, because it generates curves that are C^2 continuous (see Section 1.4).

Floater and Micchelli [1998] observe that the 4-point scheme is such that the second divided difference at a point p_{2i+1}^{j+1} is the mean of the second divided difference at the points p_i^j and p_{i+1}^j. Sabin and Dodgson [2004] "translate" this idea to the discrete interpolating circles: the new point p_{2i+1}^{j+1} is constructed such that the discrete curvature at

Figure 2.12. Limit curves generated by the circle 4-point scheme (top left) and the 4-point scheme (top right). The bottom figures zoom to the limit curves close to the point p_{10}.

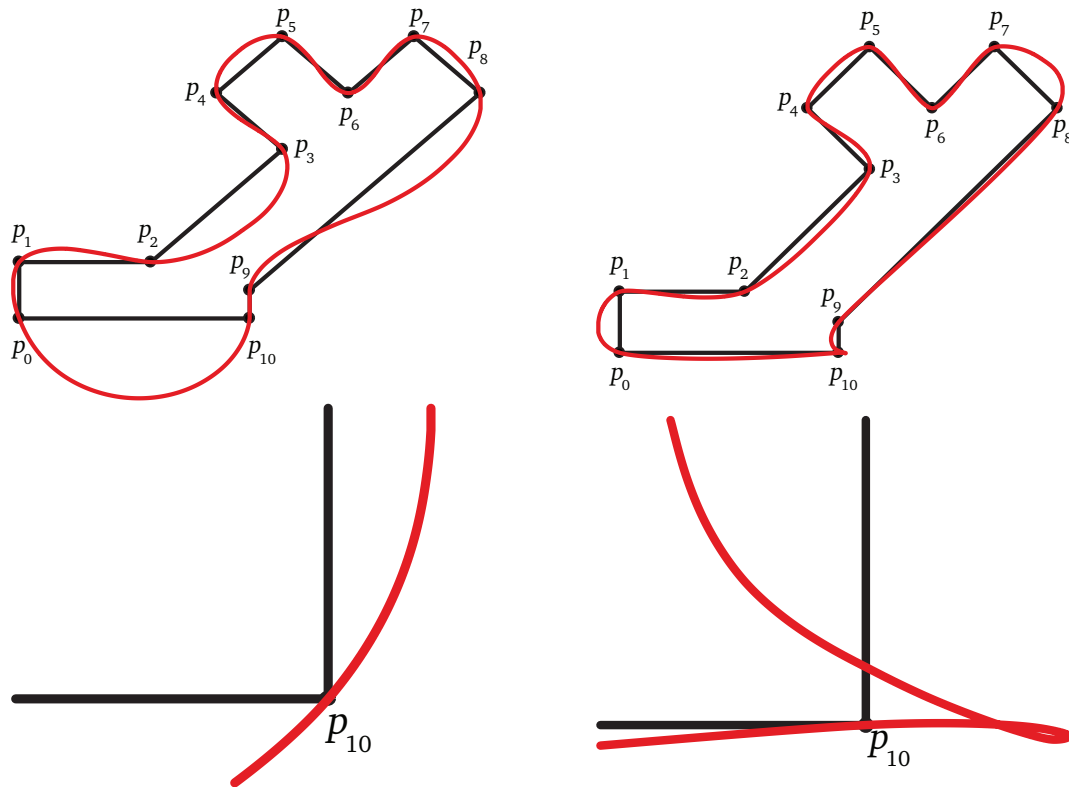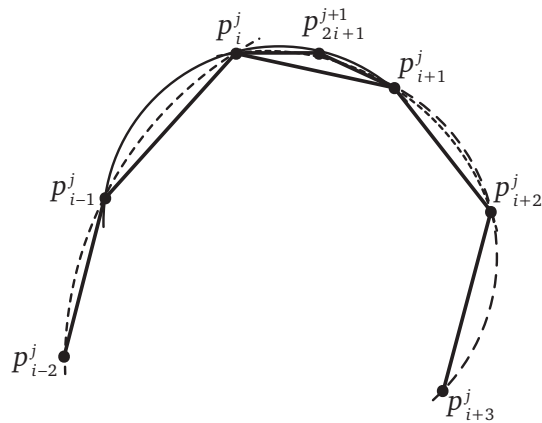Figure 2.13. Construction of the new point p_{2i+1}^{j+1} for the circle-based 6-point circle. With dash line are shown the four circles that define k_{2i+1}^{j+1}.

this point, denoted with k_{2i+1}^{j+1}, is the mean of the discrete curvatures of the old points,

$$k_{2i+1}^{j+1} = \frac{k_i^j + k_{i+1}^j}{2}. \tag{2.12}$$

The same idea is used in [Cashman et al., 2013] in a generalization of the Lane–Reisenfeld algorithm. The averaging coefficients used in (2.12) are twice the odd submask $\{1/4, 1/4\}$ of the mask of second-order differences for the 4-point scheme (1.32).

In our case, the idea is to apply twice the odd submask

$$\frac{1}{64}\{-3, 19, 19, -3\}$$

of the second-order differences of the 6-point scheme (1.34) to the discrete curvature, requiring that

$$k_{2i+1}^{j+1} = -\frac{3}{32}k_{i-1}^j + \frac{19}{32}k_i^j + \frac{19}{32}k_{i+1}^j - \frac{3}{32}k_{i+2}^j. \tag{2.13}$$

Then, the external angle δ_{2i+1}^{j+1} is computed using the definition of discrete curvature,

$$k_{2i+1}^{j+1} = \frac{2\sin(\delta_{2i+1}^{j+1})}{\left\| p_i^j - p_{i+1}^j \right\|}.$$

In order to find δ_{2i+1}^{j+1} we should have $\frac{k_{2i+1}^{j+1}}{2}\left\| p_i^j - p_{i+1}^j \right\| = \sin(\delta_{2i+1}^{j+1})$ in the interval $[-1, 1]$. Unfortunately, this is not true for an arbitrary initial control polygon. A possibility is to apply some iterations of another scheme and then the circle-based 6-point scheme. In the numerical tests if the scheme is not defined for the control polygon considered, we apply one iteration of the 4-point scheme with tension parameter $w = 1/32$ that gives a new control polygon quite close to the initial one, then we can apply safely the circle-based 6-point scheme.

With equation (2.13), we require that the discrete curvature at the new point p_{2i+1}^{j+1} is a linear combination of the discrete curvatures of the points from the previous level j. Thus, we expect that the curvature of the limit curve changes continuously. Moreover, we think that (2.13) helps to prove certain conditions on the curvature, even if the discrete curvature k_i^{j+1} does not satisfy a nice recursion formula as (2.8).

Using a different scheme in the first steps of subdivision, does not change the regularity of the limit curve. In the next chapter, we use this subdivision scheme to numerically test the proposed G^2 condition.

The circle-based 6-point scheme is a circle preserving scheme once all the initial points lie on the same circle. In this case, the discrete curvatures at the starting level are all equal $k_i^0 = k$ and, since the coefficients in (2.13) sum up to 1, we have $k_{2i+1}^{j+1} = k_i^j = k$ for all $j \geq 0$. If we consider a line as a circle with 0 curvature, then the scheme retains also lines.

Chapter 3

Geometric sufficient conditions for convergence and tangent continuity

As pointed out in Section 1.3, when dealing with geometric subdivision schemes there are few general tools that can be used to prove the convergence to a limit curve and its regularity. For a geometric subdivision scheme it is worthwhile to study the continuity of geometric quantities like tangents and curvatures. In this chapter we recall the sufficient conditions presented by Dyn and Hormann [2012] to require that an interpolatory subdivision scheme is convergent and generates curves with tangent continuity (G^1 continuity). The key feature of this work is that the conditions requested are independent on the parametrization, they only depend on geometric quantities like edge lengths and angles. The conditions given are generic and can be applied to any binary interpolatory scheme. The restriction on interpolatory schemes is necessary because the proof is point-based, in the sense that they fix a generic point of the control polygon and study the behaviour of angles, edges, secants around this point in the limit. Since the scheme is interpolatory, any generated point belongs to the limit curve and the limit behaviour of angles, edges, secants gives the behaviour of lengths and tangents of the limit curve in a neighbourhood of the point. Ewald [2016] tries to generalize the conditions given by Dyn and Hormann [2012] to the case of non planar curves and non interpolatory schemes. Ewald [2016] proves that the summability of the edge length is a necessary condition for the convergence of schemes where the even rule is continuous on a set of null points. An extension of the G^1 condition has not been found yet.

In Section 3.2 we show which geometric schemes from Section 2.2 satisfy the conditions proposed by Dyn and Hormann [2012].

3.1 G^1 sufficient conditions

The classic definition of convergence (Definition 1.12) for a subdivision scheme requires a parametrization. The notion of convergence is related to the uniform convergence of

piecewise linear functions $f^j : \mathbb{R} \to \mathbb{R}^2$, $j \in \mathbb{N}$, that interpolate the points of the scheme p_i^j at certain values of the parametrization.

In order to study the convergence without an explicit parametrization, Dyn and Hormann [2012] look at the distance between the midpoint of the edge $\overrightarrow{p_i^j p_{i+1}^j}$ and the corresponding inserted point p_{2i+1}^{j+1} (see Fig. 3.1),

$$d_i^j = \left\| \frac{p_i^j + p_{i+1}^j}{2} - p_{2i+1}^{j+1} \right\|. \tag{3.1}$$

They consider the supremum of these distances at level j,

$$d^j = \sup_{i \in \mathbb{Z}} d_i^j,$$

and the sequence of these suprema

$$\boldsymbol{d} = \{d^j\}_{j \geq 0}.$$

The value of d^j gives the distance between the two control polygons at level $j+1$ and level j

$$\left\| f^{j+1} - f^j \right\|_\infty = \sup_{t \in \mathbb{R}} \left\| f^{j+1}(t) - f^j(t) \right\| = d^j.$$

Thus, the uniform convergence of the functions f^j implies that d^j is a null sequence, namely a sequence that converges to zero.

Theorem 3.1 [Dyn and Hormann, 2012]. *If $\mathcal{S}$ is convergent, then $\boldsymbol{d}$ is a null sequence.*

A similar necessary condition can be given considering the sequence of edge lengths (see Fig. 3.1),

$$e_i^j = \left\| p_{i+1}^j - p_i^j \right\|. \tag{3.2}$$

In the same way, we study the sequence of suprema

$$e^j = \sup_{i \in \mathbb{Z}} e_i^j, \qquad \boldsymbol{e} = \{e^j\}_{j \geq 0},$$

and it is clear that the behaviour of $\boldsymbol{e}$ is equal to the behaviour of the sequence $\boldsymbol{d}$.

Proposition 3.2 [Dyn and Hormann, 2012]. *The sequence $\boldsymbol{e}$ is a null sequence if and only if $\boldsymbol{d}$ is a null sequence.*

Unfortunately, the convergence to zero is not sufficient to prove that the subdivision scheme is convergent, we need a stricter condition.

Theorem 3.3 [Dyn and Hormann, 2012]. *If $\boldsymbol{d}$ is summable then $\mathcal{S}$ is convergent.*

The summability of $\boldsymbol{d}$ is sometimes hard to verify, so Dyn and Hormann [2012] show that it is equivalent to requiring the summability of $\boldsymbol{e}$, the sequence of edge lengths.
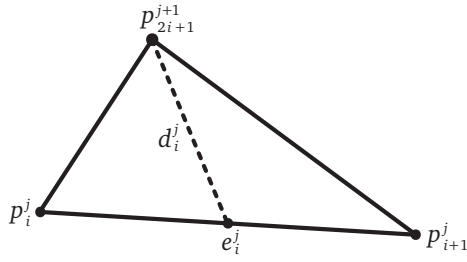
Figure 3.1. Definition of the distance d_i^j and edge length e_i^j.
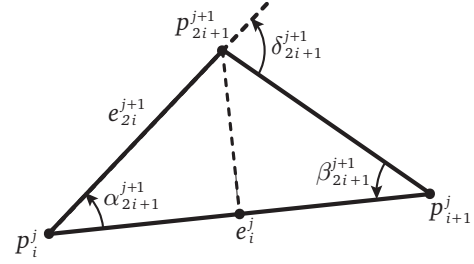
Figure 3.2. In the bisector scheme the point p_{2i+1}^{j+1} lies on the orthogonal bisector of the edge $p_i^j p_{i+1}^j$.

Proposition 3.4 [Dyn and Hormann, 2012]. *The sequence* $\boldsymbol{e}$ *is summable if and only if* $\boldsymbol{d}$ *is summable.*

It is not surprising that we ask for the summability of the edge lengths sequence. In fact, if $\boldsymbol{e}$ is a geometric sequence with ratio $\mu < 1$, then the decay

$$\frac{e^{j+1}}{e^j} = \frac{\sup_{i\in\mathbb{Z}}\left\|p_{i+1}^{j+1} - p_i^{j+1}\right\|}{\sup_{i\in\mathbb{Z}}\left\|p_{i+1}^j - p_i^j\right\|} = \mu$$

is equivalent to requiring the contractivity of the difference scheme (1.20) or the convergence condition (1.26) in the proximity setting.

In the particular case of a bisector schemes (1.9), where the new point p_{2i+1}^{j+1} lies on the bisector of the edge $\overrightarrow{p_i^j p_{i+1}^j}$, the convergence of the scheme is related to the external angles

$$\delta_i^j := \sphericalangle(\overrightarrow{p_i^j p_{i+1}^j}, \overrightarrow{p_{i-1}^j p_i^j}), \tag{3.3}$$

between two consecutive edges (see Fig. 3.3). In a bisector scheme, as shown in Figure 3.2, we have

$$e_{2i}^{j+1} = \frac{e_i^j}{2\cos\left(\delta_{2i+1}^{j+1}/2\right)}.$$

As before, we define the sequence of suprema of external angles in each level j,

$$\delta^j = \sup_{i\in\mathbb{Z}}\left|\delta_i^j\right| \quad \text{and} \quad \boldsymbol{\delta} = \{\delta^j\}_{j\geq 0}.$$

Theorem 3.5 [Dyn and Hormann, 2012]. *If* $\mathcal{S}$ *is a bisector scheme and* $\boldsymbol{\delta}$ *is a null sequence, then* $\mathcal{S}$ *is convergent.*
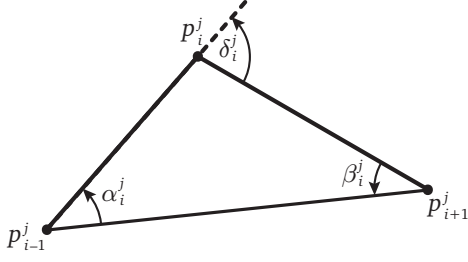
Figure 3.3. Definition of the external angle δ_i^j.
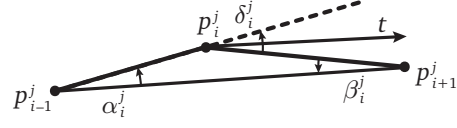
Figure 3.4. If the angle δ_i^j decays to zero, then the edges $p_{i-1}^j p_i^j$ and $p_i^j p_{i+1}^j$ both converge to the direct tangent t.

Defining the angles

$$\alpha_i^j = \measuredangle(\overrightarrow{p_{i-1}^j p_{i+1}^j}, \overrightarrow{p_{i-1}^j p_i^j}), \qquad \beta_i^j = \measuredangle(\overrightarrow{p_i^j p_{i+1}^j}, \overrightarrow{p_{i-1}^j p_{i+1}^j}), \qquad \delta_i^j = \alpha_i^j + \beta_i^j, \qquad (3.4)$$

as in Figure 3.3, the sequences

$$\alpha^j = \sup_{i \in \mathbb{Z}} \left| \alpha_i^j \right|, \quad \boldsymbol{\alpha} = \{\alpha^j\}_{j \geq 0} \quad \text{and} \quad \beta^j = \sup_{i \in \mathbb{Z}} \left| \beta_i^j \right|, \quad \boldsymbol{\beta} = \{\beta^j\}_{j \geq 0},$$

behave like $\boldsymbol{\delta}$.

Lemma 3.6 [Dyn and Hormann, 2012]. *The sequence $\boldsymbol{\delta}$ is a null sequence, if and only if both $\boldsymbol{\alpha}$ and $\boldsymbol{\beta}$ are null sequences.*

Furthermore, it turns out that the behaviour of $\boldsymbol{\delta}$ controls also the existence of continuous varying directed tangents along the curve.

Theorem 3.7 [Dyn and Hormann, 2012]. *If $\mathcal{S}$ is convergent and $\boldsymbol{\delta}$ is summable, then the limit curve is G^1 continuous.*

Corollary 3.8. *If $\mathcal{S}$ is a bisector scheme and $\boldsymbol{\delta}$ is summable, then $\mathcal{S}$ is convergent and the limit curve is G^1 continuous.*

Tangent continuity is related to the sequence of angles $\boldsymbol{\delta}$. By Definition 2.5 the tangent at a point p is the line to which both the right and the left edge converge. Requiring that $\boldsymbol{\delta}$ decays to zero, means that both edges converge to the same line, the tangent (see Fig. 3.4).

We recall some intermediate results from [Dyn and Hormann, 2012] that we need later for the proof of our new results.

The secants through the left and right neighbours of p_i^j,

$$s_i^j = \overrightarrow{p_{i-1}^j p_{i+1}^j},$$

allow to show the existence of a direct tangent in each point p_i^j of the subdivision scheme.

Lemma 3.9 [Dyn and Hormann, 2012]. *If S is convergent and δ is summable, then there exists a limit secant $\bar{s}_i^j$ through p_i^j for all $i \in \mathbb{Z}$ and $j \geq 0$.*

Lemma 3.10 [Dyn and Hormann, 2012]. *If S is convergent and δ is summable, then the limit secant $\bar{s}$ is the directed tangent line to the limit curve at p.*

In order to prove that the limit tangents $\bar{s}$ change continuously along the limit curve, they prove that for a fixed point p_0 with limit tangent $\bar{s}_0$, the points p_i^j and the edges $\overrightarrow{p_i^j p_{i+1}^j}$ in the right neighbourhood of p_0, $0 < i < 2^{j-j_0}$ and $j \geq j_0$, are in the positive ϵ–cone,

$$C^+(\epsilon) = C^+(p_0, \bar{s}_0, \epsilon) = \left\{ x : \left| \measuredangle(\overrightarrow{p_0 x}, \bar{s}_0) \right| \leq \epsilon \right\}. \tag{3.5}$$

Lemma 3.11 [Dyn and Hormann, 2012]. *If S is convergent and δ is summable, then there exists for any $\epsilon > 0$ some j_0 such that $p_i^j \in C^+(\epsilon)$ for $1 \leq i \leq 2^{j-j_0}$ and $j \geq j_0$.*

Lemma 3.12 [Dyn and Hormann, 2012]. *If S is convergent and δ is summable, then there exists for any $\epsilon > 0$ some j_0 such that $\left| \measuredangle(\overrightarrow{p_i^j p_{i+1}^j}, \bar{s}_0) \right| \leq \epsilon$ for $j \geq j_0$ and $0 \leq i < 2^{j-j_0}$.*

Summing up, Dyn and Hormann [2012] prove that the summability of edge lengths and external angles sequences are responsible for different orders of regularity of the limit curve.

Summability		Regularity	
Edge length e	$\Rightarrow$	Convergence	(3.6)
External angle δ	$\Rightarrow$	G^1 continuity	(3.7)

3.2   Examples of G^1 subdivision scheme

Dyn and Hormann [2012] introduce two subdivision schemes that satisfy the conditions (3.6) and (3.7) and both are geometric variations of the 4-point scheme: the angle-based 4-point scheme and the circle-based 4-point scheme, that we presented in Section 2.2. Both schemes are bisector schemes. By Corollary 3.8 it is sufficient to check that the δ sequence is summable, in order to prove that the schemes are convergent and G^1 continuous.

Angle-based 4-point scheme

In the angle-based 4-point scheme, the new angles are defined as the mean of the external angles δ_i^j and δ_{i+1}^j quadrisected,

$$\alpha_{2i+1}^{j+1} = \beta_{2i+1}^{j+1} = \frac{\delta_i^j + \delta_{i+1}^j}{8}.$$

Hence, the new external angles are a linear combination of the external angles from the previous level (2.9)

$$\delta_{2i}^{j+1} = \frac{-\delta_{i-1}^j + 6\delta_i^j - \delta_{i+1}^j}{8}, \qquad \delta_{2i+1}^{j+1} = \frac{\delta_i^j + \delta_{i+1}^j}{4}.$$

We look at relations of this type in order to show that the $\boldsymbol{\delta}$ sequence is summable. In this case one iteration is not sufficient, because $\left|\delta^{j+1}\right| \leq \delta^j$. Iterating another time we find

$$\delta_{4i}^{j+2} = \frac{-\delta_{i-1}^j + 4\delta_i^j - \delta_{i+1}^j}{8}, \qquad\qquad \delta_{4i+1}^{j+2} = \frac{-\delta_{i-1}^j + 8\delta_i^j + \delta_{i+1}^j}{32},$$

$$\delta_{4i+2}^{j+2} = \frac{\delta_{i-1}^j + 7\delta_i^j + 7\delta_{i+1}^j + \delta_{i+2}^j}{64}, \qquad\qquad \delta_{4i+3}^{j+2} = \frac{\delta_{i-1}^j + 8\delta_i^j - \delta_{i+1}^j}{32}.$$

So,

$$\left|\delta^{j+2}\right| \leq \max\left\{\frac{3}{4}, \frac{5}{16}, \frac{1}{4}, \frac{5}{16}\right\} \delta^j = \frac{3}{4}\delta^j,$$

and $\boldsymbol{\delta}$ is summable. Therefore, the angle-based 4-point scheme is G^1 continuous.

Circle-based 4-point scheme

For the circle-based 4-point scheme we show in (2.10) that the angles are defined as

$$\alpha_{2i+1}^{j+1} = \beta_{2i+1}^{j+1} = \frac{\alpha_i^j + \beta_{i+1}^j}{4},$$

and the external angles are

$$\delta_{2i}^{j+1} = \frac{-\alpha_i^j + 3\delta_i^j - \beta_{i+1}^j}{4}, \qquad \delta_{2i+1}^{j+1} = \frac{\alpha_i^j + \beta_{i+1}^j}{2}.$$

Whenever i is an odd index we have $\alpha_i^j = \beta_i^j = \delta_i^j/2$, by definition of the bisector scheme. So, the external angles are bounded by

$$\left|\delta_{2i}^{j+1}\right| \leq \frac{5}{4}\delta^j, \qquad \left|\delta_{2i+1}^{j+1}\right| \leq \frac{3}{4}\delta^j.$$

Unfortunately, these relations are not sufficient to prove that the $\boldsymbol{\delta}$ sequence is summable. Computing the relation for another step, we find

$$\left|\delta_{4i}^{j+2}\right| \leq \delta^j, \quad \left|\delta_{4i+1}^{j+2}\right| \leq \frac{13}{16}\delta^j, \quad \left|\delta_{4i+2}^{j+2}\right| \leq \frac{19}{16}\delta^j, \quad \left|\delta_{4i+3}^{j+2}\right| \leq \frac{13}{16}\delta^j,$$

and again we cannot conclude that $\boldsymbol{\delta}$ sequence is summable. Denoting with μ_k the maximum bound at the level $j+k$, Dyn and Hormann [2012] show that after 10 iteration they find a bound $\mu_{10} < 1$ such that $\left|\delta^{j+k}\right| \leq \mu_{10}\delta^j$. In the end, the sequence of external angles $\boldsymbol{\delta}$ turns out to be summable and the circle-based 4-point scheme is G^1 continuous.

Incenter scheme

We already mentioned that also the incenter scheme is G^1 continuous. The proof does not use the summability of δ (3.7) because, by introducing the correction terms into the tangents, the expression of the angles become complicated. Instead in [Hernández-Mederos et al., 2013], the G^1 condition (3.7) is used to prove that the generalization of the incenter scheme produces limit curves that are tangent continuous. The same is done also for two other schemes [Deng and Ma, 2012, 2014]. In both cases, (3.7) is satisfied and the schemes turn out to be G^1 continuous.

Chapter 4

Geometric condition for curvature continuity

Following the idea of Dyn and Hormann [2012], in the Section 4.1 of this chapter, we suggest a sufficient condition in order to have a limit curve with continuous curvature (G^2 continuity).

The correctness of this condition is discussed and tested in Section 4.2 with some numerical examples of G^2 continuous schemes.

In Section 4.3 we first give the idea of the proof divided in three main steps. Then, we present what we already proved: the first step is completely proved while there is missing a part of the second step. This missing part does not allow us to prove completely also the third step. In particular, we show that at any point of the subdivision scheme there exists a limit circle but we do not prove yet that this circle is the osculating circle to the limit curve. Once we prove this, the denseness of the points generated by the scheme on the limit curve allows us to conclude that the curvature of the limit curve is continuous.

4.1 G^2 sufficient condition

We saw in Section 2.1 that a curve is G^2 continuous if there exists at every point an osculating circle and if the curvatures of two osculating circles at neighbouring points are ϵ-close (cf. Definition 2.9). The osculating circle at a point p is defined as the limit position of the discrete interpolating circles at p (see Definition 2.8).

In order to satisfy these conditions we study the curvature k_i^j of the discrete interpolating circle passing through three consecutive points $p_{i-1}^j, p_i^j, p_{i+1}^j$ and we introduce

$$\nabla k_i^j := \left| k_{i+1}^j - k_i^j \right|. \tag{4.1}$$

If e_i^j measures the distance between two consecutive points and δ_i^j measures the angle

between two consecutive edges, then ∇k_i^j measures the difference between two discrete curvatures. Similar to (3.2) and (3.3) we take the supremum of ∇k_i^j over the level j and we study the behaviour of the sequence of these suprema,

$$\nabla k^j = \sup_{i \in \mathbb{Z}} \nabla k_i^j, \qquad \nabla \boldsymbol{k} = \{\nabla k^j\}_{j \geq 0}.$$

Similarly to conditions (3.6) and (3.7), we suppose the sequence $\nabla \boldsymbol{k}$ is summable in order to generate G^2 continuous limit curve. The main goal of my work is to prove this conjecture.
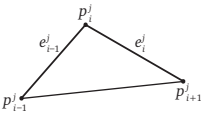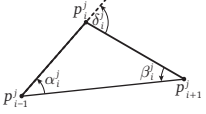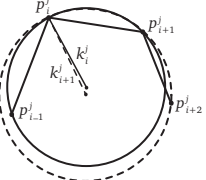
Conjecture 4.1. *Let $\mathcal{S}$ be an interpolatory subdivision scheme, such that*

1. *the sequence of edges $\boldsymbol{e}$,*

2. *the sequences of external angles $\boldsymbol{\delta}$,*

3. *the sequence of curvature differences $\nabla \boldsymbol{k}$,*

are summable, then the limit curve generated is G^2 continuous.

The request of the summability of $\nabla \boldsymbol{k}$ means that the difference between the discrete curvatures k_{i+1}^j and k_i^j decays to 0 for any $i \in \mathbb{Z}$ as j increases to infinity. In the limit, the discrete curvature k_i^j should converge pointwise to the curvature of the limit curve. Combining together these two aspects, the summability of $\nabla \boldsymbol{k}$ should imply that the curvature change continuously along the limit curve.

The sufficient geometric conditions requested for each order of regularity can be summarized as

	Summability		**Regularity**	
	Edge length $\boldsymbol{e}$		$\Rightarrow$ Convergence	
	External angle $\boldsymbol{\delta}$		$\Rightarrow$ G^1 continuity	
	Difference of curvatures $\nabla \boldsymbol{k}$	$\Rightarrow$	G^2 continuity	(4.2)

In order to prove the conjecture, at certain point, we need to consider a stricter condition on the sequences $\boldsymbol{\delta}$ and $\nabla \boldsymbol{k}$: we ask that $\boldsymbol{\delta}$ and $\nabla \boldsymbol{k}$ behave like geometric

sequences. It means that the two sequences are bounded by two geometric sequences with ratios μ_δ, $\mu_k < 1$,

$$\delta^j = O(\mu_\delta^j), \quad \text{and} \quad \nabla k^j = O(\mu_k^j).$$

These conditions allow to compare the decay of $\boldsymbol{\delta}$ with the decay of $\nabla \boldsymbol{k}$. Conjecture 4.1 requires the summability of the sequences, because much of what we prove is true with this hypothesis and we hope that we can generalise the few results that need a stricter condition.

Before trying to prove Conjecture 4.1, we would like to check, with some numerical tests, if the requirement on the summability of $\nabla \boldsymbol{k}$ (4.2) is reasonable or not.

4.2 Numerical tests

To test our condition (4.2) we consider different interpolatory subdivision schemes, both G^1 and G^2 continuous. All the subdivision schemes considered are convergent so we do not need to check the summability of $\boldsymbol{e}$. For each of them we plot the values of the discrete curvature after 2, 5 and 8 iterations of the subdivision scheme. In this way we visualise if the discrete curvatures at a point p_i^j converge in the limit and if the curvature varies continuously along the limit curve. From level to level we expect that the discrete curvature plots are close and have no jumps.

To test the G^1 (3.7) and G^2 (4.2) conditions we compute the sequences $\boldsymbol{\delta}$ and $\nabla \boldsymbol{k}$ and we display the ratios δ^{j+1}/δ^j and $\nabla k^{j+1}/\nabla k^j$ depending on j for the initial control polygon considered. If the ratio is less than 1, then it means that the corresponding sequence behaves like a geometric sequence and is summable.

In total we test 6 different schemes: the first 3 schemes are G^1 continuous, so we verify that $\boldsymbol{\delta}$ is summable while $\nabla \boldsymbol{k}$ is not. Instead, for the second 3 schemes which are G^2 continuous we verify that both $\boldsymbol{\delta}$ and $\nabla \boldsymbol{k}$ are summable.

4-point scheme

As shown in Section 1.4.1, the 4-point scheme is only C^1 continuous with Hölder regularity $C^{2-\epsilon}$. In general the generating limit curve is not G^1 continuous. If the scheme does not generate artefacts such as cusps, then the limit curve is not only C^1 but also G^1 continuous. This is the case of the limit curves in Figure 4.1. Analysing the behaviour of the discrete curvatures we expect that the limit curve is not G^2 continuous. In fact, the curvature of the discrete interpolating circles increase considerably in each step of the subdivision process. For these examples we expect that the 4-point scheme satisfies the G^1 condition (3.7) and not the G^2 condition. Figure 4.2 confirms this hypothesis, because the ratio of decay of the $\boldsymbol{\delta}$ sequence is strictly less than 1, while the ratio of $\nabla \boldsymbol{k}$ converges to 1. It is well know that we cannot say anything about the behaviour of a geometric sequence with ratio 1. The 4-point scheme is almost C^2 continuous, to verify that a C^1 scheme does not satisfy our Condition (4.2) we analyse a different scheme.

Figure 4.1. Top: Limit curve after 8 iterations of the 4-point scheme for different control polygons. Bottom: Discrete curvatures after 2, 5, 8 iterations (from dark blue to light blue).

(a) δ^{j+1}/δ^j

(b) $\nabla k^{j+1}/\nabla k^j$

Figure 4.2. Ratio of decay of the sequences $\boldsymbol{\delta}$ (a) and $\nabla \boldsymbol{k}$ (b) for the three different control polygons in the Figure 4.1, applying the 4-point scheme.

Figure 4.3. Top: Limit curve after 8 iterations of the 4-point scheme with tension parameter $w = 1/32$ for different control polygons. Bottom: Discrete curvatures after 2, 5, 8 iterations (from dark blue to light blue).

(a) δ^{j+1}/δ^j

(b) $\nabla k^{j+1}/\nabla k^j$

Figure 4.4. Ratio of decay of the sequences δ (a) and ∇k (b) for the three different control polygons in the Figure 4.3, applying the 4-point scheme with tension parameter $w = 1/32$.

Figure 4.5. Top: Limit curve after 8 iterations of the circle-based 4-point scheme for different control polygons. Bottom: Discrete curvatures after 2, 5, 8 iterations (from dark blue to light blue).

(a) δ^{j+1}/δ^{j}

(b) $\nabla k^{j+1}/\nabla k^{j}$

Figure 4.6. Ratio of decay of the sequences δ (a) and ∇k (b) for the three different control polygons in Figure 4.5, applying the circle-based 4-point scheme.

4-point scheme with tension parameter

We recall in Section 1.4.2 that the 4-point scheme with tension parameter w is C^1 continuous if we choose $w \in \left(0, \frac{\sqrt{5}-1}{8}\right)$. In the considered examples, we fix $w = 1/32$ that corresponds to taking the mean of the masks of the 2-point and 4-point scheme. Comparing with the 4-point scheme, we expect that the limit curve generated by this scheme is less regular. From Figure 4.3 we can observe that the discrete curvatures increase rapidly in each iteration of the scheme. This means that the discrete curvatures k_i^j do not converge. The behaviour of the sequences δ and ∇k confirms this. In Figure 4.4 we see that the ratio of the δ sequence is less then 1, while the ratio of ∇k is definitely larger than 1, so ∇k is not summable.

Circle-based 4-point scheme

The circle-based 4-point scheme is G^1 continuous as we show in Section 3.2. It is not G^2 continuous, in fact in Figure 4.5 the discrete curvatures increase notably as we iterate the subdivision scheme. This behaviour states that the discrete curvature does not converge at the limit. In Figure 4.6 we can observe that the ratio of δ is less than 1, while the ratio of ∇k converges to 1. Hence, the circle-based 4-point scheme satisfies the G^1 condition (3.7) but not the G^2 condition (4.2).

6-point scheme

The 6-point scheme generates limit curves that are C^2 continuous as proved in Section 1.4.1. We show that C^2 continuity does not imply G^2 continuity in general, but if we avoid some particular cases we can assume that a C^2 curve is also G^2. This is the case in the examples considered.

   The plots in Figure 4.7 (bottom) reveal that the discrete curvature is continuous: the plot after 5 iterations is almost indistinguishable from the plot at 8 iterations. The curvature does not grow indefinitely and converges to a continuous function. In this case we expect that the G^2 condition (4.2) is satisfied. Indeed, both the ratio of decay of δ and ∇k are less then 1, so the sequences are summable.

Incenter scheme

As the authors Deng and Wang [2010] claim, the incenter scheme is G^2 continuous. The plots of the discrete curvatures converge in few iterations to a continuous function (see Fig. 4.9). Moreover, we can observe that the conditions for G^1 (3.7) and G^2 (4.2) continuity are both satisfied by these examples, in fact Figure 4.10 shows that the ratio of δ and ∇k is less than 1, so both sequences are summable.
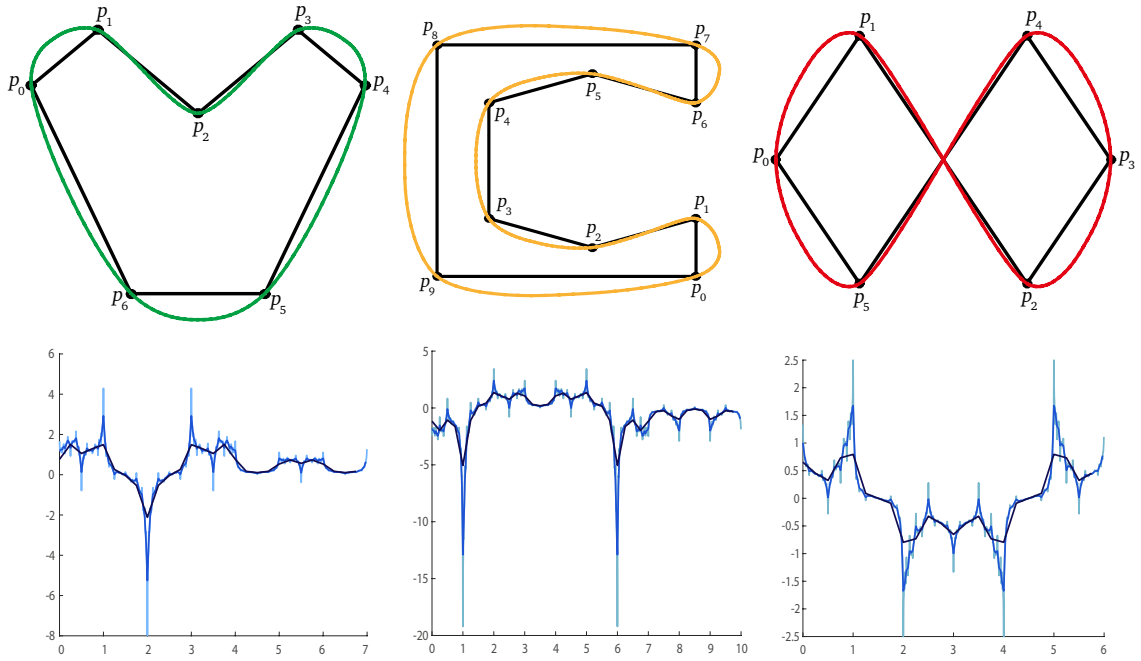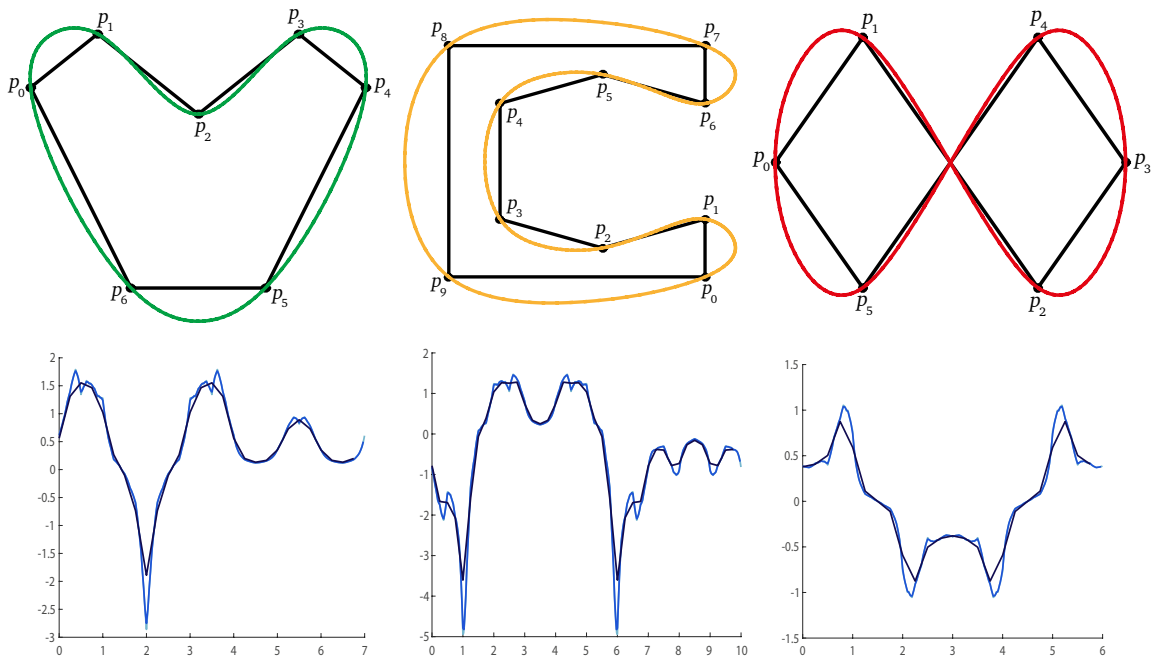
Figure 4.7. Top: Limit curve after 8 iterations of the 6-point scheme for different control polygons. Bottom: Discrete curvatures after 2, 5, 8 iterations (from dark blue to light blue).
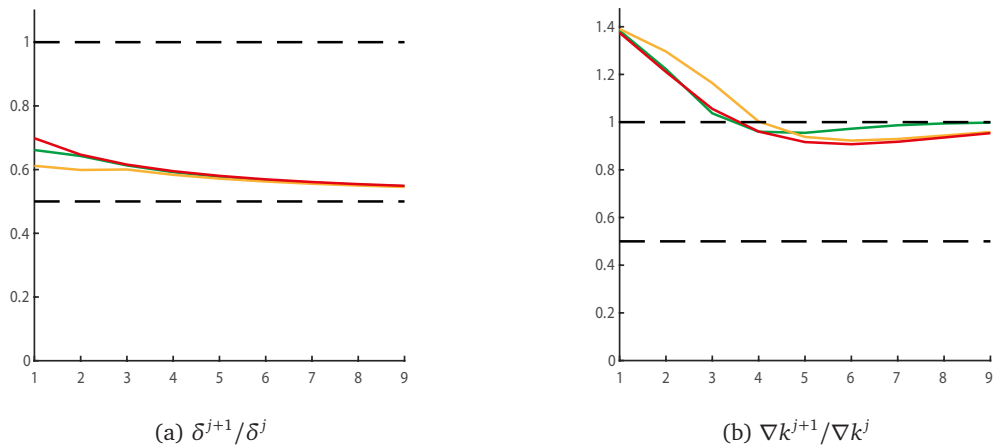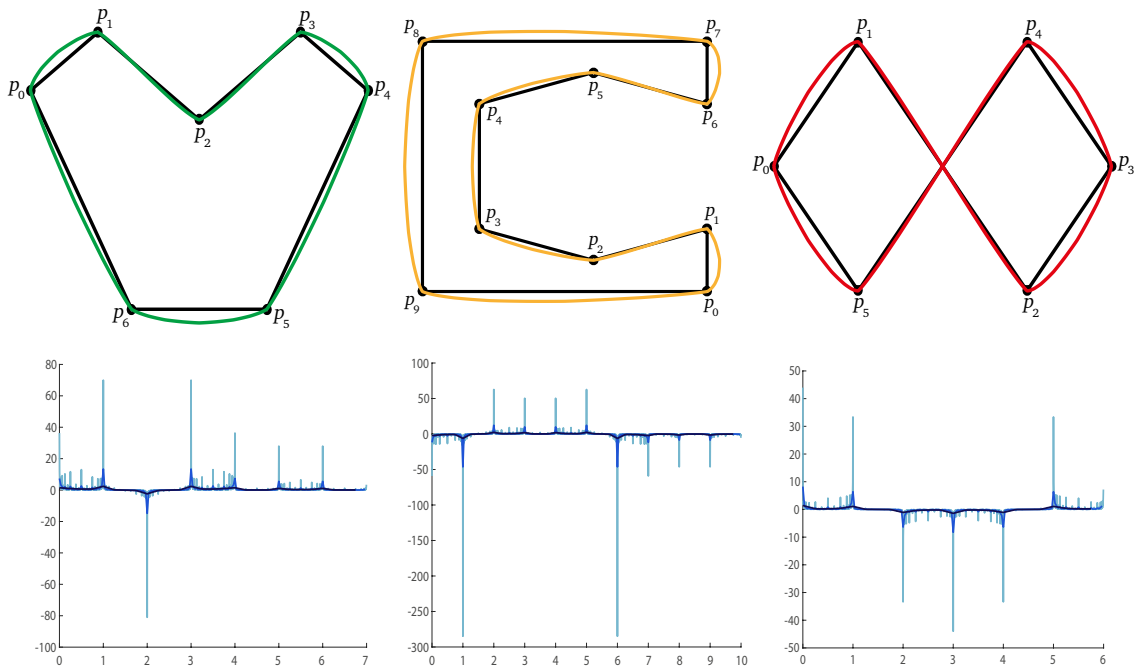

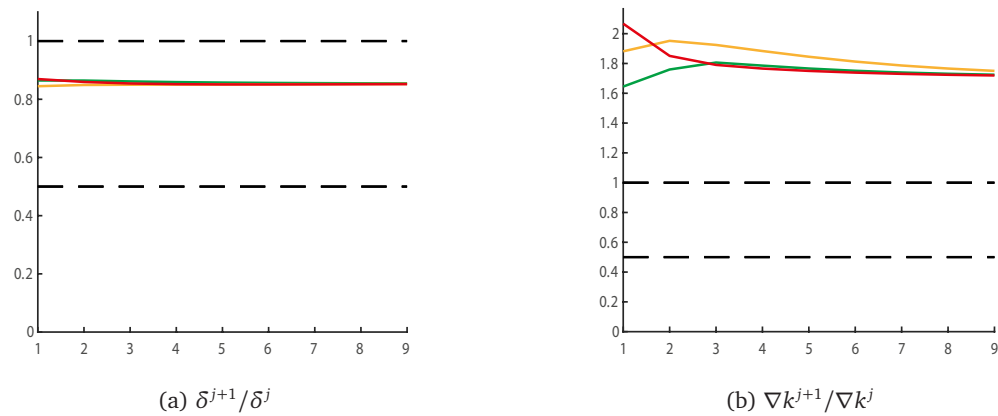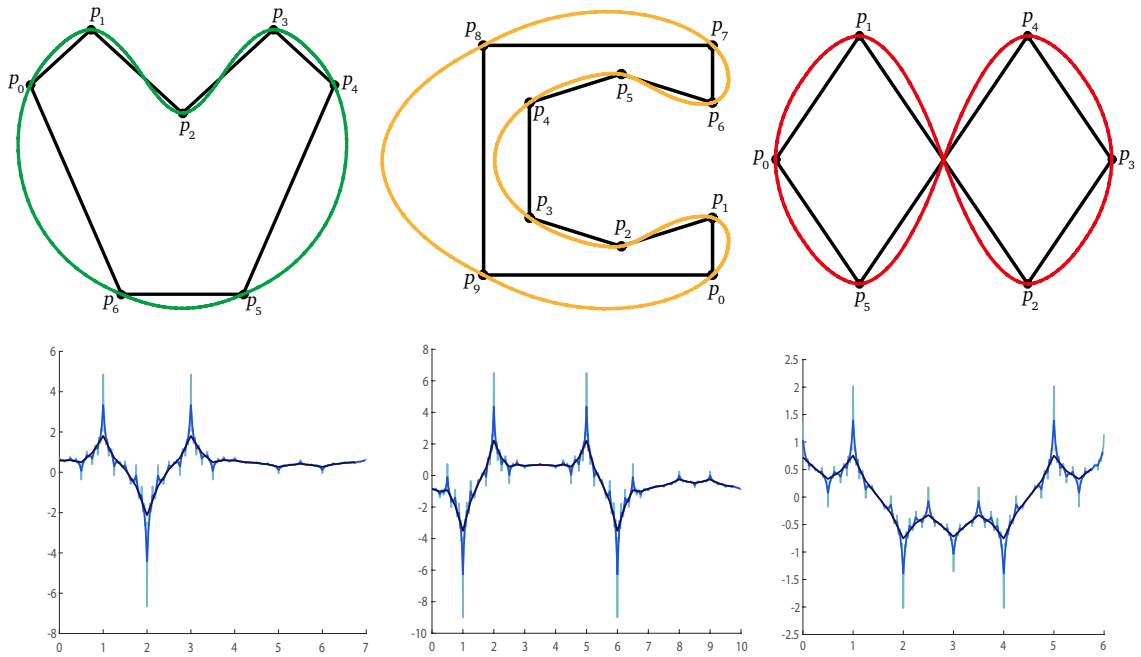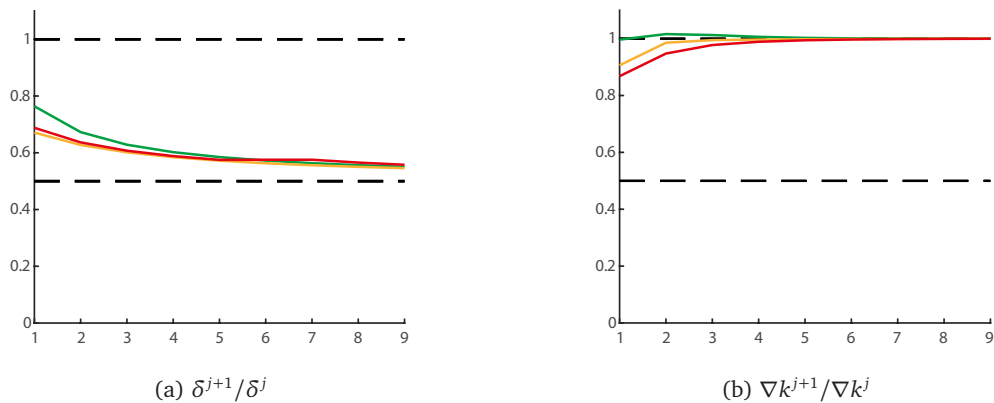(a) δ^{j+1}/δ^{j} (b) $\nabla k^{j+1}/\nabla k^{j}$

Figure 4.8. Ratio of decay of the sequences $\boldsymbol{\delta}$ (a) and $\boldsymbol{\nabla k}$ (b) for the three different control polygons in Figure 4.7, applying the 6-point scheme.
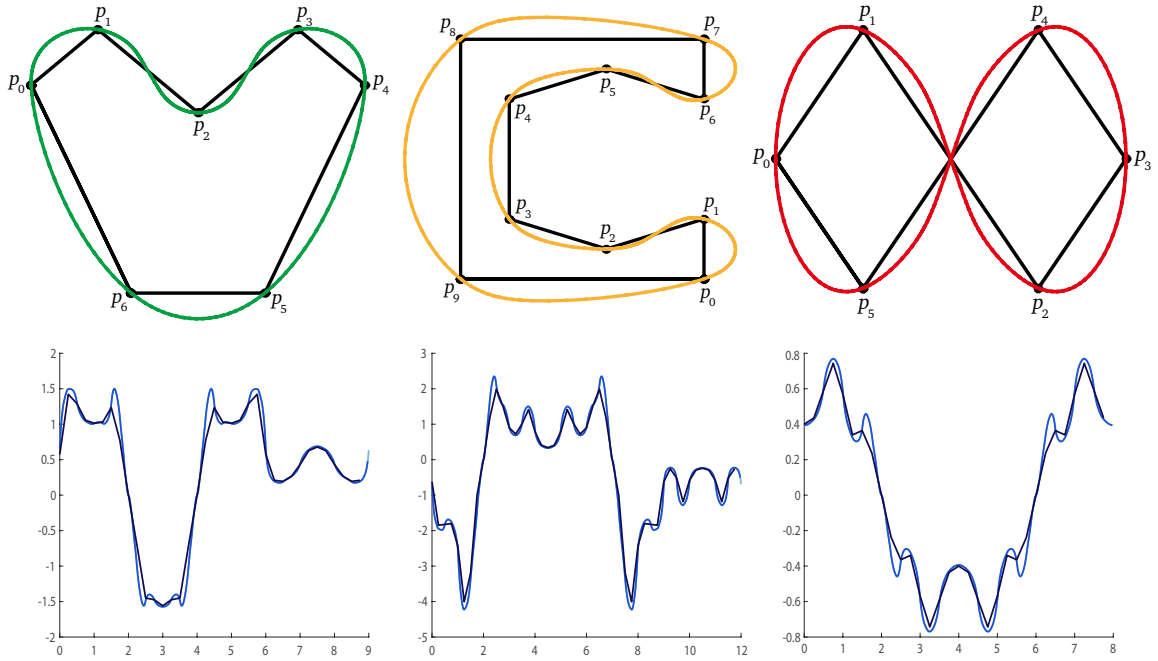
Figure 4.9. Top: Limit curve after 8 iterations of the incenter scheme for different control polygons. Bottom: Discrete curvatures after 2, 5, 8 iterations (from dark blue to light blue).

(a) δ^{j+1}/δ^{j} (b) $\nabla k^{j+1}/\nabla k^{j}$

Figure 4.10. Ratio of decay of the sequences δ (a) and ∇k (b) for the three different control polygons in Figure 4.9, applying the incenter scheme.

Figure 4.11. Top: Limit curve after 8 iterations of the circle-based 6-point scheme for different control polygons. Bottom: Discrete curvatures after 2, 5, 8 iterations (from dark blue to light blue).

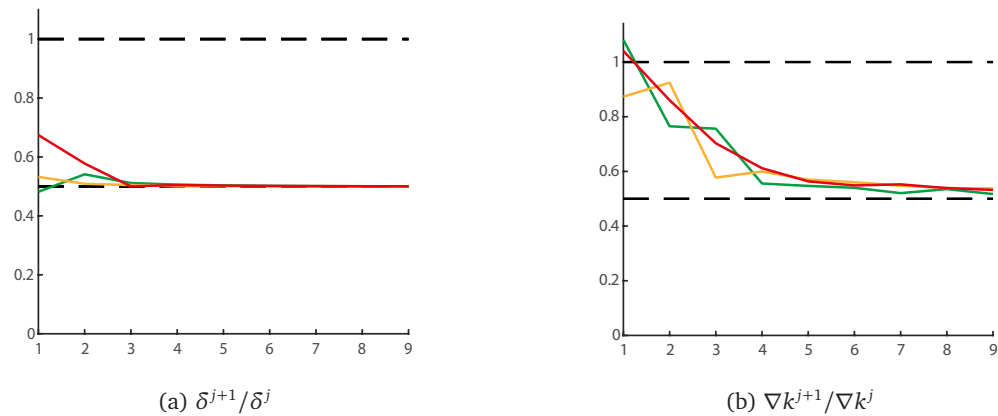(a) δ^{j+1}/δ^{j}

(b) $\nabla k^{j+1}/\nabla k^{j}$

Figure 4.12. Ratio of decay of the sequences δ (a) and ∇k (b) for the three different control polygons in Figure 4.11, applying the circle-based 6-point scheme.
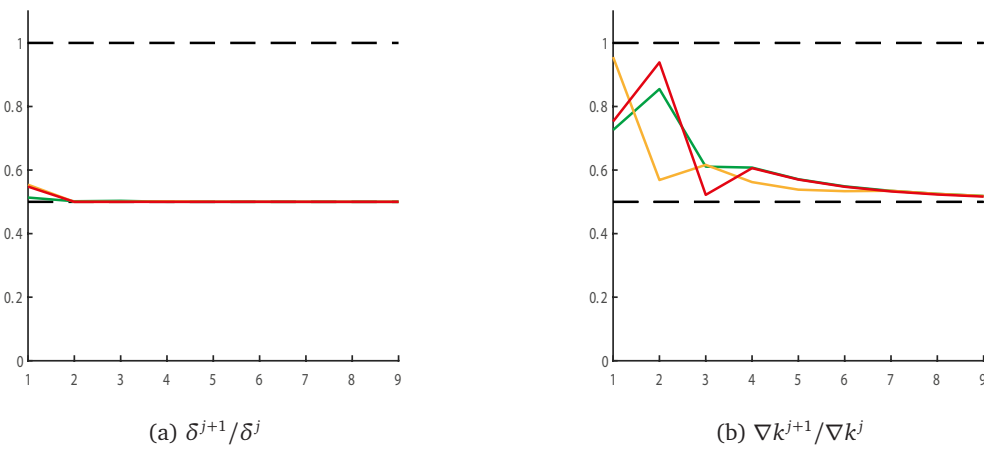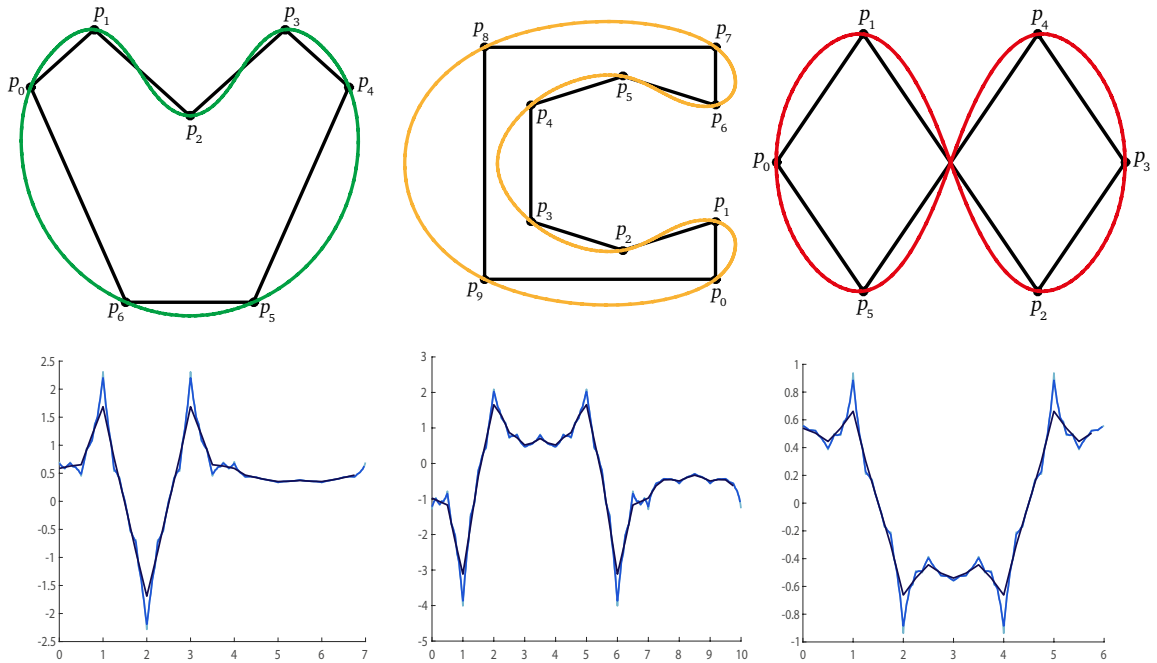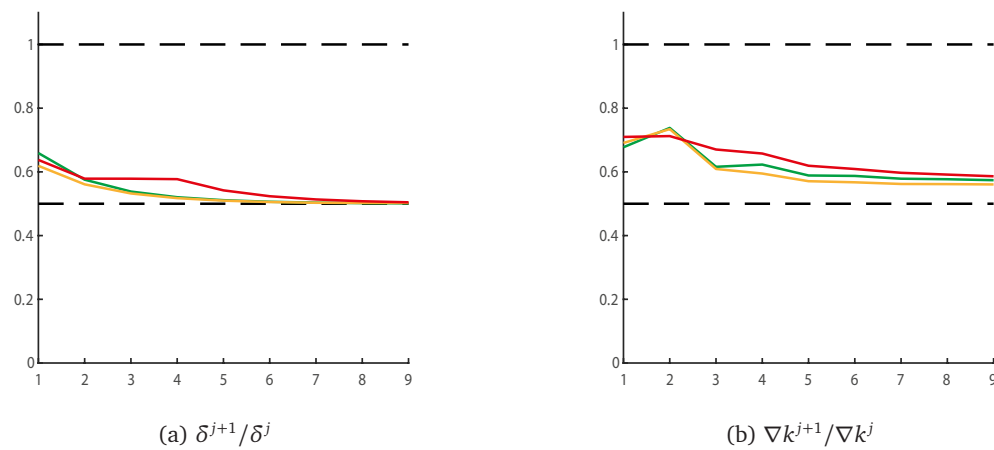
Circle-based 6-point scheme

Finally, we test the scheme that we design in order to obtain G^2 continuous limit curves:
the circle-based 6-point scheme. The difference between the discrete curvature plots
at 5 and 8 iterations of the subdivision schemes is hardly visible in Figure 4.11. The
discrete curvatures converge to a function with some spikes but without jumps and the
limit curvature is a continuous function. Looking at Figure 4.12 we see that the ratio of
δ and ∇k is strictly less then 1, so the two sequences are summable and they satisfy the
G^1 (3.7) and G^2 (4.2) conditions.

From these tests we have reason to think that the G^2 condition presented in (4.2) is
correct. Clearly, numerical examples can give us only an intuition and we still have to
prove that the summability of ∇k gives a limit curve that is G^2 continuous.

4.3   Evidence of Conjecture 4.1

Here we try to prove Conjecture 4.1: let consider an interpolatory scheme such that the
sequences e, δ and ∇k are summable then the subdivision scheme generates a limit
curve with continuous curvature. By Theorem 3.3 and 3.7 the summability of e and δ
gives respectively the convergence and the G^1 continuity of the limit curve. So, we focus
on proving that the summability of the sequence ∇k induces a limit curve that is G^2
continuous. For the concept of curvature continuity we refer to Definition 2.9.

By hypothesis the subdivision scheme $\mathcal{S}$ is interpolatory, from a level $j_0 \geq 0$ on, the
points $p_i^{j_0}$, $\forall i \in \mathbb{Z}$, are kept by the scheme $p_{2^{j-j_0}i}^{j} = p_i^{j_0}$. In the limit they belong to the
limit curve. For the sake of simplicity, all the results are proved for a point denoted by
p_0^0 but hold for any other point generated by the scheme.

From Definition 2.9 of curvature continuity we should verify that the curvature of
the limit curve is well defined at p_0^0 and it is ϵ-close to the curvatures of any point in a
neighbourhood of p_0^0. The idea of the proof of Conjecture 4.1 is explained below.

Idea of the proof:

Step 1   *The sequence of discrete interpolating circles $\{C_0^j\}_{j\geq 0}$ converges*

$$\lim_{j\to+\infty} C_0^j = \bar{C}_0,$$

where C_0^j is the discrete circle passing through p_{-1}^j, p_0, p_1^j.

As shown in Section 2.1, a circle can be defined by its tangent line and curvature. In this sense, to prove the existence of $\bar{C}_0$ is sufficient to show:

1.1 The tangents of the discrete interpolating circles at p_0 converge to the directed tangent of the limit curve at p_0 (Proposition 4.2)
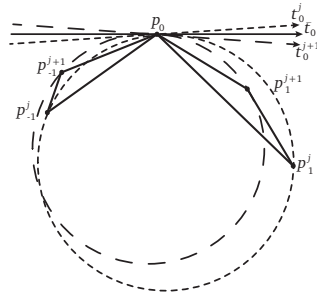
$$\lim_{j\to\infty} t_0^j = \bar{t}_0.$$

1.2 The curvatures of the discrete interpolating circles converge (Proposition 4.4)
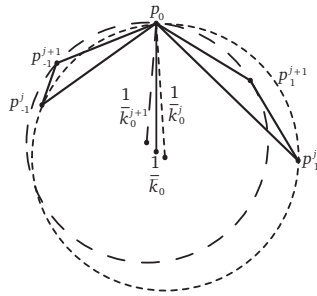
$$\lim_{j\to\infty} k_0^j = \bar{k}_0.$$

Step 2 *The circle $\bar{C}_0$ is the osculating circle at p_0 of the limit curve generated by $\mathcal{S}$.*

To prove this we exploit Proposition 2.2 where we proved that the osculating circle at p_0 can be seen as the limit of the circles with direct tangent $\bar{t}_0$ and passing through p_0 and a neighbouring point. To achieve this we have to prove:

2.1 The curvatures of the circles with tangent $\bar{t}_0$ and passing through p_0 and p_1^j converge to $\bar{k}_0$ (Proposition 4.9)
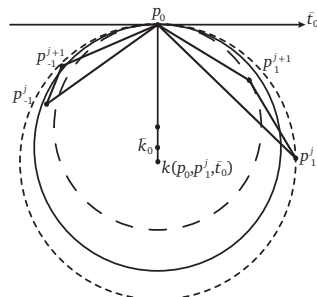
$$\lim_{j\to\infty} k(p_0, p_1^j, \bar{t}_0) = \bar{k}_0.$$

(This result is true in the stricter condition that δ and ∇k behave like geometric sequences).

2.2 In a neighbourhood of p_0 the curvatures of the circles passing through p_0 and two following points in the neighbourhood converge to $\bar{k}_0$ (Conjecture 4.13)
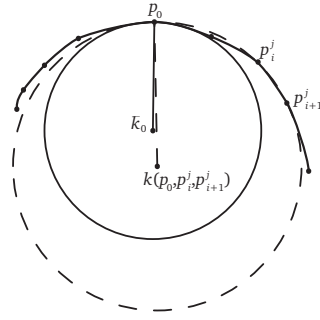
$$\exists j_0 \geq 0$$
$$\lim_{j \to \infty} k(p_0, p_i^j, p_{i+1}^j) = \bar{k}_0,$$
$$\forall i, \quad 0 < i \leq 2^{j-j_0}.$$

2.3 The curvatures of the circles with directed tangent $\bar{t}_0$ and passing through p_0 and a point in a neighbourhood of p_0, converge to $\bar{k}_0$ (Conjecture 4.14)
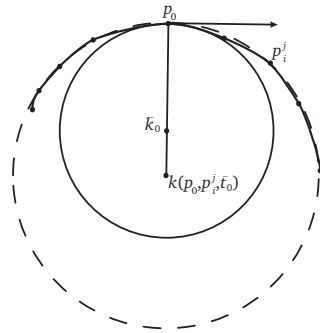
$$\exists j_0 \geq 0$$
$$\lim_{j \to \infty} k(p_0, p_i^j, \bar{t}_0) = \bar{k}_0,$$
$$\forall i, \quad 0 < i \leq 2^{j-j_0}.$$

The last two points are conjectures because they still need to be proved but we have some numerical evidences that show they are likely to be true.

Step 3 *The curvature along the limit curve varies continuously.*

We need to show that every couple of neighbouring points have curvatures that are ϵ-close.

3.1 For any ϵ there exists some level j_0 such that the limit curvature for each point p_i^j, in the neighbourhood of p_0, is ϵ-close to $\bar{k}_0$ (Proposition 4.15)

$$\exists j_0 \geq 0$$
$$\left| \bar{k}_0 - \bar{k}_i^j \right| < \epsilon,$$
$$\forall i, \quad 0 < i < 2^{j-j_0}.$$
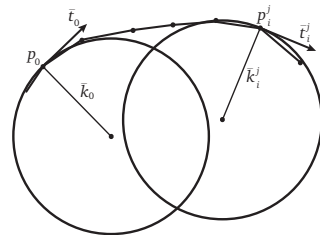
3.2 Fixed a point on the limit curve p, any point r on the limit curve that approaches p has curvature that converges to the curvature at p (Conjecture 4.16)
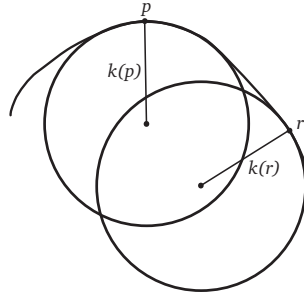
$$\lim_{r \to p} k(r) = k(p).$$

This last point is not proved yet. To prove it, we have to exploit the denseness of the points generated by the subdivision scheme $\mathcal{S}$ on the limit curve and Conjectures 4.13 and 4.14.

In the following sections we give the details for each steps.

4.3.1   Step 1

We start by proving that the sequence of discrete interpolating circles $\{C_0^j\}_{j \geq 0}$ converges to a circle $\bar{C}_0$. By Definition 2.7, the discrete interpolating circle C_0^j is the circle passing through p_{-1}^j, p_0 and p_1^j. The point p_0 is fixed at each step, while p_{-1}^j and p_1^j change. The circle C_0^j is characterize by the tangent t_0^j at p_0^j and the discrete curvature k_0^j,

$$k_0^j = \frac{2 \sin \delta_0^j}{\left\| p_1^j - p_{-1}^j \right\|}.$$

The sequence of discrete interpolating circles converges if the sequences of tangents $\{t_0^j\}_{j \geq 0}$ and discrete curvatures $\{k_0^j\}_{j \geq 0}$ converge.

Using Lemmas 3.9 and 3.10 proved in [Dyn and Hormann, 2012] we show that the sequence of tangents t_0^j converges to the direct tangent at p_0.

Proposition 4.2. *If $\mathcal{S}$ is convergent and δ is summable, then the tangents at p_0 to the discrete interpolating circles C_0^j converge to the directed tangent of the limit curve*

$$\lim_{j \to \infty} t_0^j = \bar{t}_0.$$

Proof: For every level of subdivision j we define as

$$\sigma_0^j = \sphericalangle(\overrightarrow{p_0^j p_1^j}, t_0^j) \tag{4.3}$$

the angle between the segment $\overrightarrow{p_0^j p_1^j}$ and the tangent t_0^j at p_0^j to the circle C_0^j. From Figure 4.13 we observe that $\left| \sigma_0^j \right| \leq \left| \delta_0^j \right|$ for all $j \geq 0$. By hypothesis the sequence δ
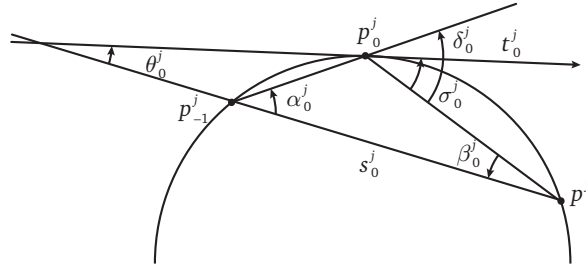
Figure 4.13. Circle passing through p_{-1}^j, p_0^j, p_1^j with tangent t_0^j at p_0^j.

is summable, which means that the general term $\delta^j = \sup_{i \in \mathbb{Z}} \left| \delta_i^j \right|$ decays to zero. In particular, for fixed ϵ, there exists an initial level, that we denote with 0, such that for all $j \geq 0$

$$\left| \delta_0^j \right| < \epsilon. \tag{4.4}$$

Since σ_0^j is bounded by δ_0^j, for all $j \geq 0$ we have

$$\left| \sigma_0^j \right| < \epsilon. \tag{4.5}$$

We call θ_0^j the angle between the secant s_0^j and the tangent t_0^j,

$$\theta_0^j = \sphericalangle(\overrightarrow{p_{-1}^j p_{+1}^j}, t_0^j) = \pi - \left(\sphericalangle(\overrightarrow{p_{-1}^j p_0^j}, \overrightarrow{p_{+1}^j p_{-1}^j}) + \sphericalangle(-t_0^j, \overrightarrow{p_0^j p_{-1}^j}) \right)$$

$$= \pi - \left(\pi - \alpha_0^j - \sigma_0^j + \alpha_0^j + \beta_0^j \right) = \sigma_0^j - \beta_0^j. \tag{4.6}$$

From (4.5) we have that for all $j \geq 0$, σ_0^j decays to zero. Moreover, $\left| \beta_0^j \right| < \epsilon$ for all $j \geq 0$ because $\delta_0^j = \alpha_0^j + \beta_0^j$ and δ is a null sequence (4.4).

If the secant s_0^j is parallel to the tangent t_0^j, then $\theta_0^j = 0$ by definition. This means that for all $\epsilon > 0$ and for all $j \geq 0$,

$$\left| \theta_0^j \right| = \left| \sphericalangle(\overrightarrow{p_{-1}^j p_1^j}, t_0^j) \right| = \left| \sphericalangle(s_0^j, t_0^j) \right| < \epsilon.$$

Then,

$$\lim_{j \to \infty} s_0^j = \lim_{j \to \infty} t_0^j.$$

From Theorem 3.9 and 3.10, we know that the limit secant $\bar{s}_0$ is the directed tangent $\bar{t}_0$ at p_0 to the limit curve. For the uniqueness of the limit, we have that

$$\lim_{j \to \infty} t_0^j = \bar{t}_0.$$

The tangents to the discrete interpolating circles converge to the directed tangent to the limit curve at each point. □

We have to prove that also the sequence of discrete curvatures k_0^j converges. In order to prove this we need a simple geometric result that follows from the well-known theorem in Euclid's *Elements*: any angle inscribed in the circle C is half of the central angle that subtends the same arc.

Lemma 4.3. *Consider a circle C, any external angle θ' measures less than any inscribed angle θ that stands on the same chord. Instead any internal angle θ'' is bigger than any inscribed angle θ that stands on the same chord (see Fig. 4.14),*

$$\theta' < \theta < \theta''.$$
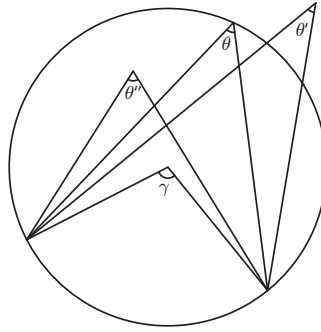
Figure 4.14. Comparison between angles outside θ', inscribed θ and inside θ'' a circle.

Proof: In this Lemma all the angles are meant as unsigned angles.

From the well known result of Euler in its *Elements*, any angle inscribed in the circle C is half of the central angle that subtends the same arc, so we can compare the external angle θ' with any angle inscribed in the circle.

We consider θ as shown in Figure 4.15a for simplicity. Then,

$$\theta' = \pi - (\alpha' + \beta') = \pi - (\pi - \theta - \gamma) - (\pi - \delta) = \theta + \gamma - \pi + \delta$$
$$= \theta - (\pi - \gamma - \delta) = \theta - \sigma.$$

All the angles are positive, thus we have

$$\theta' < \theta.$$

Otherwise, if we consider a point inside the circle, then looking to Figure 4.15b we have

$$\theta'' = \theta + (\beta - \beta''),$$

the angle $\beta - \beta''$ is positive, so we conclude

$$\theta'' > \theta.$$

$\square$
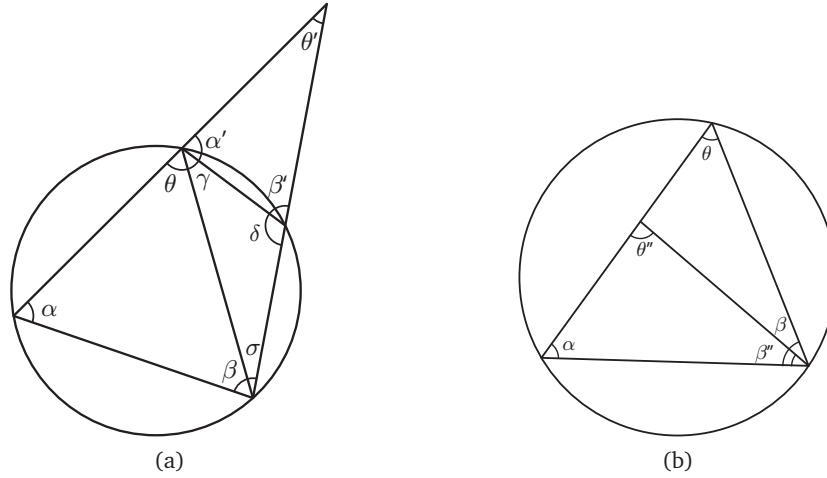
Figure 4.15. Geometric relations between angles outside θ' (a), inside θ'' (b) the circle and an inscribed angle θ.

Remark 4.1. Lemma 4.3 is true for positive angles, in case that θ, θ', $\theta'' < 0$ we simply reverse the order of the inequalities

$$\theta'' < \theta < \theta'.$$

This is helpful to give some general rules that link the point positions and the sign of the discrete curvature.

Remark 4.2. Suppose we fix one or two points in a triangle and vary the others, we study how the sign of the related discrete curvatures varies.

(a) We fix two points q and r and we move the central point p. As shown in Figure 4.16a, if p is in the half-plane above the segment $\overrightarrow{qr}$, then all the angles of the triangle are positive and also the discrete curvature is positive. Otherwise, if p is below the segment $\overrightarrow{qr}$, the angles of the triangle are negative, then also the discrete curvature is negative.

(b) Suppose we fix the central point p and the tangent t of the circle passing through q, p, r. If the two points q, r are in the half-plane below the tangent, the triangle generated has positive angles and also the curvature is positive, as shown in Figure 4.16b. Now if we move both points above the tangent, the angles of the triangle become negative and also the curvature turns out to be negative.

Proposition 4.4. *If $\mathcal{S}$ is convergent and δ, ∇k are summable, then the sequence of discrete curvatures $\{k_0^j\}_{j \geq 0}$ at point p_0 converges*

$$\lim_{j \to \infty} k_0^j = \bar{k}_0.$$
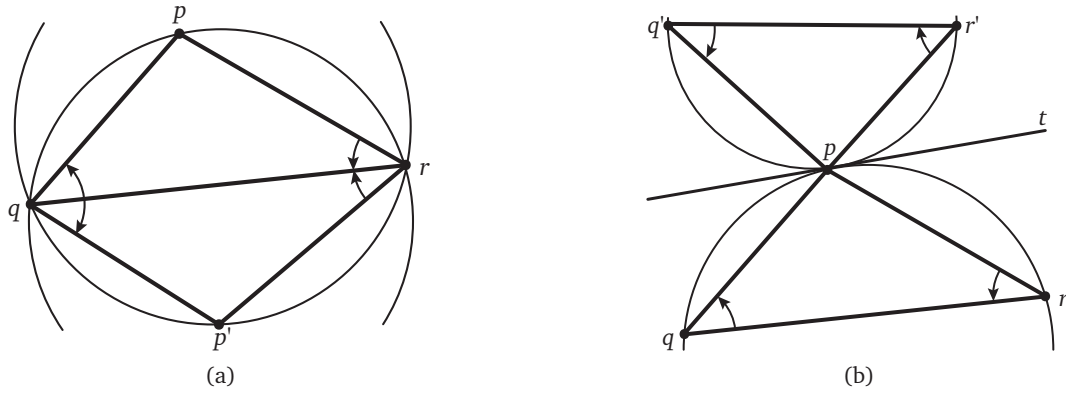
Figure 4.16. Different configurations where the curvature changes sign: (a) we fix two points q, r and we move the central point p from one half-plane to other, (b) we fix the central point p, the tangent t of the circle passing through q, p, r, and we move both points q, r above the tangent.

Proof: To prove that a limit curvature $\bar{k}_0$ exists we have to show that for all $\epsilon > 0$, there exists an initial level (in this case denoted by 0), such that $\forall j > 0$, $\left| k_0^j - k_0^{j-1} \right| < \epsilon$. We need to compare discrete interpolating circles at different levels.

Suppose we fix p_{-1}^0, p_0, p_1^0 and as a consequence k_0^0. For every configuration of points p_{-1}^1 and p_1^1 we want to prove that

$$\left| k_0^1 - k_0^0 \right| < \left| k_0^1 - k_{-1}^1 \right| + \left| k_0^1 - k_1^1 \right|. \tag{4.7}$$

Then using the hypothesis that ∇k is summable, namely $\left| k_i^j - k_{i-1}^j \right| < \epsilon$ for all i and j, we obtain the claim.

To do that, we fix the circle C_0^0 and we study the different relations between the curvatures k_0^0 and k_{-1}^1, k_1^1. Each of them corresponds to a different configuration of the points p_{-1}^1 and p_1^1. Thus, we fix the edges $\left\| p_0^0 - p_{-1}^1 \right\|$, $\left\| p_1^1 - p_0^0 \right\|$ and we rotate the points p_1^1, p_{-1}^1 such that they intersect the circle C_0^0. In such a way, we are able to compare the curvature k_0^1 with k_0^0 and to check the validity of (4.7). In the following we denote with a tilde the configuration where the rotated points are on the circle C_0^0.

For a fixed circle C_0^0, the curvature k_0^0 can be positive, negative or zero. For each one of these cases we consider all the possible relations between k_0^0 and k_{-1}^1, k_1^1.

We first of all consider the case when $k_0^0 > 0$ is positive.

(a) Let $k_{-1}^1, k_1^1 > k_0^0 > 0$.

It means that

$$k_{-1}^1 = \frac{2\sin\gamma_{-1}^1}{\left\| p_0^0 - p_{-1}^0 \right\|} > \frac{2\sin\tilde{\gamma}_{-1}^1}{\left\| p_0^0 - p_{-1}^0 \right\|} = \tilde{k}_{-1}^1 = k_0^0,$$

(a) $k_{-1}^1, k_1^1 > k_0^0$

(b) $k_{-1}^1, k_1^1 < k_0^0$

(c) $k_1^1 < k_0^0 < k_{-1}^1$
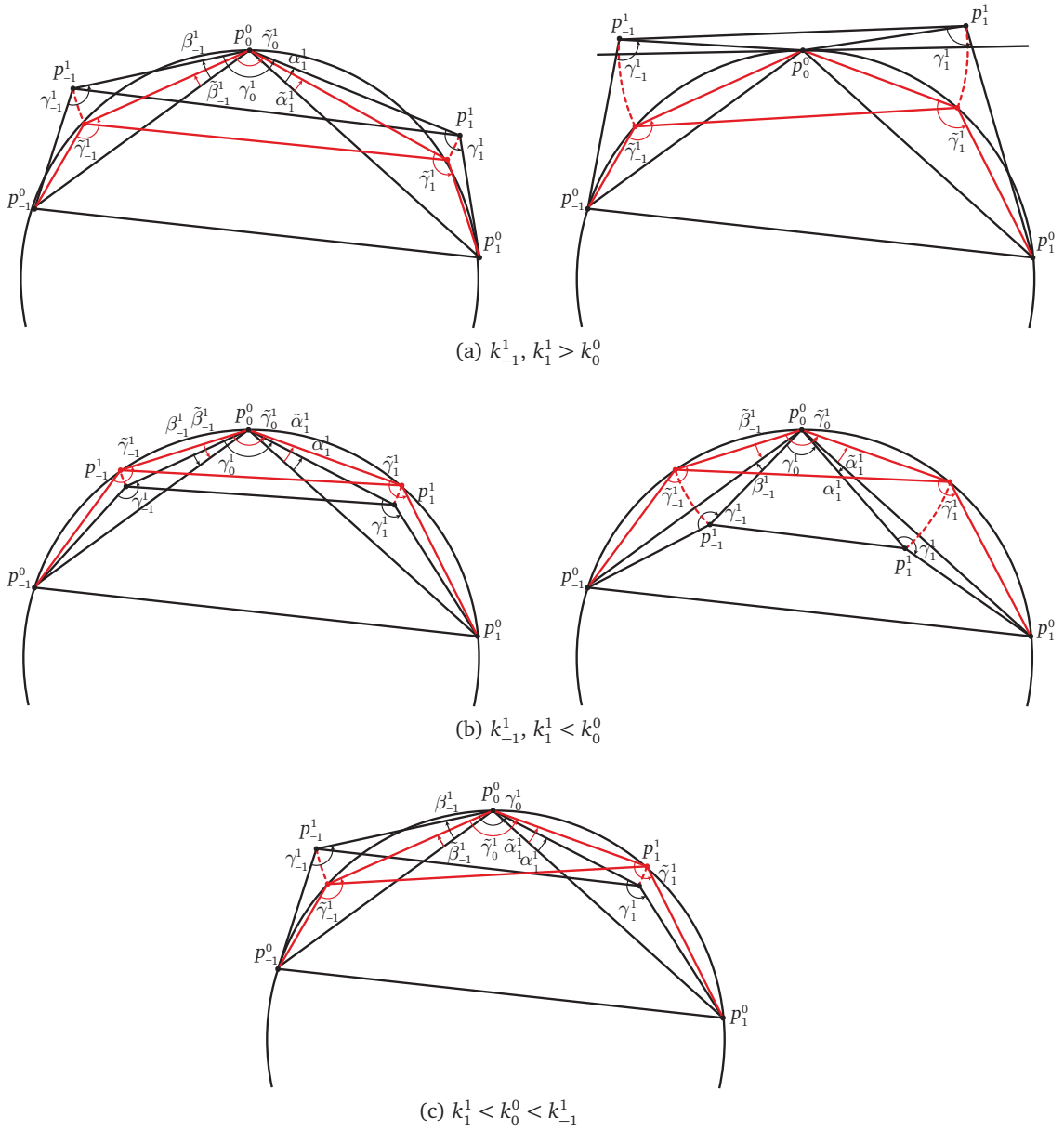
Figure 4.17. Different positions of the points p_{-1}^1, p_1^1 with respect to the circle C_0^0 with positive curvature k_0^0. The configuration where the points p_{-1}^1 and p_1^1 are rotated on the circle C_0^0 is depicted in red and any related quantities is denoted with a tilde.

where $\gamma_i^j = \pi - (\alpha_i^j + \beta_i^j) > 0$ because k_{-1}^1 is positive. By hypothesis, from a certain level on $\left|\delta_{-1}^1\right| < \pi/2$, so γ_{-1}^1 is an obtuse angle such that $\gamma_{-1}^1 < \tilde{\gamma}_{-1}^1$. From Lemma 4.3, this relation between angles means that the point p_{-1}^1 is outside the circle C_0^0. We have the same for $k_1^1 > k_0^0$, so the point p_1^1 lies outside the circle C_0^0, as shown by Figure 4.17a (left).

Now we have to compare k_0^1 with k_0^0. If the two points p_{-1}^1 and p_1^1 are above the tangent of C_0^0 the curvature has different sign respect to k_0^0 and it results $k_0^1 < k_0^0$ (see Fig 4.17a, right). Instead, if all the points are in the same half-plane, we can write

$$\gamma_0^1 = \tilde{\gamma}_0^1 + \beta_{-1}^1 - \tilde{\beta}_{-1}^1 + \alpha_1^1 - \tilde{\alpha}_1^1 > \tilde{\gamma}_0^1, \tag{4.8}$$

since the two points are outside the circle we have $\beta_{-1}^1 > \tilde{\beta}_{-1}^1$, $\alpha_1^1 > \tilde{\alpha}_1^1$. By the law of cosines we have

$$\left\|p_{-1}^1 - p_1^1\right\|^2 = \left\|p_{-1}^1 - p_0^0\right\|^2 + \left\|p_1^1 - p_0^0\right\|^2 - 2\left\|p_{-1}^1 - p_0^0\right\|\left\|p_1^1 - p_0^0\right\|\cos\gamma_0^1,$$

$$\left\|\tilde{p}_{-1}^1 - \tilde{p}_1^1\right\|^2 = \left\|p_{-1}^1 - p_0^0\right\|^2 + \left\|p_1^1 - p_0^0\right\|^2 - 2\left\|p_{-1}^1 - p_0^0\right\|\left\|p_1^1 - p_0^0\right\|\cos\tilde{\gamma}_0^1.$$

The cosine for an angle in $[\pi/2, \pi]$ is a decreasing function, so

$$\left\|p_{-1}^1 - p_1^1\right\|^2 > \left\|\tilde{p}_{-1}^1 - \tilde{p}_1^1\right\|^2. \tag{4.9}$$

With (4.8) and (4.9) we find

$$k_0^1 = \frac{2\sin\gamma_0^1}{\left\|p_{-1}^1 - p_1^1\right\|} < \frac{2\sin\tilde{\gamma}_0^1}{\left\|\tilde{p}_{-1}^1 - \tilde{p}_1^1\right\|} = \tilde{k}_0^1 = k_0^0.$$

We have all the relations between the curvatures k_1^1, k_0^1, k_1^1 and k_0^0, so we obtain

$$\left|k_0^1 - k_{-1}^1\right| + \left|k_0^1 - k_1^1\right| - \left|k_0^1 - k_0^0\right| = k_{-1}^1 - k_0^1 + k_1^1 - k_0^1 - \left(k_0^0 - k_0^1\right)$$

$$= k_{-1}^1 - k_0^1 + k_1^1 - k_0^0 > k_0^0 - k_0^0 + k_0^0 - k_0^0 = 0.$$

(b) Let $k_{-1}^1, k_1^1 < k_0^0$.

The curvatures k_{-1}^1 and k_1^1 can be positive or negative, so we have to study three different cases.

- If $k_{-1}^1, k_1^1 \geq 0$, then all the angles are positive and the relation

$$k_{-1}^1 = \frac{2\sin\gamma_{-1}^1}{\left\|p_{-1}^1 - p_0^0\right\|} < \frac{2\sin\tilde{\gamma}_{-1}^1}{\left\|p_{-1}^1 - p_0^0\right\|} = \tilde{k}_{-1}^1 = k_0^0,$$

means that $\gamma_{-1}^1 > \tilde{\gamma}_{-1}^1$. By Lemma 4.3 we know that p_{-1}^1 is inside the circle C_0^0. The same holds for the point p_1^1 that lies inside the circle C_0^0, as we see in Figure 4.17b (left). Since both points are inside the circle we can observe that

$$\beta_{-1}^1 < \tilde{\beta}_{-1}^1, \quad \alpha_1^1 < \tilde{\alpha}_1^1.$$

- If $k_{-1}^1, k_1^1 < 0$, then the points p_{-1}^1, p_1^1 are below the segments $\overrightarrow{p_{-1}^0 p_0}$ and $\overrightarrow{p_0 p_1^0}$ (Fig. 4.17b right). The points are both inside the triangle defined by p_{-1}^0, p_0, p_1^0, while the projected points $\tilde{p}_{-1}^1$, $\tilde{p}_1^1$ are outside the triangle. Then, the curvatures k_{-1}^1, k_1^1 have opposite sign with respect to $\tilde{k}_{-1}^1$, $\tilde{k}_1^1$ and

$$\beta_{-1}^1 < 0 < \tilde{\beta}_{-1}^1, \qquad \alpha_1^1 < 0 < \tilde{\alpha}_1^1.$$

- If $k_{-1}^1 > 0$ and $k_1^1 < 0$, then both the points are inside the circle C_0^0 and p_1^1 is also inside the triangle defined by p_{-1}^0, p_0, p_1^0. From the previous cases we have

$$\beta_{-1}^1 < \tilde{\beta}_{-1}^1, \qquad \alpha_1^1 < 0 < \tilde{\alpha}_1^1.$$

The angle $\tilde{\gamma}_0^1$ is greater than γ_0^1,

$$\tilde{\gamma}_0^1 = \gamma_0^1 + \tilde{\beta}_{-1}^1 - \beta_{-1}^1 + \tilde{\alpha}_1^1 - \alpha_1^1 > \gamma_0^1.$$

for all the three cases considered. Moreover, we observe that γ_0^1 and k_0^1 have to be positive because the points p_{-1}^1 and p_1^1 lie in the same half-plane of the points p_{-1}^0 and p_1^0 with respect to the tangent t_0^0. So, the curvature k_0^1 has the same sign of k_0^0, now we study which curvature is the greatest between the two.

Thanks to the relation $\tilde{\gamma}_0^1 > \gamma_0^1$ and the law of cosines,

$$\left\| p_{-1}^1 - p_1^1 \right\|^2 = \left\| p_{-1}^1 - p_0^0 \right\|^2 + \left\| p_1^1 - p_0^0 \right\|^2 - 2 \left\| p_{-1}^1 - p_0^0 \right\| \left\| p_1^1 - p_0^0 \right\| \cos \gamma_0^1,$$
$$\left\| \tilde{p}_{-1}^1 - \tilde{p}_1^1 \right\|^2 = \left\| p_{-1}^1 - p_0^0 \right\|^2 + \left\| p_1^1 - p_0^0 \right\|^2 - 2 \left\| p_{-1}^1 - p_0^0 \right\| \left\| p_1^1 - p_0^0 \right\| \cos \tilde{\gamma}_0^1,$$

we have

$$\left\| p_{-1}^1 - p_1^1 \right\|^2 < \left\| \tilde{p}_{-1}^1 - \tilde{p}_1^1 \right\|^2,$$

because γ_0^1 is obtuse and the cosine is a decreasing function in $[\pi/2, \pi]$. So, we can compare the curvature of C_0^1 with the curvature of C_0^0

$$k_0^1 = \frac{2 \sin \gamma_0^1}{\left\| p_{-1}^1 - p_1^1 \right\|} > \frac{2 \sin \tilde{\gamma}_0^1}{\left\| \tilde{p}_{-1}^1 - \tilde{p}_1^1 \right\|} = \tilde{k}_0^1 = k_0^0.$$

At this point we have all the relations between k_{-1}^1, k_1^1, k_0^1 and k_0^0 where all the points lie on the circle C_0^0,

$$\left| k_0^1 - k_{-1}^1 \right| + \left| k_0^1 - k_1^1 \right| - \left| k_0^0 - k_0^1 \right| = k_0^1 - k_{-1}^1 + k_0^1 - k_1^1 - \left(k_0^1 - k_0^0 \right)$$
$$= k_0^1 - k_{-1}^1 - k_1^1 + k_0^0 > k_0^0 - k_0^0 - k_0^0 + k_0^0 = 0.$$

(c) Let $k_1^1 < k_0^0 < k_{-1}^1$, or the case where we interchange k_1^1 and k_{-1}^1.

Similarly to the previous cases, from this relation we know that the point p_{-1}^1 is outside the circle C_0^0, instead p_1^1 lies inside C_0^0 as shown in Figure 4.17c.

In this case we do not know the relation between k_0^1 and k_0^0 but it is not necessary, because

(a) $k_{-1}^1, k_1^1 \geq k_0^0$ (b) $k_{-1}^1, k_1^1 < k_0^0$ (c) $k_{-1}^1 > k_0^0, \; k_1^1 < k_0^0$
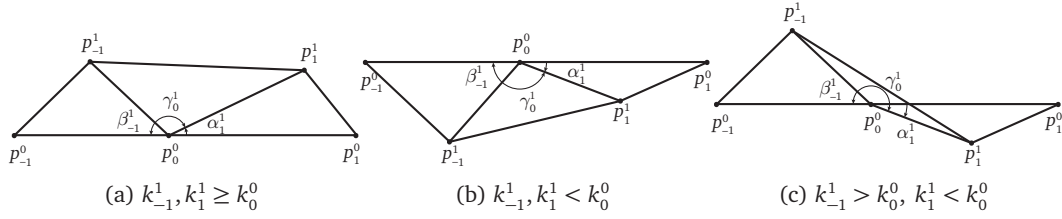
Figure 4.18. Different positions of the points p_{-1}^1 and p_1^1 when the points p_{-1}^0, p_0^0, p_1^0 are collinear ($k_0^0 = 0$).

- if $k_0^1 < k_0^0$, then $k_{-1}^1 - k_0^1 + \left| k_0^1 - k_1^1 \right| > k_{-1}^1 - k_0^1 > k_0^0 - k_0^1,$
- if $k_0^1 > k_0^0$, then $\left| k_{-1}^1 - k_0^1 \right| + k_0^1 - k_1^1 > k_0^1 - k_1^1 > k_0^0 - k_0^0.$

For each configuration of points we proved that (4.7) is true under the hypothesis that $k_0^0 > 0$.

When $k_0^0 < 0$, we have to consider three configurations that are symmetric to Figures 4.17a, 4.17b, 4.17c. The proof is similar to the previous case with $k_0^0 > 0$, the only difference is that we can only relate $\left| k_0^1 \right|$ with $\left| k_0^0 \right|$. For all the possibilities, it turns out that the relation between $\left| k_0^1 \right|$ and $\left| k_0^0 \right|$ is sufficient to prove (4.7) in the case that $k_0^0 < 0$.

It remains to study the configurations when $k_0^0 = 0$. Again we have three different configurations.

(a) Let $k_{-1}^1, k_1^1 \geq k_0^0 = 0$,

this means that both p_{-1}^1 and p_1^1 are in the same half-plane above the segment $\overrightarrow{p_{-1}^0 p_1^0}$. As shown by Figure 4.18a, the curvature k_0^1 is negative $k_0^1 < k_0^0 = 0$. Then,

$$\left| k_0^1 - k_{-1}^1 \right| + \left| k_0^1 - k_1^1 \right| - \left| k_0^1 - k_0^0 \right| = k_{-1}^1 - k_0^1 + k_1^1 - k_0^1 + k_0^1 = k_{-1}^1 - k_0^1 + k_1^1 > 0$$

and (4.7) is satisfied.

(b) Let $k_{-1}^1, k_1^1 < k_0^0 = 0$.

It is the symmetric configuration with respect to the previous one, which means that p_{-1}^1 and p_1^1 lie below the segment $\overrightarrow{p_{-1}^0 p_1^0}$. Then the curvature is positive $k_0^1 > k_0^0$, see Figure 4.18b. This allows to check the inequality (4.7),

$$\left| k_0^1 - k_{-1}^1 \right| + \left| k_0^1 - k_1^1 \right| - \left| k_0^1 - k_0^0 \right| = k_0^1 - k_{-1}^1 + k_0^1 - k_1^1 - k_0^1 = k_0^1 - k_{-1}^1 - k_1^1 > 0.$$

(c) Let $k_{-1}^1 > k_0^0$ and $k_1^1 < k_0^0$,

this means that the point p_{-1}^1 is above $\overrightarrow{p_{-1}^0 p_1^0}$ while p_1^1 is below, as in Figure 4.18c. In this case the curvature k_0^1 can be either positive and negative, but in any case the inequality (4.7) is true.

- If $k_0^1 < 0$, then

$$\left|k_0^1 - k_{-1}^1\right| + \left|k_0^1 - k_1^1\right| - \left|k_0^1 - k_0^0\right| = k_{-1}^1 - k_0^1 + \left|k_0^1 - k_1^1\right| + k_0^1 = k_{-1}^1 + \left|k_0^1 - k_1^1\right| > 0.$$

- If $k_0^1 > 0$, then

$$\left|k_0^1 - k_{-1}^1\right| + \left|k_0^1 - k_1^1\right| - \left|k_0^1 - k_0^0\right| = \left|k_0^1 - k_{-1}^1\right| + k_0^1 - k_1^1 - k_0^1 = \left|k_0^1 - k_{-1}^1\right| - k_1^1 > 0.$$

For all the cases we proved that if relation (4.7) is satisfied, then there exists an initial level j_0, depending on the position i, such that for any $j \geq j_0$ we can rewrite (4.7) in general

$$\left|k_{2i}^{j+1} - k_i^j\right| < \left|k_{2i-1}^{j+1} - k_{2i}^{j+1}\right| + \left|k_{2i}^{j+1} - k_{2i+1}^{j+1}\right|. \tag{4.10}$$

To show that the sequence of discrete curvatures $\{k_0^j\}_{j \geq j_0}$ converges we exploit (4.10) to prove that is a Cauchy sequence.

If we take two different levels $m > n > j_0$, then

$$\left|k_0^m - k_0^n\right| \leq \sum_{\ell=0}^{m-n-1} \left|k_0^{n+\ell+1} - k_0^{n+\ell}\right| \leq \sum_{\ell=0}^{m-n-1} \left|k_0^{n+\ell+1} - k_1^{n+\ell+1}\right| + \left|k_0^{n+\ell+1} - k_{-1}^{n+\ell+1}\right|$$

$$\leq 2 \sum_{\ell=0}^{m-n-1} \max_{i \in \mathbb{Z}} \left|k_i^{n+\ell+1} - k_{i+1}^{n+\ell+1}\right| = 2 \sum_{\ell=0}^{m-n-1} \nabla k^{n+\ell+1} = 2 \sum_{\ell=n+1}^{m} \nabla k^\ell.$$

By hypothesis, the sequence ∇k is summable, hence the sequence of the partial sum is a Cauchy sequence. Then, for any $\epsilon > 0$ there exists some $j_1 \geq j_0$ such that for any $m > n > j_1$

$$\sum_{\ell=n}^{m} \nabla k^\ell < \frac{\epsilon}{2} \quad \Rightarrow \quad \left|k_0^m - k_0^n\right| < \epsilon$$

and $\{k_0^j\}_{j \geq j_0}$ is a Cauchy sequence.

This allows to conclude that the sequence $\{k_0^j\}_{j \geq 0}$ is convergent and

$$\lim_{j \to \infty} k_0^j = \bar{k}_0.$$

$\square$

We already observe that the previous Proposition 4.4 applies to any point p_i^j, $i \in \mathbb{Z}$ and $j \geq j_0$, of the subdivision scheme $\mathcal{S}$.

Lemma 4.5. *The discrete curvatures k_i^j converge uniformly for any $i \in \mathbb{Z}$.*

Proof: We call $\bar{k}_i^j$ the limit of the discrete curvatures centred at p_i^j. Using the proof of Proposition 4.4,

$$\left|\bar{k}_i^j - k_i^j\right| \leq \sum_{\ell=0}^{\infty} \left|k_{2^{\ell+1}i}^{j+\ell+1} - k_{2^\ell i}^{j+\ell}\right| \leq 2 \sum_{\ell=0}^{\infty} \max_{n \in \mathbb{Z}} \left|k_{n+1}^{j+\ell+1} - k_n^{j+\ell+1}\right| = 2 \sum_{\ell=j+1}^{\infty} \nabla k^\ell.$$

Thanks to the summability of ∇k for any $\epsilon > 0$ there exists j_0 such that

$$\sum_{\ell=j_0+1}^{\infty} \nabla k^{\ell} < \frac{\epsilon}{2} \quad \Rightarrow \quad \left| \bar{k}_i^j - k_i^j \right| < \epsilon, \ \forall i \in \mathbb{Z}.$$

We have the same bound also for the points generated in the following levels, because for any $j > j_0$

$$\sum_{\ell=j}^{\infty} \nabla k^{\ell} \leq \sum_{\ell=j_0}^{\infty} \nabla k^{\ell} < \frac{\epsilon}{2}.$$

$\square$

Strictly related to the previous proposition and lemma, we can define a new sequence

$$\Delta k^j = \sup_{i \in \mathbb{Z}} \left\{ \left| k_{2i}^j - k_i^{j-1} \right| \right\}, \qquad \Delta k = \{\Delta k^j\}_{j>0}, \tag{4.11}$$

that represents the difference of discrete curvatures at the same point on two following levels.

Lemma 4.6. *If ∇k is summable, then the sequence Δk is summable.*

Proof: In Proposition 4.4 we show that from a level j_0 on, that for simplicity we call 0,

$$\left| k_{2i}^{j+1} - k_i^j \right| \leq \left| k_{2i}^{j+1} - k_{2i+1}^{j+1} \right| + \left| k_{2i}^{j+1} - k_{2i-1}^{j+1} \right|,$$

for each point p_i^j of the subdivision scheme. Then, we bound the series of Δk^j with twice the series of ∇k^j

$$\sum_{j=0}^{\infty} \Delta k^j = \sum_{j=0}^{\infty} \sup_{i \in \mathbb{Z}} \left| k_{2i}^{j+1} - k_i^j \right| \leq \sum_{j=0}^{\infty} \sup_{i \in \mathbb{Z}} \left| k_{2i}^{j+1} - k_{2i+1}^{j+1} \right| + \sup_{i \in \mathbb{Z}} \left| k_{2i}^{j+1} - k_{2i-1}^{j+1} \right| \leq 2 \sum_{j=1}^{\infty} \nabla k^j < \infty.$$

If ∇k is summable, then the sequence $\Delta k = \{\Delta k^j\}_{j>0}$ is summable. $\square$

At this point it is easy to prove that the discrete interpolating circles $\{C_0^j\}_{j\geq 0}$ at a point p_0^0 converge to a limit circle.

Theorem 4.7. *If $\mathcal{S}$ is convergent, δ and ∇k are summable then the sequence of discrete interpolating circles C_0^j passing through p_{-1}^j, p_0, p_1^j converges to a limit circle $\bar{C}_0$*

$$\lim_{j \to \infty} C_0^j = \bar{C}_0.$$

Proof: An equivalent way to define the discrete interpolating circle C_0^j passing through p_{-1}^j, p_0, p_1^j is using the tangent t_0^j at p_0 and the discrete curvature k_0^j. By Proposition 4.2 and 4.4 we have

$$\lim_{j \to \infty} t_0^j = \bar{t}_0,$$

$$\lim_{j \to \infty} k_0^j = \bar{k}_0.$$

So, there exists a circle $\bar{C}_0$ with tangent $\bar{t}_0$ at p_0 and curvature $\bar{k}_0$ such that

$$\lim_{j \to \infty} C_0^j = \bar{C}_0.$$

$\square$

4.3.2   Step 2

In this step we want to show that the limit circle $\bar{C}_0$ is the osculating circle at p_0^0. The key idea is to use Proposition 2.2. In that proposition we consider two sequences of circles, both with the direct tangent of $\mathscr{C}$ at p as tangent, but one sequence of circles passing through p and a sequence of points on the left of p, while the other circles passing through p and a sequence of points on the right. If both sequences converge to the same circle, then this is the osculating circle of $\mathscr{C}$ at p.

In our setting the right and left neighbourhoods of p_0 at level j are composed by points p_i^j and $p_{-\ell}^j$ with $0 < i, \ell \leq 2^j$. Increasing j, the neighbourhood shrinks around p_0 and we can choose a level j_0 such that $\left\| p_0 - p_i^j \right\| < \epsilon$ for any $0 < i \leq 2^j$ and $j \geq j_0$, thanks to the summability of e. We denote with $k(p_0, p_i^j, \bar{t}_0)$ the curvature of the circle with tangent $\bar{t}_0$ at p_0 and passing through p_0 and p_i^j. To apply Proposition 2.2 we need to prove that

$$\lim_{j \to \infty} k(p_0, p_i^j, \bar{t}_0) = \lim_{j \to \infty} k(p_{-\ell}^j, p_0, \bar{t}_0) = \bar{k}_0,$$

where p_i^j and $p_{-\ell}^j$ are two generic points in the left and right neighbourhood of p_0, $0 < i, \ell \leq 2^j$.

Without loss of generality, we fix on points p_i^j in the right neighbourhood of p_0 and analogously we can generalize to points $p_{-\ell}^j$ in the left neighbourhood.

The first result that we prove is that the sequence of curvatures $k(p_0, p_1^j, \bar{t}_0)$ converges to $\bar{k}_0$ (Proposition 4.9). To show this we need a general result on the edge length.

Lemma 4.8. *Let $\mathcal{S}$ a convergent scheme and δ summable, then from a certain level on, for any $i \geq 0$,*

$$\left\| p_0^{j+i} - p_1^{j+i} \right\| \leq \left\| p_0^j - p_1^j \right\|. \tag{4.12}$$

Proof: If it is true between $\overrightarrow{p_0^j p_1^j}$ and $\overrightarrow{p_0^{j+1} p_1^{j+1}}$, then it is also true in general for any positive i by induction.

By contradiction, suppose that

$$\left\| p_0^{j+1} - p_1^{j+1} \right\| > \left\| p_0^j - p_1^j \right\|.$$

It means that the point p_1^{j+1} lies outside the two circles with centres p_0^j and p_1^j and radius $\left\| p_0^j - p_1^j \right\|$ (see Fig. 4.19). Moreover, p_1^{j+1} should not be too far away from the edge $\overrightarrow{p_0^j p_1^j}$,
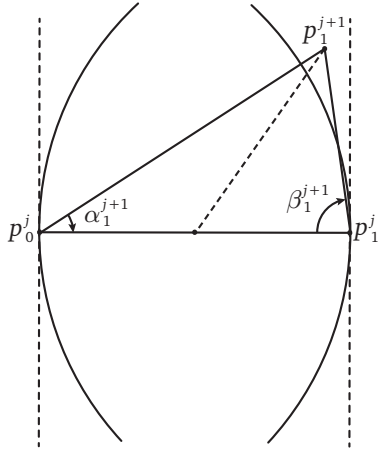
Figure 4.19. Configuration where $\left\| p_0^{j+1} - p_1^{j+1} \right\| > \left\| p_0^j - p_1^j \right\|$.
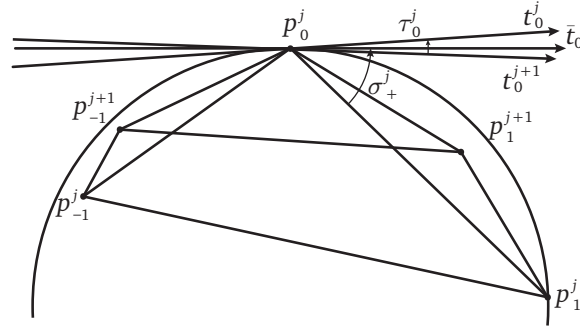
Figure 4.20. The circle $k(p_0, p_1^j, \bar{t}_0)$ and the angles $\sigma_+^j = \sphericalangle(p_0 p_1^j, \bar{t}_0)$, $\tau_0^j = \sphericalangle(t_0^j, t_0^{j+1})$.

because by Theorem 3.1 $\boldsymbol{d}$ is a null sequence. This means that α_1^{j+1} or β_1^{j+1} should be close to $\frac{\pi}{2}$ but it cannot happen because $\boldsymbol{\delta}$ is summable. So, from some level on, all the angles are strictly less than $\frac{\pi}{2}$ and decrease to zero. In the end, we have that from a certain level on the new edges are necessarily shorter than the previous ones, which agrees with the hypothesis that $\boldsymbol{e}$ is summable.   □

Furthermore, to prove Proposition 4.9 we have to restrict the hypothesis on $\boldsymbol{\delta}$ and $\nabla \boldsymbol{k}$: the two sequences should behave like convergent geometric sequences, which means that there exist two constants μ_δ and $\mu_k < 1$ such that

$$\delta^j = O(\mu_\delta^j), \qquad \nabla k^j = O(\mu_k^j). \tag{4.13}$$

The sequences $\boldsymbol{\delta}$ and $\nabla \boldsymbol{k}$ are then bounded by two convergent geometric sequences,

$$\delta^j \leq c \mu_\delta^j, \qquad \nabla k^j \leq c' \mu_k^j, \tag{4.14}$$

where $c, c' > 0$ are two positive constants. These hypotheses are not so restrictive, because in all the numerical examples that satisfy the G^1 and G^2 conditions, the sequences $\boldsymbol{\delta}$ and $\nabla \boldsymbol{k}$ are bounded by convergent geometric sequences, see Section 4.2.

Lemma 4.6 shows that the sequence $\Delta \boldsymbol{k}$ behaves like $\nabla \boldsymbol{k}$, so

$$\Delta k^j \leq 2c' \mu_k^j = c'' \mu_k^j \quad \Rightarrow \quad \Delta k^j = O(\mu_k^j).$$

Fixing a point p_i^j, the neighbouring discrete curvature k_{i+1}^j or the curvature at the next level k_{2i}^{j+1} can both be bounded by k_i^j,

$$k_{i+1}^j \leq k_i^j + c' \mu_k^j, \quad \text{and} \quad k_{2i}^{j+1} \leq k_i^j + c'' \mu_k^{j+1}. \tag{4.15}$$
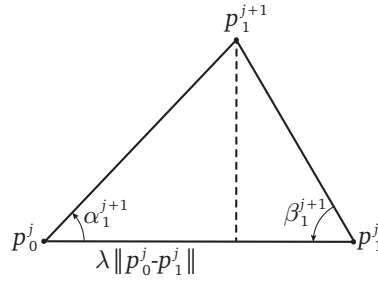
Figure 4.21. Graphic definition of lambda in (4.17).

Proposition 4.9. *If δ and ∇k behave like geometric sequences (4.14), then the sequence of curvatures $\{k(p_0, p_1^j, \bar{t}_0)\}_{j \geq j_0}$ of the circles with tangent $\bar{t}_0$ and passing through p_0^j and p_1^j, converges to $\bar{k}_0$.*

Proof: We define by $\tau_0^{j+1} = \sphericalangle(t_0^j, t_0^{j+1})$ the angle between the tangents at p_0 of the discrete interpolating circles C_0^j and C_0^{j+1}. We can split this angle into

$$\tau_0^{j+1} = \sphericalangle(t_0^j, t_0^{j+1}) = \sphericalangle(t_0^j, \overrightarrow{p_0 p_1^j}) + \sphericalangle(\overrightarrow{p_0 p_1^j}, \overrightarrow{p_0 p_1^{j+1}}) + \sphericalangle(\overrightarrow{p_0 p_1^{j+1}}, t_0^{j+1})$$
$$= -\sigma_0^j + \alpha_1^{j+1} + \sigma_0^{j+1} = -\alpha_0^j + \alpha_1^{j+1} + \alpha_0^{j+1}, \qquad (4.16)$$

where σ_0^j is defined in (4.3) and is equal to α_0^j as stated by Lemma 2.1.

We now study the behaviour of τ_0^{j+1} with respect to the behaviour of edges, angles and curvatures. To do this we use the definition of discrete curvature and the fact that $\sin(\theta) \sim \theta$ for small θ. By Lemma 3.6 in [Dyn and Hormann, 2012], each angle of the scheme α_i^j, β_i^j is bounded by the geometric sequence μ_δ^j because δ^j itself is bounded. Let us study separately the behaviour of the angles in (4.16).

- $\alpha_0^j \sim \sin(\alpha_0^j) = \frac{k_0^j}{2} \left\| p_0 - p_1^j \right\|$.

- $\alpha_1^{j+1} \sim \sin(\alpha_1^{j+1}) = \frac{k_1^{j+1}}{2} \left\| p_1^j - p_1^{j+1} \right\| \leq \frac{1}{2}(k_0^{j+1} + c'\mu_k^{j+1}) \frac{(1-\lambda)\left\| p_0 - p_1^j \right\|}{\cos(\beta_1^{j+1})}$,

  with $\lambda < 1$ that represents the ratio between the projection of $\overrightarrow{p_0 p_1^{j+1}}$ on $\overrightarrow{p_0 p_1^j}$ and $\overrightarrow{p_0 p_1^j}$ itself,

$$\lambda = \frac{\left\| p_0 - p_1^{j+1} \right\| \cos(\alpha_1^{j+1})}{\left\| p_0 - p_1^j \right\|} \qquad (4.17)$$

(see Fig. 4.21).

Using the Taylor expansion of the cosine we have

$$1 - \frac{\theta^2}{2} \leq \cos(\theta) \leq 1 \quad \Rightarrow \quad 1 \leq \frac{1}{\cos(\theta)} \leq \frac{1}{1 - \frac{\theta^2}{2}} \leq 1 + \theta^2, \qquad (4.18)$$

where the last inequality is true for $\theta < \frac{1}{2}$. From a certain level on we know that it is true for α and β, because they are null sequences.

Thus, we have

$$\alpha_1^{j+1} \lesssim \frac{1}{2}(k_0^{j+1} + c'\mu_k^{j+1})(1-\lambda)\left\|p_0^j - p_1^j\right\|\left(1 + (\beta_1^{j+1})^2\right)$$
$$\leq \frac{1}{2}(k_0^j + (c' + c'')\mu_k^{j+1})(1-\lambda)\left\|p_0^j - p_1^j\right\|\left(1 + (\beta_1^{j+1})^2\right),$$

where we apply twice (4.15). With the symbol $\lesssim$ we mean that we bound with an asymptotic quantity. The first step is always to substitute the angle with the sine, since they are asymptotically equivalent, and then to use the decays of the curvatures and the angles.

- $\alpha_0^{j+1} \sim \sin(\alpha_0^{j+1}) = \frac{k_0^{j+1}}{2}\left\|p_0^j - p_1^{j+1}\right\| \leq \frac{\lambda}{2}(k_0^j + c''\mu_k^{j+1})\frac{\left\|p_0^j - p_1^j\right\|}{\cos(\alpha_1^{j+1})}$
  $\leq \frac{\lambda}{2}(k_0^j + c''\mu_k^{j+1})\left\|p_0^j - p_1^j\right\|(1 + (\alpha_1^{j+1})^2),$
  where again we use (4.15) and (4.18).

Combining these bounds we find the following upper bound for τ_0^{j+1},

$$\tau_0^{j+1} \lesssim -\frac{k_0^j}{2}\left\|p_0^j - p_1^j\right\| + \frac{1-\lambda}{2}\left(k_0^j + (c' + c'')\mu_k^{j+1}\right)\left\|p_0^j - p_1^j\right\|\left(1 + (\delta_1^{j+1})^2\right)$$
$$+ \frac{\lambda}{2}\left(k_0^j + c''\mu_k^{j+1}\right)\left\|p_0^j - p_1^j\right\|\left(1 + (\delta_1^{j+1})^2\right)$$
$$= -\frac{k_0^j}{2}\left\|p_0^j - p_1^j\right\| + \frac{1}{2}\left(k_0^j + c''\mu_k^{j+1}\right)\left\|p_0^j - p_1^j\right\|\left(1 + (\delta_1^{j+1})^2\right)$$
$$+ \frac{1}{2}c'(1-\lambda)\mu_k^{j+1}\left\|p_0^j - p_1^j\right\|\left(1 + (\delta_1^{j+1})^2\right)$$
$$= \frac{k_0^j}{2}\left\|p_0^j - p_1^j\right\|(\delta_1^{j+1})^2 + \frac{c''}{2}\mu_k^{j+1}\left\|p_0^j - p_1^j\right\|\left(1 + (\delta_1^{j+1})^2\right)$$
$$+ \frac{1}{2}c'(1-\lambda)\mu_k^{j+1}\left\|p_0^j - p_1^j\right\|\left(1 + (\delta_1^{j+1})^2\right)$$
$$\leq c_1'\left\|p_0^j - p_1^j\right\|(\mu_\delta^{j+1})^2 + c_2'\mu_k^{j+1}\left\|p_0^j - p_1^j\right\| + c_3'\mu_k^{j+1}\left\|p_0^j - p_1^j\right\|(\mu_\delta^{j+1})^2$$
$$\leq c_1''\left\|p_0^j - p_1^j\right\|(\mu_\delta^{j+1})^2 + c_2''\mu_k^{j+1}\left\|p_0^j - p_1^j\right\|,$$

where $c_1', c_2', c_3', c_1'', c_2''$ are some constants.

We call $k(p_0, p_1^j, \bar{t}_0)$ the curvature of the circle with tangent $\bar{t}_0$ and passing through p_0 and p_1^j. In analogy with σ_0^j we define $\sigma_+^j := \sphericalangle(\overrightarrow{p_0^j p_1^j}, \bar{t}_0)$ and

$$\sigma_+^j = \sphericalangle(\overrightarrow{p_0^j p_1^j}, \bar{t}_0) = \sphericalangle(\overrightarrow{p_0^j p_1^j}, t_0^j) + \sphericalangle(t_0^j, \bar{t}_0) = \sigma_0^j + \sum_{i=0}^{\infty} \sphericalangle(t_0^{j+i}, t_0^{j+i+1}) = \sigma_0^j + \sum_{i=0}^{\infty} \tau_0^{j+i+1}.$$

Then we are able to estimate the difference between the curvature $k(p_0, p_1^j, \bar{t}_0)$ and k_0^j,

$$
\begin{aligned}
\left| k(p_0, p_1^j, \bar{t}_0) - k_0^j \right| &= \left| \frac{2\sin(\sigma_+^j)}{\left\| p_0^j - p_1^j \right\|} - \frac{2\sin(\sigma_0^j)}{\left\| p_0^j - p_1^j \right\|} \right| \sim \frac{2\left| \sigma_+^j - \sigma_0^j \right|}{\left\| p_0^j - p_1^j \right\|} = 2\frac{\left| \sum_{i=0}^{\infty} \tau_0^{j+i+1} \right|}{\left\| p_0^j - p_1^j \right\|} \\
&\lesssim 2\frac{\sum_{i=0}^{\infty} c_1'' \left\| p_0^{j+i} - p_1^{j+i} \right\| (\mu_\delta^{j+i+1})^2 + c_2'' \mu_k^{j+i+1} \left\| p_0^{j+i} - p_1^{j+i} \right\|}{\left\| p_0^j - p_1^j \right\|} \\
&\leq 2\frac{\left\| p_0^j - p_1^j \right\| \left[c_1'' (\mu_\delta^{j+1})^2 \sum_{i=0}^{\infty} (\mu_\delta^2)^i + c_2'' \mu_k^{j+1} \sum_{i=0}^{\infty} \mu_k^i \right]}{\left\| p_0^j - p_1^j \right\|} \\
&= 2c_1'' (\mu_\delta^{j+1})^2 \frac{1}{1 - \mu_\delta^2} + 2c_2'' \mu_k^{j+1} \frac{1}{1 - \mu_k} = c_1 (\mu_\delta^{j+1})^2 + c_2 \mu_k^{j+1},
\end{aligned}
$$

where in the second inequality we use (4.12). This relation allows to prove that $\forall \epsilon > 0$ there exists some j_0 such that for any $j \geq j_0$, $\left| k(p_0, p_1^j, \bar{t}_0) - k_0^j \right| < \epsilon/2$. Using the convergence of k_0^j, we have

$$
\left| k(p_0, p_1^j, \bar{t}_0) - \bar{k}_0 \right| \leq \left| k(p_0, p_1^j, \bar{t}_0) - k_0^j \right| + \left| k_0^j - \bar{k}_0 \right| < \epsilon.
$$

Note that this result can be achieved for every point in the subdivision scheme. □

The same proposition can be proved for the sequence of curvatures $k(p_{-1}^j, p_0, \bar{t}_0)$ of circles with tangent $\bar{t}_0$ and passing through p_{-1}^j and p_0. This is not enough to show that $\bar{C}_0$ is the osculating circle, because we need to show that considering circles with tangent $\bar{t}_0$ and passing through p_0 and any points in the neighbourhood of p_0, like p_i^j with $0 < i \leq 2^j$, they converge to $\bar{C}_0$.

From a certain level on we show that the maximum of edge lengths decreases, now we observe that there is a sort of order between points in a neighbourhood of p_0.

Conjecture 4.10. *Let $\mathcal{S}$ be a convergent subdivision scheme. Fix a point p_0 and consider its right neighbourhood, given by the points p_i^j with $0 < i \leq 2^{j-j_0}$ and $j \geq j_0$. The points p_i^j are ordered in the sense that*

$$
\left\| p_0 - p_i^j \right\| \leq \left\| p_0 - p_{i+1}^j \right\|,
$$

for all $0 < i \leq 2^{j-j_0}$ and $j \geq j_0$.

Numerical evidence: In Figure 4.22 we display

$$
\max_{j \geq j_0} \max_{0 < i < 2^{j-j_0}} \frac{\left\| p_0 - p_i^j \right\|}{\left\| p_0 - p_{i+1}^j \right\|}
$$

(a) 4-point scheme with $w = \frac{3}{16}$ (b) Circle-based 4-point scheme   (c) Circle-based 6-point scheme
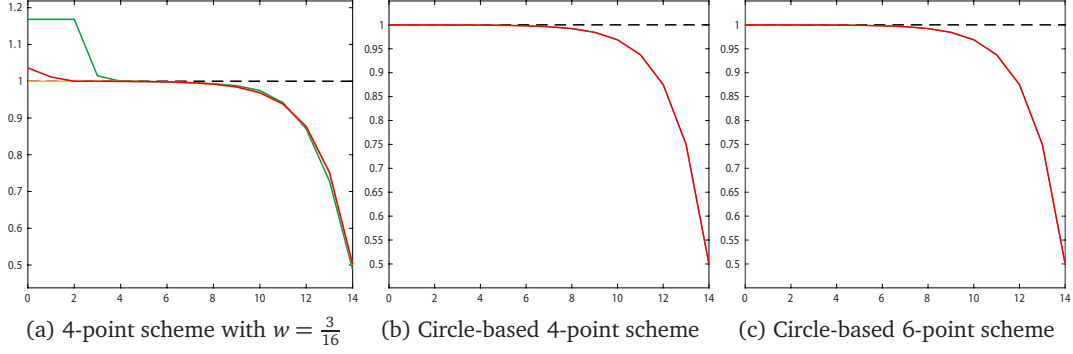
Figure 4.22. Plots of $\max_{j \geq j_0} \max_{0 < i < 2^{j-j_0}} \|p_0 - p_i^j\| / \|p_0 - p_{i+1}^j\|$ depending on j_0 with $0 \leq j_0 \leq 14$. The points are generated by the 4-point scheme with tension parameter $w = 3/16$ (a), the circle-based 4-point scheme (b) and the circle-based 6-point scheme (c) starting with the three control polygons considered in Section 4.2. The dashed line marks the value 1.

depending on j_0, for the three control polygons used in the numerical tests (Section 4.2). Figure 4.22 shows that there exists an initial level j_0 such that the ratio is less than 1 (dashed line) for all $j \geq j_0$, for all the control polygons and the subdivision schemes considered. For all the examples, Conjecture 4.10 is true.

Proposition 4.11. *If $\mathcal{S}$ is convergent and ∇k is summable, for any $\epsilon > 0$, there exists some $j_0 \in \mathbb{N}$ such that $\left|k_0^j - k_i^j\right| < \epsilon$ for any $0 < i \leq 2^{j-j_0}$ and $j \geq j_0$.*

Proof: By Definition 4.1 $\nabla k^j = \sup_{i \in \mathbb{Z}} |k_i^j - k_{i+1}^j|$, then for any points $i \in \mathbb{Z}$ and any level $j \geq 0$

$$\left|k_{i+1}^j - k_i^j\right| \leq \nabla k^j, \tag{4.19}$$

and we proved in Proposition 4.4 that

$$\left|k_{2i}^{j+1} - k_i^j\right| < 2 \nabla k^{j+1}, \tag{4.20}$$

for any $i \in \mathbb{Z}$. By Proposition 4.4 and the fact that $\{k_0^j\}_{j \geq 0}$ is a Cauchy sequence, there exists an initial level $j_0 \in \mathbb{N}$ such that

$$\left|k_0^j - k_0^{j_0}\right| < \frac{\epsilon}{2}, \quad \forall j \geq j_0. \tag{4.21}$$

We consider the right neighbourhood of p_0 composed by p_i^j, with $0 < i \leq 2^{j-j_0}$ and $j \geq j_0$, and we can split the absolute value,

$$\left|k_0^j - k_i^j\right| \leq \left|k_0^j - k_0^{j_0}\right| + \left|k_0^{j_0} - k_i^j\right|.$$

The first term is less than $\epsilon/2$ by (4.21), so we focus on the difference $\left|k_0^{j_0} - k_i^j\right|$.

We denote with i_2 the binary expression of i such that

$$i = \sum_{\ell=0}^{j-j_0} (i_2)_\ell 2^\ell. \tag{4.22}$$

To reach $k_0^{j_0}$ from k_i^j, $0 < i \leq 2^{j-j_0}$ and $j \geq j_0$, we move along the branches of the tree, displayed in Figure 4.23, following the strategy:

- if the ℓ-th digit of the binary number is 1, $(i_2)_\ell = 1$, then we move on the left to the previous curvature using (4.19) and then we go down to the previous level using (4.20),

- if the ℓ-th digit of the binary number is 0, $(i_2)_\ell = 0$, then we move directly to the previous level using (4.20).

We repeat the procedure until we reach $k_0^{j_0}$. In this way we split the absolute value using repeatedly (4.19) and (4.20),

$$
\begin{aligned}
\left| k_0^{j_0} - k_i^j \right| &\leq \sum_{\ell=0}^{j-j_0} (i_2)_\ell \left| k_{I+1}^{j-\ell} - k_I^{j-\ell} \right| + \sum_{\ell=0}^{j-j_0-1} \left| k_I^{j-\ell} - k_{I/2}^{j-\ell-1} \right| \\
&\leq \sum_{\ell=0}^{j-j_0} (i_2)_\ell \nabla k^{j-\ell} + 2 \sum_{\ell=0}^{j-j_0-1} \nabla k^{j-\ell} = \sum_{\ell=0}^{j-j_0} (i_2)_{j-j_0-\ell} \nabla k^{j_0+\ell} + 2 \sum_{\ell=0}^{j-j_0-1} \nabla k^{j_0+1+\ell} \\
&\leq 3 \nabla k^{j_0} \sum_{\ell=0}^{j-j_0} \nabla k^\ell
\end{aligned}
$$

where

$$I = i - \sum_{n=0}^{\ell} (i_2)_n 2^n$$

is the left even index, with respect to i, where we move in order to be able to use (4.20).

Since ∇k is summable, for any $\epsilon > 0$, we choose $j_0 \in \mathbb{N}$ such that

$$3 \nabla k^{j_0} \sum_{\ell=0}^{j-j_0} \nabla k^\ell < \frac{\epsilon}{2} \quad \Rightarrow \quad \left| k_0^{j_0} - k_i^j \right| < \frac{\epsilon}{2}. \tag{4.23}$$

Taking the maximum j_0 such that both (4.21) and (4.23) are bounded by $\epsilon/2$, then

$$\left| k_0^j - k_i^j \right| < \varepsilon$$

for any $0 < i \leq 2^{j-j_0}$ and $j \geq j_0$. $\qquad \square$

Corollary 4.12. *If $\mathcal{S}$ is convergent and ∇k is summable, for any $\epsilon > 0$, then there exists some $j_0 \in \mathbb{N}$ such that $\left| \bar{k}_0 - k_i^j \right| < \epsilon$ for any $0 < i \leq 2^{j-j_0}$ and $j \geq j_0$.*
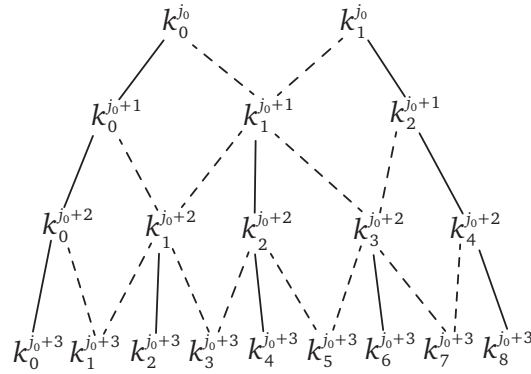
Figure 4.23. Discrete curvatures for the points p_i^j, with $0 < i \le 2^{j-j_0}$ and $j \ge j_0$. We use dashed lines to mark when we do not have a direct relation between the curvatures.

Proof: Combining the results of Proposition 4.4 and Proposition 4.11 we obtain that for any ϵ there exists some j_0 such that

$$\left| \bar{k}_0 - k_0^j \right| < \frac{\epsilon}{2}, \qquad \left| k_0^j - k_i^j \right| < \frac{\epsilon}{2}.$$

Then,

$$\left| \bar{k}_0 - k_i^j \right| \le \left| \bar{k}_0 - k_0^j \right| + \left| k_0^j - k_i^j \right| < \epsilon$$

for any $0 < i \le 2^{j-j_0}$ and $j \ge j_0$. $\qquad \square$

Proposition 4.12 shows that the discrete curvatures at different points in a neighbourhood of p_0 are ϵ-close to $\bar{k}_0$. We want to prove the same if instead we consider the curvature $k(p_0, p_i^j, p_{i+1}^j)$ of a circle passing through p_0 and two following points p_i^j, p_{i+1}^j in the right neighbourhood of p_0.

Conjecture 4.13. *If $\mathcal{S}$ is convergent, $\boldsymbol{\delta}$ and $\boldsymbol{\nabla k}$ are summable, for any $\epsilon > 0$, then there exists some $j_0 \in \mathbb{N}$ such that $\left| \bar{k}_0 - k(p_0, p_i^j, p_{i+1}^j) \right| < \epsilon$, for any $0 < i < 2^{j-j_0}$ and $j > j_0$.*

Any time we have to prove the convergence to $\bar{k}_0$ we can use Proposition 4.4 and we choose j_0 such that

$$\left| k_0^j - \bar{k}_0 \right| < \frac{\epsilon}{2},$$

in this way we can focus only on the relation with k_0^j.

Numerical evidence: The idea for the proof of Conjecture 4.13 is to use the inductive strategy, but unfortunately we did not manage to prove it. However, we show a numerical evidence of the conjecture. In Figure 4.24 we display

$$\max_{j \ge j_0} \max_{0 < i < 2^{j-j_0}} \left| k_0^j - k(p_0, p_i^j, p_{i+1}^j) \right|,$$

(a) 4-point scheme with $w = 1/32$

(b) Circle-based 4-point scheme

(c) 6-point scheme

(d) Circle-based 6-point scheme

Figure 4.24. Behaviour of $\max_{j \geq j_0} \max_{0 < i < 2^{j-j_0}} |k_0^j - k(p_0, p_i^j, p_{i+1}^j)|$ for increasing initial level j_0, with $0 \leq j_0 \leq 14$, and applying some subdivision schemes with different order of continuity: (a) the 4-point scheme with $w = 1/32$ (C^1), (b) the circle-based 4-point scheme (G^1), (c) the 6-point scheme (C^2), (d) the circle-based 6-point scheme (G^2). The colors refer to different control polygons, the same used in Section 4.2.

depending on the initial level j_0. We consider three different control polygons and we apply some subdivision schemes with different order of continuity. For C^1 or G^1 continuous schemes we can observe that shrinking the neighbourhood (for increasing j_0) the difference of curvature decreases but it does not decay to zero. While for schemes that are C^2 and G^2 continuous the difference between k_0^j and $k(p_0, p_i^j, p_{i+1}^j)$ decreases to zero as j_0 increases. This behaviour suggests that the circles $k(p_0, p_i^j, p_{i+1}^j)$ converge to k_0^j in the hypothesis of continuous curvature.

Conjecture 4.13 should help to prove the generalization of Proposition 4.9 to any point p_i^j in a right neighbourhood of p_0.

Conjecture 4.14. *Let $\mathcal{S}$ be a convergent scheme, δ and ∇k are summable, for any $\epsilon > 0$*

there exists some $j_0 \in \mathbb{N}$ such that

$$\left| \bar{k}_0 - k(p_0, p_i^j, \bar{t}_0) \right| < \epsilon$$

for any $0 < i \leq 2^{j-j_0}$ and $j \geq j_0$, where $k(p_0, p_i^j, \bar{t}_0)$ is the curvature of the circle with tangent $\bar{t}_0$ and passing through p_0 and p_i^j.

Numerical evidence: Also in this case we do not have a complete proof yet, so we can only test it numerically. Figure 4.25 shows for different initial levels j_0 the maximum of the difference between curvatures

$$\max_{j \geq j_0} \max_{0 < i < 2^{j-j_0}} \left| k_0^j - k(p_0, p_i^j, \bar{t}_0) \right|.$$

We test the conjecture using the control polygons considered in Section 4.2 and applying four subdivision schemes with different orders of regularity. The results are similar to the previous conjecture: we have that $k(p_0, p_i^j, \bar{t}_0)$ converge to k_0^j if the scheme generates curve with continuous curvature, otherwise the difference does not decay to zero or it remains constant as for the 4-point scheme with tension parameter $w = 1/32$.

The difficulties in Conjectures 4.13 and 4.14 arise by the non-linear nature of the curvature. In this sense is difficult to find relations between neighbouring circles with some common elements.

The Proposition 4.12 and Conjectures 4.13, 4.14 take into account the right neighbourhood of p_0, but similar results are true also considering the points p_{-i}^j in a left neighbourhood of p_0, $0 < i < 2^{j-j_0}$. Once we have proved these results for both sides of p_0 we can conclude that $\bar{k}_0$ is the curvature of the limit curve at p_0. In fact Proposition 2.2 states: if both the curvatures $k(p_{-\ell}, p_0, \bar{t}_0)$ and $k(p_0, p_i^j, \bar{t}_0)$, with $0 < i, \ell \leq 2^{j-j_0}$ and $j \geq j_0$, converge to the same value $\bar{k}_0$, then $\bar{k}_0$ is the curvature of the limit curve at p_0. The same proof can be repeated for any point generated by the subdivision process, since the discrete curvatures k_i^j converge pointwise at a generic point p_i^j.

4.3.3   Step 3

The final step consists of showing that the curvature changes continuously along the limit curve, namely that two neighbouring points on the limit curve have curvatures that are ϵ-close. We start by fixing p_0 and we show that the limit curvatures of all the points p_i^j in a neighbourhood of p_0 ($0 < i \leq 2^j$) differ by ϵ from $\bar{k}_0$ (see Fig. 4.26).

Proposition 4.15. *If $\mathcal{S}$ is a convergent scheme, $\boldsymbol{\delta}$ and $\nabla \boldsymbol{k}$ are summable, then for any $\epsilon > 0$, there exists some $j_0 \in \mathbb{N}$ such that for any $0 < i \leq 2^{j-j_0}$ and $j \geq j_0$,*

$$\left| \bar{k}_0 - \bar{k}_i^j \right| < \epsilon,$$

where $\bar{k}_i^j$ is the curvature of the limit curve at p_i^j.

(a) 4-point scheme with $w = 1/32$

(b) Circle-based 4-point scheme
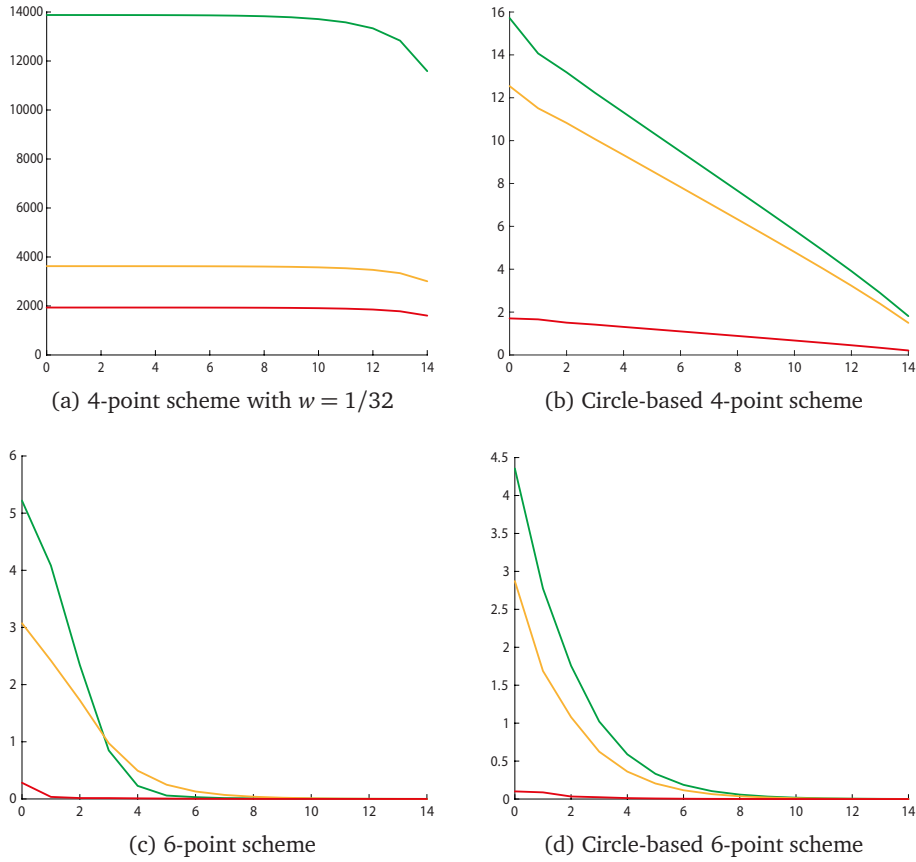
(c) 6-point scheme

(d) Circle-based 6-point scheme
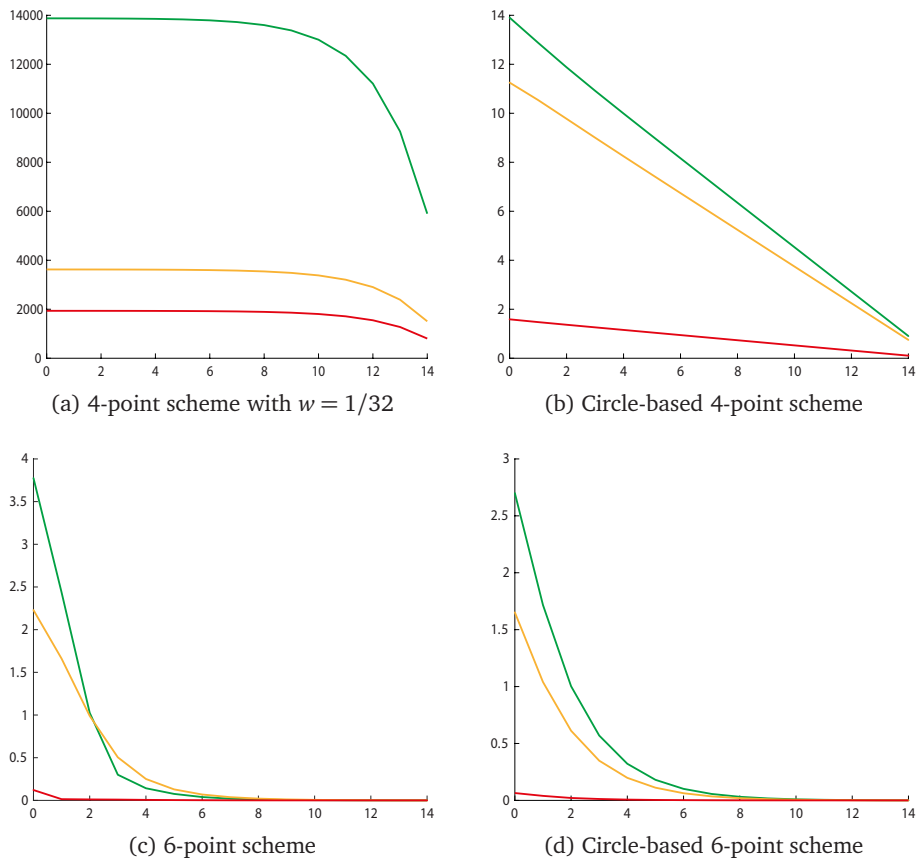
Figure 4.25. Behaviour of $\max_{j \geq j_0} \max_{0 < i < 2^{j-j_0}} |k_0^j - k(p_0, p_i^j, \bar{t}_0)|$ for increasing initial level $0 \leq j_0 \leq 14$ and applying some subdivision schemes with different order of continuity: (a) the 4-point scheme with $w = 1/32$ (C^1), (b) the circle-based 4-point scheme (G^1), (c) the 6-point scheme (C^2), (d) the circle-based 6-point scheme (G^2). The colors distinguish between different control polygons, the same used in Section 4.2.
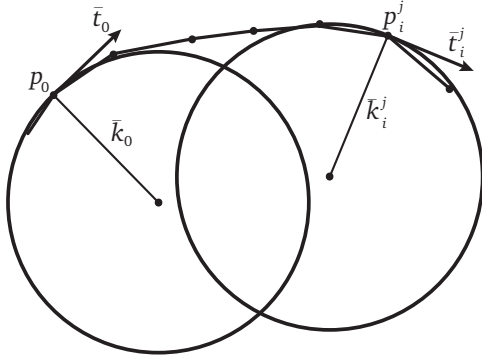
Figure 4.26. Comparison of the curvature of the osculating circles at p_0 and p_i^j.
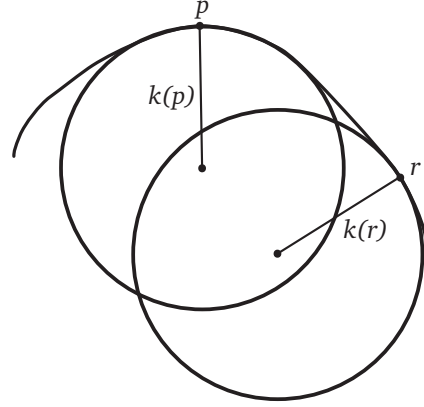
Figure 4.27. Comparison of the curvature of the osculating circles in two neighbouring points p and r of the limit curve.

Proof: In Lemma 4.5 we show that the discrete curvatures converge pointwise and uniformly, so for any $\epsilon > 0$ there exists $j_1 > 0$ such that

$$\left| \bar{k}_0 - k_0^j \right| < \frac{\epsilon}{3} \qquad \text{and} \qquad \left| \bar{k}_i^j - k_i^j \right| < \frac{\epsilon}{3},$$

for any $i \in \mathbb{Z}$ and $j > j_1$. Moreover, we prove in Proposition 4.11 that the discrete curvatures in a right neighbourhood of p_0 are ϵ-close: for any $\epsilon > 0$ there exists $j_2 > 0$ such that for $0 < i < 2^{j-j_2}$ and $j \geq j_2$,

$$\left| k_0^j - k_i^j \right| < \frac{\epsilon}{3}.$$

Defining $j_0 = \max\{j_1, j_2\}$ we obtain for any $j \geq j_0$,

$$\left| \bar{k}_0 - \bar{k}_i^j \right| \leq \left| \bar{k}_0 - k_0^j \right| + \left| k_0^j - k_i^j \right| + \left| k_i^j - \bar{k}_i^j \right| < \epsilon.$$

$\square$

Proposition 4.15 proves that the curvatures change continuously on the set of points $P = \left\{ p_i^j : j \geq 0,\ i \in \mathbb{Z} \right\}$ that it is dense on the limit curve. However, we still have to prove that the curvature is continuous for all the points on the limit curve. Considering two points p and r on the limit curve, not generated by the subdivision process, we have to prove that there exists the curvatures $k(p)$ and $k(r)$ and the difference of the curvatures decays to zero as r approaches p (see Fig. 4.27).

Conjecture 4.16. *If $\mathcal{S}$ is convergent, δ and ∇k are summable, then the limit curve $\mathcal{C}$ is G^2 continuous.*

Idea of the proof: Let us consider a point on the limit curve not generated by the subdivision process $p \in \mathscr{C} \backslash P$. We attach to this point the tangent t and the curvature k,

$$t = \lim_{n \to \infty} t_n, \qquad k = \lim_{n \to \infty} k_n, \tag{4.24}$$

where $\{p_n\}_{n \geq 0}$ is any sequence of points in P that converges to p from the right and t_n and k_n are the direct tangent and curvature at p_n. The idea of the proof is similar to the proof of Theorem 3.7, where Dyn and Hormann [2012] prove that t is the direct tangent of $\mathscr{C}$ at p. Here, to prove that the limit curve has continuous curvature we have to show that k is the osculating circle of $\mathscr{C}$ at p. The continuity of the curvature k along the limit curve $\mathscr{C}$ comes directly from Proposition 4.15.

Let us consider also a sequence of points $\{q_n\}_{n \geq 0}$ that converges to p from the left. The idea is to exploit Proposition 2.2, proving that

$$\lim_{n \to \infty} k(p, p_n, t) = \lim_{n \to \infty} k(q_n, p, t) = k.$$

Without loss of generality, we focus on the sequence $\{p_n\}_{n \geq 0}$ and the proof for the left side comes straightforward.

Suppose that there exist some $j \geq 0$ and $i \in \mathbb{Z}$ such that p and p_n are inside the piece of limit curve defined by p_i^j and p_{i+1}^j. The difference $|k - k(p, p_n, t)|$ can be bounded from above using the triangle inequality and exploiting the convergence of k_n, t_n and p_n,

$$|k - k(p, p_n, t)| \leq |k - k_n| + \left| k_n - k(p_i^j, p_n, p_{i+1}^j) \right| + \left| k(p_i^j, p_n, p_{i+1}^j) - k(p_i^j, p_n, t_n) \right|$$
$$+ \left| k(p_i^j, p_n, t_n) - k(p, p_n, t_n) \right| + |k(p, p_n, t_n) - k(p, p_n, t)|.$$

The first two terms can be bounded by ϵ by the definition of k (4.24) and Definition 2.8 of curvature of an osculating circle. In order to bound by ϵ the third and fourth terms we have to exploit the proofs of Proposition 4.9 and Conjectures 4.13, 4.14. The last term is bounded by ϵ thanks to the convergence of the tangents t_n. Unfortunately, we cannot go more into detail, because we miss the proofs of Conjectures 4.13 and 4.14 so we cannot show how to properly bound each term. $\qquad\square$

If we were able to cover the missing points (Conjecture 4.13, 4.14), then this last result would conclude the proof of Conjecture 4.1. For the missing parts we provide numerical evidence, we probably can find the missing relation between curvatures if we consider all the possible configurations, as done in Proposition 4.4.

In the end, we show, at least numerically, that the summability of the sequence ∇k is a sufficient condition to have a G^2 continuous scheme, namely a scheme that generates limit curve with continuous curvature. As we already show in Section 4.2 there are some geometric schemes as the incenter scheme and circle-based 6-point scheme that satisfy this condition and they generate a G^2 limit curve $\mathscr{C}$.

Part II

Subdivision Schemes for Image Analysis

Outline

The study of efficient representations of multidimensional functions is an important topic in signal processing, where such representations are useful in image compression and feature extraction. Applications related to phenomena that can be described as functions $f \in L^2(\mathbb{R}^d)$ (e.g. acustic signals, images, etc.) have received a strong impulse from the definition of wavelet transforms.

The success of wavelets is due to the ability to provide optimally sparse approximations of signals representing singularities much more efficiently than traditional Fourier methods and due to the existence of fast algorithms which digitalize the domain transform. Moreover, the concept of multiresolution analysis allows a unified treatment of the continuous and discrete wavelet transform (see [Chui, 1992a; Meyer, 1995; Mallat, 2008]). A multiresolution analysis is naturally related to a subdivision scheme and a filterbank that endorse the implementation of fast algorithms for the decomposition and reconstruction of a signal (cf. [Hamming, 1989; Strang and Nguyen, 1996; Vetterli and Kovačević, 2007]). All these concepts are recalled in Chapter 5.

Despite their success, wavelets are not always efficient when dealing with multivariate data. Wavelets work well to approximate data with pointwise singularities, but they may not handle efficiently singularities along curves. The reason is that wavelets are intrinsically isotropic, because they are generated by isotropically dilating a set of generators. Instead, in multivariate signals the singularities are concentrated on lower dimensional embedded manifolds, for example edges in natural images and shock fronts in the solutions of transport equations. Thus, there is the necessity of introducing a representation system that provides optimally sparse approximations of anisotropic features and a unified treatment of continuous and discrete transforms.

The first attempt are curvelets by Candès and Donoho [2004]. Curvelets form a pyramid of analysing functions defined not only at various scales and locations but also at various orientations, with the number of orientations increasing at finer scales. Since their supports become increasingly elongated at finer scales, curvelets are a good adaptive representation system to approximate images with edges. Curvelets have some drawbacks: they are defined only on bidimensional space, they do not preserve the integer lattice because they use rotations, and the lack of a multiresolution analysis that does not allow for fast decomposition algorithms. The preservation of the integer lattice is necessary to have a simple connection between the continuous and the digital setting.

The contourlets were introduced by Do and Vetterli [2005]. Contourlets are the filterbank version of curvelets. The advantage is the possibility to define efficient numerical algorithms, but the disadvantage is the absence of a continuous transform.

In the same year shearlets were introduced by Guo, Kutyniok and Labate [2006] and Labate et al. [2005]. Differently from curvelets, shearlets use shear to control directions instead of rotations. This is fundamentally different, because it allows the shearlet systems to be derived from a finite set of generators and gives a unified treatment of the continuous and digital signals, due to the fact that the shear matrix preserves the integer lattice. Thanks to their mathematical structure, shearlets are connected to a more general framework than the canonical MRA, that is the so-called multiple multiresolution analysis (MMRA). Any MMRA is related to a multiple subdivision scheme that is a scheme where in each iteration an expanding matrix and a subdivision scheme are chosen from a finite dictionary, see [Sauer, 2010]. In this way, the corresponding filterbanks allow the definition of efficient algorithms to decompose and reconstruct a signal. All these concepts are recalled and examined in detail in Chapter 6.

Multiresolution analysis, filterbanks and subdivision schemes are based on various types of scaling matrices that turns out to be the key ingredient of these tools, because they fix the way to refine the given data, to manipulate them. In other words they control the upsampling and downsampling of the data. The absolute value of the scaling matrix determinant gives the number of disjoint cosets which is strictly connected to the number of filters needed to analyse a signal and then to the computational complexity. In the wavelet setting the most popular dilation matrices are the dyadic ones with determinant 2^d and, in dimension $d = 2$, the quincunx matrix with determinant two (see [Mallat, 2008]). Each of them gives an isotropic refinement of the lattices $\mathbb{Z}^d$ and $\mathbb{Z}^2$ respectively. In the shearlet context, to gain directional flexibility, the dilation matrices are the product of a parabolic matrix

$$D_2 = \begin{pmatrix} 4\mathrm{I}_p & 0 \\ 0 & 2\mathrm{I}_{d-p} \end{pmatrix},$$

and a shear matrix. The drawback of the shearlet is the huge value of the determinant which is 2^{d+p} with respect to the determinant 2^d of the dyadic matrix used by the wavelets.

The aim of this second part of my work, presented in Chapter 7, is to develop a discrete directional transform that involves a family of dilation matrices with smaller determinant than shearlets. The idea is to keep the good properties of shearlets, such as the ability of catching signal features along different directions, and at the same time to improve the computational efficiency of the transform. In this sense, we study the crucial properties that the dilation matrices must have: to be expansive, jointly expansive and to satisfy the slope resolution property. To design a directional transform that uses these type of matrices we follow a different approach with respect to Labate et al. [2005] and Kutyniok et al. [2012], because we avoid to define explicitly the scaling function for the multiresolution analysis. We use the discrete approach of Sauer [2012], that defines the

multiple multiresolution analysis starting from a multiple subdivision scheme. This construction is convenient, because we need only to define a set of scaling matrices and the masks of the subdivision schemes associated with them. In this way, the multiresolution and the scaling functions are defined straightforwardly. Moreover, it allows to exploit the computational efficiency of the subdivision schemes in the transform computation.

In Section 7.2, we study a new family of anisotropic scaling matrices having the advantage of a smaller determinant with respect to shearlets especially when the dimension increases. Their structure is shearlet-like in the sense that they are the product of an anisotropic diagonal matrix in $\mathbb{Z}^{d \times d}$ with minimum determinant and a shear matrix. We prove that this family satisfies all the crucial properties stated above, and in particular we prove the slope resolution property (which is in general a non trivial task) in any dimension d. We provide also a family of filterbanks that allows to perform an MMRA. In Section 7.4 we present a part of the extensive experimentation done in the two dimensional case with the aim to illustrate how the directional transform defined by these matrices analyse an image. The numerical results confirm the effectiveness of these matrices to capture the details in different directions. Finally, in Section 7.3 we focus on anisotropic matrices for $d = 3$ non shearlet-like, that means they are product of a full matrix and a shear. By substituting the anisotropic diagonal matrices with a full matrix we can reduce even more the determinant. We present a choice of such matrices for which we have only a numerical evidence that they satisfy the slope resolution property.

Acknowledgement

Chapter 5

Wavelets

5.1 Wavelet system

The aim of signal processing is to give an efficient representation of signals, described as multivariate functions $f \in L^2(\mathbb{R}^d)$. Given a collection of analysing functions $\{\phi_i\}_{i \in I} \subseteq L^2(\mathbb{R}^d)$, with I a countable index set, we want to express any signal as

$$f = \sum_{i \in I} c_f(i)\phi_i.$$

This formula provides a decomposition of the function $f \in L^2(\mathbb{R}^d)$ into a countable collection of coefficients $c_f \subseteq \ell^2(I)$ (analysis process). Moreover, it also illustrates the synthesis process where the function f is reconstructed from the coefficients c_f.

Given a class of signals, the aim is to design an analysing system $\{\phi_i\}_{i \in I}$ such that for each function of the class, the corresponding coefficient sequence c_f is sparse. If a function is sparsely approximated, important features are described by coefficients with large absolute values. High approximation rates can then be achieved by storing only few coefficients.

Usually, the wavelet system in $L^2(\mathbb{R}^d)$ is composed by the dilation and translation of a single function ψ,

$$\{\psi_{M,t} = |\det M|^{d/2}\,\psi(M \cdot -t) : |\det M| \geq 2,\ t \in \mathbb{R}^d\}.$$

In general, we consider as matrix M the isotropic matrix $M = \alpha I_d$. In this case the continuous wavelet transform is the mapping

$$L^2(\mathbb{R}^d) \ni f \mapsto \mathcal{W}_\psi f(\alpha, t) = \alpha^{d/2} \int_{\mathbb{R}^d} f(x)\overline{\psi(\alpha x - t)}\,\mathrm{d}x, \quad \alpha > 0, t \in \mathbb{R}^d.$$

The only request on M is to be an *expanding* matrix.

Definition 5.1. *A matrix M is an* acceptable dilation *or an* expanding matrix *for $\mathbb{Z}^d$, if $M\mathbb{Z}^d \subset \mathbb{Z}^d$, and all its eigenvalues are greater than one in absolute value.*

Definition 5.2. *In a wavelet system, the analysing elements are obtained through the action of dilatation and translation operators on a generating function $\psi \in L^2(\mathbb{R}^d)$, called* wavelet *as*

$$\{\psi_{M,t} = |\det(M)|^{1/2}\,\psi(M(\cdot - t)) : M \in GL_d(\mathbb{R}),\ t \in \mathbb{R}^d\}.$$

The continuous wavelet transform is defined to be the mapping

$$L^2(\mathbb{R}^d) \ni f \mapsto \mathcal{W}_\psi f(M,t) = (f, \psi_{M,t}), \quad M \in GL_d(\mathbb{R}),\ t \in \mathbb{R}^d.$$

The matrix M belongs to the general linear group $GL_d(\mathbb{R})$ of $d \times d$ invertible matrices with entries in $\mathbb{R}$. Classic examples of matrices M are the dyadic matrix $2I_d$ and the quincunx matrix ($d = 2$),

$$M = \begin{pmatrix} 1 & -1 \\ 1 & 1 \end{pmatrix},$$

(see [Mallat, 2008]).

The property of the dilation matrix to leave the $\mathbb{Z}^d$ lattice invariant allows to discretize in a simpler way the continuous transform. Associated with the matrix M there is the coset $M\mathbb{Z}^d \subset \mathbb{Z}^d$ and it is possible to decompose $\mathbb{Z}^d$ into the the disjoint cosets $\xi + M\mathbb{Z}^d$,

$$\mathbb{Z}^d = \bigcup_{\xi \in E_M} \left(\xi + M\mathbb{Z}^d \right), \tag{5.1}$$

where $\xi \in E_M$ is a representative of $\mathbb{Z}^d/M\mathbb{Z}^d$ and $E_M = M[0,1)^d \cap \mathbb{Z}^d$. The vector $\xi = 0$ corresponds to the subgrid $M\mathbb{Z}^d$. The set E_M has $|\det M|$ elements and with E_M^0 we refer to $E_M \setminus \{0\}$. To define the discrete transform, it is sufficient to substitute the translation parameter $t \in \mathbb{R}^d$ with the discrete translation $\xi + k$, $\xi \in E_M$ and $k \in \mathbb{Z}^d$. The whole space $\mathbb{R}^d$ is recovered in the limit, in fact $M^{-j}\mathbb{Z}^d \to \mathbb{R}^d$ because the matrix has eigenvalues greater than one in absolute value and $\left\| M^{-j} \right\| \to 0$ for $j \to \infty$.

For example in two dimensions, choosing the dyadic matrix $\left(\begin{smallmatrix} 2 & 0 \\ 0 & 2 \end{smallmatrix}\right)$, the disjoint cosets are shown in Figure 5.1 and the representatives are

$$\xi_0 = \begin{pmatrix} 0 \\ 0 \end{pmatrix}, \quad \xi_1 = \begin{pmatrix} 1 \\ 0 \end{pmatrix}, \quad \xi_2 = \begin{pmatrix} 0 \\ 1 \end{pmatrix}, \quad \xi_3 = \begin{pmatrix} 1 \\ 1 \end{pmatrix}. \tag{5.2}$$

The corresponding discrete wavelet system is

$$\{\psi_{j,\xi,k} = 2^{jd/2}\psi(2^j \cdot -\xi - k) : j \in \mathbb{Z}, \xi \in E_{2I_2}, k \in \mathbb{Z}^d\}, \tag{5.3}$$

while the discrete wavelet transform is given by

$$\mathcal{W}_\psi f(j,\xi,k) = (f, \psi_{j,\xi,k})_{L^2(\mathbb{R}^d)}.$$

The choice of using isotropic matrices is the drawback of the wavelets because they are suitable to catch point singularities while we need a lot of coefficients to approximate discontinuities along curves. Let us consider a function f that is regular everywhere
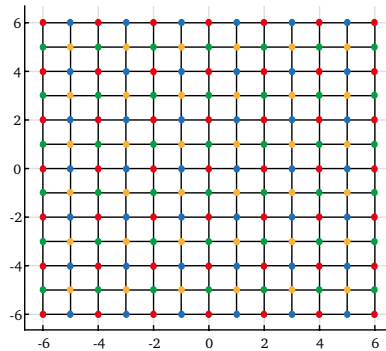
Figure 5.1. Disjoint cosets $\xi + M\mathbb{Z}^d$, where we consider the dyadic matrix $M = 2I_2$ and the representative ξ in (5.2): $\xi_0 + M\mathbb{Z}^2$ (red), $\xi_1 + M\mathbb{Z}^2$ (blue), $\xi_2 + M\mathbb{Z}^2$ (green), $\xi_4 + M\mathbb{Z}^2$ (orange).

except for a point singularity at x_0. The continuous wavelet transform $\mathcal{W}_\psi f(j, t)$ with the dyadic matrix has rapid asymptotic decay as $j \to \infty$, for all values of t, unless $t = x_0$. Continuous wavelet transforms can be used to characterize the singular support of a function, however it is unable to provide additional information about the geometry of the set of singularities. Let $f \in L^2(\mathbb{R}^2)$ be an image that contains a singularity along a smooth curve and $\{\psi_{j,\xi,k}\}$ the discrete wavelet basis in (5.3). For large j the only significant wavelet coefficients $(f, \psi_{j,\xi,k})_{L^2(\mathbb{R}^d)}$ are those associated with the singularities. At scale 2^{-j} each wavelet is supported or essentially supported inside a box $2^{-j} \times 2^{-j}$, hence there exist several elements of the wavelet basis overlapping the singularity curve and the signal representation is not sparse. We will see that shearlets overcome the problem with analysing elements ranging over several scales, orientations and locations and with the property to become very elongated.

The advantage of the wavelet is the possibility to define a multiresolution analysis that gives a unified mathematical background to the continuous and discrete transform. Moreover, a multiresolution analysis is always associate with a subdivision scheme that allows a fast implementation of the wavelet transform.

5.2 Multiresolution analysis

A multiresolution analysis allows to approximate signals at various resolutions with projections on different spaces. It is basically a way to subdivide the space $L^2(\mathbb{R}^d)$ in subspaces and to decompose a function $f \in L^2(\mathbb{R}^d)$ by projecting on these spaces.

In [Mallat, 1989; Meyer, 1995] the concept of a multiresolution analysis related to dyadic matrices $2I_d$ is presented respectively in the univariate and the multivariate setting. We recall the definition of a multiresolution analysis of $L^2(\mathbb{R}^d)$ for a generic expanding matrix $M \in \mathbb{R}^{d \times d}$ (see e.g. [Madych, 1993]).

Definition 5.3. *A sequence of nested closed subspaces $V_j \subset V_{j+1} \subset V$, $j \in \mathbb{Z}$, in a space V is called a multiresolution analysis (MRA) if*

(i) *(Traslation invariance) $f \in V_j$ if and only if $f(\cdot - M^{-j}k) \in V_j$ for all $\alpha \in \mathbb{Z}^d$.*

(ii) *(Scaling property) $f \in V_j$ if and only if $f(M\cdot) \in V_{j+1}$.*

(iii) *(Limits) The spaces are exhaustive and non redundant:*

$$\lim_{j \to \infty} V_j = V, \quad \lim_{j \to -\infty} V_j = \{0\}. \tag{5.4}$$

(iv) *(Basis) There exists a scaling function $\phi \in V$ such that $\{\phi(\cdot - k) : k \in \mathbb{Z}^d\}$ is a stable basis of V_0.*

In the case of signal analysis we consider as space $V = L^2(\mathbb{R}^d)$.

If ϕ is a stable basis of V_0, its scaled and shifted version $\{|\det M|^{jd/2} \phi(M^j \cdot - k), k \in \mathbb{Z}^d\}$ is a stable basis for V_j. Then, the projection on V_j gives information about the resolution M^j of the signal. The approximation of a function in V_{j+1} has additional information available with respect to the approximation in V_j. We define U_j as the orthogonal complement of V_j in V_{j+1}

$$V_{j+1} = V_j \oplus U_j, \tag{5.5}$$

for any $j \in \mathbb{Z}$. There exists a set of functions $\psi_\xi(x)$ such that

$$\{|\det M|^{jd/2} \psi_\xi(M^j \cdot - k), \xi \in E_M^0, k \in \mathbb{Z}^d\}$$

is an orthonormal basis of U_j. Moreover, relation (5.4) allows to decompose the space

$$L^2(\mathbb{R}^d) = \bigoplus_{j=-\infty}^{\infty} U_j$$

into the direct sum of the subspaces U_j. Then, the family of functions

$$\left\{|\det M|^{jd/2} \psi_\xi(M^j \cdot - k), j \in \mathbb{Z}, \xi \in E_M^0, k \in \mathbb{Z}^d\right\}$$

is a wavelet orthonormal basis of $L^2(\mathbb{R}^d)$.

The scaling property (ii) and the nestedness of the spaces ($V_0 \subset V_1$) provide a scaling function ϕ that is refinable, namely there exist coefficients $a \in \ell(\mathbb{Z}^d)$ such that

$$\phi(\cdot) = \sum_{k \in \mathbb{Z}^d} a(k)\phi(M \cdot - k). \tag{5.6}$$

These coefficients a can be seen as the mask of a subdivision scheme. As shown in Section 1.3, the basic limit function of a subdivision scheme is a refinable function.

The wavelet basis functions ψ_ξ, $\xi \in E_M^0$, can be defined using the scaling function ϕ. By definition of the spaces U_j (5.5), we have that $U_0 \subset V_1$ and then

$$\psi_\xi(\cdot) = \sum_{k \in \mathbb{Z}^d} b_\xi(k)\phi(M \cdot -k). \tag{5.7}$$

Using $V_1 = V_0 \oplus U_0$, we can write the basis of V_1 with respect to the basis of V_0 and U_0,

$$\phi(M \cdot -k) = \sum_{\ell \in \mathbb{Z}^d} \left(p(k - M\ell)\phi(\cdot - \ell) + \sum_{\xi \in E_M^0} q_\xi(k - M\ell)\psi_\xi(\cdot - \ell) \right), \tag{5.8}$$

where $p, q_\xi \in \ell^1(\mathbb{Z}^d)$. For simplicity, from here on we do not consider the normalization factor $|\det M|^{jd/2}$.

Any signal seen as a function $s \in L^2(\mathbb{R}^d)$ can be approximated as closely as desired by $s_j \in V_j$ and $j \in \mathbb{Z}$, due to (5.4). By the nestedness of the spaces V_j and the definition of U_j, we can write any space V_j as

$$V_j = U_{j-1} + V_{j-1},$$

thus the function s_j has a decomposition

$$s_j = u_{j-1} + s_{j-1}$$

where $s_{j-1} \in V_{j-1}$ and $u_{j-1} \in U_{j-1}$. Since ϕ and ψ_ξ are bases respectively of V_j and U_j, for any $j \in \mathbb{Z}$, we can express

$$s_j(x) = \sum_{k \in \mathbb{Z}^d} c^j(k)\phi(M^j x - k) \in V_j, \tag{5.9}$$

$$u_j(x) = \sum_{k \in \mathbb{Z}^d} \sum_{\xi \in E_M^0} d_\xi^j(k)\psi_\xi(M^j x - k) \in U_j. \tag{5.10}$$

Inserting (5.8) in the expression of s_j we obtain

$$s_j(x) = \underbrace{\sum_{k \in \mathbb{Z}^d} \sum_{\ell \in \mathbb{Z}^d} p(k - M\ell)c^j(k)\phi(M^{j-1}x - \ell)}_{s_{j-1}} + \underbrace{\sum_{k \in \mathbb{Z}^d} \sum_{\xi \in E_M^0} \sum_{\ell \in \mathbb{Z}^d} q_\xi(k - M\ell)c^j(k)\psi_\xi(M^{j-1}x - \ell)}_{u_{j-1}},$$

so the coefficients in the expression of s_j and u_j can be computed iteratively

$$c^{j-1} = \sum_{k \in \mathbb{Z}^d} p(k - M\cdot)c^j(k),$$

$$d_\xi^{j-1} = \sum_{k \in \mathbb{Z}^d} q_\xi(k - M\cdot)c^j(k), \tag{5.11}$$

with $\xi \in E_M^0$. These formulas express the decomposition algorithm where we compute the coefficients of the expression of s_{j-1} and u_{j-1}. Vice versa using (5.6) and (5.7) in the sum $s_{j-1} + u_{j-1}$ we obtain

$$
\begin{aligned}
s_j(x) &= s_{j-1}(x) + u_{j-1}(x) \\
&= \sum_{k \in \mathbb{Z}^d} \sum_{\ell \in \mathbb{Z}^d} \left(a(k - M\ell)c^{j-1}(\ell) + \sum_{\xi \in E_M^0} b_\xi(k - M\ell)d_\xi^{j-1}(\ell) \right) \phi(M^j x - k).
\end{aligned}
$$

It means that starting from the coefficients c^{j-1} and $\{d_\xi^{j-1}\}_{\xi \in E_M^0}$ we can reconstruct the signal by computing

$$
c^j = \sum_{\ell \in \mathbb{Z}^d} a(\cdot - M\ell)c^{j-1}(\ell) + \sum_{\xi \in E_M^0} b_\xi(\cdot - M\ell)d_\xi^{j-1}(\ell). \tag{5.12}
$$

This expresses the reconstruction algorithm.

Reintroducing the normalization factor $|\det M|^{jd/2}$, the relations (5.11) and (5.12) for the decomposition and reconstruction of a signal become

$$
\begin{aligned}
c^{j-1} &= \sqrt{\det M} \sum_{k \in \mathbb{Z}^d} p(k - M\cdot)c^j(k), \\
d_\xi^{j-1} &= \sqrt{\det M} \sum_{k \in \mathbb{Z}^d} q_\xi(k - M\cdot)c^j(k), \\
c^j &= \frac{1}{\sqrt{\det M}} \sum_{\ell \in \mathbb{Z}^d} a(\cdot - M\ell)c^{j-1}(\ell) + \sum_{\xi \in E_M^0} b_\xi(\cdot - M\ell)d_\xi^{j-1}(\ell).
\end{aligned} \tag{5.13}
$$

In the next section we deduce these relations from a different point of view.

5.3 Filterbank

A multiresolution analysis and a subdivision scheme lead to an efficient implementation for the analysis and synthesis of a signal by means of a filterbank. Filterbanks allow an analytic decomposition of signals using discrete operations on discrete signals. Good filterbanks reconstruct the original signal if there are no changes in the decomposition coefficients. An extensive presentation of filters can be found in [Hamming, 1989; Strang and Nguyen, 1996; Vetterli and Kovačević, 2007].

Definition 5.4. *An operator $F : \ell(\mathbb{Z}^d) \to \ell(\mathbb{Z}^d)$ is called an* LTI *filter (Linear and Time Invariant) if it is a linear operator that commutes with translation,*

$$
\tau_k(Fc) = (Fc)(\cdot + k) = F(c(\cdot + k)) = F\tau_k c
$$

for $c \in \ell(\mathbb{Z}^d)$, $k \in \mathbb{Z}^d$ and $\tau_k c = c(\cdot + k)$ is the translation operator.

Let us consider the sequence $\delta = \{\delta_{0,k}, k \in \mathbb{Z}^d\}$, the *impulse response* $f \in \ell(\mathbb{Z}^d)$ of the filter F is $f = F\delta$. A FIR (Finite Impulse Response) filter is such that $f \in \ell_{00}(\mathbb{Z}^d)$. The application of a filter to a signal c can be written as a convolution with the impulse response

$$Fc = f * c = \sum_{k \in \mathbb{Z}^d} f(\cdot - k)c(k).$$

Once we consider an expanding matrix M, any element of $\mathbb{Z}^d$ is given by the sum of a representative of cosets $\xi \in E_M$ plus an element of $M\mathbb{Z}^d$, as seen in (5.1). Thus, the application of the filter can be written as

$$(f * c)(\alpha) = (f * c)(\xi + M\beta) = (f_\xi * c)(M\beta).$$

In this way, we introduce $m = |\det M|$ impulse responses f_ξ, with $\xi \in E_M$, that define a filterbank. A filterbank is simply a set of filters and, in this case, it is called *critically sampled* because the decimation rate $|\det M|$ coincides with the number m of considered filters. In the following, we always consider critically sampled filterbanks.

The *downsampling* operator $\downarrow_M$, with respect to an expanding matrix M, is defined as

$$\downarrow_M c = c(M\cdot), \tag{5.14}$$

where $c \in \ell(\mathbb{Z}^d)$.

Using the definition of downsampling (5.14), the *analysis filters* are operators that decompose a given signal $c \in \ell(\mathbb{Z}^d)$ into the vector

$$c \mapsto \left\{ c_\xi^1 = \downarrow_M (f_\xi * c), \ \xi \in E_M \right\}. \tag{5.15}$$

The output vector has the same amount of information of the initial signal c, in fact the increase of information given by the m filters is compensated by the subsampling $\downarrow_M$.

It is natural to try to invert the process: starting with the vector $\{c_\xi^1\}_{\xi \in E_M}$, to reconstruct the signal c. So we introduce the *upsampling* operator $\uparrow_M$

$$\uparrow_M c(\alpha) = \begin{cases} c(M^{-1}\alpha) & \alpha \in M\mathbb{Z}^d, \\ 0 & \alpha \notin M\mathbb{Z}^d, \end{cases} \tag{5.16}$$

for $c \in \ell(\mathbb{Z}^d)$. It is worthwhile to remark that $\downarrow_M \uparrow_M$ is an identity, while $\uparrow_M \downarrow_M$ is a lossy operator due to the decimation involved in the upsampling,

$$\uparrow_M \downarrow_M c(\alpha) = \begin{cases} c(\alpha) & \alpha \in M\mathbb{Z}^d, \\ 0 & \alpha \notin M\mathbb{Z}^d. \end{cases} \tag{5.17}$$

Figure 5.2 shows the effect of these two operations (downsampling and upsampling) on an image.

We reconstruct the signal by convolving it with a set of filters g_ξ, $\xi \in E_M$, called *synthesis filters*

$$\tilde{c} = \sum_{\xi \in E_M} g_\xi * \uparrow_M c_\xi^1. \tag{5.18}$$

$$\begin{pmatrix} \color{red}{188} & 189 & \color{red}{191} & 191 & \color{red}{194} \\ 187 & 188 & 189 & 190 & 192 \\ \color{red}{185} & 187 & \color{red}{188} & 189 & \color{red}{189} \\ 185 & 187 & 188 & 190 & 189 \\ \color{red}{182} & 183 & \color{red}{185} & 186 & \color{red}{186} \end{pmatrix} \xrightarrow{\downarrow_M} \begin{pmatrix} 188 & 191 & 194 \\ 185 & 188 & 189 \\ 182 & 185 & 186 \end{pmatrix} \xrightarrow{\uparrow_M} \begin{pmatrix} 188 & 0 & 191 & 0 & 194 \\ 0 & 0 & 0 & 0 & 0 \\ 185 & 0 & 188 & 0 & 189 \\ 0 & 0 & 0 & 0 & 0 \\ 182 & 0 & 185 & 0 & 186 \end{pmatrix}$$
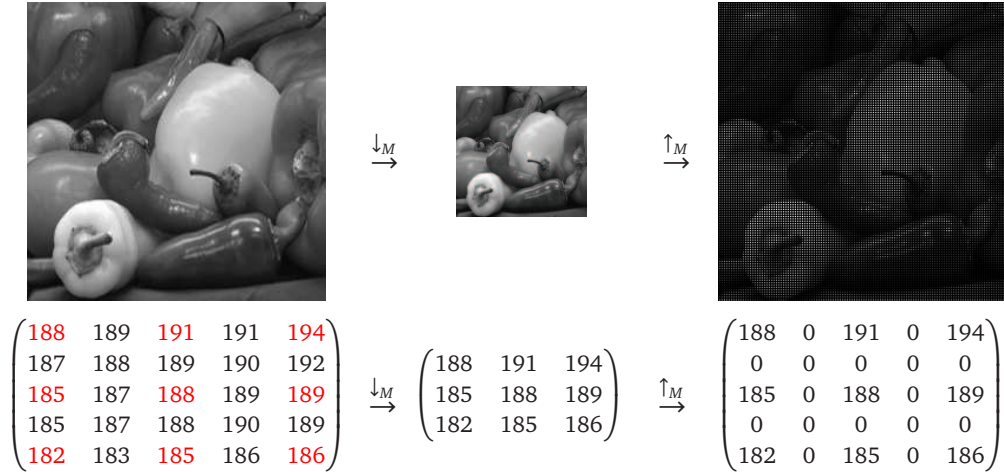
Figure 5.2. Downsampling and upsampling process with respect to the dyadic matrix $M = 2I_2$. From left to right: the original image, the downsampling and the upsampling. Below we display the same operations on a part of the data.

The whole process is sketched in Figure 5.3 and can be repeated by applying the analysis filters to the vector c_0^1.

Comparing the decomposition and reconstruction process in filter analysis (5.15), (5.18) with the relation between wavelet coefficients (5.11), (5.12), we recognise a strict relation between filterbanks and the multiresolution setting. In the analysis process,

$$\begin{aligned} c^{j-1} = \sum_{k \in \mathbb{Z}^d} p(k - M\cdot)c^j(k) & \quad \leftrightarrow \quad c_0^1 = \sum_{\alpha \in \mathbb{Z}^d} f_0(M\cdot - \alpha)c(\alpha), \\ d_\xi^{j-1} = \sum_{k \in \mathbb{Z}^d} q_\xi(k - M\cdot)c^j(k) & \quad \leftrightarrow \quad c_\xi^1 = \sum_{\alpha \in \mathbb{Z}^d} f_\xi(M\cdot - \alpha)c(\alpha). \end{aligned}$$

The two descriptions coincide if we set $f_0(\ell) = p(-\ell)$ and $f_\xi(\ell) = q_\xi(-\ell)$ for any $\ell \in \mathbb{Z}^d$. In the two different settings, the synthesis process is described by

$$\begin{aligned} c^j &= \sum_{\ell \in \mathbb{Z}^d} a(\cdot - M\ell)c^{j-1}(\ell) + \sum_{\xi \in E_M^0} b_\xi(\cdot - M\ell)d_\xi^{j-1}(\ell), \\ \tilde{c} &= \sum_{\alpha \in \mathbb{Z}^d} g_0(\cdot - M\alpha)c_0^1(\alpha) + \sum_{\xi \in E_M^0} g_\xi(\cdot - M\alpha)c_\xi^1(\alpha), \end{aligned}$$

and they coincide if we impose $g_0 = a$ and $g_\xi = b_\xi$, $\xi \in E_M^0$.

We observe that f_0 and g_0 have a formulation that is different from the other filters f_ξ and g_ξ with $\xi \in E_M^0$. The difference comes from the wavelet setting where the wavelet basis is composed by dilating and shifting the scaling function ϕ and the wavelet functions ψ_ξ, $\xi \in E_M^0$. Thus, $\{\phi(M^j \cdot - k)\}$ is the basis of V_j that contains the smooth part of the signal, while $\{\psi_\xi(M^j \cdot - k)\}$ is the basis of the space U_j that contains the details of the signal. For this reason the filters f_0 and g_0 are called low-pass filters and f_ξ, g_ξ with $\xi \in E_M^0$ are called high-pass filters.
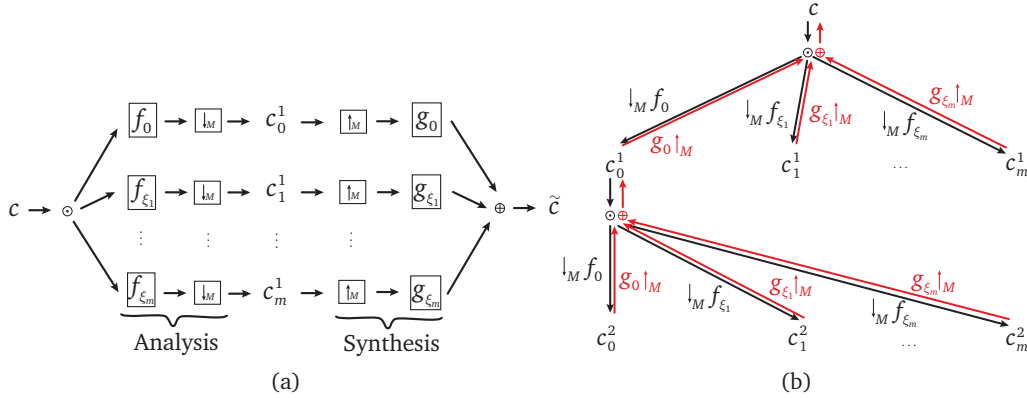
Figure 5.3. (a) Scheme of one level of decomposition and reconstruction of a signal c by convolving with the analysis filters $\{f_\xi\}_{\xi \in E_M}$ and the synthesis filters $\{g_\xi\}_{\xi \in E_M}$. (b) The process can be iterated by decomposing c_0^1. The reconstruction process is depicted in red.

A perfect reconstruction filterbank is when the analysis filters are the inverse of the synthesis filters and the reconstructed signal is exactly the initial signal c,

$$c = \sum_{\xi \in E_M} g_\xi * \uparrow_M \downarrow_M f_\xi * c. \tag{5.19}$$

A simple example of perfect reconstruction filterbank is given by the translational operator τ_ξ,

$$\sum_{\xi \in E_M} \tau_\xi \uparrow_M \downarrow_M \tau_{-\xi} = I. \tag{5.20}$$

If we expand the synthesis process (5.18) with a generic filter g, then

$$g * \uparrow_M c = \sum_{\alpha \in M\mathbb{Z}^d} g(\cdot - \alpha)c(M^{-1}\alpha) = \sum_{\alpha \in \mathbb{Z}^d} g(\cdot - M\alpha)c(\alpha) = \mathcal{S}_g c, \tag{5.21}$$

and we recognize the refinement equation of a subdivision scheme with mask g. There is a strict connection between synthesis filters and subdivision schemes. In particular it is possible to define a filterbank starting from an interpolatory subdivision scheme. This construction is called *prediction-correction* method and it is described in [Conti et al., 2010; Sauer, 2012]. A subdivision scheme with mask a takes coarse data and predicts how to refine them, thus it can be used as a synthesis filters $g_0 = a$. In this case, the best way to define the low-pass analysis filter is to set $f_0 = \delta$, so the analysis process samples the initial data c, $\downarrow_M f_0 c(\cdot) = c(M\cdot)$. With these filters and choosing an interpolatory scheme, namely $a(M\cdot) = \delta$, we reproduce data from the coarse grid $M\mathbb{Z}^d$ as reconstructed values, in fact

$$(g_0 * \uparrow_M \downarrow_M f_0 * c)(M\cdot) = (\mathcal{S}_a \downarrow_M c)(M\cdot) = \sum_{\alpha \in \mathbb{Z}^d} a(M\cdot - M\alpha)c(M\alpha) = c(M\cdot).$$

The prediction from decimated values is correct only on the coarse grid $(M\mathbb{Z}^d)$. We have to compensate the error on the other cosets. In this sense, we define the high-pass analysis filters as

$$f_\xi = \tau_{-\xi}(\delta - \uparrow_M \downarrow_M a), \quad \xi \in E_M^0,$$

where

$$\tau_{-\xi} \uparrow_M \downarrow_M a = \begin{cases} a(i - \xi) & i \in M\mathbb{Z}^d \\ 0 & i \notin M\mathbb{Z}^d \end{cases}$$

is the upsampling of the submask with respect to $\xi \in E_M$. The correction takes care also of the cosets $\xi + M\mathbb{Z}^d$. Finally, the high-pass reconstruction filters have the role to shift the correction values at the correct place

$$g_\xi = \tau_\xi \delta, \quad \xi \in E_M^0.$$

Summarizing, the impulses responses generated by an interpolatory subdivision scheme $\mathcal{S}_a$ are

	Low-pass	High-pass
Analysis	$f_0 = \delta$	$f_\xi = \tau_{-\xi}(\delta - \uparrow_M \downarrow_M a)$
Synthesis	$g_0 = a$	$g_\xi = \tau_\xi \delta$

$$(5.22)$$

for $\xi \in E_M^0$ and the corresponding filters are

$$\begin{aligned} F_0 &= I, & F_\xi &= \tau_{-\xi}(I - \uparrow_M \downarrow_M A), \\ G_0 &= A, & G_\xi &= \tau_\xi, \end{aligned}$$

where A is the operator related to the impulse response a, $Ac = a * c$. The filter A is different from the subdivision scheme $\mathcal{S}_a$ that has the upsampling inside, see (5.21). The filters F_0 and G_ξ, $\xi \in E_M^0$, are linear and time invariant filters. We have to show the same for the others filters. It is easy to verify that $\tau_\beta G_0 = G_0 \tau_\beta$, in fact

$$\tau_\beta Ac = \tau_\beta \left(\sum_{k \in \mathbb{Z}^d} a(i-k)c(k) \right) = \sum_{k \in \mathbb{Z}^d} a(i-k+\beta)c(k) = \sum_{\ell \in \mathbb{Z}^d} a(i-\ell)c(\ell+\beta) = A\tau_\beta c.$$

In a similar way we can verify that $\tau_\beta(\tau_{-\xi} \uparrow_M \downarrow_M A) = \tau_{-\xi} \uparrow_M \downarrow_M A\tau_\beta$ and also F_ξ, $\xi \in E_M^0$, are linear and time invariant filters.

In symbol calculus, these filters (5.22) can be described as

$$\begin{aligned} f_0^*(z) &= 1, & f_\xi^*(z) &= z^\xi \left(1 - \sum_{i \in \mathbb{Z}^d} a(Mi - \xi)z^{Mi-\xi} \right), \\ g_0^*(z) &= a^*(z), & g_\xi^*(z) &= z^{-\xi}, \end{aligned}$$

$$(5.23)$$

with $\xi \in E_M^0$.

It remains to prove that the filters defined in (5.22) generate a perfect reconstruction filterbank,

$$\sum_{\xi \in E_M} \left(g_\xi * \uparrow_M \downarrow_M f_\xi * c \right)(i) = (a * \uparrow_M \downarrow_M c)(i) + \sum_{\xi \in E_M^0} (g_\xi * \uparrow_M \downarrow_M f_\xi * c)(i)$$

$$= \sum_{\substack{k \in \mathbb{Z}^d \\ (i \in M\mathbb{Z}^d)}} a(i-k)c(k) + \sum_{\xi \in E_M^0} \left(\tau_\xi \uparrow_M \downarrow_M \tau_{-\xi} c \right)(i) - \sum_{\xi \in E_M^0} \left(\tau_\xi * \uparrow_M \downarrow_M (\tau_{-\xi} \uparrow_M \downarrow_M a) * c \right)(i)$$

$$= \sum_{k \in \mathbb{Z}^d} a(Mj-k)c(k) + (I - \uparrow_M \downarrow_M)c - \sum_{\xi \in E_M^0} \left(\tau_\xi * \uparrow_M \downarrow_M (\tau_{-\xi} \uparrow_M \downarrow_M a) * c \right)(i)$$

$$= \sum_{k \in \mathbb{Z}^d} a(Mj-k)c(k) + c(i) - c(Mj) - \sum_{\xi \in E_M^0} \left(\tau_\xi * \uparrow_M \downarrow_M (\tau_{-\xi} \uparrow_M \downarrow_M a) * c \right)(i).$$

We distinguish between high-pass and low-pass filters and we exploit the fact that the traslational operator is a perfect reconstruction filterbank (5.20). If the index i has to be on the subgrid $M\mathbb{Z}^d$, then we substitute i with Mj, $j \in \mathbb{Z}^d$. We analyse the last term separately in order to simplify it. First of all we can rewrite,

$$(\tau_{-\xi} \uparrow_M \downarrow_M a) * c(i) = \sum_{\substack{k \in \mathbb{Z}^d \\ (i-k \in M\mathbb{Z}^d)}} a(i-k-\xi)c(k) = \sum_{\ell \in \mathbb{Z}^d} a(M\ell - \xi)c(i - M\ell).$$

Inserting this in the last term, we get

$$\sum_{\xi \in E_M^0} \left(\tau_\xi * \uparrow_M \downarrow_M (\tau_{-\xi} \uparrow_M \downarrow_M a) * c \right)(i) = \sum_{\xi \in E_M^0} \tau_\xi * \uparrow_M \downarrow_M \left(\sum_{\ell \in \mathbb{Z}^d} a(M\ell - \xi)c(i - M\ell) \right)$$

$$= \sum_{\xi \in E_M^0} \tau_\xi \sum_{\substack{\ell \in \mathbb{Z}^d \\ (i \in M\mathbb{Z}^d)}} a(M\ell - \xi)c(i - M\ell) = \sum_{\xi \in E_M^0} \sum_{\ell \in \mathbb{Z}^d} a(M\ell - \xi)c(Mj + \xi - M\ell)$$

$$= \sum_{\xi \in E_M^0} \sum_{k \in M\mathbb{Z}^d + \xi} a(Mj - k)c(k).$$

We know that any element in $\mathbb{Z}^d$ can be written as $M\mathbb{Z}^d + \xi$ for some $\xi \in E_M$. Considering all the terms together we have

$$\sum_{\xi \in E_M} \left(g_\xi * \uparrow_M \downarrow_M f_\xi * c \right)(i)$$

$$= \sum_{k \in \mathbb{Z}^d} a(Mj - k)c(k) + c(i) - c(Mj) - \sum_{\xi \in E_M^0} \left(\tau_\xi * \uparrow_M \downarrow_M (\tau_{-\xi} \uparrow_M \downarrow_M a) * c \right)(i)$$

$$= \sum_{\xi \in E_M} \sum_{k \in M\mathbb{Z}^d + \xi} a(Mj - k)c(k) + c(i) - c(Mj) - \sum_{\xi \in E_M^0} \sum_{k \in M\mathbb{Z}^d + \xi} a(Mj - k)c(k)$$

$$= \sum_{k \in M\mathbb{Z}^d} a(Mj - k)c(k) - c(Mj) + c(i) = c(Mj) - c(Mj) + c(i) = c(i),$$

where we exploit that $\mathcal{S}_a$ is an interpolatory scheme ($a(M\cdot) = \delta$). In this way we prove that the choice of filters in (5.22) design a perfect reconstruction filterbank.

In general, an interpolatory (convergent) subdivision always allows to define a perfect reconstruction filterbank. Moreover, Derado [1999] prove that for any expanding matrix M, it is possible to define a convergent interpolatory scheme. In conclusion, we only need to have a suitable expanding matrix. This is why the thesis focuses on the problem of finding good matrices that allow to construct an alternative to shearlet providing a directional approach.

Chapter 6

Shearlets

6.1 Shearlet system

After the discussion on the limitations of wavelet systems in higher dimensions, we introduce the shearlet system as a general framework to overcome these drawbacks.

In order to achieve optimally sparse approximations of signals exhibiting anisotropic singularities, the analysing elements must consist of waveforms ranging over several scales, orientations and locations with the ability to become very elongated. These characteristics require a combination of an appropriate scaling operator to generate elements at different scales, an orthogonal operator to change their orientations, and a translation operator to displace these elements.

As scaling operator, shearlets consider the parabolic scaling matrices

$$D_\alpha = \begin{pmatrix} \alpha^2 I_p & 0 \\ 0 & \alpha I_{d-p} \end{pmatrix},$$ (6.1)

with $\alpha \geq 2$, $p \leq d$. This matrix is called *parabolic* because one eigenvalue is the square of the other, moreover it is responsible for the anisotropy of shearlets.

The parameter p in (6.1) allows to catch singularities in p-dimensional manifolds. For example, in three dimension there are different types of anisotropic features like singularities in one dimensional and two dimensional manifold. For d dimensional data, the singularities are embedded in manifolds at most $(d-1)$ dimensional. Our work mainly focuses on detecting directions of edges, so we fix $p = d-1$.

To change the orientation of waveforms, it is not possible to consider the rotation operator, because it destroys the structure of the integer lattice $\mathbb{Z}^d$ when the angle of rotation is different from $k\frac{\pi}{2}$, $k \in \mathbb{Z}$. This is one drawback of curvelets. It is important to preserve the integer lattice in order to define the discrete transform simply as a discretization of the continuous transform. An alternative orthogonal transformation is given by the *shear* matrix

$$S_W = \begin{pmatrix} I_p & W \\ 0 & I_{d-p} \end{pmatrix}$$ (6.2)

where $W \in \mathbb{R}^{p \times (d-p)}$. If W is integer, then S_W leaves the integer lattice invariant. Looking at the 2×2 matrix

$$S_w = \begin{pmatrix} 1 & w \\ 0 & 1 \end{pmatrix}, \tag{6.3}$$

we observe that the shear matrices parametrize the orientations using the slope w, rather than the angle as done by the rotations. The shear matrices are *unimodular* matrices, $\det S_W = \pm 1$, whose inverse is again a shear matrix

$$S_W^{-1} = S_{-W}, \tag{6.4}$$

and they satisfy

$$S_W^j = S_{jW} \quad \text{and} \quad S_W S_{W'} = S_{W+W'}. \tag{6.5}$$

Due to these properties, the parabolic scaling matrix and the shear matrix "pseudo-commute", i.e.

$$D_\alpha S_W = S_W^\alpha D_\alpha. \tag{6.6}$$

In general, two matrices A and B are *pseudo-commuting* matrices if there exists some $n, m \in \mathbb{N}$ such that $BA^m = A^n B$. In the shearlet case we have

$$D_\alpha S_W = \begin{pmatrix} \alpha^2 I_p & 0 \\ 0 & \alpha I_{d-p} \end{pmatrix} \begin{pmatrix} I_p & W \\ 0 & I_{d-p} \end{pmatrix} = \begin{pmatrix} \alpha^2 I_p & \alpha^2 W \\ 0 & \alpha I_{d-p} \end{pmatrix}$$
$$= \begin{pmatrix} I_p & \alpha W \\ 0 & I_{d-p} \end{pmatrix} \begin{pmatrix} \alpha^2 I_p & 0 \\ 0 & \alpha I_{d-p} \end{pmatrix} = S_{\alpha W} D_\alpha = S_W^\alpha D_\alpha.$$

Finally as translation operator, we consider the usual translation with respect to a real parameter. Given this setting we can define the continuous shearlet system and the continuous shearlet transform.

Definition 6.1. *For $\psi \in L^2(\mathbb{R}^d)$, the* continuous shearlet system *is defined by*

$$\{\psi_{\alpha, W, t} = \det D_\alpha^{1/2} \psi(D_\alpha S_W \cdot -t), \ \alpha \geq 2, \ W \in \mathbb{R}^{p \times (d-p)}, \ t \in \mathbb{R}^d\}. \tag{6.7}$$

Then the continuous shearlet transform *of $f \in L^2(\mathbb{R}^d)$ is the map*

$$L^2(\mathbb{R}^d) \in f \mapsto \mathcal{SH}_\psi f(\alpha, W, t) = (f, \psi_{\alpha, W, t})_{L^2(\mathbb{R}^d)},$$

from f to the coefficients $\mathcal{SH}_\psi f(\alpha, W, t)$ associated with the scale α, the orientation W and the localization $t \in \mathbb{R}^d$.

Since we focus on the two dimensional setting, we consider shear S_w of the form (6.3). Moreover, if the function is mostly concentrated on the vertical axis in the frequency domain, then the higher values of the continuous shearlet transform $\mathcal{SH}_\psi f(\alpha, w, t)$ are given for $w \to \infty$. This is a limit for the applications. To overcome this limitation, the *cone-adapted* shearlet transform is introduced by Guo, Kutyniok and Labate [2006].
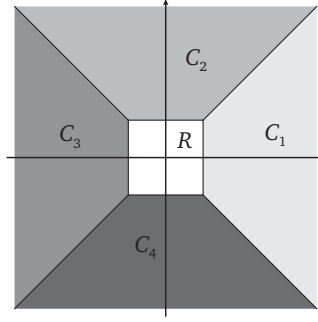
Figure 6.1. Division of the plane in four cones C_i, $i = 1, \ldots, 4$, and a square R centred in the origin.

The idea is to divide the frequency plane in four cones C_i, $i = 1, \ldots, 4$, while separating the low frequency region by cutting out a square R centred around the origin (see Fig. 6.1).

In this way the orientation parameter w varies on a finite range and we have a better distribution of the orientations that can be reached. To have a complete representation system in addition to ψ that works on the cones $C_1 \cup C_3$, we introduce another function $\tilde{\psi}$ that works on the vertical cones $C_2 \cup C_4$ and ϕ associated to the low frequency region R.

Definition 6.2. *For $\phi, \psi, \tilde{\psi} \in L^2(\mathbb{R}^2)$, the cone adapted continuous shearlet system is defined as*

$$\{\phi_t, t \in \mathbb{R}^2\} \cup \{\psi_{\alpha,w,t}, \alpha > 1, |w| \leq 1 + \alpha, t \in \mathbb{R}^2\} \cup \{\tilde{\psi}_{\alpha,w,t}, \alpha > 1, |w| \leq 1 + \alpha, t \in \mathbb{R}^2\},$$

where

$$\phi_t = \phi(\cdot - t),$$
$$\psi_{\alpha,w,t} = \det D_\alpha^{1/2} \psi(D_\alpha S_w \cdot - t),$$
$$\tilde{\psi}_{\alpha,w,t} = \det D_\alpha^{1/2} \tilde{\psi}(D_\alpha S_w \cdot - t).$$

The cone adapted continuous shearlet transform of $f \in L^2(\mathbb{R}^d)$ is the map

$$f \mapsto \mathcal{SH}_{\phi,\psi,\tilde{\psi}} f(t', (\alpha, w, t), (\tilde{\alpha}, \tilde{w}, \tilde{t})) = ((f, \phi_{t'})_{L^2(\mathbb{R}^2)}, (f, \psi_{\alpha,w,t})_{L^2(\mathbb{R}^2)}, (f, \tilde{\psi}_{\tilde{\alpha},\tilde{w},\tilde{t}})_{L^2(\mathbb{R}^2)}).$$

A simple choice for $\tilde{\psi}$ is reversing the roles of x_1 and x_2, $\tilde{\psi}(x_1, x_2) = \psi(x_2, x_1)$. A similar division of the frequency plane is operated also by contourlets [Do and Vetterli, 2005].

Shearlets give a sparse representation of the analysed signal where it is smooth, while the shearlet transform decays slowly in a neighbourhood of the discontinuity. Differently from wavelets, the shearlet system provides information about the geometry of the discontinuity, thanks to the scale α, orientation W and location t. In this way, shearlets can handle edges, corner points and junctions. The order of decay of the continuous

shearlet transform in a smooth area or in a neighbourhood of a discontinuity is studied in [Kutyniok and Labate, 2009; Guo and Labate, 2009, 2017].

In the discrete setting, we choose the orientation and localization varying on integers, while we fix an integer value for α and we consider different powers of the scaling matrix D_α. The minimum value that α can assume is 2,

$$D_2 = \begin{pmatrix} 4I_p & 0 \\ 0 & 2I_{d-p} \end{pmatrix}. \tag{6.8}$$

Definition 6.3. *A discrete shearlet system associated to $\psi \in L^2(\mathbb{R}^d)$ is composed by*

$$\{\psi_{j,W,k} = 2^{\frac{3}{4}j}\psi(D_{2^j}S_W \cdot -k), j \in \mathbb{Z}, \ W \in \mathbb{Z}^{p\times(d-p)}, \ k \in \mathbb{Z}^d\}. \tag{6.9}$$

The discrete shearlet transform *of $f \in L^2(\mathbb{R}^d)$ is the map*

$$f \mapsto \mathcal{SH}_\psi f(j,W,k) = (f,\psi_{j,W,k})_{L^2(\mathbb{R}^d)},$$

where $j \in \mathbb{Z}$ represents the scaling index, $W \in \mathbb{Z}^{p\times(d-p)}$ the orientation matrix and $k \in \mathbb{Z}^d$ the position index.

Analogously to the continuous shearlet transform, it is possible to define a cone adapted *discrete* shearlet transform [Guo, Kutyniok and Labate, 2006]. For simplicity we fix $d = 2$.

Definition 6.4. *For $\phi, \psi, \tilde{\psi} \in L^2(\mathbb{R}^2)$ the cone adapted discrete shearlet system is defined by*

$$\{\phi_k, k \in \mathbb{Z}^2\} \cup \{\psi_{j,w,k}, j \geq 0, |w| \leq 2^j, k \in \mathbb{Z}^2\} \cup \{\tilde{\psi}_{j,w,k}, j \geq 0, |w| \leq 2^j, k \in \mathbb{Z}^2\}$$

where

$$\phi_k = \phi(\cdot - k)$$
$$\psi_{j,w,k} = 2^{\frac{3}{4}j}\psi(D_{2^j}S_w \cdot -k)$$
$$\tilde{\psi}_{j,w,k} = 2^{\frac{3}{4}j}\tilde{\psi}(D_{2^j}S_w \cdot -k)$$

The cone adapted continuous shearlet transform *of $f \in L^2(\mathbb{R}^d)$ is the map*

$$f \mapsto \mathcal{SH}_{\phi,\psi,\tilde{\psi}}f(k',(j,w,k),(\tilde{j},\tilde{w},\tilde{k})) = ((f,\phi_{k'})_{L^2(\mathbb{R}^2)},(f,\psi_{j,w,k})_{L^2(\mathbb{R}^2)},(f,\tilde{\psi}_{\tilde{j},\tilde{w},\tilde{k}})_{L^2(\mathbb{R}^2)}).$$

The cone-adapted discrete shearlet transform provides a particular decomposition of the frequency space into frequency regions associated with different scales j and orientations w.

If we define the orientation W of the shear matrix to vary on the integers, then we can even restrict more by considering a finite set of shear matrices $\{S_i\}$, $i \in \{0,\ldots,s-1\} = \mathbb{Z}_s$ and defining the shearlet system

$$\{\psi_{j,i,k} = 2^{\frac{3}{4}j}\psi(M_i^j \cdot -k), \ M_i = D_2 S_i, \ i \in \mathbb{Z}_s, \ k \in \mathbb{Z}^d\}.$$

Differently to the continuous transform, we have to guarantee that this shearlet system is capable of detecting all directions in space, namely the set of matrices $\{M_i\}_{i\in\mathbb{Z}_s}$ have to satisfy the *slope resolution property*.

Definition 6.5. *A family* $\{M_i = D_2 S_i\}$, $i \in \mathbb{Z}_s$ *provides the* slope resolution property *if there exists a reference line* ℓ_0 *through the origin such that for any line* ℓ, *there exists a sequence* $\epsilon \in \mathbb{Z}_s^n$, $n \in \mathbb{N}$, *such that* $M_\epsilon \ell_0 \to \ell$.

This property ensures that the shearlet system $\{\psi_{j,i,k}\}$ is capable of deducing the direction of a singularity from the index ϵ. Of course the slope resolution property in more dimensions considers hyperplanes instead of lines.

In two dimensions, Kutyniok and Sauer [2009] consider the two matrices

$$M_0 = \begin{pmatrix} 4 & 0 \\ 0 & 2 \end{pmatrix}, \qquad M_1 = M_0 \begin{pmatrix} 1 & 1 \\ 0 & 1 \end{pmatrix} = \begin{pmatrix} 4 & 4 \\ 0 & 2 \end{pmatrix}, \tag{6.10}$$

the product of the parabolic matrix D_2 and the shear matrices $S_0 = I_2$ and S_1, defined as in (6.3).

Let ℓ be a line through the origin with slope $s(\ell)$ and let $s(\ell, \epsilon)$ denote the slope of the line $M_\epsilon^{-1} \ell$, with $\epsilon \in \mathbb{Z}_2^n$, $n \in \mathbb{N}$.

Theorem 6.1 [Kutyniok and Sauer, 2009]. *Let* ℓ *be a line through the origin with slope* $s(\ell) \in (0, \infty]$. *Then for each* $s \in \left[\frac{1}{2}, \infty\right]$ *and* $\delta > 0$, *there exist some* $n \in \mathbb{N}$ *and* $\epsilon \in \mathbb{Z}_2^n$ *such that*

$$|s(\ell, \epsilon) - s| < \delta.$$

With the matrices M_0 and M_1 we can cover all the directions with slope in $\left[\frac{1}{2}, \infty\right]$, namely we cover a cone. Now if we consider also the matrices $M_{-1} = D_2 S_{-1}$ and

$$\widetilde{M}_i = D_2 \widetilde{S}_i, \qquad \widetilde{S}_i = \begin{pmatrix} 1 & 0 \\ i & 1 \end{pmatrix}, \quad i = -1, 0, 1, \tag{6.11}$$

we can cover all the possible slopes in the plane, see Figure 6.2. Hence, the matrices $\{M_i, \widetilde{M}_i, \ i = -1, 0, 1\}$ satisfy the slope resolution property. Each pair of matrices can reach directions inside a cone, which is analogous to the cone adapted discrete shearlet system.

The generalization in higher dimension d is quite different. One important application of shearlets is the detection of tangent planes at a certain point. In order to capture directional singularities across arbitrary hyperplanes we consider shearlet scaling matrices of the form

$$M_i = D_2 S_i, \qquad D_2 = \begin{pmatrix} 4I_{d-1} & 0 \\ 0 & 2 \end{pmatrix}, \qquad S_i = \begin{pmatrix} I_{d-1} & e_i \\ 0 & 1 \end{pmatrix}, \tag{6.12}$$

where $e_i \in \mathbb{Z}^{d-1}$ are the unit vectors whose i-th component is equal to 1, $(e_i)_\ell = \delta_{i,\ell}$, $\ell = 1, \dots, d-1$.
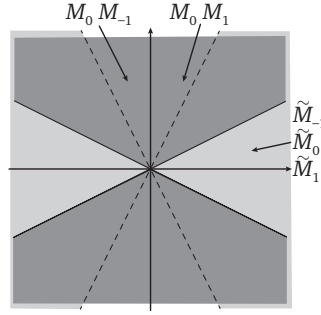
Figure 6.2. Directions covered by the application of the matrices M_j, $j = -1, 0, 1$ (dark grey) or by the application of the matrices $\widetilde{M}_j$, $j = -1, 0, 1$ (light gray).

Given a hyperplane $H = \{x \in \mathbb{R}^d : v^T x = 0\} \subset \mathbb{R}^d$ whose normal has the property $v_d \neq 0$, we normalize v such that $v_d = 1$. Writing $v = (s, 1)^T$, we call $s \in \mathbb{R}^{d-1}$ the slope of the hyperplane H. In [Sauer, 2012] it is proved that any hyperplane can be obtained from a single reference hyperplane by applying a proper matrix M_ϵ. This is the multivariate version of the slope resolution property. We denote with

$$\Delta_{d-1} := \left\{ t \in \mathbb{R}^{d-1} : t_k \geq 0, \sum_{k=1}^{d-1} t_k \leq 1 \right\}, \tag{6.13}$$

the unit simplex in $\mathbb{R}^{d-1}$.

Theorem 6.2 [Sauer, 2012]. *Let H be a hyperplane with normal $v = (s', 1)^T$, $s' \in \mathbb{R}^{d-1}$, for each vector of the form $(s, 1)^T$, $s \in 2\Delta_{d-1}$ and $\delta > 0$, then there exist some $n \in \mathbb{N}$ and $\epsilon \in \mathbb{Z}_d^n$ such that*

$$\left\| 2^n M_\epsilon^{-1} \begin{pmatrix} s' \\ 1 \end{pmatrix} - \begin{pmatrix} s \\ 1 \end{pmatrix} \right\| < \delta.$$

Theorem 6.2 exploits hyperplanes with slope in $2\Delta_{d-1}$. In order to get all the possible slopes in $\mathbb{R}^{d-1}$ we have to consider all the combinations of the unit vectors e_j with positive and negative entries and change the "fixed" coordinate. Fixing the last entry in (6.12) is completely arbitrary. To handle a complete discrete shearlet analysis we have to consider $d2^{d-1}$ sets of matrices like (6.12).

The discrete shearlet system in (6.9) is defined by a suitable function $\psi \in L^2(\mathbb{R}^d)$. As in the wavelet case (see Section 5.2), we would like to have a multiresolution analysis and avoid to give explicitly the scaling and wavelet functions. Thus, there is the necessity to generalise the concept of multiresolution analysis to a directional multiresolution analysis, see [Kutyniok and Sauer, 2009; Sauer, 2012].

6.2 Multiple multiresolution analysis and multiple subdivision scheme

The idea of Kutyniok and Sauer [2009] is to connect a multiresolution analysis to shearlets and to provide a feasible fast shearlet decomposition. Thus, they consider a new class of non-stationary bivariate subdivision schemes which incorporate directionality in a particular way. The constructed subdivision scheme provides the opportunity to adaptively change the orientation of the data during the subdivision process, since in each iteration it applies one different subdivision scheme associated with a scaling matrix chosen from a finite family. The limit function depends on the choice of subdivision scheme and scaling matrix in each step. This type of scheme is called *multiple subdivision scheme* and is presented in [Sauer, 2010, 2012]. Even thought it is developed as theoretical background of shearlets, the multiple multiresolution analysis is a general concept that can be defined by a suitable family of expanding matrices different from (6.12).

From now on we use the notation $\mathbb{Z}_s = \mathbb{Z}/s\mathbb{Z} = \{0,\dots,s-1\}$ to enumerate the s different schemes of the family and $\mathbb{Z}_s^\infty$ for the infinite sequences with values in $\mathbb{Z}_s$,

$$\mathbb{Z}_s^\infty = \bigcup_{n\in\mathbb{N}} \mathbb{Z}_s^n.$$

Definition 6.6. *A multiple subdivision scheme $\mathcal{S}_\epsilon$ consists of a finite family $\{\mathcal{S}_i\}_{i\in\mathbb{Z}_s}$ of s subdivision schemes with respect to the dilatation matrices $\{M_i\}_{i\in\mathbb{Z}_s}$, i.e.,*

$$\mathcal{S}_i c = \sum_{\alpha\in\mathbb{Z}^d} a_i(\cdot - M_i\alpha)\, c(\alpha),$$

where $c \in \ell(\mathbb{Z}^d)$ and, as usual, the masks a_i are assumed to be of finite support, $a_i \in \ell_{00}(\mathbb{Z}^d)$. In each iteration of the subdivision process we apply a subdivision scheme chosen from the family. The n-th iteration of the subdivision operator, related to the sequence $\epsilon \in \mathbb{Z}_s^n$, $\epsilon = (\epsilon_1,\dots,\epsilon_n)$, takes the form

$$\mathcal{S}_\epsilon c = \mathcal{S}_{\epsilon_n}\cdots\mathcal{S}_{\epsilon_1} c = \sum_{\alpha\in\mathbb{Z}^d} a_\epsilon(\cdot - M_\epsilon\alpha)\, c(\alpha),$$

where $a_\epsilon, c \in \ell(\mathbb{Z}^d)$ and the scaling matrix is $M_\epsilon = M_{\epsilon_n}\cdots M_{\epsilon_1}$.

We can visualize the multiple subdivision process as a tree (Fig. 6.3), in which the direction of the refined data depends on the branch that we choose.

The multiple subdivision scheme is a "generalization" of the concept of non stationary subdivision scheme where in each step of the subdivision we change the refinement rules a_i and the scaling matrix M_i, $i \in \mathbb{Z}_s$. A non stationary subdivision scheme is generally defined as a subdivision process where the mask $a^{(j)}$ is different in each iteration j, while the scaling matrix M does not change.

The operator $\mathcal{S}_\epsilon$ related to a multiple subdivision scheme defines a refinement process for any $\epsilon \in \mathbb{Z}_s^n$, if the associated scaling matrix M_ϵ is expanding and $\left\|M_\epsilon^{-1}\right\| \to 0$, for
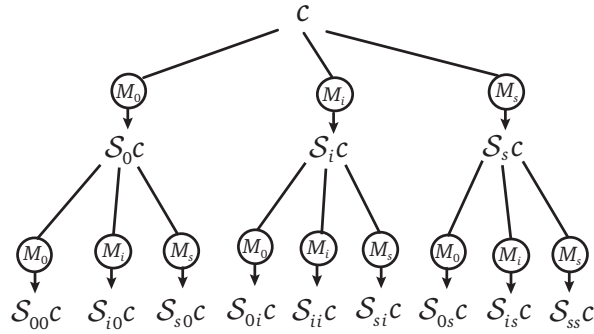
Figure 6.3. The tree shows all the possible choices of subdivision schemes after two refinement steps.

$n \to \infty$, independently of $\epsilon \in \mathbb{Z}_s^n$. This is equivalent to requiring that the *joint spectral radius* of the family $\{M_i\}_{i \in \mathbb{Z}_s}$ is less than 1,

$$\rho(\{M_i\}_{i \in \mathbb{Z}_s}) = \limsup_{n \to \infty} \max_{\epsilon \in \mathbb{Z}_s^n} \left\| M_\epsilon^{-1} \right\|^{1/n} < 1, \tag{6.14}$$

for any matrix norm, because all the norms are equivalent on finite dimensional spaces. A family of matrices that satisfies this condition is called *jointly expanding*.

As for classical subdivision schemes we can give the definition of a convergent multiple subdivision scheme.

Definition 6.7. *A multiple scheme is called uniformly* convergent *if for any sequence* $\epsilon \in \mathbb{Z}_s^n$, $n \in \mathbb{N}$, *and any* $c \in \ell(\mathbb{Z}^d)$, *there exists a uniformly continuous function* $f_{\epsilon,c} : \mathbb{R}^d \to \mathbb{R}$ *such that*

$$\lim_{n \to \infty} \sup_{\alpha \in \mathbb{Z}^d} \left| \mathcal{S}_{\epsilon_n} \cdots \mathcal{S}_{\epsilon_1} c - f_{\epsilon,c} \left(M_{\epsilon_1}^{-1} \cdots M_{\epsilon_n}^{-1} \alpha \right) \right| = 0, \tag{6.15}$$

and that $f_{\epsilon,c} \neq 0$ *for at least one choice of* c.

Remark 6.1. Choosing $\epsilon = (i, i, \dots)$, we have that the convergence of the subdivision scheme $\mathcal{S}_i$, $i \in \mathbb{Z}_s$ is a necessary condition for the convergence of the multiple subdivision scheme.

A result similar to Propositions 1.11, 1.17 can be proved for a multiple subdivision scheme. In dimension higher than 1 the forward difference operator $\nabla : \ell(\mathbb{Z}^d) \to \ell^d(\mathbb{Z}^d)$ is defined by

$$\nabla c := \begin{pmatrix} c(\cdot - e_1) - c(\cdot) \\ \vdots \\ c(\cdot - e_d) - c(\cdot) \end{pmatrix},$$

where $e_k \in \mathbb{Z}^d$ are unit vectors whose k-th component is equal to 1, $(e_k)_i = \delta_{i,k}$. The convergence of a multiple subdivision scheme depends on the existence of the difference

schemes $\mathcal{S}_{B_i}$ such that

$$\nabla \mathcal{S}_{a_i} = \mathcal{S}_{B_i} \nabla, \tag{6.16}$$

for any $i \in \mathbb{Z}_s$, and $\mathcal{S}_{B_i}$ are joint contractive. The *normalized p-joint spectral radius* of these operators is

$$\rho_p(B_i, M_i) = \limsup_{n \to \infty} \sup_{\epsilon \in \mathbb{Z}_s^n} \left((\det M_\epsilon)^{-1/p} \sup_{c \in \nabla \ell_p(\mathbb{Z}^d) \setminus \{0\}} \frac{\left\| \mathcal{S}_{B_\epsilon} c \right\|_p}{\|c\|_p} \right)^{1/n}, \tag{6.17}$$

where the determinant of the matrix M_ϵ, $\det(M_\epsilon)$ is a factor of normalization, (cf. [Charina et al., 2005a]).

Theorem 6.3 [Sauer, 2010]**.** *The multiple subdivision scheme based on (a_i, M_i), with $i \in \mathbb{Z}_s$, converges if and only if there exists the difference schemes (B_i, M_i) such that the normalized p-joint spectral radius $\rho_p(B_i, M_i) < 1$.*

This theorem is the analogous of Proposition 1.17 in the "multiple" setting.

A different option to study the convergence and regularity of a scheme is considering the Laurent formalism.

Lemma 6.4 [Sauer, 2010]**.** *If a multiple subdivision scheme $\{(a_i, M_i)\}_{i \in \mathbb{Z}_s}$ converges, then*

$$a_i^*(z) \in \langle z^{M_i} - 1 \rangle : \langle z - 1 \rangle$$

for any $i \in \mathbb{Z}_s$.

The Laurent polynomial related to the subdivision scheme $\mathcal{S}_i = \mathcal{S}_{a_i}$ is an element of the quotient of the ideals

$$\langle z^M - 1 \rangle = \left\{ \sum_{j=1}^d f_j(z)(z^{v_j} - 1), \quad f_j \in \mathbb{R}[z_1, \dots, z_d] \right\},$$

$$\langle z - 1 \rangle = \left\{ \sum_{j=1}^d f_j(z)(z_j - 1), \quad f_j \in \mathbb{R}[z_1, \dots, z_d] \right\},$$

where v_j are the column vectors of the matrix M (see [Möller and Sauer, 2004]). We recall that an ideal $I \subseteq R$ in the ring R satisfies

$$gI = \{gf \mid f \in I\} \subseteq I, \quad \forall g \in R,$$

and for $I, J \subseteq R$ the quotient ideal is defined as

$$I : J = \{f \in R \mid fJ \subseteq I\}.$$

In one dimension and choosing the isotropic matrix $M = kI$, the quotient $\langle z^k - 1 \rangle : \langle z - 1 \rangle$ is generated by the element $(1 + z + \dots + z^{k-1})$, so the symbol of the scheme has a factor

of this form. If the multiple subdivision scheme converges, then we factorize the Laurent polynomials as

$$[1-z]a_i^*(z) = B_i^*(z)[z_i^M - 1] \quad \forall i \in \mathbb{Z}_s.$$

This relation between a_i and B_i is equivalent to (6.16), because the symbol of the backward difference operator is

$$\nabla^* = \begin{bmatrix} z_1 - 1 \\ \vdots \\ z_d - 1 \end{bmatrix},$$

and

$$[z^M - 1] = \begin{bmatrix} z^{\nu_1} - 1 \\ \vdots \\ z^{\nu_d} - 1 \end{bmatrix}, \quad \text{with} \quad M = [\nu_1, \dots, \nu_d] \in \mathbb{Z}^{d \times d}.$$

Lemma 6.4 gives a necessary condition for the convergence of a scheme, which is similar to Corollary 1.9 in the univariate case. Sauer [2010] presents a sufficient condition that is the generalization of Proposition 1.11, 1.14, 1.16 to multiple subdivision schemes. In this sense we need a canonical representation of the quotient ideal $\langle z^M - 1 \rangle : \langle z - 1 \rangle$.

Proposition 6.5 [Sauer, 2010]. *Given a Smith factorization $M = \Theta \Sigma \Theta'$ of the matrix M, the quotient ideal is*

$$\langle z^M - 1 \rangle : \langle z - 1 \rangle = \langle z^M - 1, \psi_M(z) \rangle,$$

where

$$\psi_M(z) = \prod_{k=1}^{d} \sum_{\ell=0}^{\sigma_k - 1} z^{\ell \theta_k} = \prod_{k=1}^{d} \frac{z^{\sigma_k \theta_k} - 1}{z^{\theta_k} - 1}, \tag{6.18}$$

and θ_k are the column vectors of Θ and σ_k are the diagonal elements of Σ.

The polynomial $\psi_M(z)$ is called the *canonical factor* of the matrix M. In the multivariate case the canonical factor is equivalent to the factor $(z + 1)$ of the univariate binary case (1.18). Sauer [2010] gives two sufficient conditions for the convergence of a multiple subdivision scheme using the canonical factor.

Theorem 6.6 [Sauer, 2010]. *The multiple subdivision scheme defined by the dictionary of masks and scaling matrices (a_i, M_i), $i \in \mathbb{Z}_s$ with $a_i^* = \psi_{M_i}$ converges in L_1.*

Corollary 6.7 [Sauer, 2010]. *The multiple subdivision scheme defined by the dictionary (a_i, M_i), $i \in \mathbb{Z}_s$ of masks and scaling matrices with $a_i^* = \frac{1}{\det M_i} \psi_{M_i}^2$ converges to a continuous limit function.*

Corollary 6.7 arises directly from Theorem 6.6, because the autoconvolution of compactly supported L_1 functions is continuous. An analogous result for an interpolatory vector scheme is stated in [Conti et al., 2008].

Derado [1999] and Han [2003] establish the existence of convergent interpolatory subdivision schemes and refinable functions for arbitrary scaling matrices. Sauer [2010] generalizes this result to multiple subdivision schemes. To generate a multiple subdivision scheme it is sufficient to give a set of expanding matrices $\{M_i\}_{i \in \mathbb{Z}_s}$ that are jointly expanding matrices. We will see in the next section how to define it.

The limit basis function of any convergent scheme is a refinable function. The same happens in the case of multiple subdivision schemes in the sense of a joint refinement, because there is not a unique function which is scaled and shifted but all the functions ϕ_ϵ, $\epsilon \in \mathbb{Z}_s^\infty$ are related to each others. Given $\epsilon = (\epsilon_1, \epsilon^\infty) \in \mathbb{Z}_s^\infty$, the formula

$$\phi_\epsilon = \uparrow_{M_{\epsilon_1}} (\phi_{\epsilon^\infty} * a_{\epsilon_1}) = \sum_{\alpha \in \mathbb{Z}^d} a_{\epsilon_1}(\alpha) \phi_{\epsilon^\infty}(M_{\epsilon_1} \cdot -\alpha), \qquad (6.19)$$

is a *multiple refinement* equation that can be read as: ϵ_1 selects which scaling matrix is used in the refinement equation, while ϵ^∞ chooses which function is used in the refinement. This works for any decomposition of ϵ, i.e $\epsilon = (\epsilon^{(n)}, \epsilon^\infty) \in \mathbb{Z}_s^\infty$, into a finite part $\epsilon^{(n)}$ and an infinite part ϵ^∞

$$\phi_\epsilon = \sum_{\alpha \in \mathbb{Z}^d} a_{\epsilon^{(n)}}(\alpha) \phi_{\epsilon^\infty}(M_{\epsilon^{(n)}} \cdot -\alpha), \qquad (6.20)$$

where the mask $a_{\epsilon^{(n)}} = S_{\epsilon^{(n)}} \delta$. In general, the initial terms of ϵ select the mask and the scaling matrix, while the remaining infinite terms select the function used in the refinement equation. If the multiple subdivision scheme is convergent, then the limit function ϕ_ϵ is multiple refinable as in (6.20).

The multiple refinement equation (6.19) enables to define an appropriate generalization of the multiresolution analysis. In line with the definition of multiple subdivision schemes and multiple refinement equations, such a generalization is called a *multiple multiresolution analysis* (MMRA). The first attempt of this multiple multiresolution analysis is presented in [Kutyniok and Sauer, 2009] and is revisited in [Sauer, 2012].

Suppose that the limit functions ϕ_ϵ are stable, hence we can define the sets

$$V_0 = \text{span}\{\phi_\epsilon(\cdot - \alpha) : \epsilon \in \mathbb{Z}_s^\infty, \, \alpha \in \mathbb{Z}^d\},$$
$$V_j = \text{span}\{\phi_\epsilon(M_{\epsilon^{(j)}} \cdot -\alpha) : \epsilon \in \mathbb{Z}_s^\infty, \, \epsilon^{(j)} \in \mathbb{Z}_s^j, \, \alpha \in \mathbb{Z}^d\}. \qquad (6.21)$$

Thanks to (6.19), the spaces satisfy the scaling property (ii) in Definition 5.3 of a multiresolution analysis. However, V_0 is generated by a set of functions ϕ_ϵ that is not countable. In order to find a countable set of generators for the subspaces V_j, Sauer [2012] introduces

$$Z_s^* = \left\{\epsilon = (\epsilon^{(n)}, 0, \ldots) : \epsilon^{(n)} \in \mathbb{Z}_s^n, \, n \in \mathbb{N}\right\} \subset \mathbb{Z}_s^\infty,$$

the set of sequences with finitely many non zeros entries. We can substitute the functions ϕ_ϵ with $\epsilon \in Z_s^*$ in (6.21). The functions ϕ_ϵ, $\epsilon \in \mathbb{Z}_s^*$, are limit functions of a subdivision

scheme where $\mathcal{S}_0$ is repeated infinitely many times. With this choice of functions we can define the subspaces

$$V_j^* = \text{span}\{\phi_\epsilon(M_{\epsilon^{(j)}} \cdot -\alpha) : \ \epsilon \in \mathbb{Z}_s^*, \ \epsilon^{(j)} \in \mathbb{Z}_s^j, \ \alpha \in \mathbb{Z}^d\}. \qquad (6.22)$$

By definition the spaces V_j^* are translation invariant. They satisfy the scaling property (ii) and they are nested thanks to (6.19): for any $\epsilon = (\epsilon_1, \epsilon^\infty) \in \mathbb{Z}_s^*$, the function $\phi_\epsilon \in V_0^*$ is

$$\phi_\epsilon = \sum_{\alpha \in \mathbb{Z}^d} a_{\epsilon_1}(\alpha)\phi_{\epsilon^\infty}(M_{\epsilon_1} \cdot -\alpha),$$

a linear combination of functions in V_1^*, because $\epsilon^\infty \in \mathbb{Z}_s^*$.

Guo, Labate, Lim, Weiss and Wilson [2006a,b] present a different generalization of the multiresolution analysis that they call *AB-multiresolution analysis* (*AB*-MRA). They consider two groups of matrices A and B, where A contains the expanding matrices, while B contains the matrices that are responsible of the directionality. The shearlets fit in this theory if A is defined by the powers of the scaling matrix, $A = \{D_2^j, j \in \mathbb{Z}\}$, while B contains the shear matrices, $B = \{S_W, W \in \mathbb{Z}^{d-1}\}$. Let us denote by $D_a \in A$ and $D_b \in B$ the elements of the two groups A and B. Then, the nested spaces of the *AB*-MRA are defined by

$$V_0 = \text{span}\{D_b\phi(\cdot - k), k \in \mathbb{Z}^d, D_b \in B\},$$
$$V_j = \text{span}\{D_a^j D_b\phi(\cdot - k), k \in \mathbb{Z}^d, D_b \in B, j \in \mathbb{Z}\}.$$

The descriptions of $L^2(\mathbb{R}^d)$ given by MMRA and *AB*-MRA are different. In the *AB*-MRA setting the spaces V_j are generated by a scaled, rotated, shifted version of a unique scaling function ϕ while in MMRA we have to consider a countable number of scaling functions ϕ_ϵ, with $\epsilon \in \mathbb{Z}_s^*$. Vice versa in MMRA we consider a finite set of shear matrices $\{S_i, i \in \mathbb{Z}_s\}$ while the group B contains all the possible shear matrices in the space, $B = \{S_W, W \in \mathbb{Z}^{d-1}\}$. Moreover, the spaces in *AB*-MRA are the span with respect to translation and shear while in the MMRA setting we take the span only with respect to translation. This is the reason why in an MMRA we need a countable set of scaling functions to compensate for the finite number of shear matrices considered. We decide in our work to consider the MMRA setting because it is more flexible to consider the scaling and shear matrices together: when we move from one level to the next we do not have to consider all the possible shears. The *AB*-MRA decomposes the space as if in each step we consider all the branches of the tree together. Moreover, the MMRA setting is related to a multiple subdivision scheme that allows us to concentrate only on the choice of the jointly expanding matrices. In fact, we show in the following how we can define a convergent multiple subdivision scheme by giving a set of jointly expanding matrices.

6.2.1 Construction of a multiple subdivision scheme

Following [Sauer, 2012; Cotronei et al., 2015] we present a construction of a multiple subdivision scheme given a generic set of jointly expanding matrices $\{M_i\}_{i\in\mathbb{Z}_s}$. Choosing a scaling matrix M_i, $i \in \mathbb{Z}_s$, from the family, we consider the *Smith factorization*

$$M_i = \Theta_i \Sigma_i \Theta_i', \tag{6.23}$$

where $\Theta_i, \Theta_i' \in \mathbb{Z}^d$ are unimodular matrices, i.e. $|\det \Theta_i| = |\det \Theta_i| = 1$, and Σ_i is a diagonal matrix with eigenvalues σ_ℓ, $\ell = 1, \ldots, d$. Such a factorization always exists even if it is not unique in general. It can be computed by a combination of Gauss elimination and Euclidean division and, if we order the diagonal values with respect to divisibility, then we call it the *Smith normal form*; see [Marcus and Minc, 1992] for details.

To define a convergent subdivision scheme associated with M_i, we first construct a subdivision scheme for the diagonal matrix Σ_i. Considering a diagonal matrix, we can associate a scheme that is the tensor product of univariate interpolatory schemes b_ℓ with arity equal to the diagonal values σ_ℓ of the matrix, $\ell = 1, \ldots, d$. The tensor product of convergent interpolatory schemes is a convergent interpolatory scheme. Thus, we have for free that the designed subdivision scheme is convergent. The mask b_{Σ_i} is given by

$$b_{\Sigma_i} := \bigotimes_{\ell=1}^{d} b_\ell, \qquad b_{\Sigma_i}(\alpha) = \prod_{\ell=1}^{d} b_\ell(\alpha_\ell), \qquad \alpha \in \mathbb{Z}^d,$$

and the corresponding symbol is

$$b_{\Sigma_i}^*(z) = \sum_{\alpha \in \mathbb{Z}^d} b_{\Sigma_i}(\alpha) z^\alpha = \prod_{\ell=1}^{d} b_\ell^*(z_\ell), \qquad z \in (\mathbb{C} \setminus \{0\})^d. \tag{6.24}$$

The mask a_i of the scheme associated with M_i is computed using the mask of Σ_i as

$$a_i = b_{\Sigma_i}(\Theta_i^{-1}\cdot),$$

and its symbol is

$$a_i^*(z) = \sum_{\alpha \in \mathbb{Z}^d} b_{\Sigma_i}(\Theta_i^{-1}\alpha) z^\alpha = \sum_{\alpha \in \mathbb{Z}^d} b_{\Sigma_i}(\alpha) z^{\Theta_i \alpha} = b_{\Sigma_i}^*(z^{\Theta_i}). \tag{6.25}$$

The unimodular matrix Θ_i takes the role of a resampling operator. In general, for any unimodular matrix $\Theta \in \mathbb{Z}^{d\times d}$, the resampled sequence $c(\Theta^{-1}\cdot)$ has the symbol

$$\big(c(\Theta^{-1}\cdot)\big)^*(z) = c^*(z^\Theta), \qquad z^\Theta := \big(z^{\theta_1}, \ldots, z^{\theta_d}\big), \quad \Theta = [\theta_1, \ldots, \theta_d].$$

Once we have constructed in this way a subdivision scheme $\mathcal{S}_{a_i}$ for each matrix M_i, $i \in \mathbb{Z}_s$, the convergence of the multiple subdivision scheme (a_i, M_i) has to be studied. Theorem 6.3 or Theorem 6.6 and Corollary 6.7 are the tools to prove the convergence.

Let us show an example of such a construction. We select a collection of univariate interpolatory subdivision schemes with arity σ_ℓ, $\ell = 1, \ldots, d$. For each matrix M_i, $i \in \mathbb{Z}_s$, we define the scheme as the tensor product of the interpolatory schemes and we prove that the multiple subdivision scheme generated converges to a continuous limit function.

Example 6.1. We consider the 2-point scheme with arity σ_ℓ which has the mask

$$b_\ell = \frac{1}{\sigma_\ell}\{0, 1, 2, \ldots, \sigma_\ell - 1, \sigma_\ell, \sigma_\ell - 1, \ldots, 2, 1, 0\},$$

and symbol

$$b_\ell^*(z) = \frac{z^{-(\sigma_\ell - 1)}}{\sigma_\ell}(1 + z + z^2 + \ldots + z^{\sigma_\ell - 1})^2, \qquad \ell = 1, \ldots, d.$$

According to (6.24), the symbol of Σ_i takes the form

$$b_{\Sigma_i}^*(z) = \prod_{\ell=1}^{d} \frac{z_\ell^{-(\sigma_\ell - 1)}}{\sigma_\ell} \left(\sum_{k=0}^{\sigma_\ell - 1} z_\ell^k \right)^2,$$

and according to (6.25) the symbol of the scheme associated with M_i is

$$a_i^*(z) = b_{\Sigma_i}^*(z^{\Theta_i}) = \prod_{\ell=1}^{d} \frac{z^{-(\sigma_\ell - 1)\theta_\ell}}{\sigma_\ell} \left(\sum_{k=0}^{\sigma_\ell - 1} z^{k\theta_\ell} \right)^2. \tag{6.26}$$

With this construction we obtain a convergent multiple subdivision scheme.

Lemma 6.8. *The multiple subdivision scheme generated by (a_i, M_i), as defined in* (6.26) *for all $i \in \mathbb{Z}_s$, is convergent and converges to a continuous function.*

Proof: For each matrix M_i, $i \in \mathbb{Z}_s$, the corresponding canonical factor is

$$\psi_{M_i}(z) = \prod_{\ell=1}^{d} \frac{z^{\sigma_\ell \theta_\ell} - 1}{z^{\sigma_\ell} - 1} = \prod_{\ell=1}^{d}(1 + z^{\theta_\ell} + \ldots + z^{(\sigma_\ell - 1)\theta_\ell}) = \prod_{\ell=1}^{d} \left(\sum_{k=0}^{\sigma_\ell - 1} z^{k\theta_\ell} \right).$$

We observe that

$$\frac{1}{\det M_i} \psi_{M_i}^2(z) = \prod_{\ell=1}^{d} \frac{1}{\sigma_\ell} \left(\sum_{k=0}^{\sigma_\ell - 1} z^{k\theta_\ell} \right)^2$$

is equal to a_i^* in (6.26) without the shift factors $z^{-(\sigma_\ell - 1)\theta_\ell}$. Corollary 6.7 yields that the multiple subdivision scheme generated by (a_i, M_i), $i \in \mathbb{Z}_s$, converges to a continuous limit function. $\square$

This example proves that for any family of jointly expanding matrices $\{M_i\}_{i \in \mathbb{Z}_s}$, there exists at least a multiple subdivision scheme that converges to a continuous function. Obviously, it is possible to choose in different ways the univariate interpolatory subdivision schemes b_ℓ with arity σ_ℓ, but in this case we have to prove the convergence using Theorem 6.3. This simple construction justifies our choice to focus on matrices that can substitute shearlet scaling matrices. In fact, we show that whenever we have a family of jointly expanding matrices $\{M_i\}_{i \in \mathbb{Z}_s}$ we can construct a convergent multiple subdivision scheme and a multiple mutiresolution analysis.
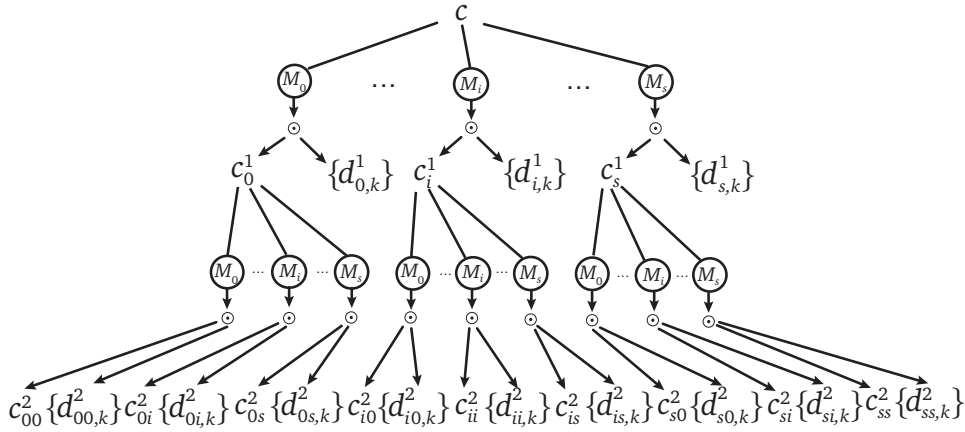
Figure 6.4. Scheme of the possible decompositions of the signal c for the different choices of filterbanks after two levels.

6.3 Filterbanks

Similar to the MRA (cf. Section 5.3) also in the multiple multiresolution setting we can define a filterbank that allows to decompose and to reconstruct a signal. The difference to the theory developed for MRA is that here we consider a set of scaling matrices $\{M_i\}_{i\in\mathbb{Z}_s}$ and we have to define a filterbank for each matrix M_i,

$$\text{Analysis filters:} \quad F_{i,k}, \qquad \text{Synthesis filters:} \quad G_{i,k},$$

where $k \in \mathbb{Z}_{m_i}$, $|\det M_i| = m_i$.

Considering a signal $c \in \ell(\mathbb{Z}^d)$ and choosing a matrix from the family $\{M_i\}_{i\in\mathbb{Z}_s}$, the convolution with the corresponding analysis filters $\{F_{i,k}\}_{k\in\mathbb{Z}_{m_i}}$ decomposes the signal into

$$c_i^1 = \downarrow_{M_i} F_{i,0} c \qquad \text{and} \qquad d_{i,k}^1 = \downarrow_{M_i} F_{i,k} c, \quad k \in \mathbb{Z}_{m_i} \setminus \{0\},$$

an approximation component and $m_i - 1$ details. Repeating the decomposition process n times and choosing different matrices for each iteration, we decompose the signal c into

$$c_\epsilon^n, \qquad \text{and} \qquad d_{\epsilon,k}^n, \quad k \in \mathbb{Z}_{m_{\epsilon_n}}. \tag{6.27}$$

with $\epsilon \in \mathbb{Z}_s^n$. The whole decomposition process can be visualized as a tree, see Figure 6.4.

Even if the filters are critically sampled after n decomposition steps we have s^n different branches and coefficients to be stored. In fact, in each step the coefficients $c_{\epsilon'}^{n'}$ with $\epsilon' \in \mathbb{Z}_s^{n'}$ and $n' < n$, can be decomposed by choosing one of the s matrices M_i, $i \in \mathbb{Z}_s$. Further, if the number of matrices of the set $\{M_i\}_{i\in\mathbb{Z}_s}$ is less than $\min_{i\in\mathbb{Z}_s}|\det M_i|$ and we do not save the approximation coefficients $c_{\epsilon'}^{n'}$ until the last level n, then the total

storage is a constant multiple of the storage for the original signal c. The set $\{M_i\}_{i\in\mathbb{Z}_s}$ of s matrices is said to be *sufficiently expansive* if

$$s < \min_{i\in\mathbb{Z}_s}|\det M_i|. \tag{6.28}$$

The following result is a slight modification of Lemma 2 in [Sauer, 2012].

Lemma 6.9. *If the set of matrices $\{M_i\}_{i\in\mathbb{Z}_s}$ is sufficiently expansive (6.28), then the storage requirement for an MMRA's tree of depth n is $O(|c|)$, where $|c| = \{\alpha \in \mathbb{Z}^d : c(\alpha) \neq 0\}$.*

Proof: We define $C \in \mathbb{N}$ such that

$$C = \max_{i\in\mathbb{Z}_s} \max_{k\in\mathbb{Z}_{m_i}} \left|f_{i,k}\right|.$$

Convolving a signal c with one of the filters $f_{i,k}$ requires a storage less than $|c| + C$. Downsampling by M_i reduces the storage by a factor of $|\det M_i|$. After one level of decomposition the storage requirement σ is

$$\sigma(1) = \sum_{\epsilon_1\in\mathbb{Z}_s}\left(\frac{|c|+C}{\left|\det M_{\epsilon_1}\right|} + \sum_{k=1}^{m_{\epsilon_1}}\frac{|c|+C}{\left|\det M_{\epsilon_1}\right|}\right) = \sum_{\epsilon_1\in\mathbb{Z}_s}\left(\frac{|c|+C}{\left|\det M_{\epsilon_1}\right|} + (m_{\epsilon_1}-1)\frac{|c|+C}{\left|\det M_{\epsilon_1}\right|}\right)$$

$$= \sum_{\epsilon_1\in\mathbb{Z}_s}|c|+C = s(|c|+C),$$

where $m_{\epsilon_1} = \left|\det M_{\epsilon_1}\right|$, $\epsilon_1 \in \mathbb{Z}_s$. The first term of the equation is the storage for $c^1_{\epsilon_1}$ while the second term represents the storage of $d^1_{\epsilon_1,k}$ with $k \in \mathbb{Z}_{m_{\epsilon_1}} \setminus \{0\}$. At the second step we decompose $c^1_{\epsilon_1}$ for any $\epsilon_1 \in \mathbb{Z}_s$, and the storage requirement becomes

$$\sigma(2) = \sum_{\epsilon\in\mathbb{Z}_s^2}\left(\frac{|c|+2C}{|\det M_\epsilon|} + (m_{\epsilon_2}-1)\frac{|c|+2C}{|\det M_\epsilon|}\right) + \sum_{\epsilon_1\in\mathbb{Z}_s}(m_{\epsilon_1}-1)\frac{|c|+C}{|\det M_{\epsilon_1}|}.$$

After n iterations of the decomposition process, the storage amounts to

$$\sigma(n) = \sum_{\epsilon\in\mathbb{Z}_s^n}\left(\frac{|c|+nC}{|\det M_\epsilon|} + (m_{\epsilon_n}-1)\frac{|c|+nC}{|\det M_\epsilon|}\right) + \sum_{j=1}^{n-1}\sum_{\epsilon\in\mathbb{Z}_s^j}(m_{\epsilon_j}-1)\frac{|c|+jC}{|\det M_\epsilon|}$$

$$= \sum_{\epsilon\in\mathbb{Z}_s^n}\frac{|c|+nC}{|\det M_\epsilon|} + \sum_{j=1}^{n}\sum_{\epsilon\in\mathbb{Z}_s^j}(m_{\epsilon_j}-1)\frac{|c|+jC}{|\det M_\epsilon|}.$$

For any $\epsilon \in \mathbb{Z}_s^n$,

$$|\det M_\epsilon| = \prod_{j=1}^{n}\left|\det M_{\epsilon_j}\right| > \prod_{j=1}^{n}\min_{i\in\mathbb{Z}_s}|\det M_i| = \left(\min_{i\in\mathbb{Z}_s}|\det M_i|\right)^n.$$

Then,

$$\sum_{\epsilon \in \mathbb{Z}_s^n} \frac{1}{|\det M_\epsilon|} < \sum_{\epsilon \in \mathbb{Z}_s^n} \frac{1}{(\min_{i \in \mathbb{Z}_s} |\det M_i|)^n} = \left(\frac{s}{\min_{i \in \mathbb{Z}_s} |\det M_i|}\right)^n.$$

We call this ratio q and by hypothesis we have

$$q = \frac{s}{\min_{i \in \mathbb{Z}_s} |\det M_i|} < 1.$$

Including this bound into the storage computation we have

$$\sigma(n) < (|c| + nC)q^n + \sum_{j=1}^n (|c| + jC) \sum_{\epsilon \in \mathbb{Z}_s^j} \frac{\max_{i \in \mathbb{Z}_s} |\det M_i| - 1}{(\min_{i \in \mathbb{Z}_s} |\det M_i|)^j}$$

$$= (|c| + nC)q^n + \left(\max_{i \in \mathbb{Z}_s} |\det M_i| - 1\right) \sum_{j=1}^n (|c| + jC)q^j$$

$$= (|c| + nC)q^n + |c|\left(\max_{i \in \mathbb{Z}_s} |\det M_i| - 1\right) \frac{1 - q^{n+1}}{1 - q} + \left(\max_{i \in \mathbb{Z}_s} |\det M_i| - 1\right) C \sum_{j=1}^n j q^j.$$

For any $n \in \mathbb{N}$ we can understand the last term as a Riemann sum that can be bounded by the integral on all positive numbers,

$$\sum_{j=1}^n j q^j \leq \int_1^n x q^x \, dx < \int_0^\infty x q^x \, dx = \frac{1}{\ln q^2}.$$

Finally, $\sigma(n)$ is bounded,

$$\sigma(n) < |c| \, q^n + |c|\left(\max_{i \in \mathbb{Z}_s} |\det M_i| - 1\right) \frac{1 - q^{n+1}}{1 - q} + \left(\max_{i \in \mathbb{Z}_s} |\det M_i| - 1\right) \frac{C}{\ln q^2}$$

$$< \frac{|c| \, q^n + |c|\left(\max_{i \in \mathbb{Z}_s} |\det M_i| - 1\right) - |c| \max_{i \in \mathbb{Z}_s} |\det M_i| q^{n+1}}{1 - q} + \frac{C}{\ln q^2} \max_{i \in \mathbb{Z}_s} |\det M_i|$$

$$= |c| \, q^n \frac{1 - q \max_{i \in \mathbb{Z}_s} |\det M_i|}{1 - q} + |c| \frac{\max_{i \in \mathbb{Z}_s} |\det M_i| - 1}{1 - q} + \frac{C}{\ln q^2} \max_{i \in \mathbb{Z}_s} |\det M_i|$$

$$< |c| \frac{1 - q \max_{i \in \mathbb{Z}_s} |\det M_i|}{1 - q} + |c| \frac{\max_{i \in \mathbb{Z}_s} |\det M_i| - 1}{1 - q} + \frac{C}{\ln q^2} \max_{i \in \mathbb{Z}_s} |\det M_i|$$

$$= |c| \max_{i \in \mathbb{Z}_s} |\det M_i| \frac{1 - q}{1 - q} + \frac{C}{\ln q^2} \max_{i \in \mathbb{Z}_s} |\det M_i|$$

$$< |c| \max_{i \in \mathbb{Z}_s} |\det M_i| + |c| \frac{C}{\ln q^2} \max_{i \in \mathbb{Z}_s} |\det M_i| < |c| \max_{i \in \mathbb{Z}_s} |\det M_i| \left(\frac{C}{\ln q^2} + 1\right) = O(|c|).$$

In the last terms we use that $q < 1$ and $\left(\frac{C}{\ln q^2} + 1\right) < 1$. This proves the statement. $\square$

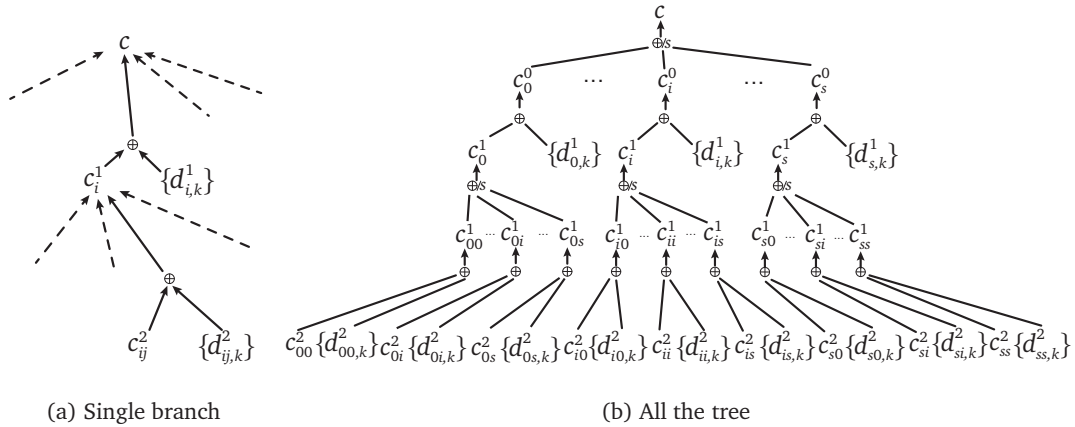(a) Single branch   (b) All the tree

Figure 6.5. Scheme of the reconstruction process after two levels of decomposition: (a) the signal is reconstructed following one branch of the tree, (b) the signal is reconstructed at each level by taking the mean of all the reconstructed coefficients at the same knot. In this way all the branches of the tree are taken into account.

Now in order to reconstruct the original signal, we have to read the tree backward. Considering a branch denoted by $\epsilon = (\epsilon', \epsilon_n) \in \mathbb{Z}_s^n$, we reconstruct the coefficient $c_{\epsilon'}^{n-1}$ by upsampling and convolving $\{c_\epsilon^n; d_{\epsilon,k}^n, k \in \mathbb{Z}_{m_{\epsilon_n}}\}$ with the synthesis filters $G_{\epsilon_n,k}, k \in \mathbb{Z}_{m_{\epsilon_n}}$,

$$c_{\epsilon'}^{n-1} = G_{\epsilon_n,0} \uparrow_{M_{\epsilon_n}} c_\epsilon^n + \sum_{k=1}^{m_{\epsilon_n}-1} G_{\epsilon_n,k} \uparrow_{M_{\epsilon_n}} d_{\epsilon,k}^n. \tag{6.29}$$

In this way, we reconstruct the signal following a branch of the tree. An example of such a reconstruction is shown in Figure 6.5a.

Exploiting all the branches independently we have s^n different ways to reconstruct c. Each branch has different features, because it works along different directions. In the reconstruction process, particularly after compression, it can be useful to exploit all the tree to keep advantages from the different reconstructions. In this case we reconstruct the signal c using all the branches of the tree. The one level reconstruction formula (6.29) is the same; the difference is that at each node of the tree we take the mean of the s different reconstructions. Suppose as before to have a tree with n levels of decomposition, from a node at level $n-1$ we have s children. Each of these branches is denoted by $\epsilon^i = (\epsilon', i)$, with $\epsilon' \in \mathbb{Z}_s^{n-1}$ and $i \in \mathbb{Z}_s$. If we apply one level of reconstruction using (6.29) to each branch ϵ^i, then we obtain s different reconstructions which can be denoted by $c_{\epsilon^i}^{n-1}$. Choosing one of these reconstructed coefficients $c_{\epsilon^i}^{n-1}$ and following the branch indicated with ϵ', we reconstruct the initial signal c by following only the branch ϵ^i, as explained above. If instead we want to exploit all the different reconstructions

$c_{\epsilon^i}^{n-1}$ for all $i \in \mathbb{Z}_s$, then we take the mean (or a weighted average)

$$c_{\epsilon'}^{n-1} = \sum_{i=0}^{s-1} \frac{c_{\epsilon^i}^{n-1}}{s} = \frac{1}{s} \sum_{i=0}^{s-1} \left(G_{i,0} \uparrow_{M_i} c_{\epsilon^i}^n + \sum_{k=1}^{m_i-1} G_{i,k} \uparrow_{M_i} d_{\epsilon^i,k}^n \right),$$

and we repeat the process. The whole reconstruction process after two levels of decomposition is shown in Figure 6.5b.

In Section 5.3, we recall that any expanding matrix defines a subdivision scheme and such scheme allows to construct a filterbank with the prediction-correction method. The multiple subdivision scheme proposed in Section 6.2.1 is composed by a set of expanding matrices $\{M_i\}_{i \in \mathbb{Z}_s}$ and their corresponding interpolatory subdivision schemes $\mathcal{S}_i = \mathcal{S}_{a_i}$. Using the prediction-correction method we can provide a filterbank for each subdivision scheme $\mathcal{S}_{a_i}$ and any expanding matrix M_i, $i \in \mathbb{Z}_s$. By (5.22), the filterbank related to M_i is defined as

$$\begin{aligned} F_{i,0} &= I, & F_{i,k} &= \tau_{-\xi_k}(I - \uparrow_{M_i}\downarrow_{M_i} A_i), \\ G_{i,0} &= A_i, & G_{i,k} &= \tau_{\xi_k}, \end{aligned} \tag{6.30}$$

where A_i is the operator related to the mask a_i and the impulse responses are

$$\begin{aligned} f_{i,0} &= \delta, & f_{i,k} &= \tau_{-\xi_k}(\delta - \uparrow_{M_i}\downarrow_{M_i} a_i) \\ g_{i,0} &= a_i, & g_{i,k} &= \tau_{\xi_k}\delta \end{aligned}$$

where $k \in \mathbb{Z}_{m_i} \setminus \{0\}$ and $\xi_k \in E_{M_i}^0$. The symbols of the impulse response becomes

$$\begin{aligned} f_{i,0}^*(z) &= 1, & f_{i,k}^*(z) &= z^{\xi_k} - \sum_{\ell \in \mathbb{Z}^d} a_i(M_i\ell - \xi_k)z^{M_i\ell}, \\ g_{i,0}^*(z) &= a_i^*(z), & g_{i,k}^*(z) &= z^{-\xi_k}, \end{aligned} \tag{6.31}$$

where $k \in \mathbb{Z}_{m_i} \setminus \{0\}$ and $\xi_k \in E_{M_i}^0$. Note that in the shearlet case we have to consider s filterbanks, one for each expanding matrix M_i and subdivision schemes $\mathcal{S}_{a_i}$, $i \in \mathbb{Z}_s$.

This framework is defined for shearlet scaling matrices, but it works for any type of expanding matrices M_i, $i \in \mathbb{Z}_s$. Now we study which properties the matrices M_i, $i \in \mathbb{Z}_s$, need to satisfy in order to generate a directional transform similar to shearlets and a multiple multiresolution analysis with lower complexity.

Chapter 7

Anisotropic Scaling Matrices

As we already saw, the concepts of multiple multiresolution analysis and multiple subdivision schemes are general and are characterized by a set of expanding matrices. In Section 7.1 we summarize which properties are sufficient for a set of matrices to generate a directional transform and a multiple multiresolution analysis. Indeed, the aim of our work is to substitute shearlets by keeping all the good properties they have and by improving the computational cost of the analysis process. The determinant of the scaling matrices gives the number of filters needed to decompose and reconstruct a signal, so it is connected to the computational efficiency of the signal processing. The determinant of the parabolic scaling matrix is quite high (2^{d+p}), which is the drawback of the shearlet transform. To improve this drawback we propose some matrices that satisfy all the required properties and have smaller determinant. We focus on matrices that are the product of an expanding matrix and a shear matrix and we distinguish the case of shear-like matrices where we take a diagonal expanding matrix (Section 7.2) from general expanding matrices (Section 7.3). For this family of matrices we prove that they satisfy the required properties and we show some illustrations of the behaviour of these matrices for image analysis by comparing them to shearlets (see Section 7.4).

The results given here are presented in [Bozzini et al., submitted; Rossini and Volontè, 2017] with the joint effort of Mira Bozzini, Milvia Rossini and Tomas Sauer.

7.1 Fundamental properties of scaling matrices

In order to find a family of matrices $\{M_i\}_{i \in \mathbb{Z}_s}$ that can substitute shearlet scaling matrices, we study which properties are sufficient to define a directional transform. The conditions are already presented in Chapters 5 and 6 and we recall them here for clarity.

1. **Anisotropic expanding matrices**

$$\begin{cases} |\lambda_j^i| > 1 \\ |\lambda_j^i| \neq |\lambda_k^i| \end{cases} \qquad \forall j \neq k \in \mathbb{Z}_d,$$

where λ_j^i are the eigenvalues of the matrix M_i, for all $i \in \mathbb{Z}_s$.

In order to detect anisotropic features like edges along curves and wavefronts in an image we need to consider elongated elements, thus we ask for matrices M_i that are anisotropic. Instead, the request to consider expanding matrices, allows to define a convergent subdivision scheme. Interpolatory schemes with scaling matrices M_i, $i \in \mathbb{Z}_s$, are defined by (6.25).

Note that anisotropic expanding matrices must have determinant greater or equal to 3, because determinant equal to 2 does not give anisotropic effects.

2. **Jointly expanding matrices**
   A set of matrices $\{M_i\}_{i \in \mathbb{Z}_s}$ is jointly expanding if for any $\epsilon \in \mathbb{Z}_s^n$, $n \in \mathbb{N}$, the composed matrix M_ϵ is expanding or the joint spectral radius is bounded by 1

$$\rho(\{M_i\}_{i \in \mathbb{Z}_s}) = \lim_{n \to \infty} \max_{\epsilon \in \mathbb{Z}_d^n} \left\| M_\epsilon^{-1} \right\|^{\frac{1}{n}} < 1.$$

This request is necessary for the convergence of a multiple subdivision scheme. In Section 6.2.1 we show that this property is sufficient to define a convergent interpolatory multiple subdivision scheme by following a particular construction.

3. **Slope resolution property**
   Let H be a hyperplane with normal $v = (s', 1)^T$, $s' \in \mathbb{R}^{d-1}$, then for each vector of the form $(s, 1)^T$, with $s \in \mathbb{R}^{d-1}$ and $\delta > 0$, there exist some $n \in \mathbb{N}$ and $\epsilon \in \mathbb{Z}_d^n$ such that

$$\left\| \begin{pmatrix} s' \\ 1 \end{pmatrix} - M_\epsilon \begin{pmatrix} s \\ 1 \end{pmatrix} \right\| < \delta.$$

This property ensures that the directional transform defined by the matrices $\{M_i\}_{i \in \mathbb{Z}_s}$ is able to detect all directions in space. In general we prove this property under the strict hypothesis $s \in I \subset \mathbb{R}^{d-1}$. This is sufficient if we show that we recover all the space by considering different sets of matrices $\{M_i\}_{i \in \mathbb{Z}_s}$ and different intervals I. It is the equivalent of the cone-adapted shearlets system.

4. **Pseudo commuting property** (not necessary)
   Suppose that the matrices M_i are the product of a diagonal matrix D with a set of matrices S_i, $M_i = DS_i$, then

$$\exists m, n \in \mathbb{N}, \quad \text{such that} \quad DS_i^m = S_i^n D.$$

The pseudo commuting property is not necessary for defining a directional transform but it turns out to be useful because it allows to write simple explicit formulas for the iterated matrices. For example in the shearlet case with matrices $\{M_i = D_2 S_{W_i}\}_{i \in \mathbb{Z}_s}$, we have

$$M_\epsilon = \prod_{j=1}^n D_2 S_{W_j} = S_{W'} D_2^n, \quad \text{where} \quad W' = \sum_{j=1}^n 2^j W_j.$$

By recalling that the shear matrices are unimodular, the identity

$$M_\epsilon^{-1}\mathbb{Z}^d = D_2^{-n}S_{-W'}\mathbb{Z}^d = D_2^{-n}\mathbb{Z}^d,$$

allows us to conclude that $M_\epsilon^{-1}\mathbb{Z}^d$ is a refinement of $\mathbb{Z}^d$ for any $n \in \mathbb{N}$ and $\epsilon \in \mathbb{Z}_s^n$. The existence and the form of unimodular matrices that pseudo commute with an anisotropic diagonal matrix is given in [Bozzini et al., 2015] depending on the dimension d.

Proposition 7.1 [Bozzini et al., 2015]. *Let D be an anisotropic diagonal expanding matrix in $\mathbb{Z}^{2\times2}$ and A be a non-diagonal unimodular matrix in $\mathbb{Z}^{2\times2}$. The identity*

$$DA^m = A^n D$$

is satisfied if and only if one of the following three cases holds:

(a) $A^q = I$, and m, n are such that $m = \ell_1 q$, $n = \ell_2 q$, for some $\ell_1, \ell_2 \in \mathbb{Z}$;

(b) $D = \begin{pmatrix} rk & 0 \\ 0 & k \end{pmatrix}$, with m, n such that $r = \frac{n}{m}$ and $A = \pm\begin{pmatrix} 1 & w \\ 0 & 1 \end{pmatrix}$;

(c) $D = \begin{pmatrix} rk & 0 \\ 0 & k \end{pmatrix}$, with m, n such that $r = \frac{m}{n}$ and $A = \pm\begin{pmatrix} 1 & 0 \\ w & 1 \end{pmatrix}^T$.

In particular, any 2×2 matrix that pseudo commutes with an anisotropic scaling matrix has to be of shear type. For $d = 3$, the situation is already different.

Proposition 7.2 [Bozzini et al., 2015]. *Let*

$$D = \begin{pmatrix} krs & 0 & 0 \\ 0 & kr & 0 \\ 0 & 0 & k \end{pmatrix}, \qquad r, s \in \mathbb{Q}_+,\ r, s \neq 1,$$

and

$$A = \left(\begin{array}{c|c} B & v \\ \hline 0 & \lambda \end{array}\right),$$

where B is a unimodular 2×2 matrix and v is a column vector of dimension 2. The pseudo-commuting property $DA = A^n D$ holds whenever A has one of the following forms:

(a) $v = 0$, $\lambda = \pm1$, B is a shear matrix and $s = n$, or B is n-periodic and $s = 1$ if $\lambda = -1$, n is odd;

(b) for some $v \neq 0$,

    i. $\lambda = 1$ and

        A. $B = \pm\begin{pmatrix} 1 & w \\ 0 & 1 \end{pmatrix}$, $s = n$, and $r = 1$ or $r = n$;

$\qquad$ B. $B = \pm \begin{pmatrix} 1 & w \\ 0 & 1 \end{pmatrix}^T$, $s = \frac{1}{n}$, and $r = 1$ or $r = \frac{1}{n}$;

$\quad$ ii. $\lambda = -1$ and

$\qquad$ A. $B = \pm \begin{pmatrix} 1 & w \\ 0 & 1 \end{pmatrix}$, $s = n$ (odd), and $r = 1$ or $r = \frac{1}{n}$;

$\qquad$ B. $B = \pm \begin{pmatrix} 1 & w \\ 0 & 1 \end{pmatrix}^T$, $s = \frac{1}{n}$ (n odd), and $r = 1$ or $r = n$;

$\quad$ iii. $\lambda = 1$, B is a n-periodic matrix such that $Bv = v$, with $s = 1$ and $r = n$.

A matrix B is an n-periodic matrix if $B^n = B$, $n \in \mathbb{N}$. This proposition shows that in contrast to $d = 2$ there exist matrices that pseudo commute with dilations without being shear matrices. The same extends to higher dimensions.

Proposition 7.3 [Bozzini et al., 2015]. *For $d > 3$ consider*

$$D := \left(\begin{array}{c|c} krI_p & 0 \\ \hline 0 & kI_{d-p} \end{array} \right),$$

and let

$$A := \left(\begin{array}{c|c} B & W \\ \hline 0 & I_{d-p} \end{array} \right),$$

where $B \in \mathbb{Z}^{p \times p}$ is a unimodular n-periodic matrix, $W \in \mathbb{Z}^{p \times d-p}$, and $BW = W$. Then the relation $DA = A^n D$ holds if $r = n$.

In the following we look for sets of matrices $\{M_i\}_{i \in \mathbb{Z}_s}$ that satisfy all the prescribed properties and with determinant smaller than shearlet scaling matrices. In particular, we focus on matrices $M_i = DS_i$ that are the product of an anisotropic expanding matrix D and a shear matrix S_i. If D is a diagonal matrix we call the matrices M_i shear-like because they mimic the shearlet matrices (Sec. 7.2). Furthermore, we study also the case where D is a full matrix (Sec. 7.3).

7.2 Shear-like anisotropic expanding matrices

In the first part of the work we focus on a set of shear-like matrices M_i that are the product of an integer diagonal matrix of the form

$$D = \begin{pmatrix} \alpha I_p & 0 \\ 0 & \beta I_{d-p} \end{pmatrix}, \qquad p < d, \qquad \alpha \neq \beta > 1, \qquad (7.1)$$

and a set of unimodular matrices S_i that give the directionality. By definition (7.1) of the matrix D we have that the matrices $M_i = DS_i$ satisfy the first property, in fact M_i are anisotropic expanding matrices. For $\alpha = 4$ and $\beta = 2$ we get back to the parabolic scaling matrix D_2 of the shearlet in (6.8).

d	$\det D_2$	$\det D$
2	8	6
3	32	18
4	128	54
5	512	162
6	2048	486

Table 7.1. Comparison between $\det D_2$ and $\det D$ for increasing dimension $d \geq 2$.

To overcome the disadvantage of the shearlet scaling matrices, we look for matrices with determinant smaller than 2^{d+p}. In the set of matrices of the form (7.1) we have the minimal determinant if $\alpha = 3$ and $\beta = 2$,

$$D = \begin{pmatrix} 3I_p & 0 \\ 0 & 2I_{d-p} \end{pmatrix}. \tag{7.2}$$

One important application of a directional transform is the detection of tangential hyperplanes at a point, because it allows to catch discontinuities of a signal. For this reason, in the following, we fix $p = d - 1$ and the dilation matrix becomes

$$D = \begin{pmatrix} 3I_{d-1} & 0 \\ 0 & 2 \end{pmatrix}. \tag{7.3}$$

In two dimensions the difference between the parabolic matrix D_2 (6.8) and D (7.3) is still small, $\det D_2 = 8$ and $\det D = 6$, but increasing the dimension, the difference increases rapidly,

$$\det D_2 = 2^{2d-1}, \quad \det D = 2^d \left(1 + \frac{1}{2}\right)^{d-1},$$

see Table 7.1.

We choose unimodular matrices S_i that pseudo commute with D in (7.3). The pseudo commuting property helps to find an explicit formula for the iterated matrices M_ϵ, $\epsilon \in \mathbb{Z}_s^n$, $n \in \mathbb{N}$. We use Theorems 7.1, 7.2 and 7.3 to see which form the matrices S_i should have.

In order to prove the remaining properties, to be jointly expanding matrices and the slope resolution property, we consider separately the bidimensional case and the multivariate case, because we have slightly different proofs.

7.2.1   Matrices in dimension $d = 2$

In two dimensions we consider the diagonal matrix

$$D = \begin{pmatrix} 3 & 0 \\ 0 & 2 \end{pmatrix}, \tag{7.4}$$

and using Theorem 7.1 we state that only (up to a sign) the shear matrices can pseudo-commute with this matrix. If we choose S_w as in (6.3),

$$S_w = \begin{pmatrix} 1 & w \\ 0 & 1 \end{pmatrix}, \tag{7.5}$$

then D and S_w satisfy

$$DS_w^2 = S_w^3 D. \tag{7.6}$$

The same relation is true for any power n.

Lemma 7.4. *For each $n \in \mathbb{N}$,*

$$D^n S_w^{2^n} = S_w^{3^n} D^n. \tag{7.7}$$

Proof: The proof is by induction over n. If $n = 1$, then (7.7) reduces to $DS_w^2 = S_w^3 D$. We observe that for any $\ell \in \mathbb{N}$, $S_w^\ell = S_{\ell w}$ is again a shear matrix and

$$D(S_w^\ell)^2 = (S_w^\ell)^3 D. \tag{7.8}$$

We assume that the claim is true for some $n \in \mathbb{N}$, and consider the case for $n + 1$. Using (7.8) and the induction assumption, we have

$$D^{n+1} S_w^{2^{n+1}} = D^n D \left(S_w^{2^n}\right)^2 = D^n \left(S_w^{2^n}\right)^3 D = D^n \left(S_w^3\right)^{2^n} D$$
$$= \left(S_w^3\right)^{3^n} D^n D = S_w^{3^{n+1}} D^{n+1}.$$

$$\square$$

We fix $w = -1$ and for simplicity we call $S_{-1} = S$. We consider two scaling matrices M_i, $i \in \mathbb{Z}_2$,

$$M_0 = D = \begin{pmatrix} 3 & 0 \\ 0 & 2 \end{pmatrix}, \qquad M_1 = DS^2 = \begin{pmatrix} 3 & -6 \\ 0 & 2 \end{pmatrix}, \tag{7.9}$$

whose inverses are

$$M_0^{-1} = D^{-1} = \begin{pmatrix} \frac{1}{3} & 0 \\ 0 & \frac{1}{2} \end{pmatrix}, \qquad M_1^{-1} = S^{-2} D^{-1} = \begin{pmatrix} \frac{1}{3} & 1 \\ 0 & \frac{1}{2} \end{pmatrix}. \tag{7.10}$$

Let us consider the iterated matrix $M_\epsilon = M_{\epsilon_n} \ldots M_{\epsilon_1}$, $\epsilon = (\epsilon_1, \ldots, \epsilon_n) \in \mathbb{Z}_2^n$ and its inverse M_ϵ^{-1}.

Lemma 7.5. *If $n \in \mathbb{N}$ and $\epsilon \in \mathbb{Z}_2^n$, then*

$$M_\epsilon^{-1} = \begin{pmatrix} 3^{-n} & 2^{1-n} p_\epsilon \left(\frac{2}{3}\right) \\ 0 & 2^{-n} \end{pmatrix}, \tag{7.11}$$

with the polynomial

$$p_\epsilon(x) = \sum_{j=1}^n \epsilon_j x^{j-1}, \qquad x \in [0, 1].$$

Proof: The proof is by induction. For $n = 1$, the claim holds. In fact if $\epsilon_1 = 0$ or $\epsilon_1 = 1$,

$$M_0^{-1} = \begin{pmatrix} 3^{-1} & 0 \\ 0 & 2^{-1} \end{pmatrix}, \quad \text{or} \quad M_1^{-1} = \begin{pmatrix} 3^{-1} & 1 \\ 0 & 2^{-1} \end{pmatrix}.$$

We suppose the claim is true for some $n \in \mathbb{N}$ and we consider $\epsilon = (\epsilon', \epsilon_{n+1}) \in \mathbb{Z}_2^{n+1}$. The inverse of the matrix M_ϵ is

$$M_\epsilon^{-1} = M_{\epsilon'}^{-1} M_{\epsilon_{n+1}}^{-1},$$

with

$$p_\epsilon\left(\frac{2}{3}\right) = \sum_{j=1}^{n+1} \epsilon_j \left(\frac{2}{3}\right)^{j-1} = p_{\epsilon'}\left(\frac{2}{3}\right) + \epsilon_{n+1}\left(\frac{2}{3}\right)^n.$$

If $\epsilon_{n+1} = 0$, then

$$\begin{aligned}
M_\epsilon^{-1} &= \begin{pmatrix} 3^{-n} & 2^{1-n} p_{\epsilon'}\left(\frac{2}{3}\right) \\ 0 & 2^{-n} \end{pmatrix} \begin{pmatrix} 3^{-1} & 0 \\ 0 & 2^{-1} \end{pmatrix} = \begin{pmatrix} 3^{-(n+1)} & 2^{-n} p_{\epsilon'}\left(\frac{2}{3}\right) \\ 0 & 2^{-(n+1)} \end{pmatrix} \\
&= \begin{pmatrix} 3^{-(n+1)} & 2^{-n} p_\epsilon\left(\frac{2}{3}\right) \\ 0 & 2^{-(n+1)} \end{pmatrix}.
\end{aligned}$$

If $\epsilon_{n+1} = 1$, then we have $p_\epsilon\left(\frac{2}{3}\right) = p_{\epsilon'}\left(\frac{2}{3}\right) + \left(\frac{2}{3}\right)^n$, and

$$\begin{aligned}
M_\epsilon^{-1} &= \begin{pmatrix} 3^{-n} & 2^{1-n} p_{\epsilon'}\left(\frac{2}{3}\right) \\ 0 & 2^{-n} \end{pmatrix} \begin{pmatrix} 3^{-1} & 1 \\ 0 & 2^{-1} \end{pmatrix} = \begin{pmatrix} 3^{-(n+1)} & 3^{-n} + 2^{-n} p_{\epsilon'}\left(\frac{2}{3}\right) \\ 0 & 2^{-(n+1)} \end{pmatrix} \\
&= \begin{pmatrix} 3^{-(n+1)} & 2^{-n} p_\epsilon\left(\frac{2}{3}\right) \\ 0 & 2^{-(n+1)} \end{pmatrix}.
\end{aligned}$$

This concludes the induction. $\qquad\qquad\square$

By computing directly the inverse of (7.11), we can write M_ϵ, $\epsilon \in \mathbb{Z}_2^n$, as

$$M_\epsilon = \begin{pmatrix} 3^n & 3^{n+1} q_\epsilon\left(\frac{2}{3}\right) \\ 0 & 2^n \end{pmatrix}, \tag{7.12}$$

where we introduce the polynomial

$$q_\epsilon(x) = \sum_{j=1}^{n} -\epsilon_j x^j.$$

In the previous section we show that it is important to prove that the matrices M_0, and M_1 are jointly expanding, which allows the grids $M_\epsilon^{-n} \mathbb{Z}^d$ to tend to $\mathbb{R}^d$ as n increases.

Proposition 7.6. *M_ϵ are expanding matrices for any $\epsilon \in \mathbb{Z}_2^n$ for n sufficiently large.*

Proof: We have to prove that the joint spectral radius of the set $\{M_i\}_{i\in\mathbb{Z}_2}$ is less than 1,

$$\rho(\{M_i^{-1}\}_{i\in\mathbb{Z}_2}) = \limsup_{n\to\infty} \sup_{\epsilon\in\mathbb{Z}_2^n} \left\|M_\epsilon^{-1}\right\|^{1/n} = \limsup_{n\to\infty} \sup_{\epsilon\in\mathbb{Z}_2^n} \left\|\prod_{j=1}^n M_{\epsilon_j}^{-1}\right\|^{1/n} < 1.$$

By the equivalence of norms on finite dimensional spaces, we can choose the underlying matrix norm arbitrarily, for example $\|\cdot\|_1$. Using the general expression of M_ϵ^{-1} in (7.11) we have

$$\begin{aligned}
\sup_{\epsilon\in\mathbb{Z}_2^n} \left\|M_\epsilon^{-1}\right\|_1^{1/n} &= \sup_{\epsilon\in\mathbb{Z}_2^n} \left\|\begin{pmatrix} 3^{-n} & 2^{1-n} p_\epsilon\left(\frac{2}{3}\right) \\ 0 & 2^{-n} \end{pmatrix}\right\|_1^{1/n} = \sup_{\epsilon\in\mathbb{Z}_2^n} \left(2^{1-n} p_\epsilon\left(\frac{2}{3}\right) + 2^{-n}\right)^{1/n} \\
&= \left(2^{1-n} \sum_{j=0}^{n-1} \left(\frac{2}{3}\right)^j + 2^{-n}\right)^{1/n} = \left(2^{1-n} 3\left(1-\left(\frac{2}{3}\right)^n\right) + 2^{-n}\right)^{1/n} \\
&= \frac{1}{2}\left(7 - 6\left(\frac{2}{3}\right)^n\right)^{1/n} < 1
\end{aligned}$$

for $n \geq 3$ and

$$\rho(\{M_i\}_{i\in\mathbb{Z}_2}) = \limsup_{n\to\infty} \sup_{\epsilon\in\mathbb{Z}_2^n} \left\|\prod_{j=1}^n M_{\epsilon_j}^{-1}\right\|_1^{1/n} = \frac{1}{2}.$$

$\square$

Thus, the matrices M_0 and M_1 are suitable for defining a multiple refinement process because they are jointly expanding. Given $\epsilon = (\epsilon_1,\ldots,\epsilon_n) \in \mathbb{Z}_2^n$ with $n \in \mathbb{N}$ we also have an explicit way to compute the points on the coarse and the refined lattice. For instance, we can rewrite (7.12) as

$$M_\epsilon = \begin{pmatrix} 1 & 3^{n+1} 2^{-n} q_\epsilon\left(\frac{2}{3}\right) \\ 0 & 1 \end{pmatrix} D^n = \begin{pmatrix} 1 & -3\sum_{j=1}^n \epsilon_j \left(\frac{3}{2}\right)^{n-j} \\ 0 & 1 \end{pmatrix} D^n. \qquad (7.13)$$

Using the shear matrix properties and (7.7) we get

$$M_\epsilon = \begin{pmatrix} 1 & 3\,2^{-n} q_n\left(\frac{2}{3}\right) \\ 0 & 1 \end{pmatrix}^{3^n} D^n = D^n \begin{pmatrix} 1 & 3\,2^{-n} q_n\left(\frac{2}{3}\right) \\ 0 & 1 \end{pmatrix}^{2^n} = D^n \begin{pmatrix} 1 & 3 q_n\left(\frac{2}{3}\right) \\ 0 & 1 \end{pmatrix}. \qquad (7.14)$$

Instead, inverting (7.13) we obtain

$$M_\epsilon^{-1} = D^{-n} \begin{pmatrix} 1 & 3\sum_{j=1}^n \epsilon_j \left(\frac{3}{2}\right)^{n-j} \\ 0 & 1 \end{pmatrix}. \qquad (7.15)$$

We can use (7.14), (7.15) to compute easily the coarse grid $M_\epsilon\mathbb{Z}^2$ and the refined grid $M_\epsilon^{-1}\mathbb{Z}^2$.

At this point, we can follow [Kutyniok and Sauer, 2009] to show that the matrices M_0 and M_1 enjoy the slope resolution property. Note that for $d > 2$ we need a more

general approach for the proof (see Theorem 7.11) so that it applies also in this case. Let ℓ be a line through the origin with slope $s(\ell)$ and we denote with $s(\ell, \epsilon)$ the slope of $M_\epsilon^{-1}\ell$ with $\epsilon \in \mathbb{Z}_2^n$ and $n \in \mathbb{N}$.

Lemma 7.7. *Let ℓ be a line passing through the origin with slope $s(\ell) \in [0, \infty]$ and $\epsilon \in \mathbb{Z}_2^n$ with $n \in \mathbb{N}$.*

(i) If $s(\ell) \in (0, \infty)$, then

$$s(\ell, \epsilon) = \frac{1}{\left(\frac{2}{3}\right)^n \frac{1}{s(\ell)} + 2p_\epsilon\left(\frac{2}{3}\right)}. \tag{7.16}$$

(ii) If $\ell = \{0\} \times \mathbb{R}$, i.e $s(\ell) = \infty$, then

$$s(\ell, \epsilon) = \frac{1}{2p_\epsilon\left(\frac{2}{3}\right)}. \tag{7.17}$$

(iii) If $\ell = \mathbb{R} \times \{0\}$, i.e. $s(\ell) = 0$, then

$$s(\ell, \epsilon) = 0. \tag{7.18}$$

Proof:

(i) If $s(\ell) \in (0, \infty)$, then we can consider the point $(1, s(\ell)) \in \ell$ that becomes

$$M_\epsilon^{-1}\begin{pmatrix} 1 \\ s(\ell) \end{pmatrix} = \begin{pmatrix} 3^{-n} & 2^{1-n}p_\epsilon\left(\frac{2}{3}\right) \\ 0 & 2^{-n} \end{pmatrix}\begin{pmatrix} 1 \\ s(\ell) \end{pmatrix} = \begin{pmatrix} 3^{-n} + 2^{1-n}p_\epsilon\left(\frac{2}{3}\right)s(\ell) \\ 2^{-n}s(\ell) \end{pmatrix}.$$

Thus, the slope of the line $M_\epsilon^{-1}\ell$ is

$$s(\ell, \epsilon) = \frac{2^{-n}s(\ell)}{3^{-n} + 2^{1-n}p_\epsilon\left(\frac{2}{3}\right)s(\ell)} = \frac{1}{\left(\frac{2}{3}\right)^n \frac{1}{s(\ell)} + 2p_\epsilon\left(\frac{2}{3}\right)}.$$

(ii) If $s(\ell) = \infty$, then the point $(0, 1) \in \ell$ is transformed into

$$M_\epsilon^{-1}\begin{pmatrix} 0 \\ 1 \end{pmatrix} = \begin{pmatrix} 3^{-n} & 2^{1-n}p_\epsilon\left(\frac{2}{3}\right) \\ 0 & 2^{-n} \end{pmatrix}\begin{pmatrix} 0 \\ 1 \end{pmatrix} = \begin{pmatrix} 2^{1-n}p_\epsilon\left(\frac{2}{3}\right) \\ 2^{-n} \end{pmatrix}$$

and

$$s(\ell, \epsilon) = \frac{2^{-n}}{2^{1-n}p_\epsilon\left(\frac{2}{3}\right)} = \frac{1}{2p_\epsilon\left(\frac{2}{3}\right)}.$$

(iii) If $s(\ell) = 0$, then the point $(1, 0) \in \ell$ is transformed into

$$M_\epsilon^{-1}\begin{pmatrix} 1 \\ 0 \end{pmatrix} = \begin{pmatrix} 3^{-n} & 2^{1-n}p_\epsilon\left(\frac{2}{3}\right) \\ 0 & 2^{-n} \end{pmatrix}\begin{pmatrix} 1 \\ 0 \end{pmatrix} = \begin{pmatrix} 3^{-n} \\ 0 \end{pmatrix}$$

and $s(\ell, \epsilon) = 0$.

$$\square$$

Lemma 7.7 helps us to prove a result similar to Theorem 6.1 for shearlets (cf. [Kutyniok and Sauer, 2009]).

Theorem 7.8. *Let ℓ be a line through the origin with slope $s(\ell) \in (0, \infty]$. Then for each $s \in [1/6, \infty]$ and $\delta > 0$ there exist some $n \in \mathbb{N}$ and $\epsilon \in \mathbb{Z}_2^n$ such that*

$$|s(\ell, \epsilon) - s| < \delta.$$

Proof: Let $s \in \left(\frac{1}{6}, \infty\right)$ and $\delta > 0$. Due to the denseness of rational numbers there exist $n \in \mathbb{N}$ and $\epsilon \in \mathbb{Z}_2^n$ such that

$$\left|2p_\epsilon\left(\frac{2}{3}\right) - \frac{1}{s}\right| = \left|2\sum_{j=1}^n \epsilon_j \left(\frac{2}{3}\right)^{j-1} - \frac{1}{s}\right| < \frac{\delta}{s(s+\delta)} = \tilde{\delta}. \tag{7.19}$$

From this inequality we have

$$2\sum_{j=1}^n \epsilon_j \left(\frac{2}{3}\right)^{j-1} > \frac{1}{s} - \tilde{\delta}.$$

Since we can always enlarge n, without loss of generality, we may assume

$$0 < \left(\frac{2}{3}\right)^n \frac{1}{s(\ell)} < \tilde{\delta}. \tag{7.20}$$

Using these inequalities and (7.16), we have

$$|s(\ell, \epsilon) - s| = \left|\frac{1}{\left(\frac{2}{3}\right)^n \frac{1}{s(\ell)} + 2\sum_{j=1}^n \epsilon_j \left(\frac{2}{3}\right)^{j-1}} - s\right| = \left|\frac{1 - s\left[\left(\frac{2}{3}\right)^n \frac{1}{s(\ell)} + 2\sum_{j=1}^n \epsilon_j \left(\frac{2}{3}\right)^{j-1}\right]}{\left(\frac{2}{3}\right)^n \frac{1}{s(\ell)} + 2\sum_{j=1}^n \epsilon_j \left(\frac{2}{3}\right)^{j-1}}\right|$$

$$= s\left|\frac{\frac{1}{s} - \left(\frac{2}{3}\right)^n \frac{1}{s(\ell)} - 2\sum_{j=1}^n \epsilon_j \left(\frac{2}{3}\right)^{j-1}}{\left(\frac{2}{3}\right)^n \frac{1}{s(\ell)} + 2\sum_{j=1}^n \epsilon_j \left(\frac{2}{3}\right)^{j-1}}\right| \le s\left|\frac{\frac{1}{s} - \left(\frac{2}{3}\right)^n \frac{1}{s(\ell)} - 2\sum_{j=1}^n \epsilon_j \left(\frac{2}{3}\right)^{j-1}}{2\sum_{j=1}^n \epsilon_j \left(\frac{2}{3}\right)^{j-1}}\right|$$

$$\le s\left|\frac{\frac{1}{s} - \left(\frac{2}{3}\right)^n \frac{1}{s(\ell)} - 2\sum_{j=1}^n \epsilon_j \left(\frac{2}{3}\right)^{j-1}}{\frac{1}{s} - \tilde{\delta}}\right| \le s^2\left|\frac{\frac{1}{s} - 2\sum_{j=1}^n \epsilon_j \left(\frac{2}{3}\right)^{j-1}}{1 - s\tilde{\delta}}\right|$$

$$\le \left|\frac{s^2\tilde{\delta}}{1 - s\tilde{\delta}}\right| = \delta.$$

Let $\epsilon \in \mathbb{Z}_2^\infty$ such that $\epsilon_j = 0$ for any $j \ge j_0$. For $K > 0$, using (7.20), there exists $n_0 \in \mathbb{N}$ such that

$$\left(\frac{2}{3}\right)^n \frac{1}{s(\ell)} + 2\sum_{j=1}^n \epsilon_j \left(\frac{2}{3}\right)^{j-1} < \frac{1}{K} \quad \forall n \ge n_0,$$
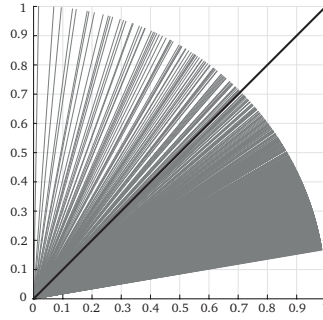
Figure 7.1. Fixing a line ℓ through the origin (black), the grey lines are the directions reached after the application of M_ϵ^{-1} where we consider all possible $\epsilon \in \mathbb{Z}_2^{10}$.

which implies

$$s(\ell, \epsilon) = \frac{1}{\left(\frac{2}{3}\right)^n \frac{1}{s(\ell)} + 2\sum_{j=1}^n \epsilon_j \left(\frac{2}{3}\right)^{j-1}} > K,$$

hence $\lim_{n\to\infty} s(\ell, \epsilon) = \infty$.

Let $\epsilon \in \mathbb{Z}_2^\infty$ such that $\epsilon_j = 1$ for any $j > j_0$. With this hypothesis we can rewrite $s(\ell, \epsilon)$ as

$$s(\ell, \epsilon) = \frac{1}{\left(\frac{2}{3}\right)^n \frac{1}{s(\ell)} + 2\sum_{j=1}^n \epsilon_j \left(\frac{2}{3}\right)^{j-1}} = \frac{1}{\left(\frac{2}{3}\right)^n \frac{1}{s(\ell)} + 2\left[3 - 3\left(\frac{2}{3}\right)^n - \sum_{j=1}^{j_0}(1-\epsilon_j)\left(\frac{2}{3}\right)^{j-1}\right]}$$

$$= \frac{1}{\left(\frac{2}{3}\right)^n \frac{1}{s(\ell)} + 6 - 6\left(\frac{2}{3}\right)^n - 2\sum_{j=1}^{j_0}(1-\epsilon_j)\left(\frac{2}{3}\right)^{j-1}},$$

hence,

$$\lim_{n\to\infty} s(\ell, \epsilon) = \lim_{n\to\infty} \frac{1}{\left(\frac{2}{3}\right)^n \frac{1}{s(\ell)} + 6 - 6\left(\frac{2}{3}\right)^n - 2\sum_{j=1}^{j_0}(1-\epsilon_j)\left(\frac{2}{3}\right)^{j-1}} = \frac{1}{6 - 2\sum_{j=1}^{j_0}(1-\epsilon_j)\left(\frac{2}{3}\right)^{j-1}}.$$

If $\epsilon_1 = \ldots = \epsilon_{j_0} = 0$, then

$$\lim_{n\to\infty} s(\ell, \epsilon) = \frac{1}{6\left(\frac{2}{3}\right)^{j_0}}.$$

Otherwise, if $\epsilon_1 = \ldots = \epsilon_{j_0} = 1$, then

$$\lim_{n\to\infty} s(\ell, \epsilon) = \frac{1}{6}.$$

This concludes the proof. $\square$

Using only M_0 and M_1 we can move any line ℓ, with slope $s(\ell) \in (0, \infty]$, close to any other line with slope in $\left[\frac{1}{6}, \infty\right]$, as can be seen in Figure 7.1.

Focusing on the matrices M_0 and M_1 of the form (7.9) does not allow to reach certain directions as shown in Theorem 7.8. This situation is similar to what Kutyniok and Sauer

[2009] prove in Theorem 6.1. As for the shearlet case, in order to obtain a system that resolves all possible directions we have to consider all the matrices

$$\begin{pmatrix} 3 & -6 \\ 0 & 2 \end{pmatrix}, \qquad \begin{pmatrix} 3 & 0 \\ 0 & 2 \end{pmatrix}, \qquad \begin{pmatrix} 3 & 6 \\ 0 & 2 \end{pmatrix},$$

$$\begin{pmatrix} 2 & 0 \\ -6 & 3 \end{pmatrix}, \qquad \begin{pmatrix} 2 & 0 \\ 0 & 3 \end{pmatrix}, \qquad \begin{pmatrix} 2 & 0 \\ 6 & 3 \end{pmatrix},$$

where we also change the order of 3 and 2 in the diagonal matrix and the shear acts on the second variable. For each pair of matrices we can prove similar results to Theorems 7.6 and 7.8.

7.2.2   Matrices in dimension $d \geq 3$

In dimension d we concentrate on the dilation matrix

$$D = \begin{pmatrix} 3I_{d-1} & 0 \\ 0 & 2 \end{pmatrix}. \tag{7.21}$$

Theorems 7.2 and 7.3 tell us which type of matrices pseudo-commute with D. We choose to work with shear matrices of the form

$$S_i = \begin{pmatrix} I_{d-1} & -e_i \\ 0 & 1 \end{pmatrix}, \qquad i \in \mathbb{Z}_d, \tag{7.22}$$

that satisfy

$$DS_i^2 = S_i^3 D. \tag{7.23}$$

The vectors e_i, $i \in \mathbb{Z}_d$, are such that $e_0 = 0$ and $(e_i)_k = \delta_{ik}$, for $k = 1, \dots, d-1$.

As for shearlets in [Kutyniok and Sauer, 2009] and the bivariate case, this choice of matrices is arbitrary and it creates an asymmetry between the variables. The last variable is treated differently with respect to the first $d-1$ variables where the shear acts. This choice does not allow to reach certain directions. To obtain a system that resolves all possible directions, d multiresolution systems should be considered where the role of the non shear variable is taken by all variables. We should take matrices that are a permutation of the rows of (7.21) and (7.22). The results are always the same only with respect to another variable.

We define the scaling matrices M_i, $i \in \mathbb{Z}_d$, as

$$M_i = DS_i^2 = \begin{pmatrix} 3I_{d-1} & -6e_i \\ 0 & 2 \end{pmatrix} = S_i^3 D, \tag{7.24}$$

whose inverses can be easily computed,

$$M_i^{-1} = S_i^{-2}D^{-1} = \begin{pmatrix} \frac{1}{3}I_{d-1} & e_i \\ 0 & \frac{1}{2} \end{pmatrix}. \tag{7.25}$$

The multiple subdivision scheme is governed by the matrices

$$M_\epsilon := M_{\epsilon_n} \dots M_{\epsilon_1}, \qquad \epsilon = (\epsilon_1, \dots, \epsilon_n) \in \mathbb{Z}_d^n, \qquad n \in \mathbb{N},$$

for which we have an explicit expression similar to (7.11) in the bivariate case.

Lemma 7.9. *For $n \in \mathbb{N}$ and $\epsilon \in \mathbb{Z}_d^n$ we have*

$$M_\epsilon^{-1} = \begin{pmatrix} 3^{-n} I_{d-1} & 2^{1-n} p_\epsilon\left(\frac{2}{3}\right) \\ 0 & 2^{-n} \end{pmatrix}, \tag{7.26}$$

with the $d-1$ vector valued polynomial

$$p_\epsilon(x) = \sum_{j=1}^n x^{j-1} e_{\epsilon_j}, \qquad x \in [0,1].$$

Proof: By induction over n, we first note that for $n = 1$ we have exactly the matrices M_ϵ^{-1}, $\epsilon \in \mathbb{Z}_d$ in (7.25).

Let us suppose that the claim is true for $n \geq 1$ and we verify it for $n + 1$ and $\epsilon = (\epsilon', \epsilon_{n+1}) \in \mathbb{Z}_d^{n+1}$. The matrix M_ϵ^{-1} has the form

$$M_\epsilon^{-1} = M_{\epsilon'}^{-1} M_{\epsilon_{n+1}}^{-1} = \begin{pmatrix} 3^{-n} I_{d-1} & 2^{1-n} p_{\epsilon'}(2/3) \\ 0 & 2^{-n} \end{pmatrix} \begin{pmatrix} 3^{-1} & e_{\epsilon_{n+1}} \\ 0 & 2^{-1} \end{pmatrix}$$

$$= \begin{pmatrix} 3^{-(n+1)} I_{d-1} & 2^{-n} p_{\epsilon'}(2/3) + 3^{-n} e_{\epsilon_{n+1}} \\ 0 & 2^{-(n+1)} \end{pmatrix},$$

and taking into account that

$$2^{-n} p_{\epsilon'}\left(\frac{2}{3}\right) + 3^{-n} e_{\epsilon_{n+1}} = 2^{-n} \left(p_{\epsilon'}\left(\frac{2}{3}\right) + \left(\frac{2}{3}\right)^n e_{\epsilon_{n+1}} \right) = 2^{-n} p_\epsilon\left(\frac{2}{3}\right),$$

we obtain the general expression (7.26). $\qquad\qquad\qquad\qquad\qquad\qquad\qquad\square$

Inverting M_ϵ^{-1} in (7.26), we get a formula for M_ϵ, namely

$$M_\epsilon = \begin{pmatrix} 3^n I_{d-1} & 3^{n+1} q_\epsilon(2/3) \\ 0 & 2^n \end{pmatrix}, \tag{7.27}$$

with

$$q_\epsilon(x) = -\sum_{j=1}^n x^j e_{\epsilon_j}, \qquad \epsilon \in \mathbb{Z}_d^n, \quad n \in \mathbb{N}.$$

These matrices are able to define a directional multiresolution analysis if they satisfy all the properties listed in Section 7.1: they are jointly expanding, i.e., the grid $M_\epsilon^{-1} \mathbb{Z}^d$ tends to $\mathbb{R}^d$ and they satisfy the slope resolution property.

Proposition 7.10. *The set of matrices $\{M_i\}_{i \in \mathbb{Z}_d}$ is jointly expanding.*

Proof: We have to show that the joint spectral radius of the scaling matrices

$$\rho\left(\{M_i^{-1}\}_{i\in\mathbb{Z}_d}\right) = \limsup_{n\to\infty} \sup_{\epsilon\in\mathbb{Z}_d^n} \left\|M_\epsilon^{-1}\right\|^{1/n}$$

is strictly less than one. Using $\|\cdot\|_1$, we obtain for $n\in\mathbb{N}$

$$\sup_{\epsilon\in\mathbb{Z}_d^n}\left\|M_\epsilon^{-1}\right\|_1^{1/n} = \sup_{\epsilon\in\mathbb{Z}_d^n}\left\|\begin{pmatrix} 3^{-n} & 2^{1-n}p_\epsilon(2/3) \\ 0 & 2^{-n} \end{pmatrix}\right\|_1^{1/n} = \sup_{\epsilon\in\mathbb{Z}_d^n}\left(2^{1-n}\left\|p_\epsilon\left(\frac{2}{3}\right)\right\|_1 + 2^{-n}\right)^{1/n}$$

$$\leq \frac{1}{2}\left(2\sum_{j=0}^{n-1}\left(\frac{2}{3}\right)^j + 1\right)^{1/n} \leq \frac{1}{2}\left(2\sum_{j=0}^{\infty}\left(\frac{2}{3}\right)^j + 1\right)^{1/n} = \frac{7^{1/n}}{2}$$

and therefore $\sup_{\epsilon\in\mathbb{Z}_d^n}\left\|M_\epsilon^{-1}\right\|_1^{1/n} < 1$ for $n\geq 3$ independently of ϵ. $\square$

In dimension d, the slope resolution property allows to obtain any hyperplane by applying a suitable matrix M_ϵ to a single reference hyperplane. A hyperplane $H = \{x\in\mathbb{R}^d : v^Tx = 0\} \subset \mathbb{R}^d$ whose normal has the property $v_d \neq 0$, can be described by $v = (s,1)^T$ where $s\in\mathbb{R}^{d-1}$ is the slope of the hyperplane H. The slope of the reference hyperplane can be chosen arbitrarily in a scaled version of the standard simplex Δ_{d-1} defined in (6.13).

We now generalize Theorem 7.8 to dimension d. In this case the proof is different from the bivariate case and involves contractive maps and the fix point theorem.

Theorem 7.11. *For any reference hyperplane H with slope $s\in 6\Delta_{d-1}$, the family of matrices $\{M_i\}_{i\in\mathbb{Z}_d}$ has the slope resolution property: for any hyperplane H' with slope $s'\in\mathbb{R}^{d-1}$ and any $\delta > 0$ there exists $\epsilon\in\mathbb{Z}_d^n$, $n\in\mathbb{N}$, such that*

$$\left\|\begin{pmatrix} s' \\ 1 \end{pmatrix} - 2^{-n}M_\epsilon\begin{pmatrix} s \\ 1 \end{pmatrix}\right\| < \delta.$$

Proof: Let H be any hyperplane with slope $t\in\mathbb{R}^{d-1}$. Multiplying with M_i^{-1}, $i\in\mathbb{Z}_d$, we obtain a hyperplane with slope

$$M_i^{-1}\begin{pmatrix} t \\ 1 \end{pmatrix} = \begin{pmatrix} \frac{1}{3}I_{d-1} & e_i \\ 0 & \frac{1}{2} \end{pmatrix}\begin{pmatrix} t \\ 1 \end{pmatrix} = \frac{1}{2}\begin{pmatrix} \frac{2}{3}t + 2e_i \\ 1 \end{pmatrix}, \qquad t\in\mathbb{R}^{d-1}.$$

We define the affine contractions $h_i : \mathbb{R}^{d-1}\to\mathbb{R}^{d-1}$ by

$$h_i(t) = \frac{2}{3}t + 2e_i, \qquad i\in\mathbb{Z}_d, \tag{7.28}$$

which satisfy

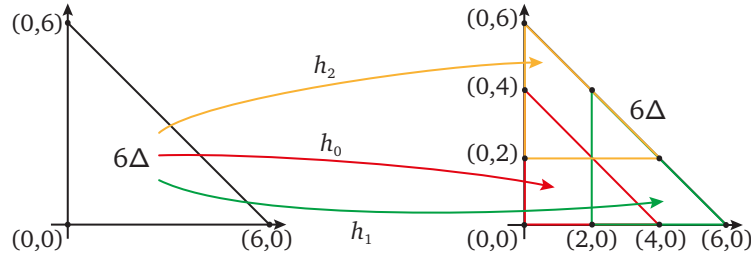$$h_i(6\Delta_{d-1}) = \frac{2}{3}6\Delta_{d-1} + 2e_i = 4\Delta_{d-1} + 2e_i \subset 6\Delta_{d-1} \tag{7.29}$$

Figure 7.2. In two dimensions $(d-1=2)$, we have three contractive maps h_i, $i \in \{0,1,2\}$ and the union of $h_0(6\Delta)$ (red), $h_1(6\Delta)$ (green), $h_2(6\Delta)$ (orange) gives again 6Δ.

and

$$\bigcup_{i \in \mathbb{Z}_d} h_i(6\Delta_{d-1}) = 6\Delta_{d-1}, \tag{7.30}$$

as visualized in Figure 7.2 for $d = 3$. Thus, the compact set $6\Delta_{d-1}$ is an invariant space with respect to the contractions h_i, $i \in \mathbb{Z}_d$. Hutchinson [1981] shows that any compact subset $X \subset \mathbb{R}^{d-1}$ satisfy a generating property,

$$6\Delta_{d-1} = \lim_{n \to \infty} \bigcup_{\epsilon \in \mathbb{Z}_d^n} h_\epsilon(X) \tag{7.31}$$

with respect to an invariant space in the Hausdorff metric. For general $\epsilon \in \mathbb{Z}_d^n$ we have

$$M_\epsilon^{-1}\begin{pmatrix} t \\ 1 \end{pmatrix} = \begin{pmatrix} 3^{-n}\mathrm{Id}_{d-1} & 2^{1-n}p_\epsilon\left(\frac{2}{3}\right) \\ 0 & 2^{-n} \end{pmatrix}\begin{pmatrix} t \\ 1 \end{pmatrix} = 2^{-n}\begin{pmatrix} \left(\frac{2}{3}\right)^n t + 2p_\epsilon\left(\frac{2}{3}\right) \\ 1 \end{pmatrix},$$

so h_ϵ is the composition of affine contractions

$$h_\epsilon(t) = h_{\epsilon_n}\left(h_{(\epsilon_1,\dots,\epsilon_{n-1})}(t)\right) = \left(\frac{2}{3}\right)^n t + 2p_\epsilon\left(\frac{2}{3}\right), \qquad \epsilon \in \mathbb{Z}_d^n, \qquad n \in \mathbb{N}.$$

This iterative definition and (7.29) yield that

$$h_\epsilon(6\Delta_{d-1}) \subset 6\Delta_{d-1}, \qquad \forall \epsilon \in \mathbb{Z}_d^n, \quad n \in \mathbb{N}. \tag{7.32}$$

Hence, the scaled simplex $6\Delta_{d-1}$ is an invariant space for any combination of the contraction h_i, $i \in \mathbb{Z}_d$.

Given a hyperplane H' with slope $s' \in \mathbb{R}^{d-1}$, and $0 < \delta' < \delta$, we consider the compact set

$$R_{\delta'}(s') = \{t \in \mathbb{R}^{d-1} : \left\|s' - t\right\|_1 \leq \delta'\}.$$

The generating property (7.31) implies that there exist some $n_1 \in \mathbb{N}$ and $\epsilon^1 \in \mathbb{Z}_d^{n_1}$ such that

$$I = h_{\epsilon^1}\left(R_{\delta'}(s')\right) \cap 6\Delta_{d-1} \neq \emptyset.$$

Figure 7.3. Definition of the contractive map h_ϵ such that $s \in h_\epsilon(R_{\delta'}(s'))$.

Applying (7.32) to the closure of I, there exist some $n_2 \in \mathbb{N}$ and $\epsilon^2 \in \mathbb{Z}_d^{n_2}$ such that

$$s \in h_{\epsilon^2}(I) \subset h_{\epsilon^2}\left(h_{\epsilon^1}\left(R_{\delta'}(s')\right)\right) = h_\epsilon\left(R_{\delta'}(s')\right), \qquad \text{with } \epsilon = (\epsilon^2, \epsilon^1) \in \mathbb{Z}_d^n, \qquad (7.33)$$

see Figure 7.3. Hence, $h_\epsilon^{-1}(s) \in R_{\delta'}(s')$ or equivalently,

$$\left\| \binom{s'}{1} - 2^{-n} M_\epsilon \binom{s}{1} \right\|_1 \le \delta' < \delta$$

as claimed.   □

Finally for each $\epsilon \in \mathbb{Z}_d^n$, we can rewrite (7.27) as

$$M_\epsilon = \begin{pmatrix} 3^n \mathrm{I}_{d-1} & 3^{n+1} q_\epsilon(2/3) \\ 0 & 2^n \end{pmatrix} = D^n \begin{pmatrix} \mathrm{I}_{d-1} & 3 q_\epsilon(2/3) \\ 0 & 1 \end{pmatrix} = D^n S_\epsilon \qquad (7.34)$$

and we can rewrite (7.26) as

$$M_\epsilon^{-1} = \begin{pmatrix} 3^{-n} \mathrm{I}_{d-1} & 2^{1-n} p_\epsilon(2/3) \\ 0 & 2^{-n} \end{pmatrix} = D^{-n} \begin{pmatrix} \mathrm{I}_{d-1} & 3 \sum_{j=1}^n \left(\frac{3}{2}\right)^{n-j} e_{\epsilon_j} \\ 0 & 1 \end{pmatrix} = D^{-n} \widehat{S}_\epsilon. \quad (7.35)$$

Taking the inverses of (7.34) and (7.35) yields

$$M_\epsilon = \widehat{S}_\epsilon^{-1} D^n, \qquad M_\epsilon^{-1} = S_\epsilon^{-1} D^{-n}. \qquad (7.36)$$

These formulations of M_ϵ and M_ϵ^{-1} allow us to compute efficiently the grids $M_\epsilon \mathbb{Z}^d$ and $M_\epsilon^{-1} \mathbb{Z}^d$ as transformations of the D^n or D^{-n} refined grid. These transformations are still shears, however, in contrast to the shearlet case, the translation is not integer any more because it depends on $q_\epsilon(2/3)$ and $p_\epsilon(2/3)$.

7.3   General anisotropic expanding matrices

We show that considering the expanding matrices M_i, as product of an anisotropic diagonal matrix D and a shear S_i, the minimum determinant is achieved by $2^d \left(1 + \frac{1}{2}\right)^{d-1}$ given by (7.3). This determinant is less than the determinant of the shearlet case (6.12)

which is 2^{2d-1}. Indeed, it is not the minimal determinant possible for an expanding matrix. In fact in two dimensions, from a theoretical point of view, an expanding matrix should have determinant greater than 2 and we have to restrict to a determinant greater or equal to 3 if we want anisotropic matrices. Cotronei et al. [2015] present a set of two anisotropic expanding matrices

$$M_0 = \begin{pmatrix} 1 & 1 \\ 1 & -2 \end{pmatrix}, \qquad M_1 = \begin{pmatrix} 1 & 1 \\ 0 & 1 \end{pmatrix} M_0 = \begin{pmatrix} 2 & -1 \\ 1 & -2 \end{pmatrix},$$

with determinant 3 that are jointly expanding and they satisfy the slope resolution property. Cotronei et al. [2015] show that it is possible to have a determinant smaller than the diagonal matrix D in (7.4) if full matrices are considered. One could ask if focusing on full matrices we can find anisotropic expanding matrices that satisfy all the properties requested (jointly expanding matrices, slope resolution property) with determinant less than the shear-like matrices (7.3) in dimension $d > 2$. Thanks to some numerical experiments we conjecture that the answer is yes. We set up an algorithm that searches integer matrices in $\mathbb{Z}^{3\times 3}$ that satisfy some of the requested properties. The idea is to consider matrices with integer entries in a sub interval of $\mathbb{Z}$ centred in 0 (we are looking for matrices with minimum determinant). Once the interval is fixed, we generate all the matrices with entries in this interval and we perform a sequence of tests that in each step allow to eliminate the undesired matrices:

1. We first check for matrices with determinant less than $2^d \left(1 + \frac{1}{2}\right)^{d-1}$, the determinant of the shear-like case in (7.3).

2. We compute the eigenvalues λ_k, $k = 1, \ldots, d$ and we keep only the matrices with all eigenvalues $|\lambda_k| > 1$ and with at least two different eigenvalues $|\lambda_j| \neq |\lambda_k|$, $j \neq k$. In this way we select the anisotropic expanding matrices.

3. For the remaining matrices M, we define the set

$$M_i = M S_i, \qquad S_i = \begin{pmatrix} 1 & -e_i \\ 0 & 1 \end{pmatrix}, \tag{7.37}$$

   with the vectors $(e_i)_k = \delta_{ik}$, $k = 1, \ldots, d-1$ and $e_0 = 0$. We save the matrices for which there exists some $n_0 \in \mathbb{N}$ such that $\left\| M_\epsilon^{-1} \right\| < 1$ for any $\epsilon \in \mathbb{Z}_d^{n_0}$. We choose n_0 quite small. This allows to conclude that the matrices M_i are jointly expanding matrices as shown in the following proposition.

Proposition 7.12. *If there exists some $n_0 \in \mathbb{N}$ such that $\left\| M_\epsilon^{-1} \right\| < 1$ for any $\epsilon \in \mathbb{Z}_d^{n_0}$, then the set of matrices $\{M_i\}_{i \in \mathbb{Z}_d}$ are jointly expanding matrices.*

Proof: The proof follows straightforwardly from the definition of the joint spectral radius, in fact for any type of norm

$$\left\| M_\epsilon^{-1} \right\| = \left\| \prod_{j=1}^{n} M_{\epsilon_j}^{-1} \right\| \leq \prod_{j=1}^{n} \left\| M_{\epsilon_j}^{-1} \right\|.$$

By hypothesis there exists some $n_0 \in \mathbb{N}$ such that $\left\| M_\epsilon^{-1} \right\| < 1$ for all $\epsilon \in \mathbb{Z}_d^{n_0}$, and we define $\mu = \max_{\epsilon \in \mathbb{Z}_d^{n_0}} \left\| M_\epsilon^{-1} \right\| < 1$, thus

$$\prod_{j=1}^{n} \left\| M_{\epsilon_j}^{-1} \right\| \leq \prod_{k=1}^{\lfloor n/n_0 \rfloor} \left\| M_{\epsilon'_k}^{-1} \right\| \leq \prod_{k=1}^{\lfloor n/n_0 \rfloor} \mu = \mu^{\lfloor n/n_0 \rfloor},$$

where ϵ'_k are sub sequences of ϵ such that $\left| \epsilon'_k \right| \leq n_0$. So the joint spectral radius of this set of matrices is

$$\rho(\{M_i\}_{i \in \mathbb{Z}_d}) = \limsup_{n \to \infty} \sup_{\epsilon \in \mathbb{Z}_d^n} \left\| M_\epsilon^{-1} \right\|^{1/n} \leq \limsup_{n \to \infty} (\mu^{\lfloor n/n_0 \rfloor})^{1/n} = \sqrt[n_0]{\mu} < 1.$$

$\square$

In this way we obtain some sets of anisotropic expanding matrices that are also jointly expanding. An example of such matrices is

$$M = \begin{pmatrix} -1 & 1 & 0 \\ 1 & 1 & 1 \\ 1 & 1 & -2 \end{pmatrix} \tag{7.38}$$

and the product with shear matrices give the set

$$M_0 = M = \begin{pmatrix} -1 & 1 & 0 \\ 1 & 1 & 1 \\ 1 & 1 & -2 \end{pmatrix},$$

$$M_1 = MS_1 = M \begin{pmatrix} 1 & 0 & -1 \\ 0 & 1 & 0 \\ 0 & 0 & 1 \end{pmatrix} = \begin{pmatrix} -1 & 1 & 1 \\ 1 & 1 & 0 \\ 1 & 1 & -3 \end{pmatrix}, \tag{7.39}$$

$$M_2 = MS_2 = M \begin{pmatrix} 1 & 0 & 0 \\ 0 & 1 & -1 \\ 0 & 0 & 1 \end{pmatrix} = \begin{pmatrix} -1 & 1 & -1 \\ 1 & 1 & 0 \\ 1 & 1 & -3 \end{pmatrix}.$$

These matrices have $\det M_i = 6$ for $i \in \mathbb{Z}_3$ and the eigenvalues are $\pm\sqrt{3}$ and -2. So, as expected, they are anisotropic expanding matrices with determinant smaller than the shear-like matrix ($\det D = 18$) but also smaller than the dyadic matrix $2I_3$ ($\det 2I_3 = 8$) considered in the wavelet case. Moreover, computing the inverse of the matrices in

(7.39) we have

$$M_0^{-1} = M^{-1} = \begin{pmatrix} -\frac{1}{2} & \frac{1}{3} & \frac{1}{6} \\ \frac{1}{2} & \frac{1}{3} & \frac{1}{6} \\ 0 & \frac{1}{3} & -\frac{1}{3} \end{pmatrix},$$

$$M_1^{-1} = S_1^{-1} M^{-1} = \begin{pmatrix} 1 & 0 & 1 \\ 0 & 1 & 0 \\ 0 & 0 & 1 \end{pmatrix} M^{-1} = \begin{pmatrix} -\frac{1}{2} & \frac{2}{3} & -\frac{1}{6} \\ \frac{1}{2} & \frac{1}{3} & \frac{1}{6} \\ 0 & \frac{1}{3} & -\frac{1}{3} \end{pmatrix}, \qquad (7.40)$$

$$M_2^{-1} = S_2^{-1} M^{-1} = \begin{pmatrix} 1 & 0 & 0 \\ 0 & 1 & 1 \\ 0 & 0 & 1 \end{pmatrix} M^{-1} = \begin{pmatrix} -\frac{1}{2} & \frac{1}{3} & \frac{1}{6} \\ \frac{1}{2} & \frac{2}{3} & -\frac{1}{6} \\ 0 & \frac{1}{3} & -\frac{1}{3} \end{pmatrix},$$

and $\left\| M_i^{-1} \right\|_2 < 1$ for any $i \in \mathbb{Z}_3$.

For the matrices in (7.39) it remains to prove the slope resolution property, which is not a trivial task in the general case. In fact, differently to shear-like matrices, we have no explicit expression for the matrices M_ϵ with $\epsilon \in \mathbb{Z}_d^n$ and $n \in \mathbb{N}$, because this set of matrices does not satisfy the pseudo commuting property. In this case, it is difficult to find contracting maps and an invariant space as done in Theorem 7.11 for any d. For the moment we only have numerical evidence of the slope resolution property. As numerical test we fix $n \in \mathbb{N}$ and a hyperplane H' with normal $(s', 1)^T$, $s' \in \mathbb{R}^2$, and we apply the matrices M_ϵ^{-1}, with all possible $\epsilon \in \mathbb{Z}_d^n$ of length n, to the normal $(s', 1)$. This procedure displays an output similar to Figure 7.1 in the bivariate case. To provide numerical evidence of the slope resolution property we have to repeat the test considering all the possible shear matrices and all the permutations of matrix rows. If in the end the resulting normals span approximately all the directions, then the slope resolution property is satisfied from a numerical point of view.

This is still work in progress. An idea to prove the slope resolution property is to consider as contractions not the maps generated by M_i^{-1}, $i \in \mathbb{Z}_3$, but some finite combinations of these matrices, as done in [Cotronei et al., 2015] for $d = 2$. Another possibility is to look for general anisotropic matrices that satisfy the pseudo commuting property even if this means to consider a set of matrices with higher determinant than 6.

7.4   Numerical examples for $d = 2$

Finally, in this section we show some illustrations of how the MMRA based on the matrices presented in Section 7.2 performs when analysing a signal.

We focus on the family of matrices

$$M_0 = \begin{pmatrix} 3 & 0 \\ 0 & 2 \end{pmatrix}, \quad M_1 = \begin{pmatrix} 3 & -6 \\ 0 & 2 \end{pmatrix}, \qquad (7.41)$$

with $\det(M_i) = 6$, for $i \in \mathbb{Z}_2$. This means that we have to consider 6 analysis filters and 6 synthesis filters for each M_i, $i \in \mathbb{Z}_2$.

Following the construction proposed in Sections 6.2.1 and 6.3, we define for the family of matrices $\{M_i\}_{i\in\mathbb{Z}_2}$ a convergent multiple subdivision scheme and the relative filterbanks. The Smith factorization form of the matrices is trivial,

$$M_0 = IDI, \qquad M_1 = \begin{pmatrix} 3 & -6 \\ 0 & 2 \end{pmatrix} = \begin{pmatrix} 1 & -3 \\ 0 & 1 \end{pmatrix}\begin{pmatrix} 3 & 0 \\ 0 & 2 \end{pmatrix}\begin{pmatrix} 1 & 0 \\ 0 & 1 \end{pmatrix} = S^3 DI. \qquad (7.42)$$

Thus, we need two univariate interpolatory subdivision schemes with arity $\sigma_1 = 3$ and $\sigma_2 = 2$, respectively. For example, we consider the ternary and dyadic 2-point schemes with masks

$$b_1 = \left(\ldots, 0, \frac{1}{3}, \frac{2}{3}, 1, \frac{2}{3}, \frac{1}{3}, 0, \ldots\right), \quad b_2 = \left(\ldots, 0, \frac{1}{2}, 1, \frac{1}{2}, 0, \ldots\right),$$

and symbols

$$b_1^*(z) = \frac{z^{-2}}{3}(1 + z + z^2)^2, \quad b_2^*(z) = \frac{z^{-1}}{2}(1 + z)^2.$$

By (6.24), the symbol of the diagonal matrix D is the tensor product of b_1 and b_2,

$$b_D^*(z) = \frac{z_1^{-2} z_2^{-1}}{6}(1 + z_1 + z_1^2)^2(1 + z_2)^2,$$

and using (6.25) the symbols related to the matrices M_0 and M_1 are

$$b_{M_0}^*(z) = b_D^*(z) = \frac{z_1^{-2} z_2^{-1}}{6}(1 + z_1 + z_1^2)^2(1 + z_2)^2, \qquad (7.43)$$

$$b_{M_1}^*(z) = b_D^*(z^{S^3}) = \frac{z_1 z_2^{-1}}{6}(1 + z_1 + z_1^2)^2(1 + z_1^{-3} z_2)^2. \qquad (7.44)$$

The multiple subdivision scheme generated by the two symbols b_{M_0}, b_{M_1} and the two matrices M_0, M_1 converges to a continuous function, as stated by Lemma 6.8. Once we define the multiple subdivision scheme, we compute the filters using the prediction-correction method and the formulas (6.30), (6.31). The analysis filters for the diagonal matrix M_0 are

$$f_{0,0} = \begin{pmatrix} 0 & 0 & 0 & 0 & 0 \\ 0 & 0 & 0 & 0 & 0 \\ 0 & 0 & 1 & 0 & 0 \\ 0 & 0 & 0 & 0 & 0 \\ 0 & 0 & 0 & 0 & 0 \end{pmatrix}, \quad f_{0,1} = \begin{pmatrix} 0 & 0 & 0 & 0 & 0 \\ 0 & 0 & 0 & 0 & 0 \\ 0 & -\frac{2}{3} & 1 & 0 & -\frac{1}{3} \\ 0 & 0 & 0 & 0 & 0 \\ 0 & 0 & 0 & 0 & 0 \end{pmatrix}, \quad f_{0,2} = \begin{pmatrix} 0 & 0 & 0 & 0 & 0 \\ 0 & 0 & 0 & 0 & 0 \\ 0 & -\frac{1}{3} & 0 & 1 & -\frac{2}{3} \\ 0 & 0 & 0 & 0 & 0 \\ 0 & 0 & 0 & 0 & 0 \end{pmatrix},$$

$$f_{0,3} = \begin{pmatrix} 0 & 0 & -\frac{1}{2} & 0 & 0 \\ 0 & 0 & 1 & 0 & 0 \\ 0 & 0 & -\frac{1}{2} & 0 & 0 \\ 0 & 0 & 0 & 0 & 0 \\ 0 & 0 & 0 & 0 & 0 \end{pmatrix}, \quad f_{0,4} = \begin{pmatrix} 0 & -\frac{1}{3} & 0 & 0 & -\frac{1}{6} \\ 0 & 0 & 1 & 0 & 0 \\ 0 & -\frac{1}{3} & 0 & 0 & -\frac{1}{6} \\ 0 & 0 & 0 & 0 & 0 \\ 0 & 0 & 0 & 0 & 0 \end{pmatrix}, \quad f_{0,5} = \begin{pmatrix} 0 & -\frac{1}{6} & 0 & 0 & -\frac{1}{3} \\ 0 & 0 & 0 & 1 & 0 \\ 0 & -\frac{1}{6} & 0 & 0 & -\frac{1}{3} \\ 0 & 0 & 0 & 0 & 0 \\ 0 & 0 & 0 & 0 & 0 \end{pmatrix},$$

and the synthesis filters are

$$g_{0,0} = \begin{pmatrix} \frac{1}{6} & \frac{1}{3} & \frac{1}{2} & \frac{1}{3} & \frac{1}{6} \\ \frac{1}{3} & \frac{2}{3} & \mathbf{1} & \frac{2}{3} & \frac{1}{3} \\ \frac{1}{6} & \frac{1}{3} & \frac{1}{2} & \frac{1}{3} & \frac{1}{6} \end{pmatrix}, \quad g_{0,1} = \begin{pmatrix} 0 & 0 & 0 & 0 & 0 \\ 0 & 1 & \mathbf{0} & 0 & 0 \\ 0 & 0 & 0 & 0 & 0 \end{pmatrix}, \quad g_{0,2} = \begin{pmatrix} 0 & 0 & 0 & 0 & 0 \\ 1 & 0 & \mathbf{0} & 0 & 0 \\ 0 & 0 & 0 & 0 & 0 \end{pmatrix},$$

$$g_{0,3} = \begin{pmatrix} 0 & 0 & 0 & 0 & 0 \\ 0 & 0 & \mathbf{0} & 0 & 0 \\ 0 & 0 & 1 & 0 & 0 \end{pmatrix}, \quad g_{0,4} = \begin{pmatrix} 0 & 0 & 0 & 0 & 0 \\ 0 & 0 & \mathbf{0} & 0 & 0 \\ 0 & 1 & 0 & 0 & 0 \end{pmatrix}, \quad g_{0,5} = \begin{pmatrix} 0 & 0 & 0 & 0 & 0 \\ 0 & 0 & \mathbf{0} & 0 & 0 \\ 1 & 0 & 0 & 0 & 0 \end{pmatrix},$$

where we highlight the $(0,0)$ element in bold. In the same way the analysis and synthesis filters for the matrix M_1 are

$$f_{1,0} = \begin{pmatrix} 0 & 0 & 0 & 0 & 0 \\ 0 & 0 & \mathbf{1} & 0 & 0 \\ 0 & 0 & 0 & 0 & 0 \end{pmatrix}, \qquad\qquad f_{1,1} = \begin{pmatrix} 0 & 0 & 0 & 0 & 0 & 0 \\ 0 & -\frac{2}{3} & \mathbf{1} & 0 & -\frac{1}{3} & 0 \\ 0 & 0 & 0 & 0 & 0 & 0 \end{pmatrix},$$

$$f_{1,2} = \begin{pmatrix} 0 & 0 & 0 & 0 & 0 \\ 0 & -\frac{1}{3} & \mathbf{0} & 1 & -\frac{2}{3} \\ 0 & 0 & 0 & 0 & 0 \end{pmatrix}, \qquad\qquad f_{1,3} = \begin{pmatrix} -\frac{1}{2} & 0 & 0 & 0 & 0 & 0 & 0 \\ 0 & 0 & 0 & \mathbf{1} & 0 & 0 & 0 \\ 0 & 0 & 0 & 0 & 0 & 0 & -\frac{1}{2} \end{pmatrix},$$

$$f_{1,4} = \begin{pmatrix} -\frac{1}{3} & 0 & 0 & -\frac{1}{6} & 0 & 0 & 0 & 0 & 0 & 0 \\ 0 & 0 & 0 & 0 & \mathbf{1} & 0 & 0 & 0 & 0 & 0 \\ 0 & 0 & 0 & 0 & 0 & 0 & -\frac{1}{3} & 0 & 0 & -\frac{1}{6} \end{pmatrix}, \quad f_{1,5} = \begin{pmatrix} -\frac{1}{6} & 0 & 0 & -\frac{1}{3} & 0 & 0 & 0 & 0 & 0 & 0 \\ 0 & 0 & 0 & 0 & 0 & \mathbf{1} & 0 & 0 & 0 & 0 \\ 0 & 0 & 0 & 0 & 0 & 0 & -\frac{1}{6} & 0 & 0 & -\frac{1}{3} \end{pmatrix}$$

$$g_{1,0} = \begin{pmatrix} \frac{1}{6} & \frac{1}{3} & \frac{1}{2} & \frac{1}{3} & \frac{1}{6} & 0 & 0 & 0 & 0 & 0 & 0 \\ 0 & 0 & 0 & \frac{1}{3} & \frac{2}{3} & \mathbf{1} & \frac{2}{3} & \frac{1}{3} & 0 & 0 & 0 \\ 0 & 0 & 0 & 0 & 0 & 0 & \frac{1}{6} & \frac{1}{3} & \frac{1}{2} & \frac{1}{3} & \frac{1}{6} \end{pmatrix}, \quad g_{1,1} = \begin{pmatrix} 0 & 0 & 0 & 0 & 0 \\ 0 & 1 & \mathbf{0} & 0 & 0 \\ 0 & 0 & 0 & 0 & 0 \end{pmatrix},$$

$$g_{1,2} = \begin{pmatrix} 0 & 0 & 0 & 0 & 0 \\ 1 & 0 & \mathbf{0} & 0 & 0 \\ 0 & 0 & 0 & 0 & 0 \end{pmatrix}, \qquad\qquad g_{1,3} = \begin{pmatrix} 0 & 0 & 0 & 0 & 0 \\ 0 & \mathbf{0} & 0 & 0 & 0 \\ 0 & 0 & 0 & 0 & 1 \end{pmatrix},$$

$$g_{1,4} = \begin{pmatrix} 0 & 0 & 0 & 0 & 0 \\ 0 & 0 & \mathbf{0} & 0 & 0 \\ 0 & 0 & 0 & 0 & 1 \end{pmatrix}, \qquad\qquad g_{1,5} = \begin{pmatrix} 0 & 0 & 0 & 0 & 0 \\ 0 & 0 & \mathbf{0} & 0 & 0 \\ 0 & 0 & 0 & 1 & 0 \end{pmatrix}.$$
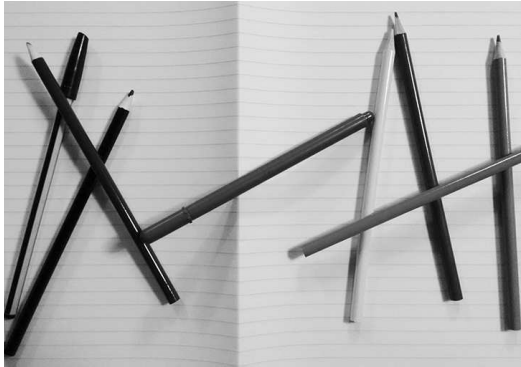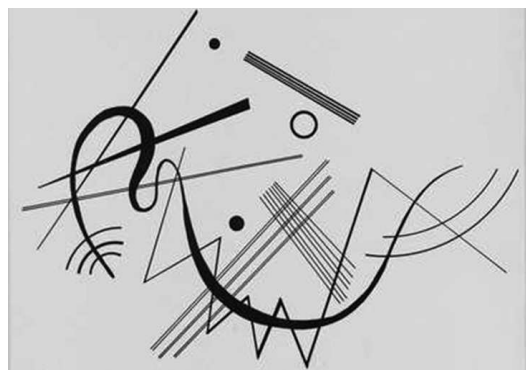
(a) Pencils

(b) Expo

(c) Boots

(d) Leaf

(e) Lighthouse

(f) Kandinsky

Figure 7.4. Test images of sizes 729×512 pixels except (e) Lighthouse of size 512×512 pixels.
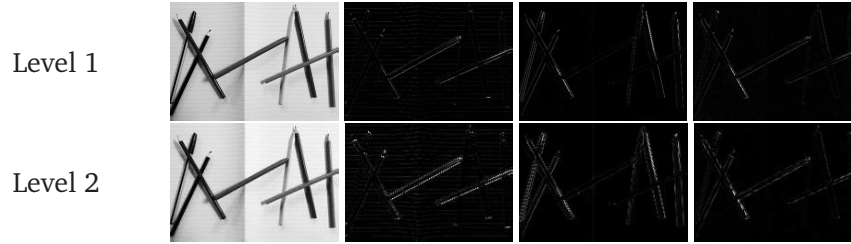
Figure 7.5. Two level decomposition of the image in Figure 7.4a using Daubechies wavelets of order 2. In each row, from left to right, the 4 images are the approximation coefficients and the details coefficients along the horizontal, vertical and diagonal direction.

To show the potential of the directional transform defined by the matrices M_i, $i \in \mathbb{Z}_2$ in (7.41), we use these filters to analyse and synthesize some test images represented in Figure 7.4.

For comparison, with the same construction we compute the filterbanks of the shearlet scaling matrices

$$M_0^{[S]} = \begin{pmatrix} 4 & 0 \\ 0 & 2 \end{pmatrix}, \qquad M_1^{[S]} = \begin{pmatrix} 4 & -4 \\ 0 & 2 \end{pmatrix}. \tag{7.45}$$

With the computed filters we implement a full decomposition process for all the branches of the tree and a reconstruction process following a single branch or averaging all the branches of the tree, as explained in Section 6.3. The implementation is not trivial because the shear matrices have some intrinsic problems. Applying a shear transformation on an image we obtain a pseudo rotated image that cannot be stored in a rectangular matrix. We decide to embed the pseudo rotated image in a larger matrix with zero entries even if this increases the storage space. As first implementation of a directional transform using the MMRA setting, we focus on the comparison of the analysed signal with the new matrices in (7.41) and the well-known transforms. In the following we consider some examples of the decomposition and compression process. Moreover, we study the reconstructed details in order to see if the new matrices can be used for an edge detection tool.

7.4.1 Decomposition

The first stage of any application with images is the decomposition process where we convolve the image with the analysis filters f_ξ, $\xi \in E_M$, and we downsample it. The low-pass filter f_0 gives the approximation coefficients c^1 while the high-pass filters f_ξ, $\xi \in E_M^0$, generate the so-called detail coefficients d_ξ^1. The process can be repeated starting from the approximation coefficients c^1. The decomposition process with wavelets is shown in Figure 7.5.

In the MMRA setting, at each step of the decomposition process we choose a matrix M_i from the set, with $i \in \mathbb{Z}_2$. After two decomposition steps we have 4 different ways to
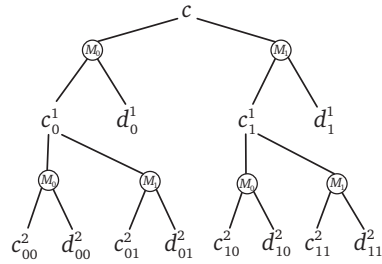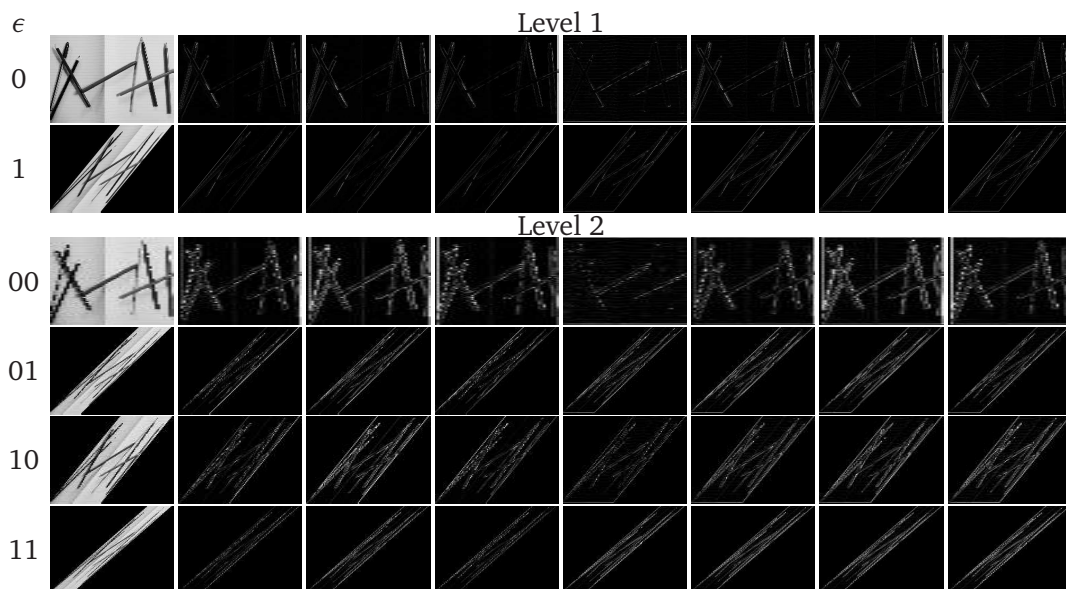
Figure 7.6. Multiple decomposition tree up to level 2.

Figure 7.7. Two level decomposition of the image in Figure 7.4a with shearlets. The eight images in each row are the approximation coefficients c_ϵ^2 and detail coefficients $d_{\epsilon,k}^2$ with $\epsilon \in \mathbb{Z}_2$ and $k = 1,\ldots,7$. Each row represents a branch of the tree in Figure 7.6.
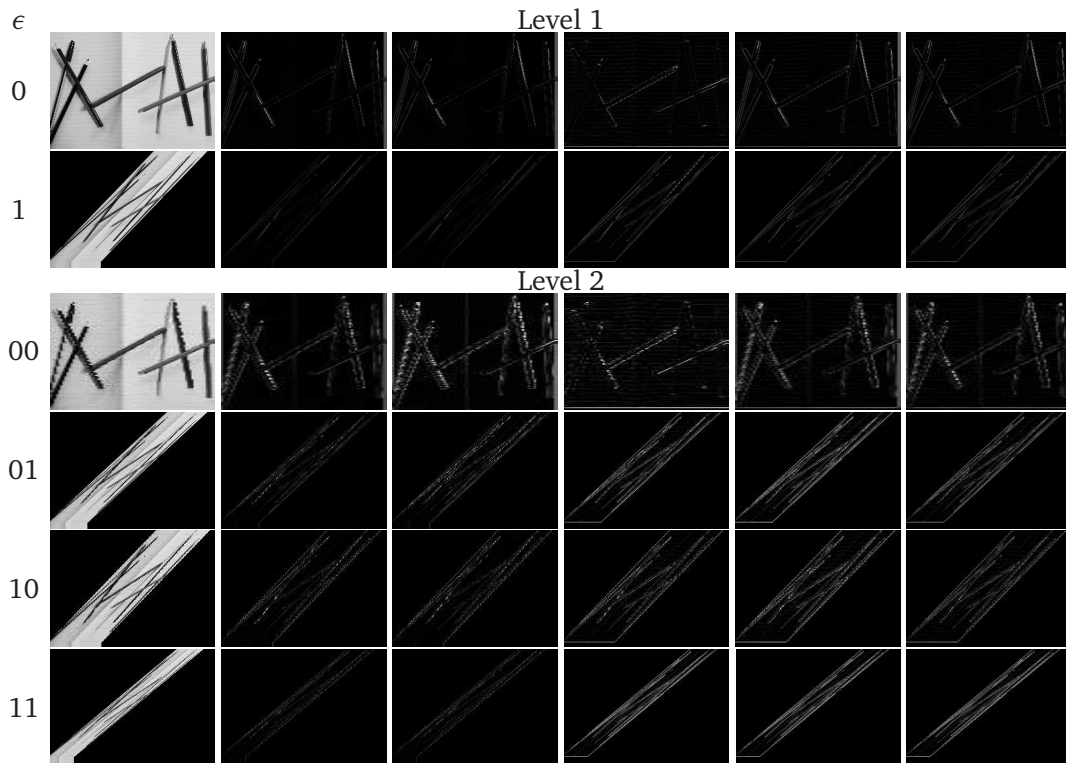
Figure 7.8. Two level decomposition of the image in Figure 7.4a with respect to the family of matrices in (7.41). The six images in each row are the approximation coefficients c_ϵ^2 and detail coefficients $d_{\epsilon,k}^2$ with $\epsilon \in \mathbb{Z}_2$ and $k = 1,\dots,5$. Each row represents a branch of the tree in Figure 7.6.

decompose an image, as depicted by the tree in Figure 7.6. Applying this decomposition process to Figure 7.4a with the shearlet matrices (7.45) and the new matrices (7.41), we obtain the approximation and detail coefficients displayed respectively in Figures 7.7 and 7.8. The decomposition with the matrices that contain the shear, $M_1^{[S]}$ and M_1, produces a pseudo rotated image. The more often we apply $M_1^{[S]}$ or M_1, the more the resulting image is pseudo rotated and stretched, as shown in the last row of Figures 7.7 and 7.8. The decomposition with the new matrices M_i is similar to the decomposition by the shearlet matrices $M_i^{[s]}$, but the main difference is the number of detail coefficients (5 vs 7). In this sense the new matrices produce less computational effort and they require less storage space. In addition, the smaller determinant of the matrices $\{M_i\}_{i \in \mathbb{Z}_2}$ in (7.41) gives detail and approximation coefficients that are less stretched with respect to shearlets.

We observe that the decomposition process in the wavelet and shear-like setting are completely different. For wavelets, each detail coefficient detects features only along the horizontal, vertical and diagonal directions, see Figure 7.5. Instead, for the new matrices, the detail directions ξ_k combine with the pseudo rotation of the image and allow to detect different directions for each branch of the tree. The new matrices can be exploited in the edge detection problem thanks to this capability of considering different directions. In Figures 7.7 and 7.8 it is not easy to see which directions are covered because the details are quite stretched. In the following sections we reconstruct the details and we study which directions are detected by the different branches.

7.4.2 Compression

The perfect reconstruction filterbanks guarantee that if no changes occur in the approximation and detail coefficients, then the initial signal is perfectly reconstructed. However, since the representation produced by the transform is sparse, we can save space by keeping only the largest coefficients. This is the idea of the compression process: produce a good quality approximation of the signal by storing few coefficients.

In order to evaluate the difference between the reconstructed signal from the initial signal we consider some metrics: the peak signal-to-noise ratio ($PSNR$) and the structural similarity index ($SSIM$). The peak signal-to-noise ratio measures the ratio between the maximum value of the signal and the mean square error between the reconstructed and initial signal. Let I be our test image and denote with $\tilde{I}$ the reconstructed image, then the mean square error between these two images is

$$MSE(I, \tilde{I}) = \frac{1}{mn} \sum_{i=1}^{m} \sum_{l=1}^{n} (I(i,l) - \tilde{I}(i,l))^2, \tag{7.46}$$

and the peak signal-to-noise ratio is defined as

$$PSNR(I, \tilde{I}) = 10 \log_{10} \left(\frac{255^2}{MSE(I, \tilde{I})} \right), \tag{7.47}$$

where m, n are the dimensions of the signal I and the maximum value of an image is 255 (cf. [Mallat, 2008; Vetterli and Kovačević, 2007]). If the image is perfectly reconstructed ($\tilde{I} = I$), then the mean square error is 0 and $PSNR$ is ∞. Hence, the higher the value of $PSNR$, the better the reconstructed image. With values of $PSNR$ greater than 30 it is difficult for the human eye to distinguish the differences between the reconstructed and the initial image. The peak signal-to-noise ratio is not always a good indicator for the perceived quality of the reconstructed image. There are other indicators that take care of the characteristics of the human visual system. One of these indicators is the structural similarity index ($SSIM$) introduced by Wang et al. [2004]. The $SSIM$ measures the changes in structural information, luminance and contrast between neighbouring pixels. Let x, y be two parts of the images I and $\tilde{I}$ of size $n \times n$, then the structural similarity index $SSIM$ is defined as

$$SSIM(x, y) = \ell(x, y) c(x, y) s(x, y) = \frac{(2\mu_x \mu_y + k_1)(2\sigma_{xy} + k_2)}{(\mu_x^2 + \mu_y^2 + k_1)(\sigma_x^2 + \sigma_y^2 + k_2)}, \qquad (7.48)$$

where k_1, k_2 are constants needed to stabilize the division, μ is the average of x and y, σ^2 is the variance and σ_{xy} is the covariance defined by

$$\mu_x = \frac{1}{n^2} \sum_{i,j=1}^{n} x(i, j), \qquad \sigma_x = \left(\frac{1}{n^2 - 1} \sum_{i,j=1}^{n} (x(i, j) - \mu_x) \right)^{\frac{1}{2}},$$

$$\sigma_{xy} = \frac{1}{n^2 - 1} \sum_{i,j=1}^{n} (x(i, j) - \mu_x)(y(i, j) - \mu_y).$$

The functions $\ell(x, y)$, $c(x, y)$, $s(x, y)$ measure respectively the luminance, the contrast and the structure,

$$\ell(x, y) = \frac{2\mu_x \mu_y + k_1}{\mu_x^2 + \mu_y^2 + k_1}, \quad c(x, y) = \frac{2\sigma_x \sigma_y + k_2}{\sigma_x^2 + \sigma_y^2 + k_2}, \quad s(x, y) = \frac{2\sigma_{xy} + k_2}{2\sigma_x \sigma_y + k_2}.$$

The values of $SSIM$ vary in $[-1, 1]$ and if the images I and $\tilde{I}$ are the same we get $SSIM = 1$.

The idea behind an (M)MRA is to express a signal in a sparse way. The key features of the signal and the singularities correspond to the largest coefficients in the decomposition process. So the compression process saves only the biggest coefficients in the approximation and detail coefficients. The choice of which coefficients to save and which ones to set to zero can be made in two different ways: fixing a hard threshold or a compression rate. In both cases the approximation coefficients are kept and we apply the compression only to the detail coefficients. The hard threshold saves all the detail coefficients greater than $thr \geq 0$ and sets the other coefficients to zero. Instead, fixing a compression rate of $CR : 1$ means that we save one coefficient out of CR detail coefficients. That is, we store a fixed percentage of the initial coefficients. Let n be the total

amount of coefficients and n_d, n_a be respectively the number of detail and approximation coefficients such that $n = n_d + n_a$. With a compression rate $CR : 1$, the number of coefficients saved is $n' = n/CR$. In particular we save the $n'_d = n/CR - n_a$ largest detail coefficients.

Considering more levels of decomposition, the coefficients become smaller in absolute value. When we compress the details we have to be careful. Otherwise we throw away all the details of the highest levels. To avoid this, we reintroduce the scaling factor $|\det M|^{(j/2)}$ that is present in the definition of the shearlet system, see e.g. (6.7). With this scaling factor the coefficients are well distributed and we can decide which coefficients to keep and which to throw away.

A summary of the whole process is given by:

1. Decomposition,

2. Compression with a hard threshold thr or a compression rate $CR : 1$, we keep the largest detail coefficients after we multiply them by the scaling factor $|\det M|^{j/2}$,

3. Reconstruction by following a single branch of the tree or averaging all branches.

Fixing a threshold value of 150, in Figure 7.9 we show the reconstructed images using the new matrices in (7.41) and the shearlet matrices in (7.45). We observe that the behaviour of the new matrices is similar to shearlets. In fact in both cases, the reconstructed images along the branch $\epsilon = (1, 1, 1, 1)$ present some artefacts near the edges of the figure. These artefacts are less visible in the reconstructed images that take care of all the branches, because the artefacts are generated by several applications of the matrix M_1. In Figures 7.7 and 7.8 we see that repeated application of M_1 stretches the image. So, if we introduce some computational error or we eliminate a detail coefficient, then the reconstruction amplifies this error and produces these flaws. To compare the reconstruction with the new matrices and shearlets we compare the values of *PSNR* and *SSIM*, see Fig. 7.10. Both the *PSNR* and *SSIM* values confirm that the reconstruction averaging all the branches of the tree is better than following a single branch. Moreover, the values of *PSNR* and *SSIM* show that the reconstruction with shearlets is better than the reconstruction with the new matrices in this case. In fact, in Figure 7.9 the reconstructed images with shearlets are more delineated with respect to the reconstructed images with the new matrices.

We repeat the comparison between the new matrices in (7.41) and shearlets where we fix a compression rate of 8 : 1. Figure 7.11 shows the reconstructed images using both families of matrices and following a branch of the tree, $\epsilon = (1, 1, 1, 1)$, or taking the average of all the branches. As before, the compression generates some flaws and the reconstruction averaging all the branches performs better than considering a single branch. Differently from the previous example, in this case the reconstructed images using the new matrices give higher values of *PSNR* and *SSIM* than shearlets, see Figure 7.12. From Figure 7.11 we see that the reconstructed images with the new matrices are more delineated with respect to the reconstructed images with shearlets.
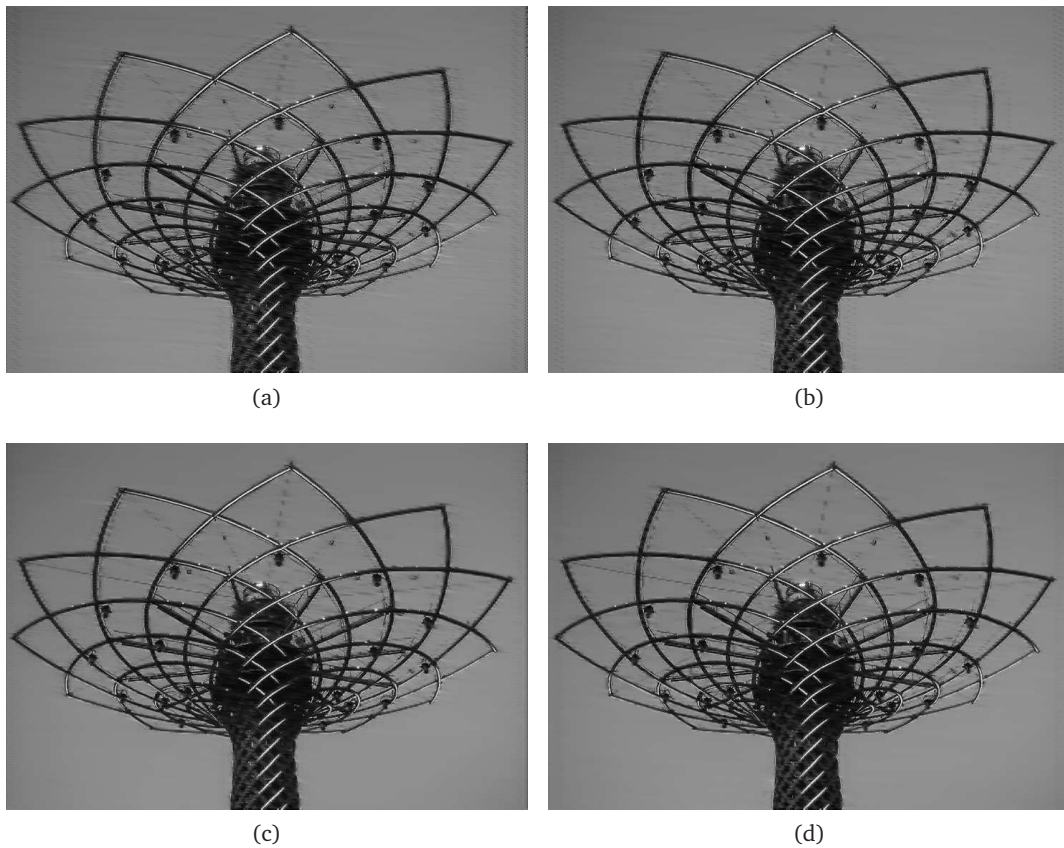
(a)   (b)

(c)   (d)

Figure 7.9. Compression with a hard threshold $thr = 150$ of Figure 7.4b. The images are re-constructed following the branch $\epsilon = (1,1,1,1)$ (top) or all branches together (bottom). In the whole process we use the new matrices (7.41) (left) and the shearlet matrices (7.45) (right).
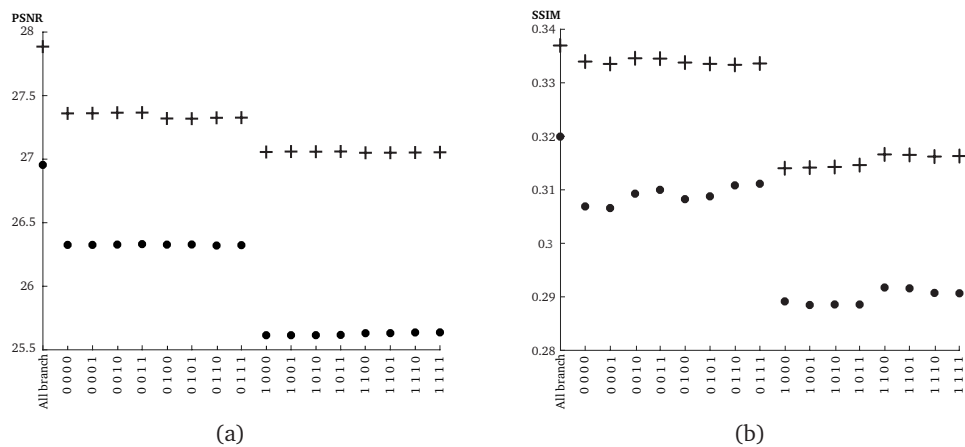

(a)   (b)

Figure 7.10. Values of $PSNR$ (left) and $SSIM$ (right) for the reconstructed images after a compression with threshold $thr = 150$ using the new matrices (7.41) (dot) or shearlets (cross).
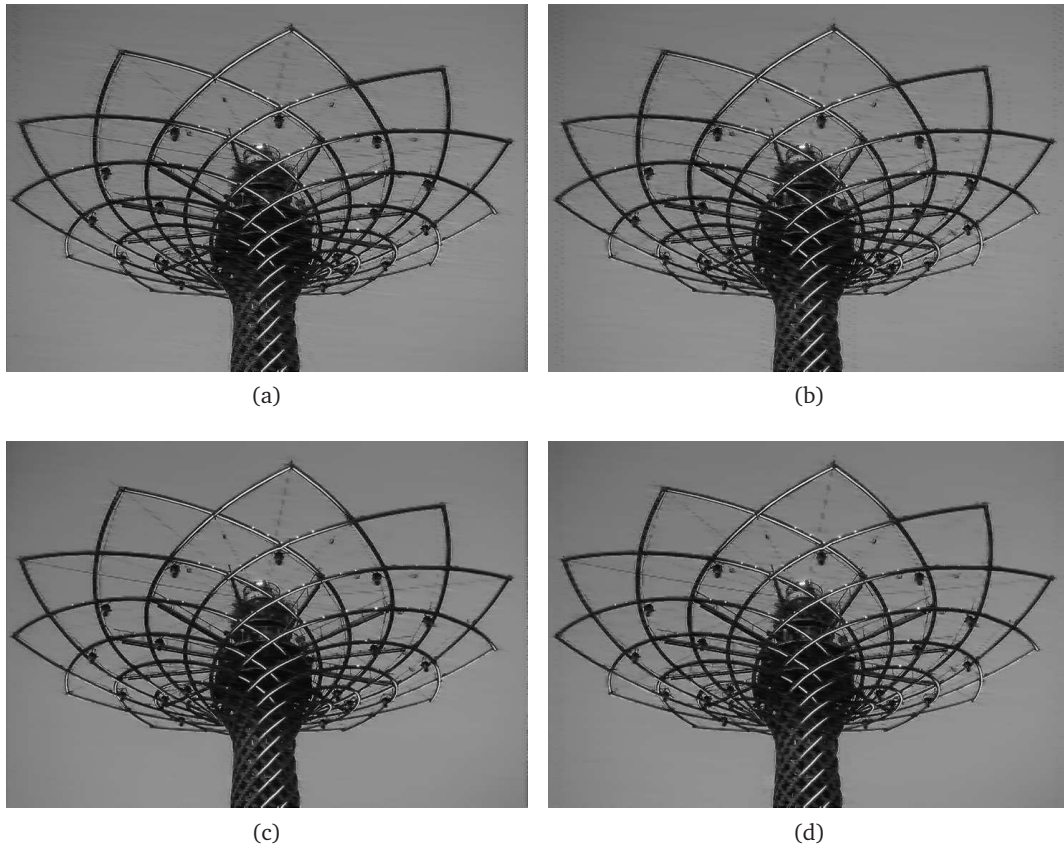
(a)   (b)

(c)   (d)

Figure 7.11. Compression of Figure 7.4b with compression rate $8:1$. The images are reconstructed following the branch $\epsilon = (1,1,1,1)$ (top) or all branches together (bottom). In the whole process we use the new matrices (7.41) (left) and the shearlet matrices (7.45) (right).
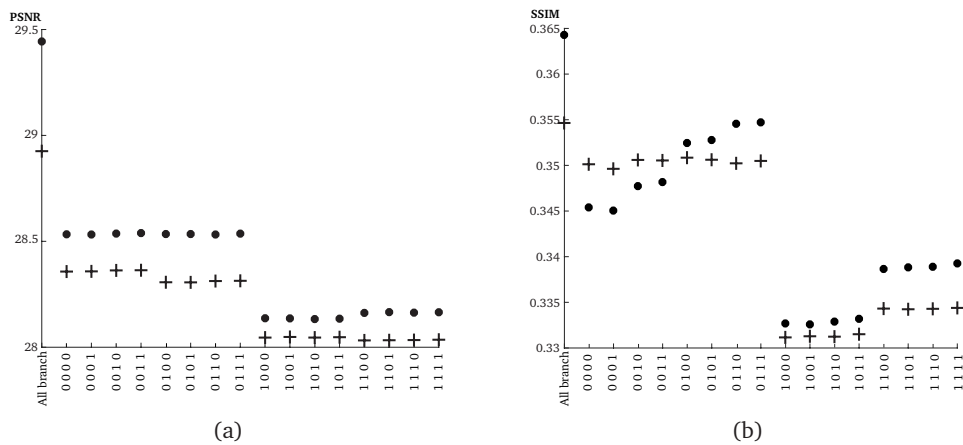

(a)   (b)

Figure 7.12. Values of *PSNR* (left) and *SSIM* (right) for the reconstructed images after compression with rate $8:1$ using the new matrices (7.41) (dot) or shearlets (cross).

An interesting test is to study the quality of the reconstructed images for increasing values of thresholds and compression rates. Figure 7.13 shows the reconstructed images using all the branches of the tree and the new matrices, after we compress with increasing values of threshold. For $thr = 0$ the resulting image is equal to Figure 7.4a, in fact the *PSNR* is high and *SSIM* is equal to 1 (see Fig. 7.14). Increasing the value of the threshold we loose from small to essential details of the image: for $thr = 50$ the lines on the white sheet are not well reproduced; for $thr = 100$ the contours of the pencils are not smooth and for $thr = 200$ all the edges are not well defined. For increasing values of threshold the quality of the image decreases and with it also the *PSNR* and the *SSIM* values. We see in Figure 7.14 that for values of $thr > 0$ the *PSNR* decreases slowly. In this sense the *SSIM* index can represent better the quality of the reconstructed image. Figure 7.15a shows the distribution of the details coefficients with respect to their values. With red stars we depict the increasing values of threshold. Most of the detail coefficients are around 0, so introducing a threshold $thr >> 0$ we save only few coefficients. Figure 7.14a shows the percentage of non zero coefficients saved by each value of threshold.

We expect the same behaviour if we consider increasing values of compression rate, see Figure 7.16. Eliminating half of the coefficients seems not to affect the quality of the image, indeed the value of *PSNR* and *SSIM* are quite high (see Fig. 7.17). As for increasing values of threshold also by increasing the compression rate the reconstructed images get worse, loosing an increasing number of details. In Figure 7.16 with compression rate 4 : 1 the quality of the image is good but we loose some wood grain. At compression rate 8 : 1, small details are cancelled but the main edges are still visible in Figure 7.4c while a lot of edges are not defined at compression rate 12 : 1. This decline in the quality of the reconstructed images is measured by *PSNR* and *SSIM* in Figure 7.17. Figure 7.15b shows that the distribution of the detail coefficients depends on the image considered, thus the compression rate and the threshold to obtain a good reconstructed image depend on the initial image considered. As expected, with the new matrices we can have a good approximation of the initial image storing few coefficients because the features of the signal are given by largest detail coefficients. This is effective to save storage space.

7.4.3   Detail reconstruction

Shearlets are suitable for dealing with anisotropic signals and give some geometric information, like position and orientation, about the discontinuities. In this sense we say that they are able to catch edges and singularities along curves. As for wavelet also for shearlets, near a discontinuity the transform coefficients decay slowly. The velocity of this decay is given in [Guo and Labate, 2009, 2017] in the case of a continuous shearlet system (6.7). So the idea is to use the maxima of the shearlet transform to detect discontinuities and to exploit the scale, orientation and location parameters to give more information about this discontinuity (cf. [Yi et al., 2009]).

For the proposed matrices we do not have the exact decay rate of the coefficients around a discontinuity but we can visualise if the largest coefficients detect the edges of

(a) $thr = 0$ (b) $thr = 50$

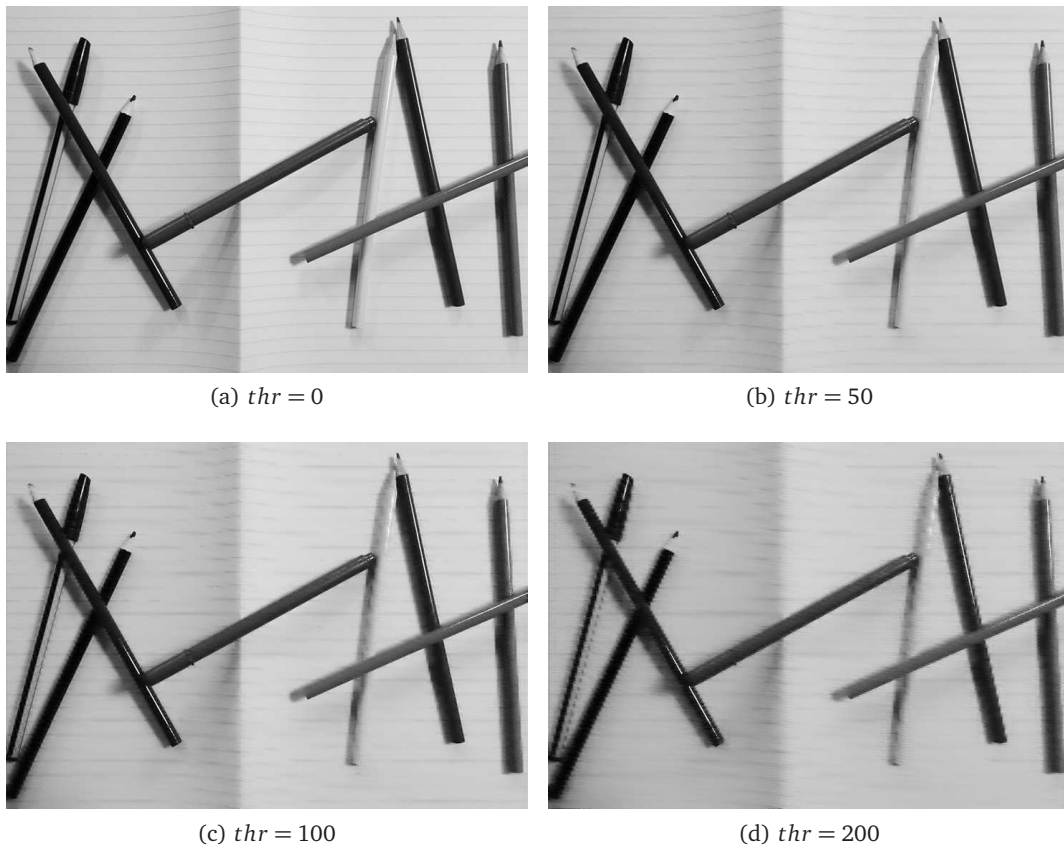(c) $thr = 100$ (d) $thr = 200$

Figure 7.13. Compressed images applying increasing values of threshold $thr = 0, 50, 100, 200$. In order to reconstruct the images we exploit all the coefficients of the 3 levels tree and we use the matrices in (7.41).

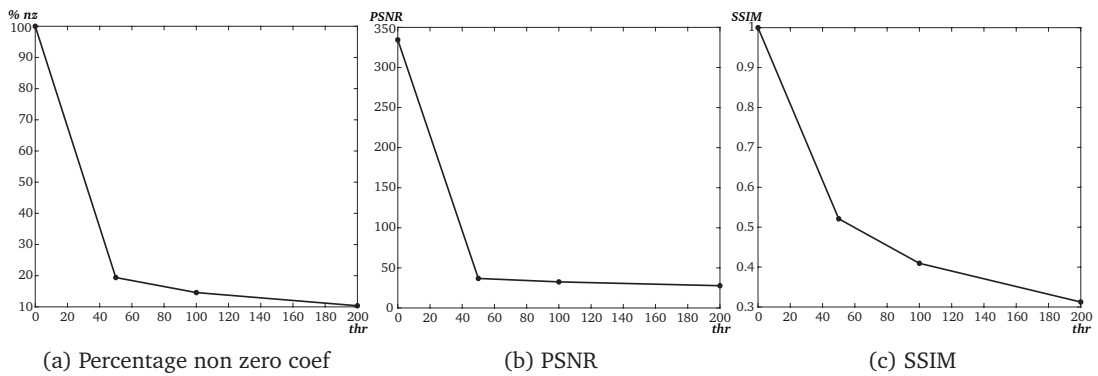(a) Percentage non zero coef   (b) PSNR   (c) SSIM

Figure 7.14. Metrics on compressed images (Fig. 7.13) with new matrices in (7.41) for increasing values of threshold: (a) percentage of non zero coefficients kept after the compression, (b) *PSNR* (7.47), (c) *SSIM* (7.48).
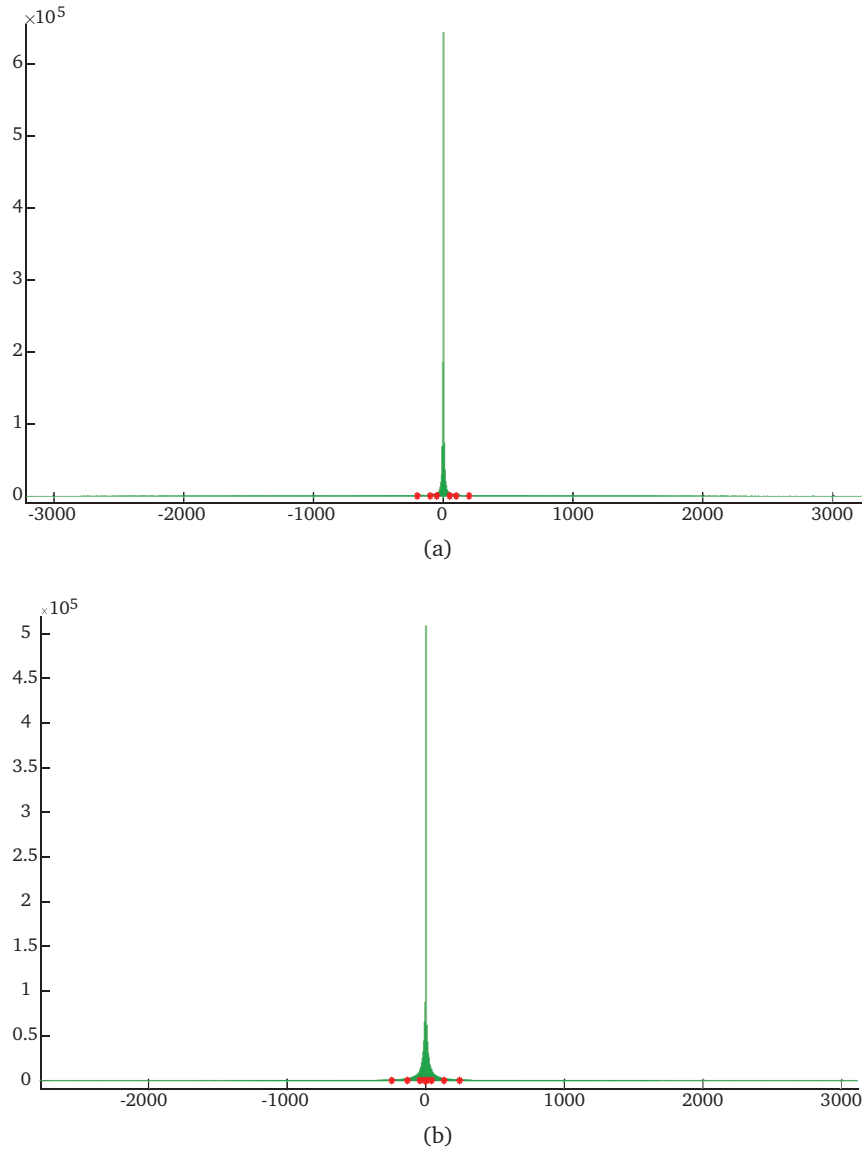
(a)

(b)

Figure 7.15. Histograms of the numbers of detail coefficients with a certain value. The decomposition is done with the matrices in (7.41). (a) Histogram of Figure 7.4a with increasing values of threshold $thr = 50, 100, 200$. (b) Histogram of Figure 7.4c with increasing compression rate CR 2, 4, 8, 12.

(a) $CR\ 2:1$

(b) $CR\ 4:1$

(c) $CR\ 8:1$

(d) $CR\ 12:1$

Figure 7.16. Compressed images of Figure 7.4c applying increasing compression rates $CR = 2, 4, 8, 12$. In order to reconstruct the images we exploit all the coefficients of the 3 levels tree and we use the new matrices in (7.41).
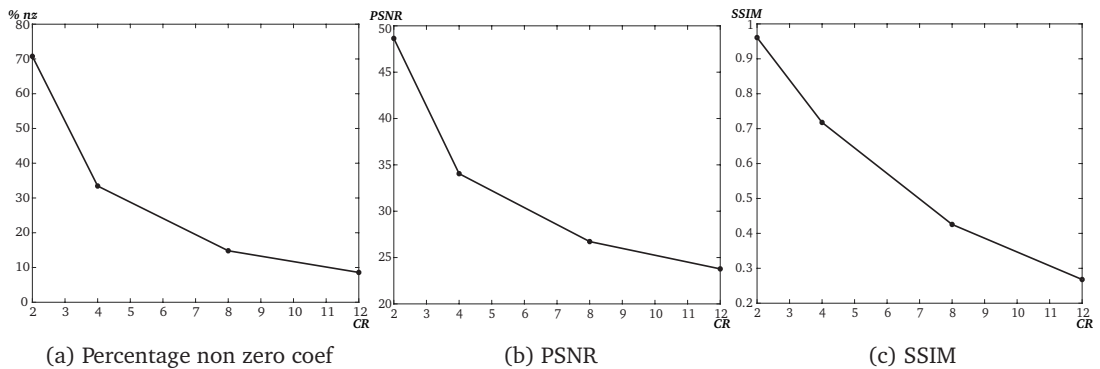

(a) Percentage non zero coef

(b) PSNR

(c) SSIM

Figure 7.17. Metrics on compressed images (Fig. 7.16) with new matrices in (7.41) for increasing compression rates: (a) percentage of non zero coefficients kept after the compression, (b) *PSNR* (7.47), (c) *SSIM* (7.48).

<div align="center">(a)   (b)</div>
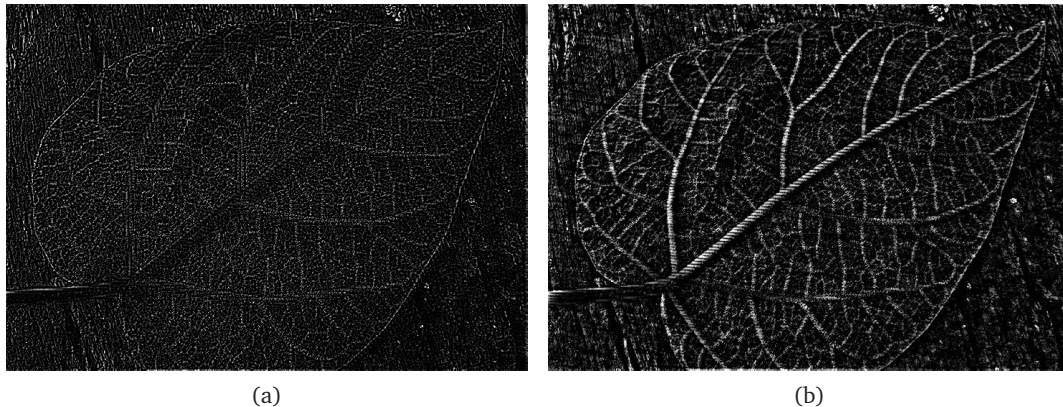
Figure 7.18. Reconstructed details after two levels of decomposition with wavelets (left) and with the new matrices in (7.41) (right). In our case we reconstruct by exploiting all branches of the tree.

the image. So we look at the maxima in the detail coefficients at different scaling levels and different branches. The index ϵ of the branch gives information about the direction of the discontinuity. Since the detail coefficients can be stretched and elongated, it is difficult to visualize the maxima of the details from Figures 7.7 and 7.8. Therefore, the idea is to reconstruct the detail after putting to zero the approximation coefficients. In this way we visualize the contribution of the details in the reconstruction process and we check if the largest detail coefficients correspond to the discontinuities of the initial image. The process can be summed up in three steps:

1. Decomposition,

2. Setting to zero the approximation coefficients,

3. Reconstruction by following a single branch of the tree or averaging all branches.

The resulting images give us the perception if the directional transform is able to detect all the discontinuities and to distinguish between small changes in gray scale and big jumps between two areas with flat color. This gives us the insight if the new matrices in (7.41) are able to detect edges or not.

Figure 7.18 compares the reconstructed details for Figure 7.4d considering the wavelet transform and the new matrices in (7.41). In the reconstruction process with the new matrices we average all the branches of the tree in order to consider all the elements detected by the different branches. The new matrices highlight better the discontinuities, the wood grains and the veins in the leaf, with respect to the wavelet case where the direction of some edges is not clearly visible. This confirms our expectation: anisotropic matrices identify discontinuities along some directions better than isotropic matrices. Moreover, the new matrices seem to distinguish between big jumps (big veins in the

leaf) represented by light color and small jumps (wood grains) represented by darker gray.

We repeat the test to compare the behaviour of the new matrices in (7.41) with respect to shearlets. Figure 7.19 shows the reconstructed details with the new matrices and shearlets considering each branch separately. We observe that the different branches detect different features and they work along different directions. The reconstruction of a single coefficient influences also neighbouring pixels with an interval of influence that depends on the support size of the filters. This creates the flaws that are visible in Figure 7.19 and also in the previous Figures 7.9 and 7.11. The flaws show clearly along which directions we are working. Even if we consider the same branch of the tree, the new matrices (7.41) and the shearlet matrices (7.45) work along different directions, because we consider a different set of matrices. The details reconstructed by averaging all branches are similar to the new matrices and shearlets, see Figure 7.20. The difference is that the flaws generated by shearlets are more elongated, because the determinants of the matrices are higher then the determinants of the new matrices. So, the details reconstructed with the new matrices (7.41) perturb a smaller region than the details reconstructed with shearlets. For this reason the new matrices localize better the discontinuity with respect to shearlets. Moreover, the reconstructed details with shearlets exhibit some black holes along the edges. This means that a part of the edge is not detected. The new matrices produce less holes, meaning that the edge is detected almost completely. In this example the new matrices offer a better edge detection than shearlets.

An effective edge detection is given by Canny's algorithm, presented in [Canny, 1986]. This procedure convolves the signal with a Gaussian, computes the gradient, and the maxima of the gradient correspond to edges. In order to not detect small changes and to attach together different edges, the maxima are selected with a threshold and also relative maxima are kept if they are close to global maxima. At the end, we obtain a logical image where we have 1 in correspondence to an edge and 0 elsewhere. Mallat and Zhong [1992] state that looking at the maxima of the gradient is equivalent to looking at the maxima in the wavelet transform. This observation endorses Yi et al. [2009] to look at maxima of the shearlet transform to detect edges. We do the same with the new matrices in (7.41).

In Figures 7.21 and 7.22 we analyse Figures 7.4e and 7.4f with Canny's edge detection and we reconstruct the detail coefficients with the new matrices in (7.41). The resulting images are completely different, because for Canny's algorithm we obtain a logical image, while in our case we have a grayscale image. In this case we cannot compare the quality of the images but we study if the new matrices detect all the edges recognized by Canny's algorithm. In particular, Figures 7.21 and 7.22 show two drawbacks of Canny's edge detection: closed edges and noise. In Figure 7.21 Canny's algorithm is not able to recognize a part of the fence because it is too dense while it recognizes edges in the grass. For the same image, the reconstructed details with the new matrices

(a) $\epsilon = (0,0)$ (b)

(c) $\epsilon = (0,1)$ (d)

(e) $\epsilon = (1,0)$ (f)

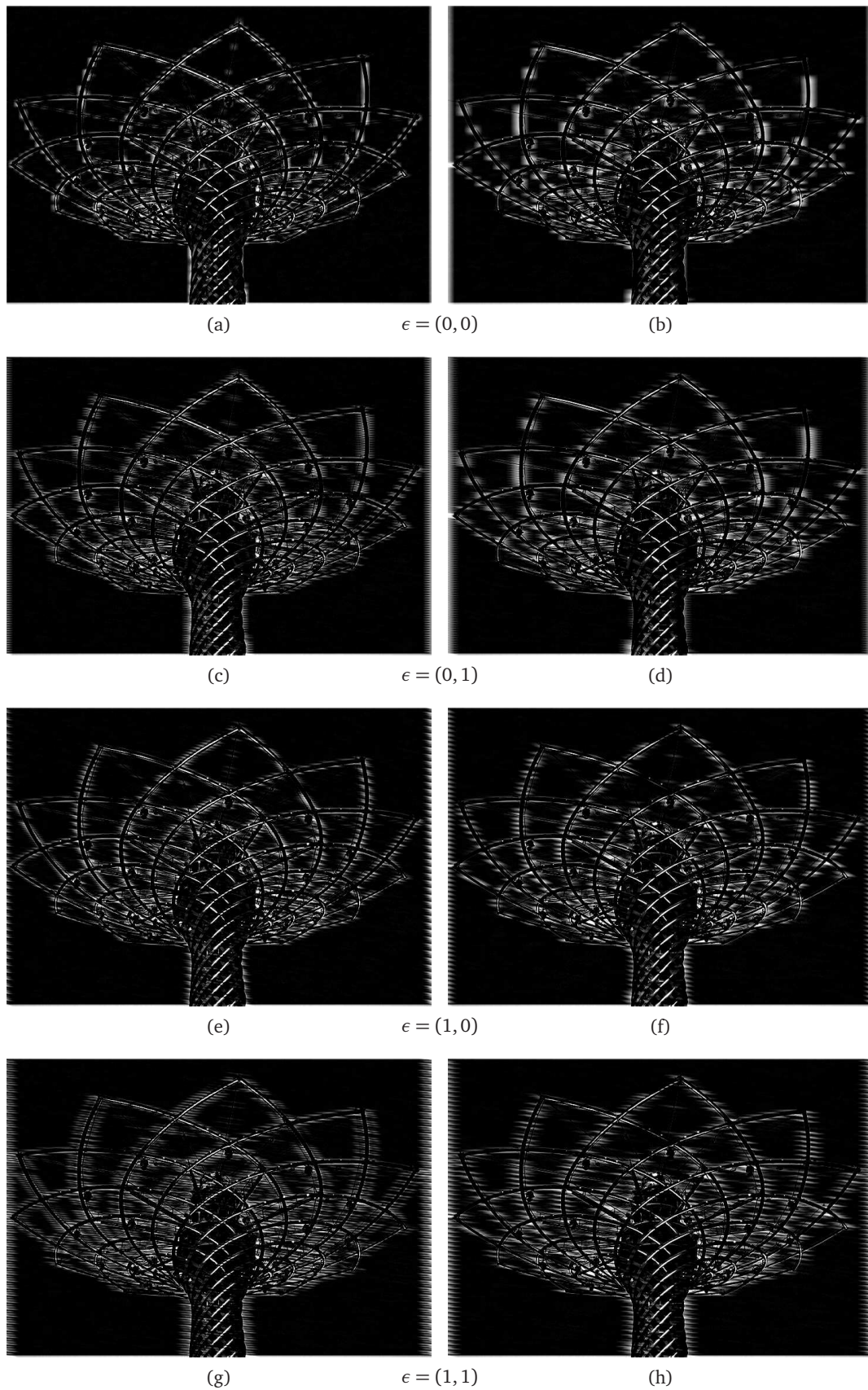(g) $\epsilon = (1,1)$ (h)

Figure 7.19. Comparison between reconstructed details with the new matrices (7.41) (left) and shearlets (7.45) (right) after two levels of decomposition of Figure 7.4b. Each row gives the reconstruction along a single branch of the tree (Fig. 7.6).

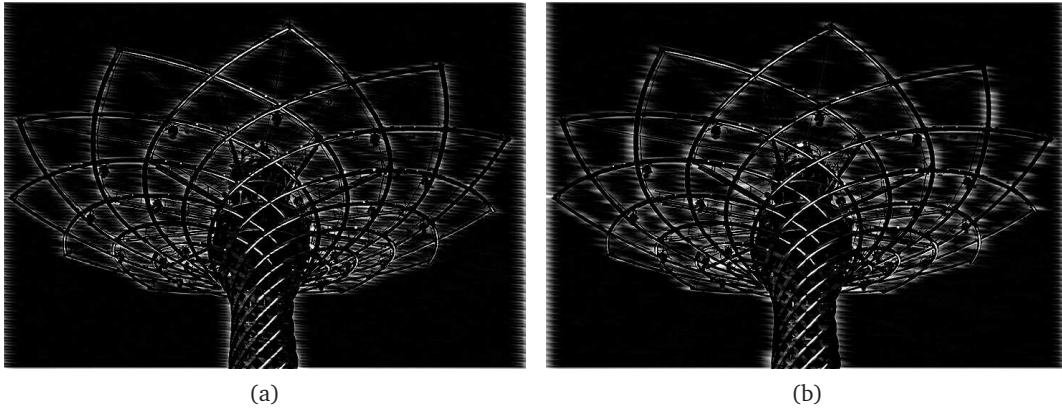<div align="center">(a)   (b)</div>

Figure 7.20. Comparison between reconstructed details with the new matrices (7.41) (left) and shearlets (7.45) (right) after two levels of decomposition of Figure 7.4b. We reconstruct by averaging all branches of the tree (Fig. 7.6).
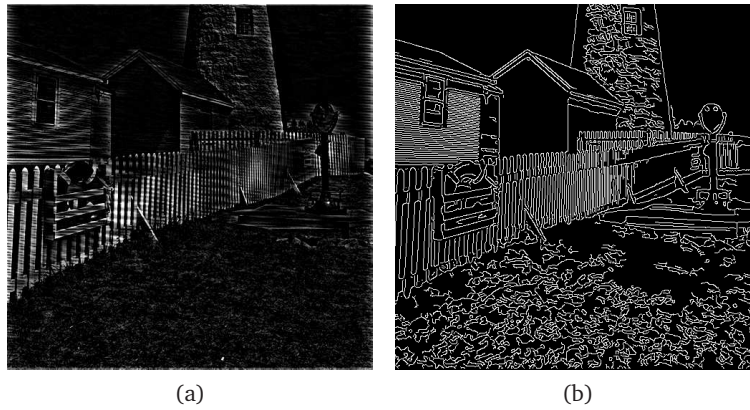

<div align="center">(a)   (b)</div>

Figure 7.21. Comparison between the reconstructed details with the new matrices (7.41) (left) and Canny's edge detection of Figure 7.4e.

(a)   (b)
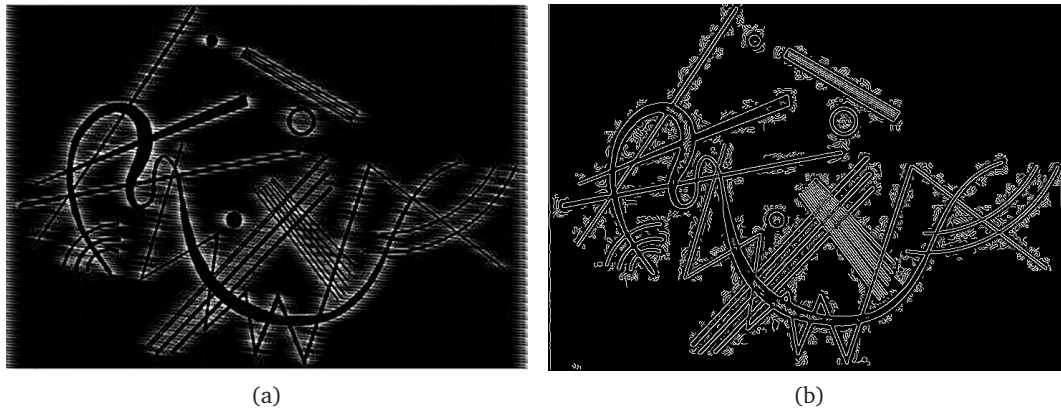
Figure 7.22. Comparison between the reconstructed details with the new matrices (7.41) (left) and Canny's edge detection of Figure 7.4f.

detect the fence even when the boards are very close and in the grass they detect only small discontinuities. Another drawback of Canny's algorithm is shown in Figure 7.22. Figure 7.4f is not of high quality and presents some blur near the edges of the image. Canny's edge detection recognizes these blurs as edges. This problem does not effect the reconstructed details with the new matrices even if some flaws are present in the image. Thus, the reconstructed edges with the new matrices are not effected by noise and can also detect closed edges.

We observe that the transform generated by the new matrices in (7.41) detects discontinuities and distinguishes between big and small jumps into the colormap of the initial image. So it could be interesting in the future to implement a true edge detection with these matrices. The algorithm should find the location of the maximal detail coefficients inside the image and take care of the orientation information given by the tree in order to connect the edges in the right way. Moreover, we should mark with different colors the edges in correspondence to big and small jumps.

With these examples we test the directional MMRA generated by the matrices in (7.41) in comparison with wavelets and shearlets. The new transform behaves similar to shearlets but with a smaller number of details for each branch of the tree which corresponds to less storage space to save all the decomposition tree. Moreover, the reconstruction with the new matrices generates smaller flaws in comparison to shearlets. The proposed transform is also promising for the edge detection problem. For the future it will be interesting to also test different types of filters, for example orthogonal filters that could give a better approximation of the initial image.

Conclusions

Subdivision schemes are effective in several areas of data approximation, and are well exploited for their computational efficiency. In this work we analyse two different applications of subdivision schemes, specifically to curve design and image analysis.

In the first part we consider geometric subdivision schemes that can be useful to require some geometric features of the limit curve. We study the regularity of the limit curve, in particular the curvature. Dyn and Hormann [2012] present sufficient conditions for the convergence and G^1 continuity that depend respectively on edges and angles. Precisely, they require that the sequences of maxima of edges and angles are summable. A curve is G^2 continuous if at each point there exists the osculating circle, and if the curvatures of these circles change continuously along the curve. In the subdivision setting we consider the discrete interpolating circles that pass through three neighbouring points and the difference between neighbouring discrete curvatures. We conjecture that the sequence of maxima of these differences has to be summable in order to generate a G^2 continuous limit curve. To verify the correctness of our hypothesis, we use subdivision schemes with different orders of regularity and several control polygons. The proposed condition seems to be correct, because it is satisfied only in those examples where the limit curve is known to be G^2 continuous. Moreover, we introduce a new geometric scheme that is tailored to satisfy the given condition.

We put a lot of effort into proving that the summability of the differences of curvatures is sufficient to obtain a G^2 continuous curve. Most of the proof is done, but it is not complete because we miss one point. The problem is to prove some relations between the curvatures of discrete interpolating circles with common elements: a common edge or the same tangent at a point. This difficulty arises from the non linear nature of the curvature: in fact, the curvature of a discrete interpolating circle is the ratio between an angle and the opposite edge of the inscribed triangle. For these quantities it is rather easy to find relations between neighbouring edges on angles. Considering two triangles with a common edge, we can use the triangle inequality and the sum of interior angles to relate edges and angles of the two triangles. However, what complicates the study is the ratio between these quantities, because to have the convergence of the curvature it is not sufficient to know that the maximum of edges and angles are summable, but we also need that these sequences decay in the same way. We give numerical evidence that the prescribed relations between neighbouring discrete curvatures are satisfied by schemes

175

that generate G^2 limit curves. To prove these relations we probably have to consider all the possible configurations of points, as done in the other parts of the proof.

In the second part of the thesis we exploit a generalization of the subdivision schemes: the multiple subdivision scheme, which allows to choose an expanding matrix and a subdivision scheme from a finite dictionary in each step of the refinement. In image analysis, subdivision schemes define a filterbank in a simple way. In this sense, a multiple subdivision scheme defines filterbanks that can be used in the setting of a directional transform. The key ingredient to define a directional transform is a family of anisotropic expanding matrices that are jointly expanding, and satisfy the slope resolution property. For any dimension d, we present a set of shear-like matrices which are product of an anisotropic diagonal matrix and a shear, and we prove that these matrices satisfy all the required properties. The advantage of these matrices is that they have a smaller determinant than shearlets. This is important, because the determinant of the matrices gives the number of filters, so it is strictly related to the computational efficiency of the process. Furthermore, it is interesting to study which is the minimal determinant of a family of matrices that satisfies all the prescribed properties, when we give up to consider anisotropic diagonal matrices. For $d = 3$ we implement a routine to find a general set of anisotropic matrices with small determinant that are jointly expanding. We find an example of matrices with determinant (det $= 6$) less than the dyadic case (det $2I_3 = 8$) but, for the moment, we do not have the proof of the slope resolution property. In general, to prove the slope resolution property for a family of matrices we have to find a set of contractive maps and their invariant space. Moreover, as for the cone adapted shearlet system or the presented shear-like matrices, we have to be sure that the union of the invariant spaces covers every possible direction. It is complicated to check all these requests with an automatic routine.

For the shear-like matrices in (7.9) we show some applications on images to test their efficiency in decomposition, compression and edge detection settings. The obtained results are promising, and the proposed matrices enjoy all the features of the directional transform. With respect to wavelets, they are able to analyse different directions. Moreover, the smaller determinant with respect to shearlets generates less artefacts in the reconstruction process. For the future it will be interesting to study how the results change by considering different filterbanks. For example we want to construct orthogonal filters.

By reconstructing the detail coefficients we observe that the proposed matrices can be used to detect edges. In fact, they give good results compared both to shearlets and Canny's algorithm. They are able to detect different directions of edges with low fragmentation, they are robust to noise, and they distinguish between big and small jumps. These promising results suggest that it will be worthwhile to study a true edge detection with these matrices. The algorithm will take maxima in the detail coefficients and will find their location in the image. We also have to exploit the scale and direction information given by the branch of the tree in order to attach in the right way the edges and to classify if they represent strong edges or small changes.

Bibliography

Bozzini, M., Ghisi, D., Rossini, M. and Sauer, T. [2015]. Directional transforms and pseudo-commuting properties, *Monografías Matemáticas* **40**: 29–41.

Bozzini, M., Rossini, M., Sauer, T. and Volontè, E. [submitted]. Anisotropic scaling matrices and subdivisions schemes, *IMA Journal of Numerical Analysis* .

Candès, E. J. and Donoho, D. L. [2004]. New tight frames of curvelets and optimal representations of objects with piecewise c2 singularities, *Communications on pure and applied mathematics* **57**(2): 219–266.

Canny, J. [1986]. A computational approach to edge detection, *IEEE Transactions on pattern analysis and machine intelligence* (6): 679–698.

Cashman, T. J., Hormann, K. and Reif, U. [2013]. Generalized lane–riesenfeld algorithms, *Computer Aided Geometric Design* **30**(4): 398–409.

Chaikin, G. M. [1974]. An algorithm for high-speed curve generation, *Computer graphics and image processing* **3**(4): 346–349.

Chalmovianskỳ, P. and Jüttler, B. [2007]. A non-linear circle-preserving subdivision scheme, *Advances in Computational Mathematics* **27**(4): 375–400.

Charina, M., Conti, C., Guglielmi, N. and Protasov, V. [2017]. Regularity of non-stationary subdivision: a matrix approach, *Numerische Mathematik* **135**(3): 639–678.

Charina, M., Conti, C. and Sauer, T. [2005a]. Lp–convergence of subdivision schemes: joint spectral radius versus restricted spectral radius, *Approximation theory XI (Gatlinburg, TN, 2004), M. Neamtu and LL Schumaker, eds., Nashboro Press, Nashville, TN* pp. 129–150.

Charina, M., Conti, C. and Sauer, T. [2005b]. Regularity of multivariate vector subdivision schemes, *Numerical algorithms* **39**(1): 97–113.

Chui, C. K. [1992a]. *An introduction to wavelets*, Elsevier.

Chui, C. K. [1992b]. Wavelets: a tutorial in theory and applications, *Wavelet Analysis and its Applications, San Diego, CA: Academic Press,| c1992, edited by Chui, Charles K.* **1**.

Conti, C., Cotronei, M. and Sauer, T. [2008]. Full rank positive matrix symbols: interpolation and orthogonality, *BIT Numerical Mathematics* **48**(1): 5–27.

Conti, C., Cotronei, M. and Sauer, T. [2010]. Full rank interpolatory subdivision schemes: Kronecker, filters and multiresolution, *Journal of Computational and Applied Mathematics* **233**(7): 1649–1659.

Conti, C., Dyn, N., Manni, C. and Mazure, M.-L. [2015]. Convergence of univariate nonstationary subdivision schemes via asymptotic similarity, *Computer Aided Geometric Design* **37**: 1–8.

Conti, C. and Hormann, K. [2011]. Polynomial reproduction for univariate subdivision schemes of any arity, *Journal of Approximation Theory* **163**(4): 413–437.

Cotronei, M., Ghisi, D., Rossini, M. and Sauer, T. [2015]. An anisotropic directional subdivision and multiresolution scheme, *Advances in Computational Mathematics* **41**(3): 709–726.

Daubechies, I. and Lagarias, J. C. [1992]. Two-scale difference equations ii. local regularity, infinite products of matrices and fractals, *SIAM Journal on Mathematical Analysis* **23**(4): 1031–1079.

De Rham, G. [1947]. Un peu de mathématiques à propos d'une courbe plane., *Elemente der Mathematik* **2**: 73–76.

Deng, C. and Ma, W. [2012]. Matching admissible g2 hermite data by a biarc-based subdivision scheme, *Computer Aided Geometric Design* **29**(6): 363–378.

Deng, C. and Ma, W. [2014]. A biarc based subdivision scheme for space curve interpolation, *Computer Aided Geometric Design* **31**(9): 656–673.

Deng, C. and Wang, G. [2010]. Incenter subdivision scheme for curve interpolation, *Computer Aided Geometric Design* **27**(1): 48–59.

Derado, J. [1999]. Multivariate refinable interpolating functions, *Applied and Computational Harmonic Analysis* **7**(2): 165–183.

Deslauriers, G. and Dubuc, S. [1989]. Symmetric iterative interpolation processes, *Constructive approximation*, Springer, pp. 49–68.

Do Carmo, M. P. [1976]. *Differential geometry of curves and surfaces*, Vol. 2, Prentice-hall Englewood Cliffs.

Do, M. N. and Vetterli, M. [2005]. The contourlet transform: an efficient directional multiresolution image representation, *IEEE Transactions on image processing* **14**(12): 2091–2106.

Dyn, N. [1992]. Subdivision schemes in cagd, *Advances in Numerical Analysis*, Citeseer.

Dyn, N. [2002]. Analysis of convergence and smoothness by the formalism of laurent polynomials, *Tutorials on Multiresolution in Geometric Modelling*, Springer, pp. 51–68.

Dyn, N., Gregory, J. A. and Levin, D. [1991]. Analysis of uniform binary subdivision schemes for curve design, *Constructive Approximation* **7**(1): 127–147.

Dyn, N. and Hormann, K. [2012]. Geometric conditions for tangent continuity of interpolatory planar subdivision curves, *Computer Aided Geometric Design* **29**(6): 332–347.

Dyn, N. and Levin, D. [1995]. Analysis of asymptotically equivalent binary subdivision schemes, *Journal of mathematical analysis and applications* **193**(2): 594–621.

Dyn, N., Levin, D. and Gregory, J. A. [1987]. A 4-point interpolatory subdivision scheme for curve design, *Computer aided geometric design* **4**(4): 257–268.

Erdélyi, A. [2010]. Asymptotic expansions.

Ewald, T. [2016]. Convergence of geometric subdivision schemes, *Applied Mathematics and Computation* **272**: 41–52.

Ewald, T., Reif, U. and Sabin, M. [2015]. Hölder regularity of geometric subdivision schemes, *Constructive Approximation* **42**(3): 425–458.

Farin, G. E. [2002]. *Curves and surfaces for CAGD: a practical guide*, Morgan Kaufmann.

Floater, M. S. and Micchelli, C. A. [1998]. Nonlinear stationary subdivision, *In Memory of A.K. Varma*, Elsevier, pp. 209–224.

Guo, K., Kutyniok, G. and Labate, D. [2006]. Sparse multidimensional representations using anisotropic dilation and shear operators.

Guo, K. and Labate, D. [2009]. Characterization and analysis of edges using the continuous shearlet transform, *SIAM journal on Imaging Sciences* **2**(3): 959–986.

Guo, K. and Labate, D. [2017]. Microlocal analysis of edge flatness through directional multiscale representations, *Advances in Computational Mathematics* **43**(2): 295–318.

Guo, K., Labate, D., Lim, W.-Q., Weiss, G. and Wilson, E. [2006a]. The theory of wavelets with composite dilations, *Harmonic analysis and applications* pp. 231–250.

Guo, K., Labate, D., Lim, W.-Q., Weiss, G. and Wilson, E. [2006b]. Wavelets with composite dilations and their mra properties, *Applied and Computational Harmonic Analysis* **20**(2): 202–236.

Hamming, R. W. [1989]. *Digital filters*, Courier Corporation.

Han, B. [2003]. Compactly supported tight wavelet frames and orthonormal wavelets of exponential decay with a general dilation matrix, *Journal of Computational and Applied Mathematics* **155**(1): 43–67.

Han, B. and Jia, R.-Q. [1998]. Multivariate refinement equations and convergence of subdivision schemes, *SIAM Journal on Mathematical Analysis* **29**(5): 1177–1199.

Harten, A., Engquist, B., Osher, S. and Chakravarthy, S. R. [1987]. Uniformly high order accurate essentially non-oscillatory schemes, iii, *Journal of computational physics* **71**(2): 231–303.

Hernández-Mederos, V., Estrada-Sarlabous, J. and Ivrissimtzis, I. [2013]. Generalization of the incenter subdivision scheme, *Graphical Models* **75**(2): 79–89.

Hutchinson, J. E. [1981]. Fractals and self similarity, *Indiana University Journal of Math* **30**(5): 713–747.

Knuth, D. E. [1976]. Big omicron and big omega and big theta, *ACM Sigact News* **8**(2): 18–24.

Kutyniok, G. and Labate, D. [2009]. Resolution of the wavefront set using continuous shearlets, *Transactions of the American Mathematical Society* **361**(5): 2719–2754.

Kutyniok, G., Labate, D. et al. [2012]. *Shearlets: Multiscale analysis for multivariate data*, Springer Science & Business Media.

Kutyniok, G. and Sauer, T. [2009]. Adaptive directional subdivision schemes and shearlet multiresolution analysis, *SIAM Journal on Mathematical Analysis* **41**(4): 1436–1471.

Labate, D., Lim, W.-Q., Kutyniok, G. and Weiss, G. [2005]. Sparse multidimensional representation using shearlets, *Optics & Photonics 2005*, International Society for Optics and Photonics, pp. 59140U–59140U.

Liu, X.-D., Osher, S. and Chan, T. [1994]. Weighted essentially non-oscillatory schemes, *Journal of computational physics* **115**(1): 200–212.

Madych, W. R. [1993]. Some elementary properties of multiresolution analyses of l 2 (r n), *Wavelets: A tutorial in Theory and Applications*, Academic Press Professional, Inc., pp. 259–294.

Mallat, S. [2008]. *A wavelet tour of signal processing, the sparse way*, Academic press.

Mallat, S. G. [1989]. Multiresolution approximations and wavelet orthonormal bases of $l^2(\mathbb{R})$, *Transactions of the American mathematical society* **315**(1): 69–87.

Mallat, S. and Zhong, S. [1992]. Characterization of signals from multiscale edges, *IEEE Transactions on pattern analysis and machine intelligence* **14**(7): 710–732.

Marcus, M. and Minc, H. [1992]. *A survey of matrix theory and matrix inequalities*, Vol. 14, Courier Corporation.

Meyer, Y. [1995]. *Wavelets and operators*, Vol. 1, Cambridge university press.

Micchelli, C. A. and Prautzsch, H. [1989]. Uniform refinement of curves, *Linear Algebra and its Applications* **114**: 841–870.

Möller, H. M. and Sauer, T. [2004]. Multivariate refinable functions of high approximation order via quotient ideals of laurent polynomials, *Advances in Computational Mathematics* **20**(1): 205–228.

Moosmüller, C. [2016]. Cˆ1 analysis of hermite subdivision schemes on manifolds, *SIAM Journal on Numerical Analysis* **54**(5): 3003–3031.

Oswald, P. [2004]. Smoothness of nonlinear median-interpolation subdivision, *Advances in Computational Mathematics* **20**(4): 401–423.

Peters, J. and Reif, U. [2008]. *Subdivision surfaces*, Springer.

Rossini, M. and Volontè, E. [2017]. On directional scaling matrices in dimension d= 2, *Mathematics and Computers in Simulation* .

Rudin, W. et al. [1964]. *Principles of mathematical analysis*, Vol. 3, McGraw-Hill New York.

Sabin, M. A. and Dodgson, N. A. [2004]. A circle-preserving variant of the four-point subdivision scheme, *Mathematical Methods for Curves and Surfaces: Tromsø* pp. 275–286.

Sauer, T. [2010]. Multiple subdivision schemes, *International Conference on Curves and Surfaces*, Springer, pp. 612–628.

Sauer, T. [2012]. Shearlet multiresolution and multiple refinement, *Shearlets*, Springer, pp. 199–237.

Schaefer, S., Vouga, E. and Goldman, R. [2008]. Nonlinear subdivision through nonlinear averaging, *Computer Aided Geometric Design* **25**(3): 162–180.

Strang, G. and Nguyen, T. [1996]. *Wavelets and filter banks*, SIAM.

Vetterli, M. and Kovačević, J. [2007]. Wavelets and subband coding.

Wallner, J. [2006]. Smoothness analysis of subdivision schemes by proximity, *Constructive Approximation* **24**(3): 289–318.

Wallner, J. and Dyn, N. [2005]. Convergence and c^1 analysis of subdivision schemes on manifolds by proximity, *Computer Aided Geometric Design* **22**(7): 593–622.

Wang, Z., Bovik, A. C., Sheikh, H. R. and Simoncelli, E. P. [2004]. Image quality assessment: from error visibility to structural similarity, *IEEE transactions on image processing* **13**(4): 600–612.

Warren, J. [1995]. Binary subdivision schemes for functions over irregular knot sequences.

Xie, G. and Yu, T. P.-Y. [2005]. Smoothness analysis of nonlinear subdivision schemes of homogeneous and affine invariant type, *Constructive Approximation* **22**(2): 219–254.

Xie, G. and Yu, T. P.-Y. [2007]. Smoothness equivalence properties of manifold-valued data subdivision schemes based on the projection approach, *SIAM Journal on Numerical Analysis* **45**(3): 1200–1225.

Yang, X. [2006]. Normal based subdivision scheme for curve design, *Computer Aided Geometric Design* **23**(3): 243–260.

Yi, S., Labate, D., Easley, G. R. and Krim, H. [2009]. A shearlet approach to edge analysis and detection, *IEEE Transactions on Image Processing* **18**(5): 929–941.

Zhao, H., Qiu, X., Liang, L., Sun, C. and Zou, B. [2009]. Curvature normal vector driven interpolatory subdivision, *Shape Modeling and Applications, 2009. SMI 2009. IEEE International Conference on*, IEEE, pp. 119–125.